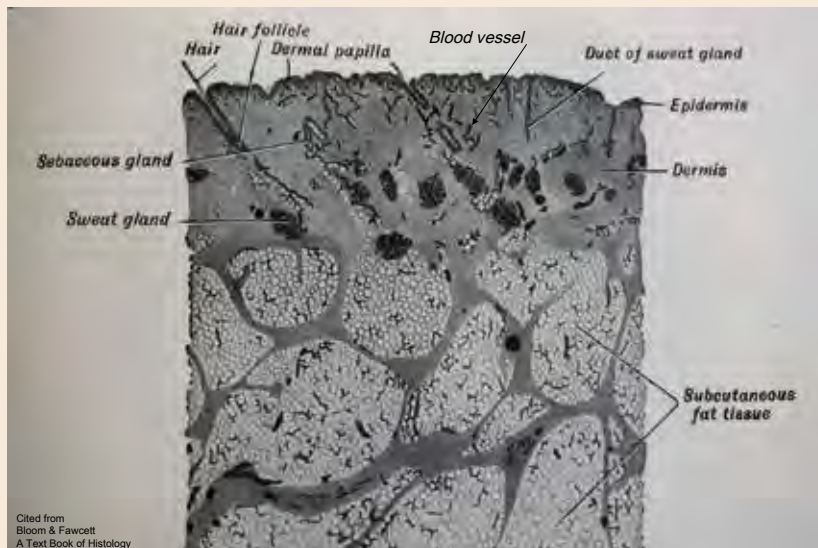


Forum for Nordic Dermato-Venereology

Official journal of the Nordic Dermatology Association

The Dermis – Ultrastructural Histopathology of Connective Tissue



By TAKASI KOBAYASI



The Dermis – Ultrastructural Histopathology of Connective Tissue

TAKASI KOBAYASI, MD

Laboratories for Connective Tissue Research, Department of Dermato-venereology University of Copenhagen, Bispebjerg Hospital, Rigshospital, Copenhagen, Denmark. Former Associate Professor of Dermato-Venereology, Member of Danish Dermatological Association. Member of the Society of Cutaneous Ultrastructure Research. Honorary member of Japanese Dermatological Association. Member of Dansk Dermatologisk Selskab and Society of Cutaneous Ultrastructure Research

Summary

Dermis is composed of connective tissue, namely, elastic system fibre, collagen fibrils, ground substance. Basal lamina is a binding structure secreted by keratinocytes of ectodermal origin and mesenchymal cells of mesenchymal cell tissue. Axon of neural ectodermal cells also produces basal lamina. Schwann cells and perineural cells of nerve are also mesenchymal. Mast cells and cells of mesenchymal cell lineage, function for maintenance of dermal connective tissue.

Elastic system fibre is composed of elastic microfibrils and matrix and reveals various shapes after developing, aging and inheritance and by external influence. Amyloid, Hyaline and calcium are the pathological products of elastic fibre matrix.

Collagen fibrils present characteristic axial periodicity of 10 nm. Thickness of the fibrils varies for fibrosis and atrophy. High ratio of type I/III is found in thicker collagen fibril. Collagen aggregate shows distinguished shape after collagenase degradation. Twisted collagen fibrils are the sign for inherited anomaly.

Ground substance appears in typical shape of "Filaments with dots" (Filaments of type VI collagen and globular acid mucopolysaccharide) and form glove networks in the interfibrillar space. Myxoedema is the condition after accumulation of ground substance.

Junction is constructed by basal lamina, anchoring filaments, anchoring fibrils and elastic microfibrils. Junction is well developed under epidermis but poor under mesenchymal cell tissues. Separation in dermoepidermal junction is specific sign for bullous dermatoses. Productive form is found in some fibrotic dermatoses.

Mast cells and myofibroblasts play distinct roles in some connective tissue disorders.

Pericytes transform to myofibroblast and play distinct roles for fibrotic and atrophic dermatoses and tissue repair. Pericyte transformation to myofibroblast is the fundamental process of fibrosis. Pericyte is the cell reservoir for myofibroblast. Seemingly, pericytes develop from vascular endothelial cells.

Introduction

Skin covers the whole surface of the human body, maintaining human body in a stable condition and protecting the body against external injury. Skin consists of the epidermis, covering the outer surface, and the dermis, supporting the epidermis and continuing deeply to the subcutaneous adipose tissue. The epidermis is the parenchymal tissue of skin and consists of keratinocytes in strata. Keratinocytes are ectodermal in origin. The dermis is composed of connective tissue and mesenchymal cells of mesodermal origin. Myofibroblasts and mast cells are mesenchymal cells, which occur free in the dermis. Mesenchymal cells also form cellular tissues in the dermis, i.e. vessels, smooth-muscle tissue, adipose tissue and perineurium. Dermis embeds epidermal appendages and mesenchymal cell tissues and hold these tissues in stable condition. Mast cells and myofibroblasts migrate freely into the dermis and maintain the connective tissue in normal proper form. In addition, peripheral nerves are also embedded in dermis. A peripheral nerve is constructed by axon, Schwann cells and perineurium. Axon is neuroectodermal, Schwann cell is neuro-mesenchymal. Perineurium is mesenchymal constructed of perineural collagen fibrils and perineural cells of mesenchymal origin.

Dermal connective tissue is constructed of elastic system fibres, collagen fibrils and ground substance. Epidermis, mesenchymal cell tissues and peripheral nerves anchor to dermal connective tissue via the basal lamina (Figure). Connective tissue of the dermis varies in structure according to inheritance, age, disease and environmental injuries. In addition, dendritic cells migrate into the dermis and epidermis of normal skin. The function of dendritic cells is incompletely explained. Dendritic cells take part in allergic inflammatory reactions and are thought to regulate the mitotic activity of keratinocytes.

This paper reports the research for the ultrastructural histopathology of dermis, based on more than 200 studies, published, presented and unpublished, performed during the period 1962–2008 in the Section for Ultrastructural Histopathology in the Connective Tissue Research Laboratories Department of Dermato-venereology, University of Copenhagen, Rigshospital

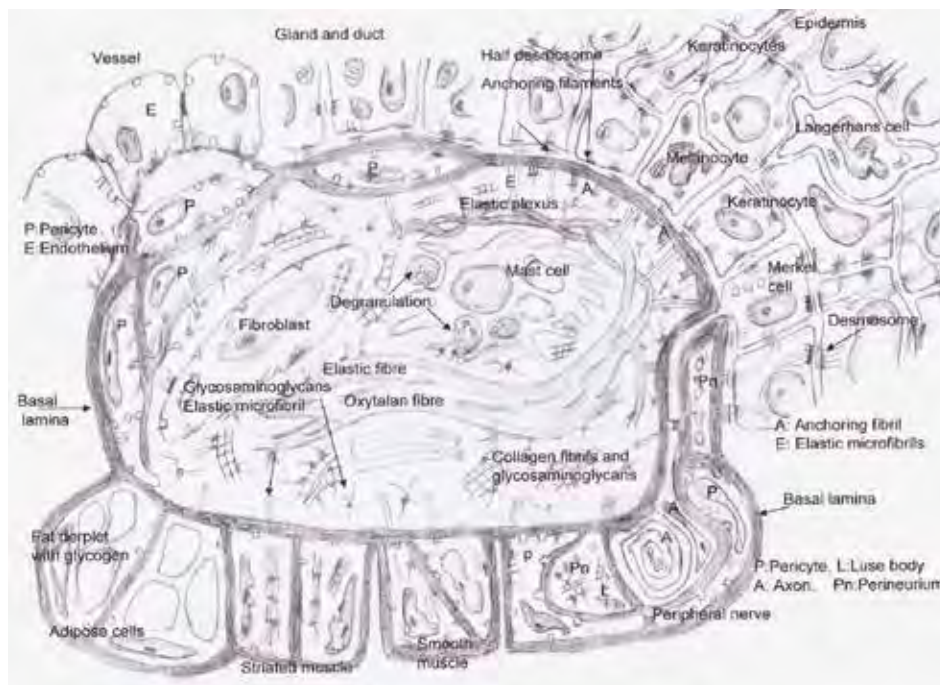


Figure. Dermis. Schema on structural components of dermis in a view-point of basal lamina.

and Bispebjerg Hospital, Copenhagen, Denmark. The material for these studies included more than 4,000 specimens of various dermatoses, obtained mainly in own clinic and partly from other hospitals both inside and outside Denmark. Study material was also obtained from cell and organ culture studies of skin in own laboratory. The tissue samples were prepared using routine methods and immune electron microscopy developed in the laboratory (see Appendix).

The Connective Tissue Research Laboratories were founded in the Institute of Medical Anatomy, Copenhagen University at the end of the 1950s by Professor Dr med. Gustav Asboe-Hansen. The ultrastructure research section began working with the Philips 100B electron microscope. When Dr Gustav Asboe-Hansen was appointed as Professor of Dermato-venere-

ology at the University of Copenhagen, the connective tissue research laboratories moved into Department H, Rigshospital and the study proceeded using a Siemens Elmiskop IA and, later, a JEOL Electron microscope 100CX.

In 1978, the laboratory arranged the 5th European Meeting for Electron Microscopy, applied for cutaneous pathology, and established the Society of Cutaneous Ultrastructure Research (SCUR). In 1982, Professor G. Asboe-Hansen retired, and the laboratory function was taken over by Associate Professor Dr med. Takasi Kobayasi. In 1992, Department H Rigshospital merged with the Dermatology Department Bispebjerg Hospital and moved into Bispebjerg Hospital following system re-organization in the Rigshospital. The laboratories were moved into Bispebjerg Hospital and the ultrastructural study proceeded there. In 1 March 2007, Dr Takasi Kobayasi retired.

Illustration of electronic micrographs

I. Elastic system fibre

Overview	
• Ultrastructure	Figures 1–5
• Histochemistry	Figures 6–8
• Age and age-exposure-dependent variations	Table I
• Age and exposure-dependent changes	Figures 9–21
• Calcification	Figures 22–23
• Disorders	
- Pseudoxanthoma elasticum	Figures 24–27
- Salpeter-induced calcinosis	Figure 28
- Calcinosis cutis	Figure 29
- Amyloidosis	Figures 30–32
- Pretibial myxoedema	Figure 33
- Necrobiosis lipoidica diabetorum	Figure 34
- Morphoea	Figure 35
- Acrosclerotic scleroderma	Figures 36–37
- Lupus erythematosus	Figure 38
• Inheritance-dependent disorders	
- Disseminated cutaneous nevi	Figure 39
- Juvenile elastoma	Figures 40–41
- Inherited hypermobile disorders	Figure 42–49

Ultrastructure [1, 2]

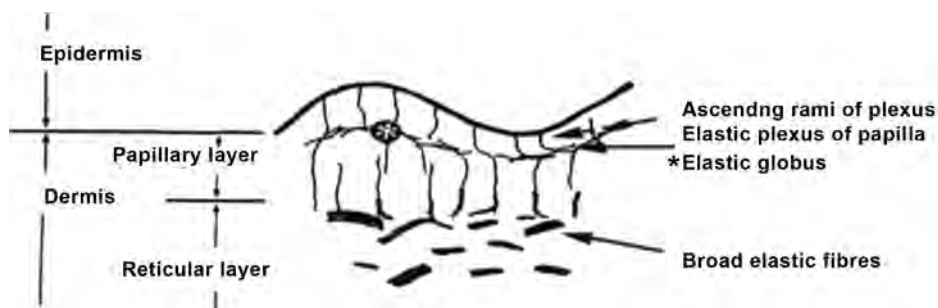


Fig. 1. Elastic system fibre in dermis. Elastic system fibre consists of elastic microfibrils and matrix, and presents some structural variants of the fibres in normal dermis. Elastic fibre is the common name. The construction and names of the variants in dermis are shown in the figure. Elastic system fibre constructs net-works along to the direction of skin tension. Elastic fibres and microfibrils construct plexus in papillary dermis and elastic microfibrils ascend from the plexus and fuse to basal lamina (Ascending rami) [1a, 1b, 2]. Elastic fibre starts to form microfibril-bundle and spots of matrix in the bundle. The matrix expands gradually after age and covers over the bundle (Elastic fibre proper). Broad elastic fibre is a normal, non-degenerate variant of the elastic system fibre which matrix is covered almost all the fibril-bundle. Broad elastic fibre is found in reticular dermis, earliest on adolescent age. Elastic globus is also an age-dependent variant of normal shape, found in papillary dermis of adult [6]. Some inherited dermatoses reveal specific structural variants [20, 21, 22]. Elastic fibres degenerate after age, external and internal factors. Net-works of elastic fibres are supposedly to maintain skin tension in a stable condition against external forces. Elastic microfibrils are said to form mesenchymal cells. Turn-over rate of elastic fibre is unknown, presumably for many years or no renewal. Oxytalan fibre is a bundle of microfibrils, seemingly a variant of elastic system fibre [7].

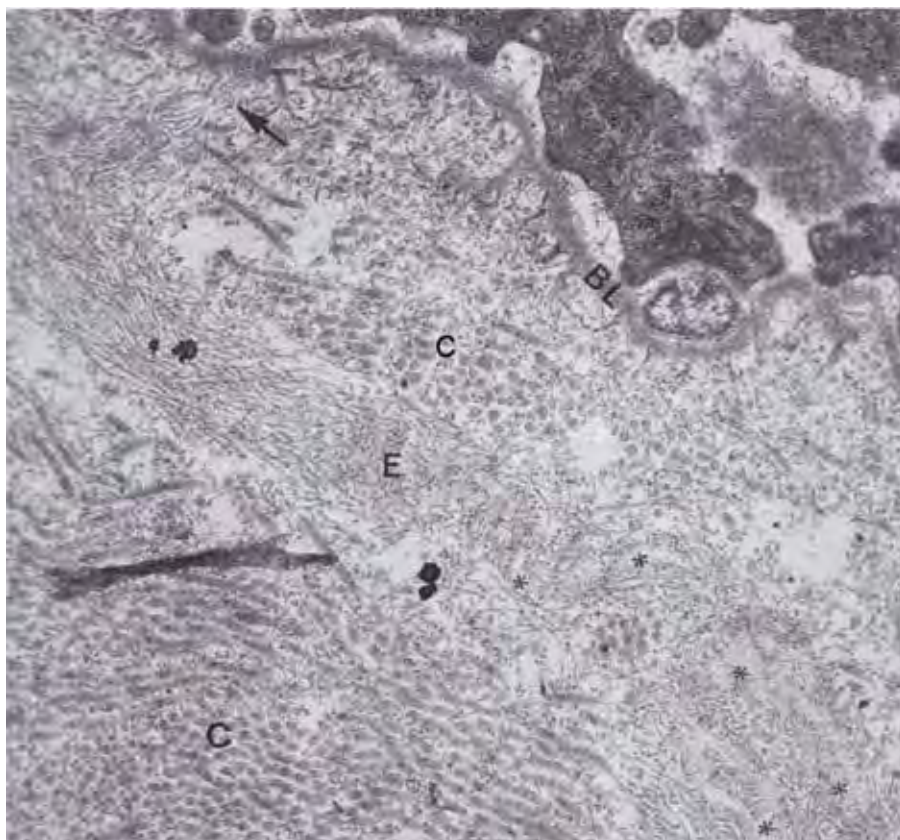


Fig. 2. Elastic system fibre in the upper part of dermis. Elastic microfibrils ascend from the subpapillary plexus of elastic fibre (E and asterisks) and fuse to basal lamina (BL). Arrow points ascending microfibrils fuse to basal lamina. C: Collagen fibrils. × 10,000

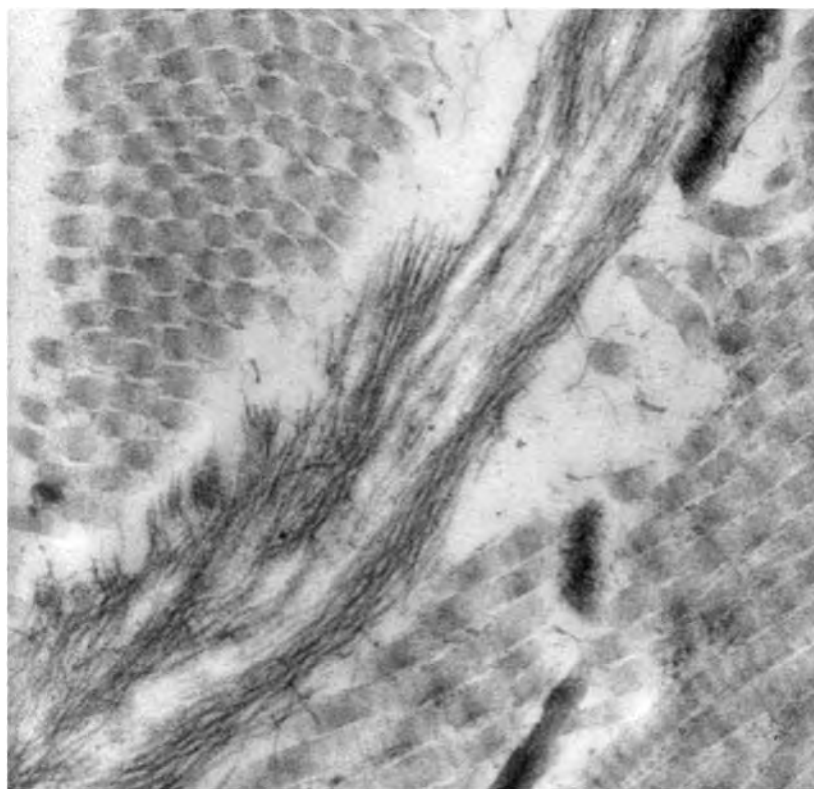


Fig. 3. Elastic fibre proper. Longitudinal section. Normal elastic fibre showing typical ultrastructure is named “Elastic fibre proper”. Such a fibre is commonly found in dermis of baby, children and young person, though matrix covers wider areas of the fibre after age. Elastic fibre proper presents lucent homogenous matrix with internal dense stripes and the microfibrils on the fibre surface. Microfibrils array parallel to the fibre direction. × 20,000.

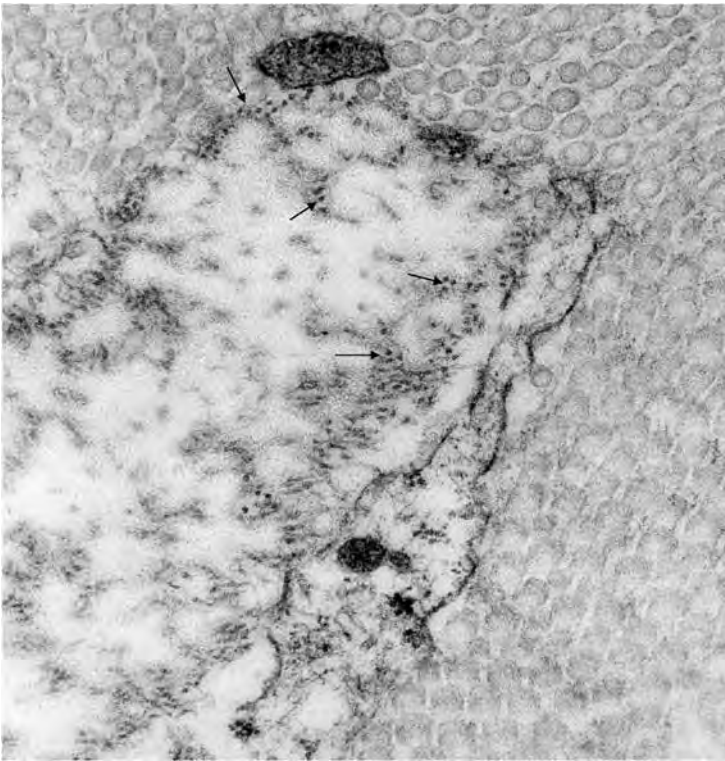


Fig. 4. Elastic fibre proper. Cross-cut section. Elastic microfibrils are seen on the surface of matrix. Elastic microfibrils reveal round cut-surfaces on the matrix surface (arrows). Elastic matrix is homogeneous lucent and internal dense stripes are seen as dense spots. $\times 20,000$.

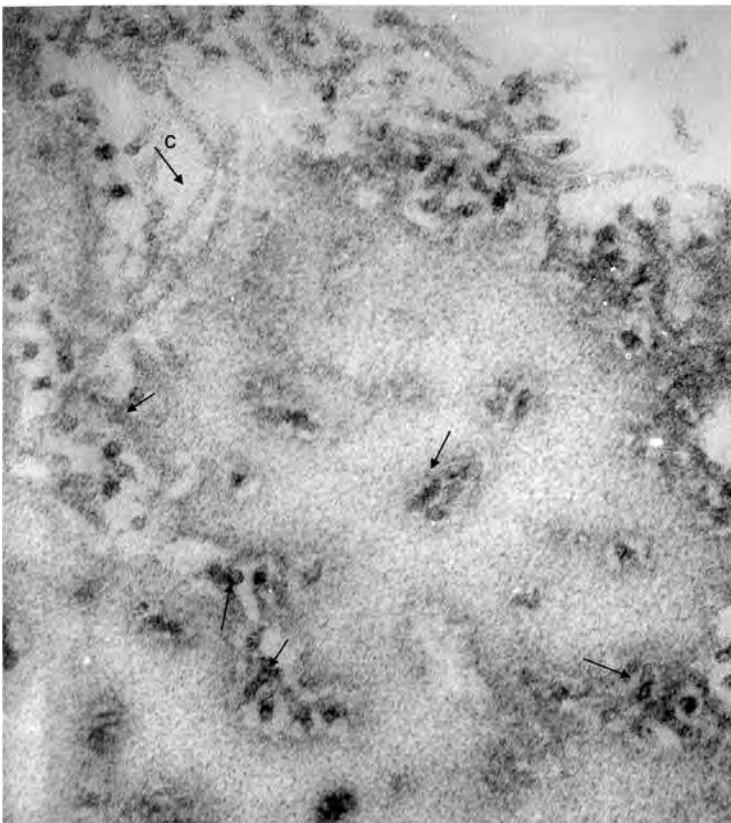


Fig. 5. Elastic fibre proper in details. Cross-cut section. Elastic microfibrils are hollow fibrils, showing round cut-surface in 10 nm across (arrows) and faint cross-bands in longitudinal section (arrow C). Matrix is lucent homogeneous. Elastic microfibrils are formed of fibrillin and disulfide bounds. Elastic microfibrils are not stained by light microscopic elastic fibre stain, but stained by aldehyde fuchsin after oxidation by potassium permanganate. Matrix is also called elastin which contains mucoprotein (Elastmucin). Elastin is stained by acid orcein, aldehyde fuchsin in light microscopy. $\times 40,000$.

Histochemistry [3]



Fig. 6. Influence by pancreatic elastase [3]. The picture shows normal dermis, influenced by pancreatic elastase, at pH 8, for 6 h. Elastic fibre matrix and basal lamina are removed, while elastic microfibrils remain unaffected (arrow). C: Collagen fibrils. $\times 5,000$.



Fig. 7. Elastic fibre after treatment with dithioerythritol solution (10 mg/ml in Hanks' balanced salt solution) for 6 hours [3]. Elastic microfibrils appear beaded (arrows), while elastic matrix (E) is seen grainy. $\times 20,000$.

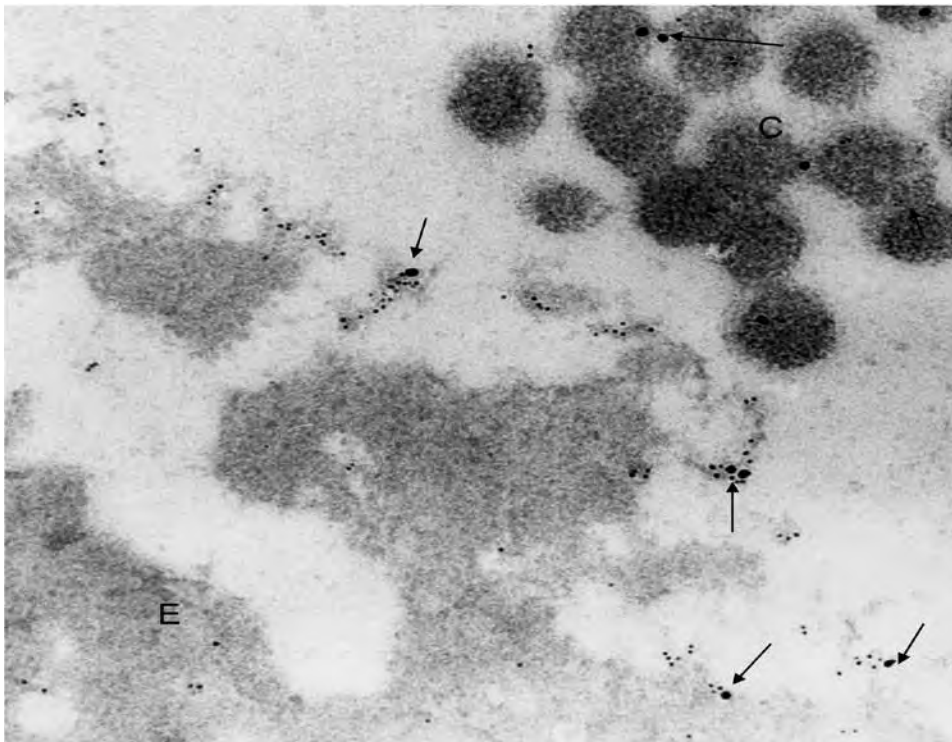


Fig. 8. Immunoelectronmicroscopy. Types V and VI collagen [4]. Type V collagen, marked by 5 nm gold particles. Type V collagen is a binding collagen, found on the surfaces of elastic microfibrils and matrix surface (as well as on surfaces of collagen fibrils). Type VI collagen (marked by 10 nm gold particles) is found on the surface of matrix and microfibrils. Type VI collagen forms core protein of ground substance and associates with glycosaminoglycans. C: Collagen fibrils. E: Elastic matrix. × 40,000.

Age -and sun-exposure-dependent variation. Inheritance dependent variation

Age, years	0-4	5-9	10-14	15-19	20-24	25-29	30-34	35-39	40-44	45-49	50-54	55-59	≥60
<i>Patients with Ehlers-Danlos syndrome (BI 6-9) and Hypermobile syndrome with TCF (BI 3-5); n=73</i>													
Biopsy, n	2	1	4	14	5	4	10	15	6	6	2	1	3
<i>Control subjects (BI 0-2) in elbow without TCF; n=62</i>													
Biopsy, n	3	2	1	2	3	3	2	8	4	10	9	8	7
<i>Control subjects in covered area, selected in the laboratory's archive, without TCF; n=14</i>													
Buttocks:	22, 43, 60 years of age												
Waist:	31, 35, 49, 60, 67 years of age												
Thigh:	17, 27, 43 years of age												
Breast fold:	18, 35, 47 years of age												
<i>Patients with Marfan syndrome, Osteogenesis imperfecta, type I and Homocysteinuria. Age (BI and TCF +, -)</i>													
Marfan syndrome	62 (6+), 55 (6+), 39 (9+), 35 (4+), 33 (9+), 18 (8+), 17 (8+); n=7												
Osteogenesis imperfecta, type I	37 (2-), 27 (7+), 26 (3-), 19 (6+), 4 (5+); n=5												
Homocysteinuria	15 (2+); n=1												

Table I. Biopsies for the study [5]. Elastic system fibre of clinically normal dermis is widely varied in the structure among ages, locations of body surface (external influence), inheritance and internal disorders. Biopsy specimens are mostly taken in the half-exposed area, for instance extensor surface of elbow, and covered area of clinically normal skin. Biopsy material is selected in the laboratory's archive and shown in the table. Inherited hypermobile disorders reveal altered shapes of elastic fibres in normal dermis and vary after age. The ultrastructure is different among normal persons. Inherited disorders are Ehlers-Danlos syndrome, Hypermobile syndrome, Marfan syndrome, Osteogenesis imperfecta, type I and Homocysteinuria. Clinical sign of Beighton's Score Index for hypermobility (BI) and ultrastructural sign of twisted collagen fibrils (TCF) suggest hypermobility, i.e. inherited anomaly of connective tissue [12 in the Section of Collagen fibrils]. Age-dependent variation is demonstrated in infantile, adolescent adult and senile pattern. The changes are recognized by altered elastic matrix and microfibrils. Biopsies studied appear in the table. Ultrastructure of each age-patterns are summarized in Fig. 10. Age-dependent changes are further intensified by sun exposure. Individual changes are shown in the following figures.

Age and exposure-dependent changes

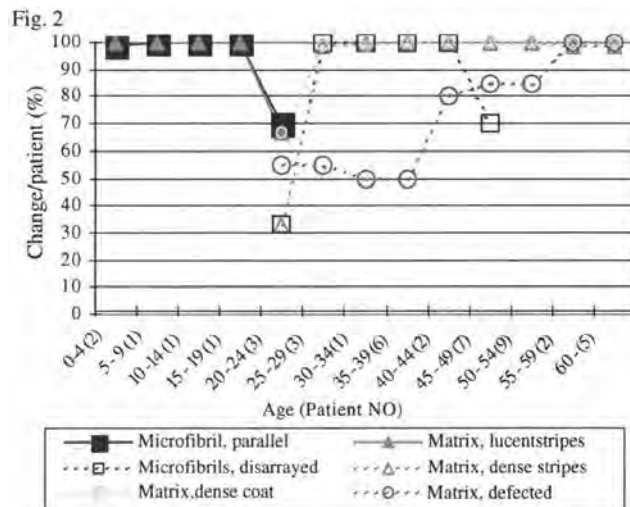
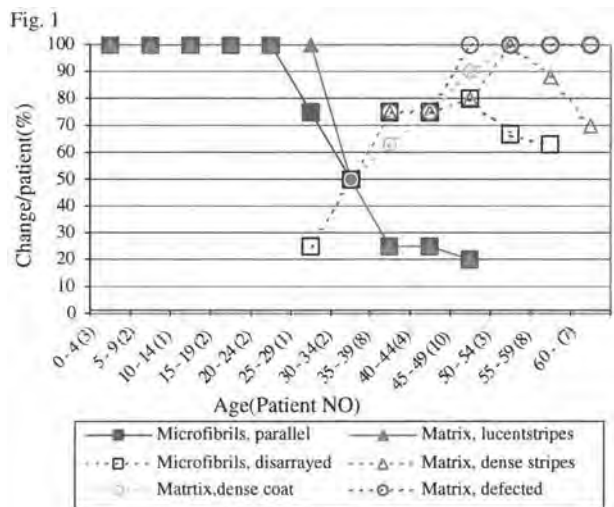


Fig. 9. Elastic fibre changes in age-dependent pattern. Fig. 1: Reticular dermis, Fig. 2: Papillary dermis. A finding at 70% is the border value to interpret the results as positive. Reticular dermis shows infantile pattern till 25–29 year-period and senile pattern from 45–49 year-period. Transforming age-period of adolescent pattern to adult pattern is unclear. Papillary dermis presents infantile pattern till 20–24 year-period and senile pattern probably begins at 45–49 year-period. Transforming age-period for infantile pattern to adolescent pattern is 20–24 year-period for papillary dermis. Senile pattern begins 50–54 year-period for reticular dermis. Transforming age-period of adolescent pattern to adult pattern can not be estimated. Whole degeneration pattern presents 5 years earlier in papillary dermis than reticular dermis. The results suggest sol-exposure probably provoke and stimulate degeneration of elastic fibres. The degeneration occurs 5 years earlier in papillary dermis than those in reticular dermis. It is impossible to separate sol-exposure dependent change from age-dependent change by ultrastructural figures.

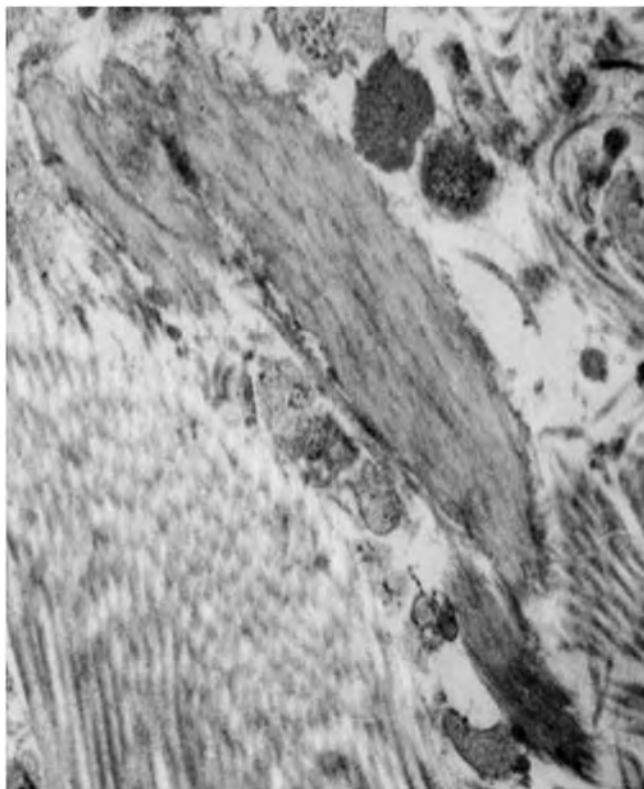


Fig. 10. Elastic fibres of Infantile pattern. Reticular dermis. Biopsy from thigh in a 9-year-old girl. Elastic fibres show homogeneous matrix with distinct stripes and microfibrils on the surface. × 10,000.

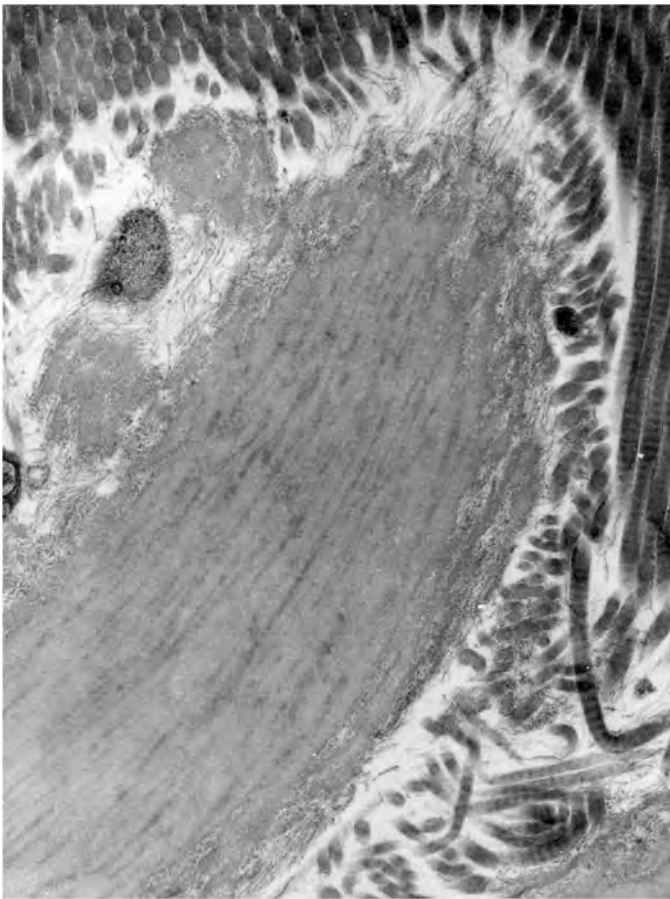


Fig. 11. Broad elastic fibre. Adolescent pattern. Reticular dermis of elbow of a 17-year-old female. A thick variant of normal elastic fibre may also be called broad elastic fibre. A broad elastic fibre presents lucent homogenous matrix with internal stripes and elastic microfibrils on the surface. $\times 20,000$.

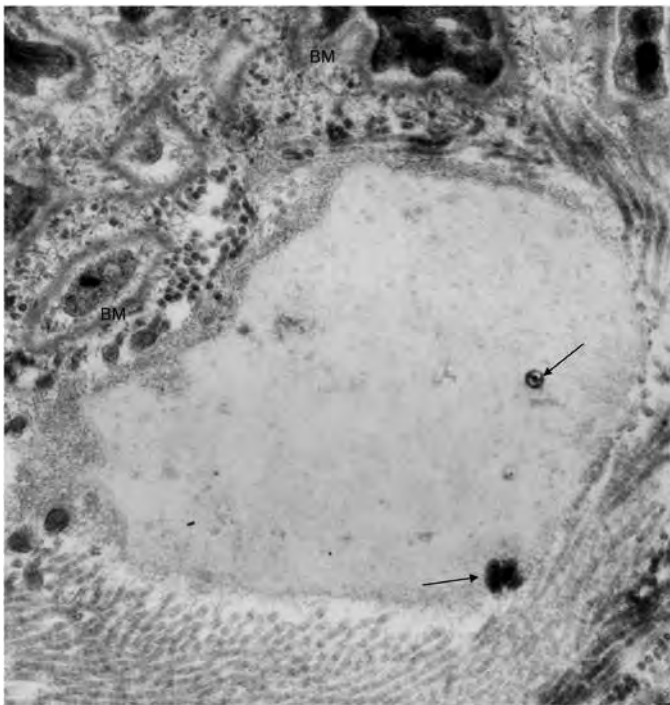


Fig. 12. Globus elasticus after Ebner [6]. Globus elasticus is found in papillary dermis of adult. Globus elasticus shows homogeneous lucent matrix without internal stripes. Calcium spot is often found in small spots (arrows). Globus elasticus is seemingly age change. BM: Basal lamina of epidermis. $\times 5,000$.

Addendum: Oxytalan fibre [Cotta-Peveria et al.] [7] is found in reticular dermis of adult. Oxytalan fibre is a bundle of microfibrils, seen as a bundle of straight microfibrils. Oxytalan fibre is stained light-microscopically after intensive oxydaion like elastic microfibrils stain. Oxytalan fibre could be elastic in nature.

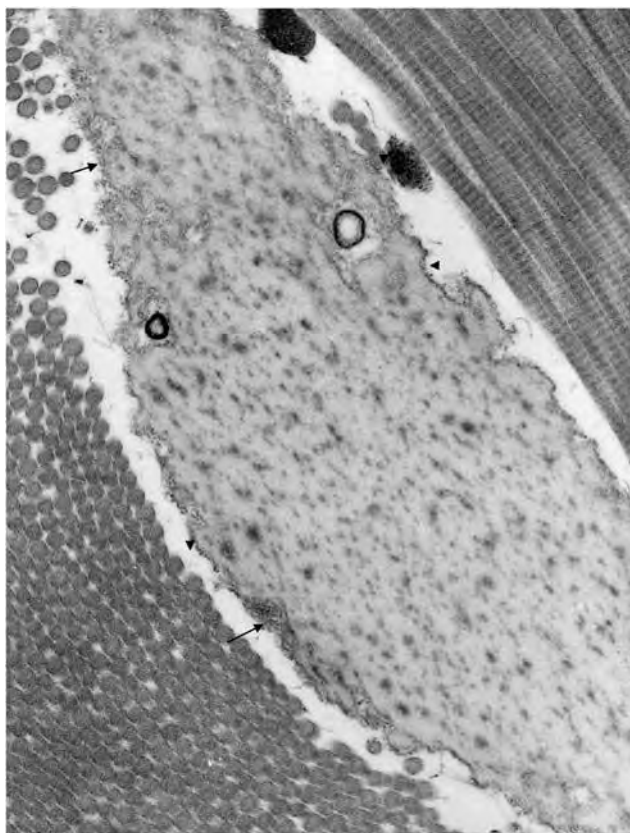


Fig. 13. Adult pattern in the reticular dermis of elbow of a 31-year-old woman. Few disarrayed microfibrils (arrows) and dense surface coat on the matrix surface (arrow-heads). Dense rings in the matrix are calcium precipitants. × 20,000.

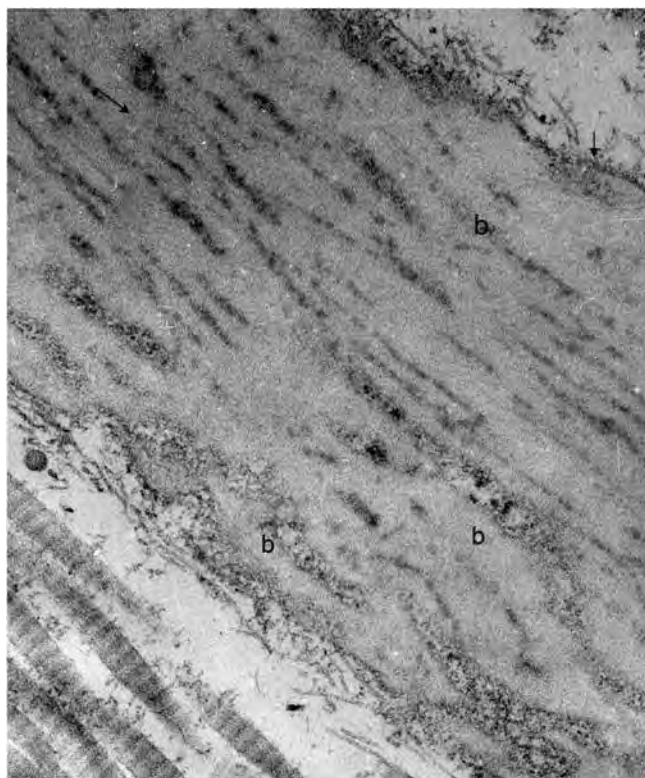


Fig. 14. Adult/senile pattern. Reticular dermis in a 35-year-old woman. Internal stripes of matrix are wide and dense. The matrix is separated in bands (b). Surface coat of matrix are dense (arrows). Microfibrils are scarce on the matrix surface. × 20,000.

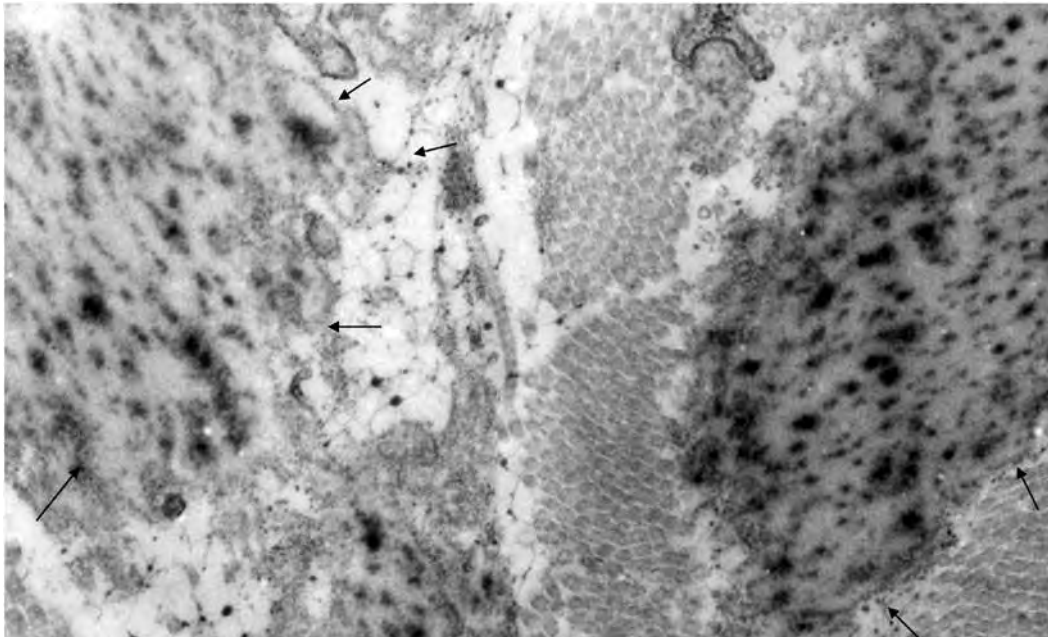


Fig. 15. Adult/Senile pattern. Elastic fibres in the reticular dermis of the elbow in a 41-year-old woman. The matrix shows degenerated figure, such as dense wide stripes and dense surface coat (arrows). The surface of matrix shows defects. Microfibrils are scarce. Numerous glycosaminoglycan figures are seen on the matrix surface and in the vicinity of the matrix. $\times 20,000$.

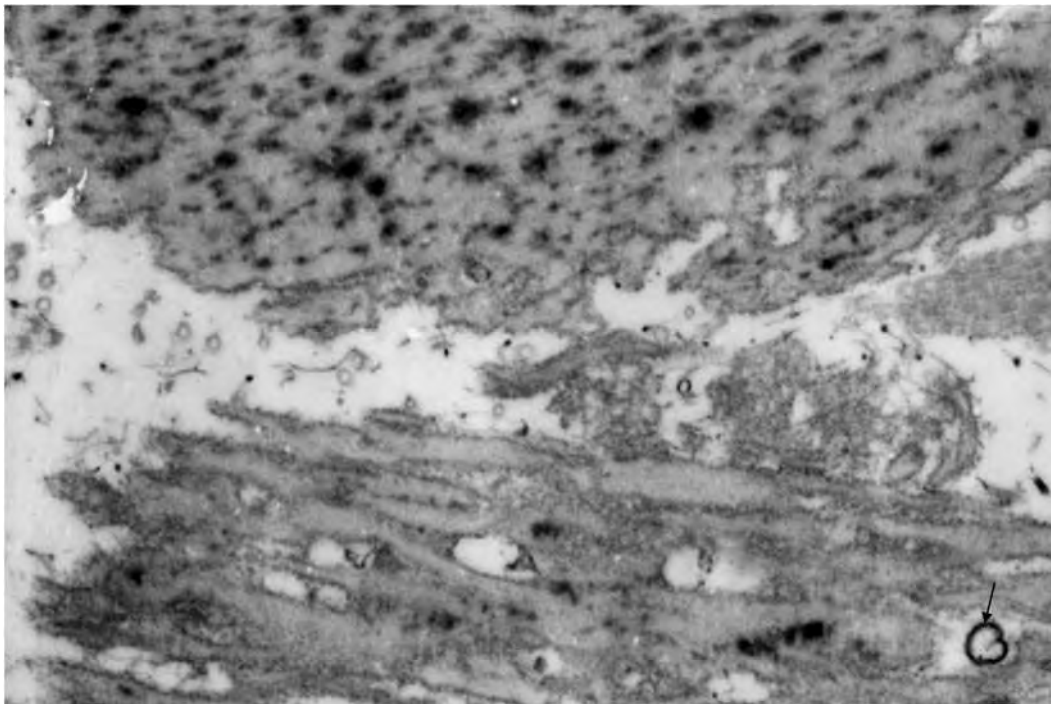


Fig. 16. Senile pattern. Reticular dermis of the elbow in a 60-year-old woman. Broad elastic fibre in the upper part of the picture resembles to the adult pattern in the former slide. No disarrayed microfibrils are seen. The other broad elastic fibre in the lower shows matrix in degenerate figure with round holes and separate bands. Calcium precipitates in ring is seen in the right-lower corner (arrow). Glycosaminoglycan figures are seen in the interfibrous space. $\times 20,000$.

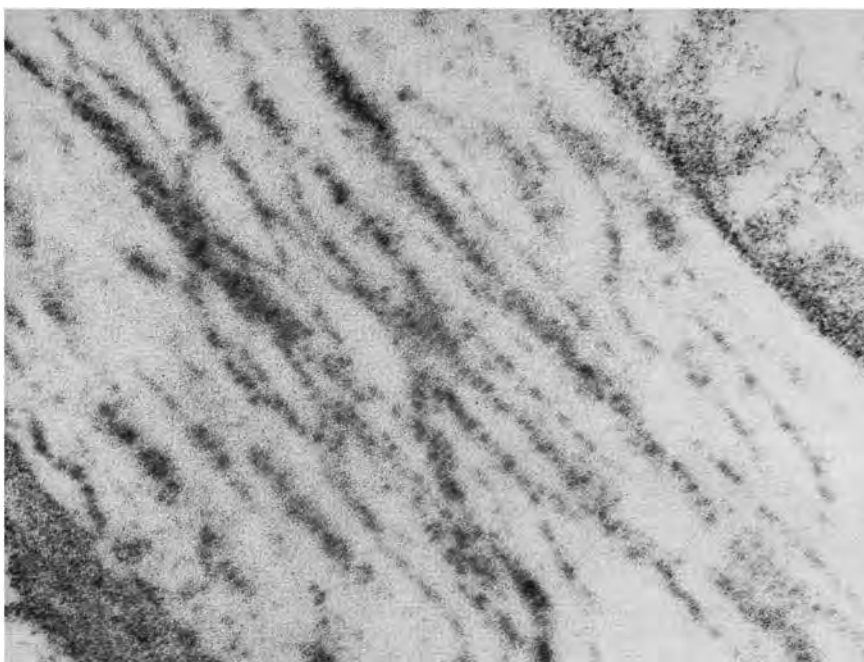


Fig. 17. Senile pattern. Broad elastic fibre in heavily sun-exposed reticular dermis (Armpit, relatively covered body area of an 84-year-old man). Internal stripes of matrix are widened and contain dense granular material. Matrix surface shows no microfibrils and are coated by dense material. $\times 20,000$.

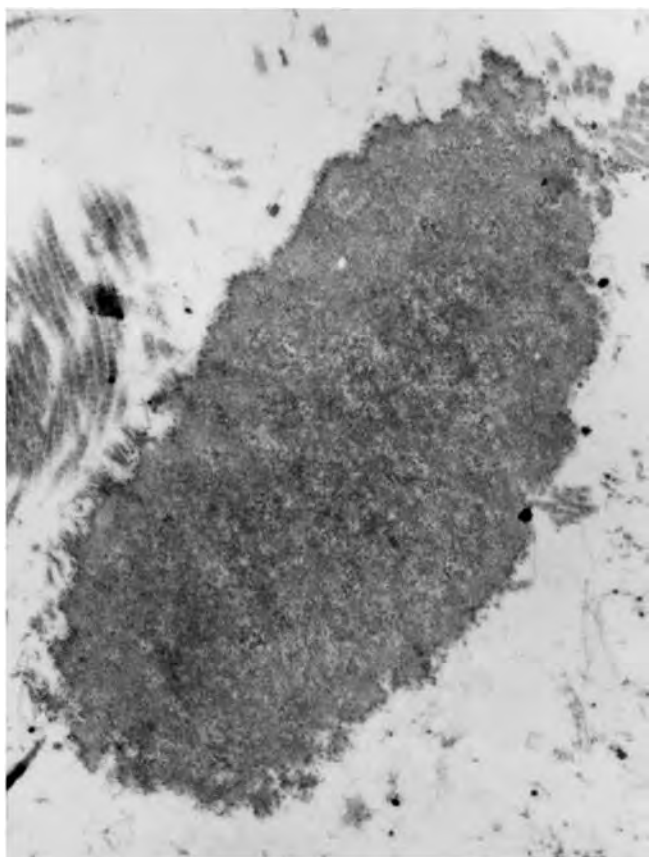


Fig. 18. Senile pattern in a intensively sun-exposed area [8]. Degenerated broad elastic fibre in the reticular dermis. Elastic matrix is grainy without internal stripes. The matrix surface is covered by dense coat and shows no microfibrils. The elastic fibre could be stained by acid-orcein. This type of elastic fibre seems to correspond with elacin fibre of optical microscopy. $\times 5,000$.

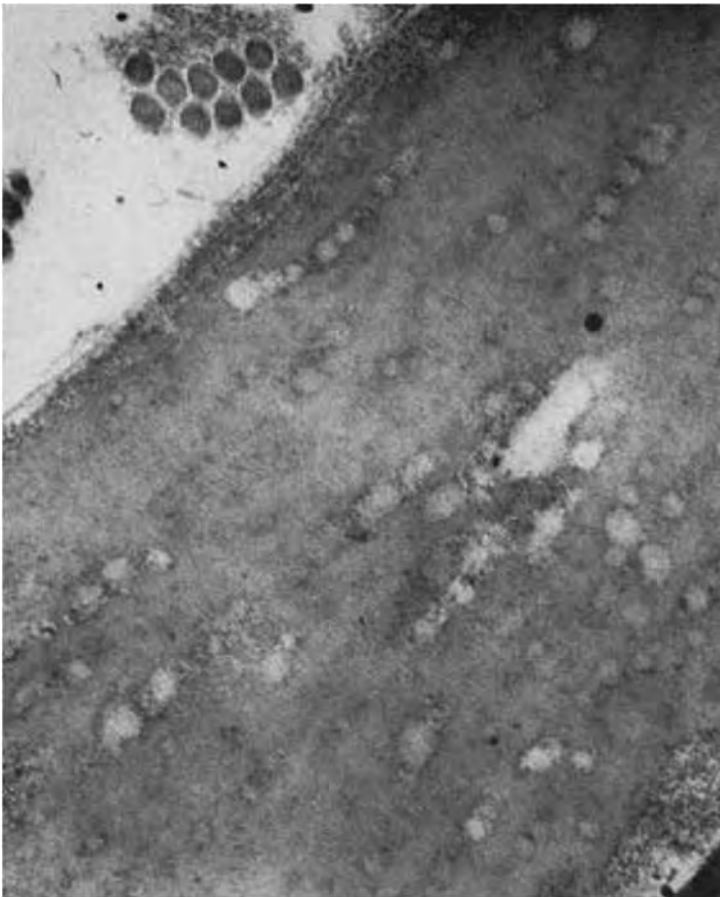


Fig. 19. Senile pattern. Broad elastic fibre in armpit of an 80-year-old man [8]. Small round holes in the internal stripes of matrix. Thin matrix coat and no microfibrils on the matrix surface. $\times 20,000$.

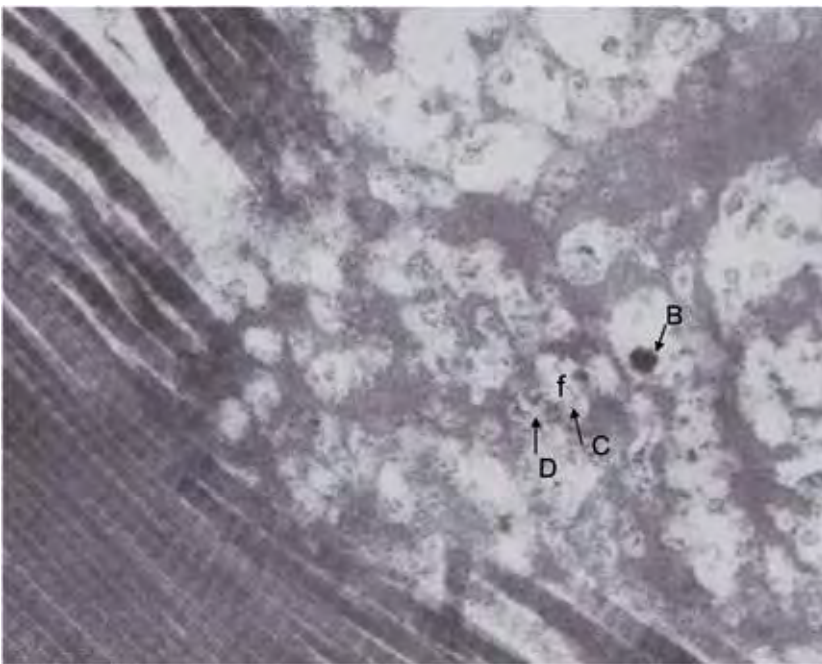


Fig. 20. Severely sun-exposed area. Broad elastic fibre on the back of the neck in an 84-year-old person [8]. Severe vacuole formation and disintegration of the fibre. Calcium spot (arrow B) and round phospholipids (arrows C and D). Details are shown in Figs 21, 22. $\times 10,000$.

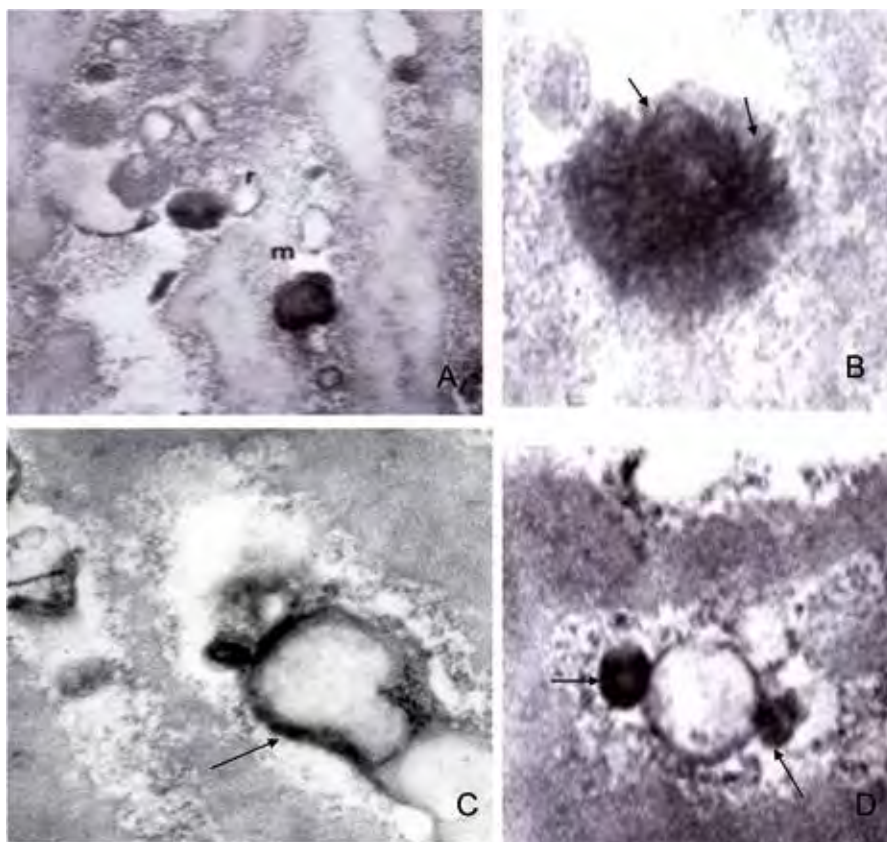


Fig. 21. Details of Fig. 20. Round particles seen in the spaces of broad elastic fibre. A: Holes and dense spots. $\times 20,000$. B: Dense spot with needle-form crystal of Calcium apatite (arrows). $\times 40,000$. C, D: Spots showing myelin-figure in the periphery (arrows), suggesting phospholipids content. $\times 40,000$.

Calcification [8,10]

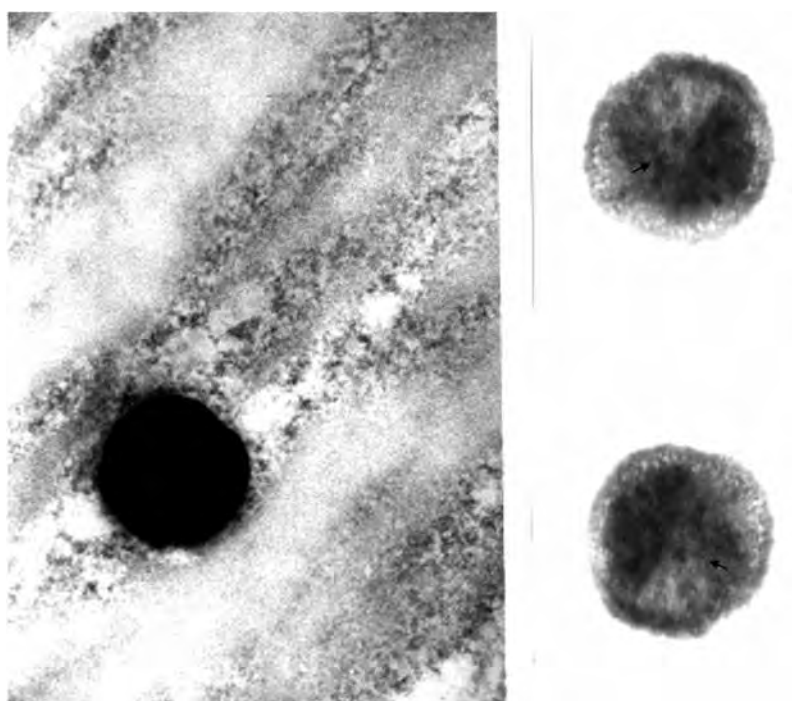


Fig. 22. Calcification in normal elastic fibre. Round spot are usual figure of calcification in normal elastic fibre in adult and senile patterns. Dense round spot of calcium. Usually found in the dilated space of the internal stripes of matrix. The dense spots shows needle-form crystals of calcium apatite. (Arrows points at examples of the crystal). $\times 40,000$.

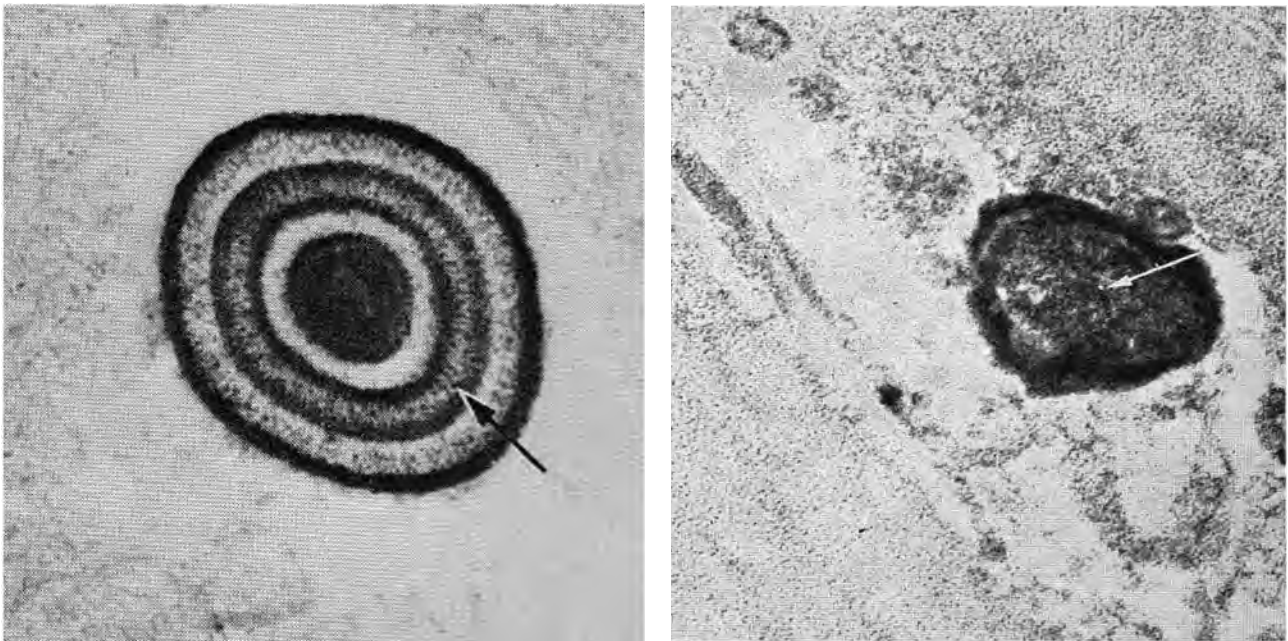


Fig. 23. A) Calcium spot in a nodule of cutaneous amyloidosis [11]. Calcium precipitant is seen annular in some layers. Arrow indicates needle-like crystal of calcium apatite. $\times 20,000$. B) Gastric artery of a 40-year-old healthy man, no sign for pseudoxanthoma elasticum [10]. Elastic fibres show age-dependent change. Arrow points at calcium apatite crystals of needle-form in radial array. The finding indicates calcification in age change. $\times 20,000$.

Disorders

Pseudoxanthoma elasticum [9]



Fig. 24. Pseudoxanthoma elasticum [16]. Elastic fibres in the reticular dermis are irregular in shape and show bizarre-shaped heavy precipitants of calcium in the matrix. $\times 2,000$.

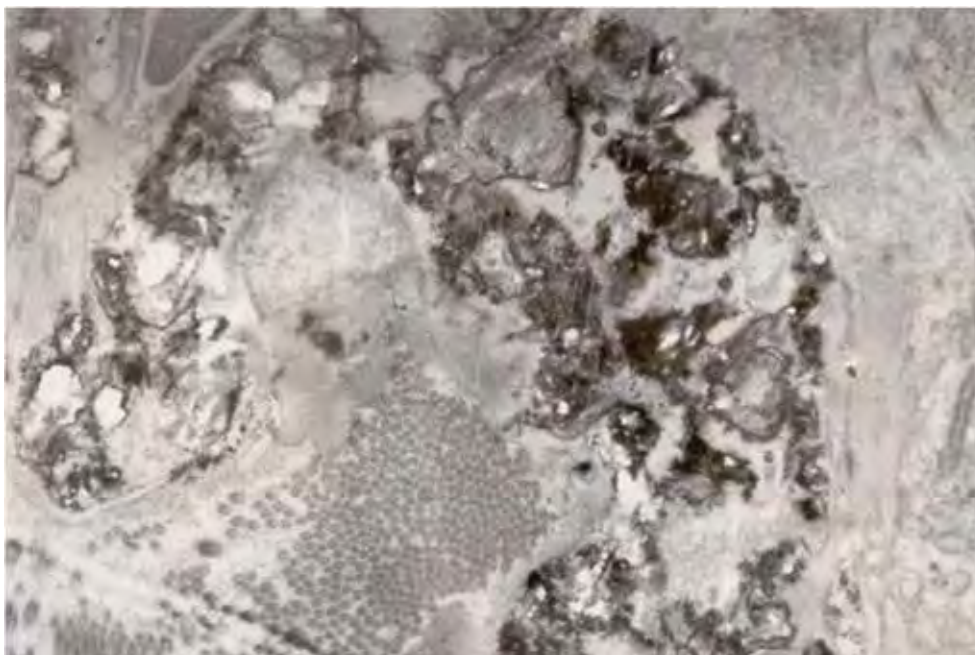


Fig. 25. Pseudoxanthoma elasticum. A larger magnification of Fig. 24. A broad elastic fibre presents bizarre shaped calcification in the matrix. Matrix around calcified area shows homogenous without internal stripes and microfibrils on the matrix surface. $\times 5,000$.

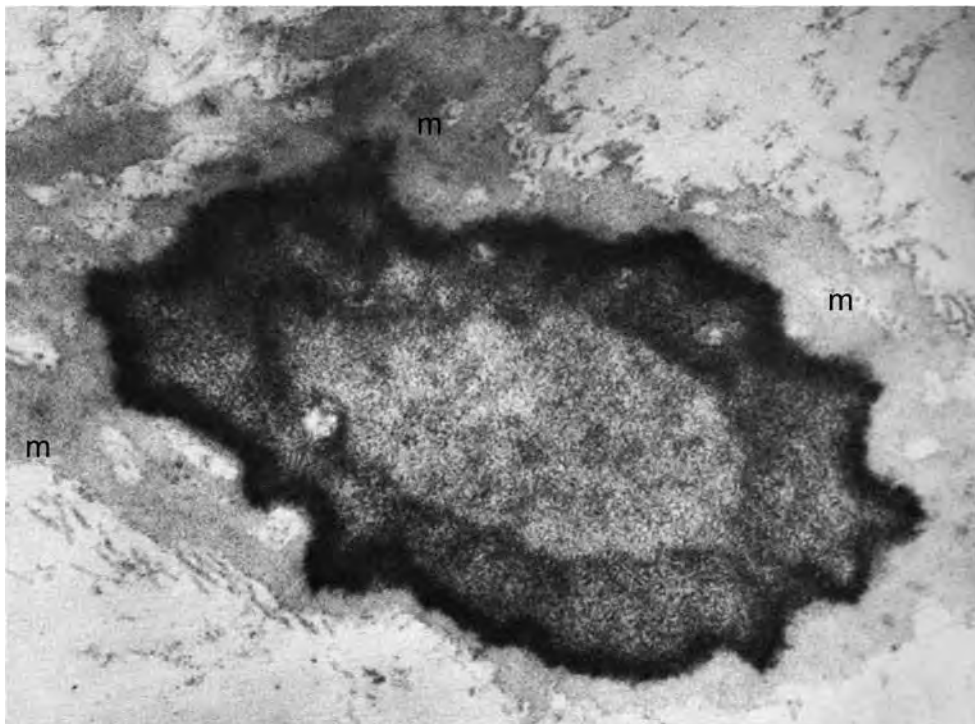


Fig. 26. Pseudoxanthoma elasticum. An annular shaped calcification in the matrix. Calcium precipitant presents bizarre annular form with needle-like crystals inside the matrix. Matrix (m) is lucent homogenous without dense stripes. Microfibrils are scarce on the matrix surface. $\times 50,000$.

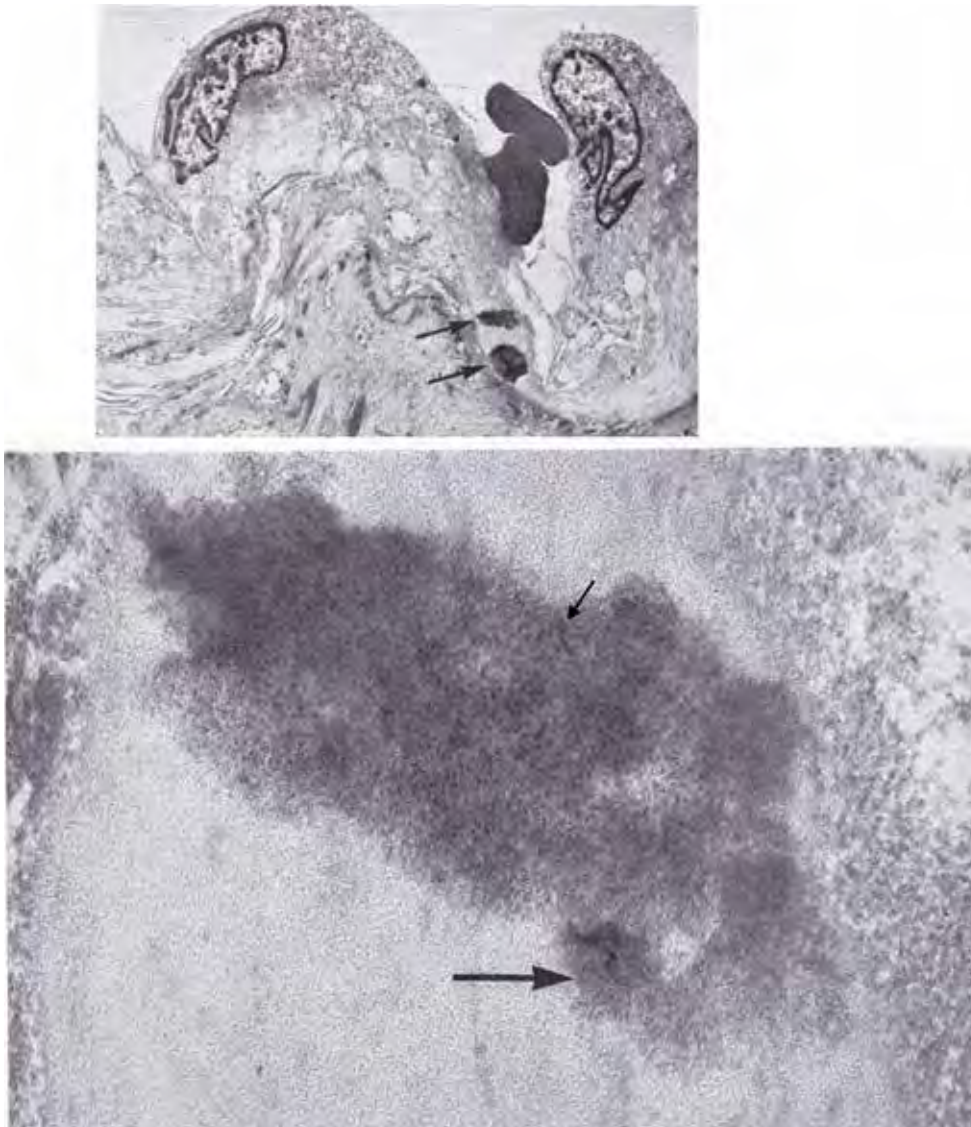


Fig. 27. Internal elastic lamina of gastric artery in a 31-year-old patient of pseudoxanthoma elasticum [10]. Upper picture: Survey of vascular wall. Arrows show calcification in optical microscopy. The upper arrow-pointed spot appears in the lower picture. Lower picture: One of the calcification in the upper figure. Granules and thin needles (thin and thick arrows) of calcium apatite are identified in the dense spot. $\times 80,000$.

Salpeter-induced calcinosis

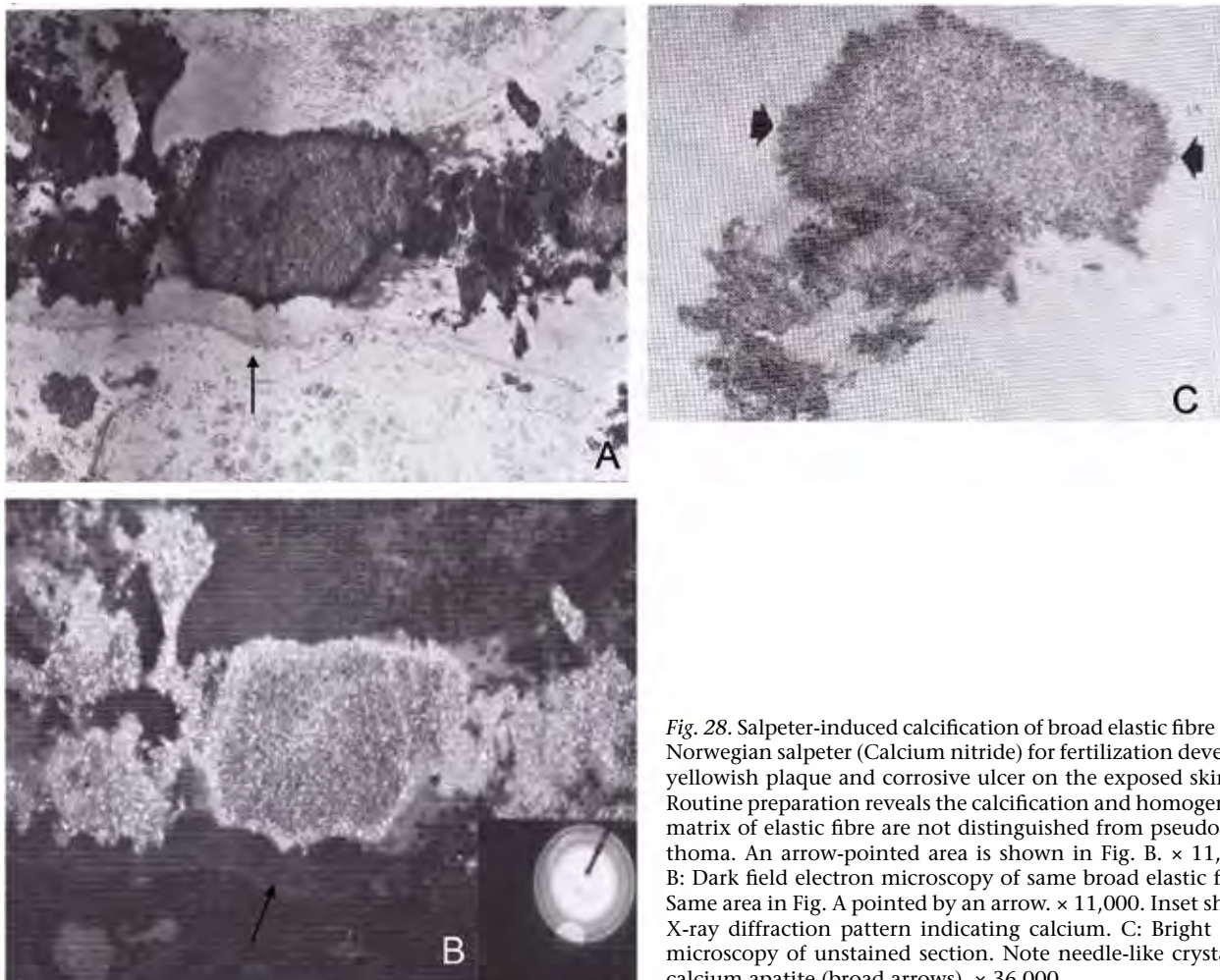


Fig. 28. Salpeter-induced calcification of broad elastic fibre [12]. Norwegian salpeter (Calcium nitride) for fertilization develops yellowish plaque and corrosive ulcer on the exposed skin. A: Routine preparation reveals the calcification and homogenous matrix of elastic fibre are not distinguished from pseudoxanthoma. An arrow-pointed area is shown in Fig. B. $\times 11,000$. B: Dark field electron microscopy of same broad elastic fibre. Same area in Fig. A pointed by an arrow. $\times 11,000$. Inset shows X-ray diffraction pattern indicating calcium. C: Bright field microscopy of unstained section. Note needle-like crystal of calcium apatite (broad arrows). $\times 36,000$.

Calcinosis cutis

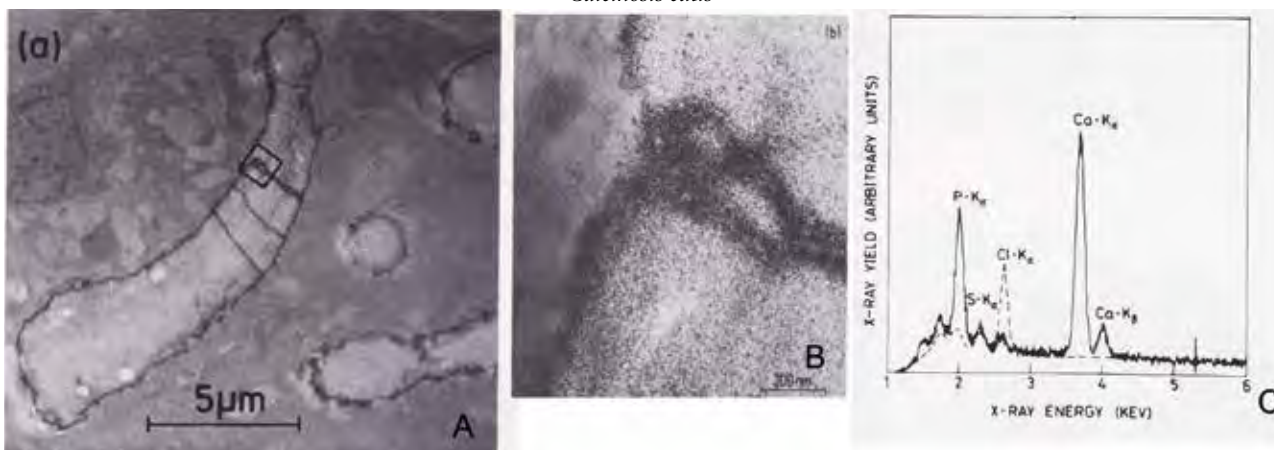


Fig. 29. Universal calcinosis of dermatomyositis [13]. A: Calcium phosphate is precipitated and deposited on the surface of broad elastic fibre. Fig. B shows the square in Fig. A. Fig. C: X-ray fluorescence spectrum. Solid line shows calcified elastic fibre. Broken line is from dermal collagen fibre.

Amyloidosis

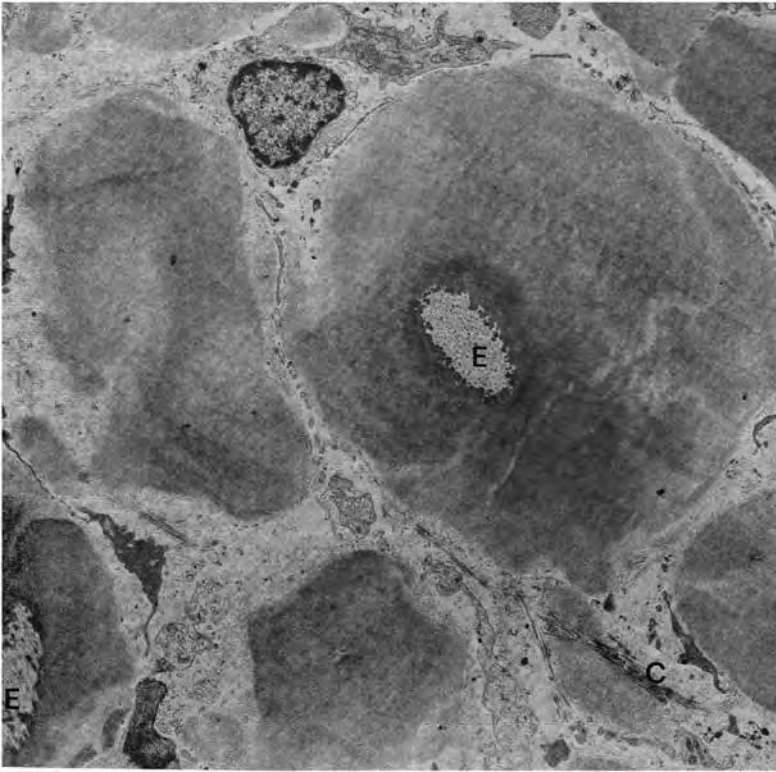


Fig. 30. Systemic amyloidosis [11, 14]. Large amyloid masses in reticular dermis show elastic fibre (E) in the middle of the amyloid mass. Collagen fibrils (C). $\times 4,000$.

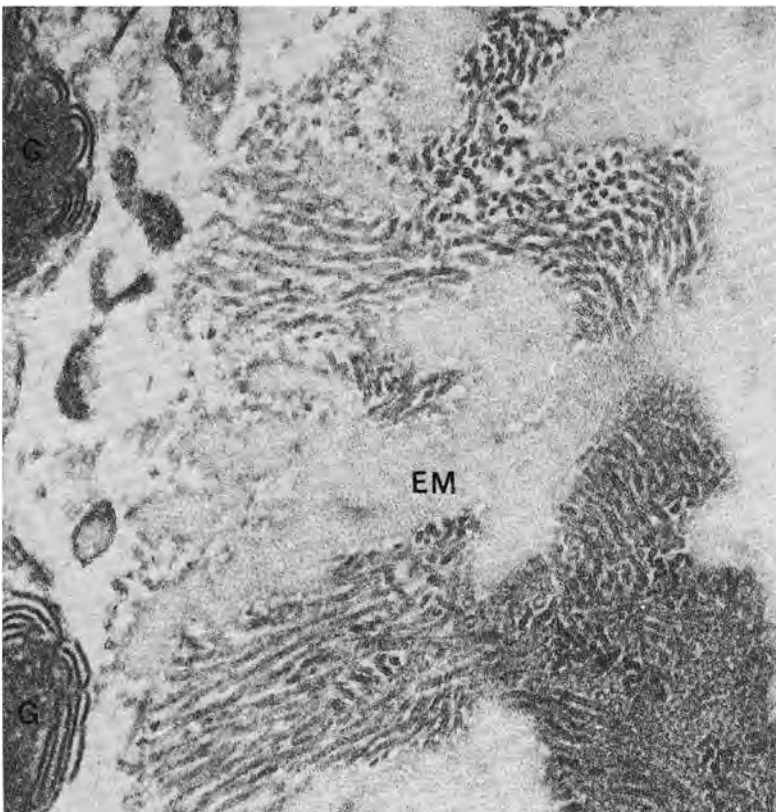


Fig. 31. Systemic amyloidosis [11, 14]. Elastic fibre and amyloid fibrils. Elastic matrix is invaginated on the surface (EM). Mass of amyloid fibrils are on the surface. Amyloid fibrils seem to grow from elastic matrix. Amyloid fibrils are wavy on the matrix surface and straight in the periphery. $\times 28,000$.

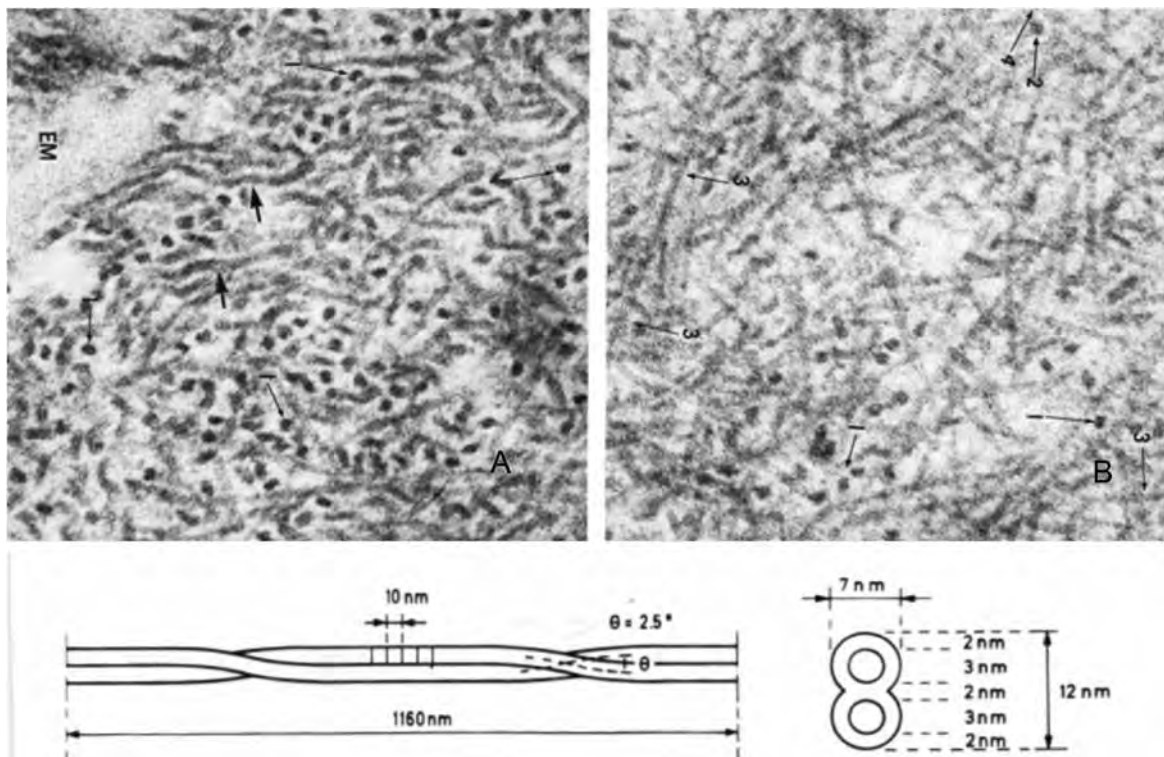


Fig. 32. Amyloid fibrils and the schematic explanation [14]. Picture to the left shows amyloid fibrils in wavy form close to the elastic matrix (EM). Picture to the right shows straight form in the middle of the mass. An amyloid fibril is a twin fibril. Drawing shows the structure of an amyloid fibrils. $\times 45,000$.

Pretibial myxoedema [15]

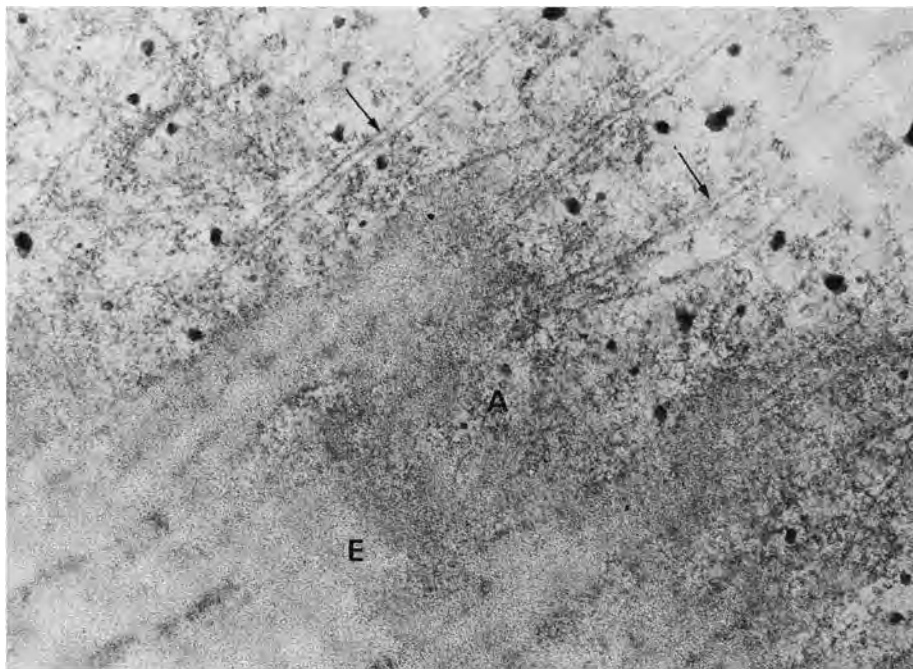


Fig. 33. Localized myxoedema [15]. Broad elastic fibre in reticular dermis in a 31-year-old women. Elastic fibre degenerates on the matrix surface and is covered by granular material, dense thin coat and straight elastic microfibrils (arrows). Dense spots are glycosaminoglycans. E: Elastic matrix. A: Surface coat. $\times 20,000$.

Necrobiosis lipoidica diabetorum [16]



Fig. 34. *Necrobiosis lipoidica* [16]. Broad elastic fibre in the reticular dermis. Elastic matrix (E) is disintegrated and shows granular material. Dense spots are glycosaminoglycans. Microfibrils are disappeared and internal stripes are grainy. Collagen fibrils (C). $\times 20,000$.

Morphoea

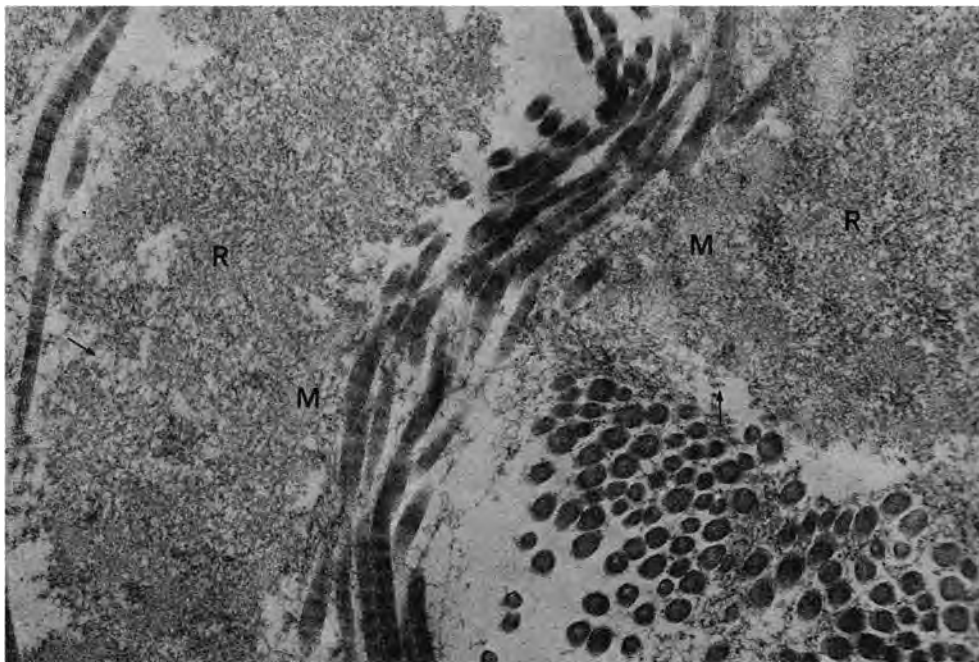


Fig. 35. *Morphoea* [17]. Matrix is reticular and grainy (R). No microfibrils are seen. M: Rest of matrix. $\times 20,000$.

Acrosclerotic scleroderma

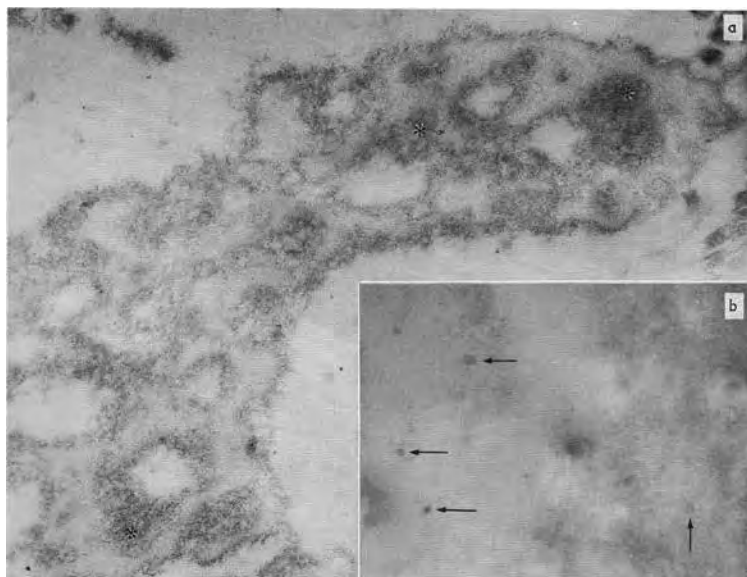


Fig. 36. Acrosclerotic scleroderma [18]. Elastic fibre shows holes and uneven surface of the matrix. No elastic microfibrils are found. Fig. a shows elastic fibre after periodic acid-silver proteinate stain. Elastic matrix is covered by neutral proteoglycans. Fig. b shows elastic fibre after Ruthenium red stain and demonstrates positive spots (Glycosaminoglycans) in the surface coat of the matrix (arrows) (Fig. b). × 20,000.

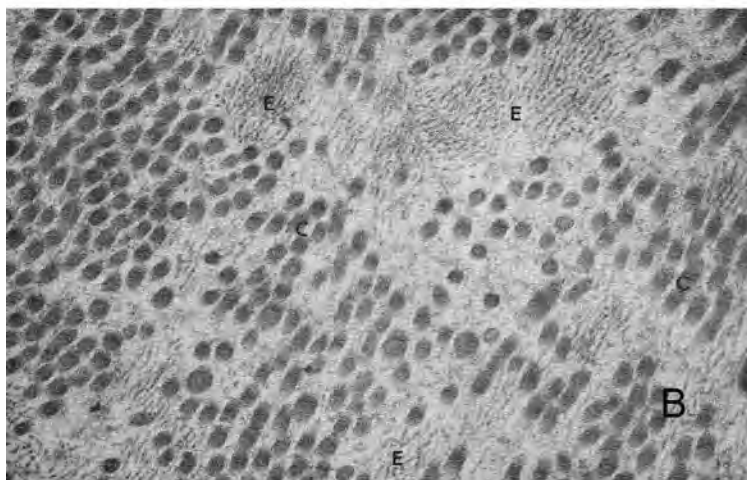
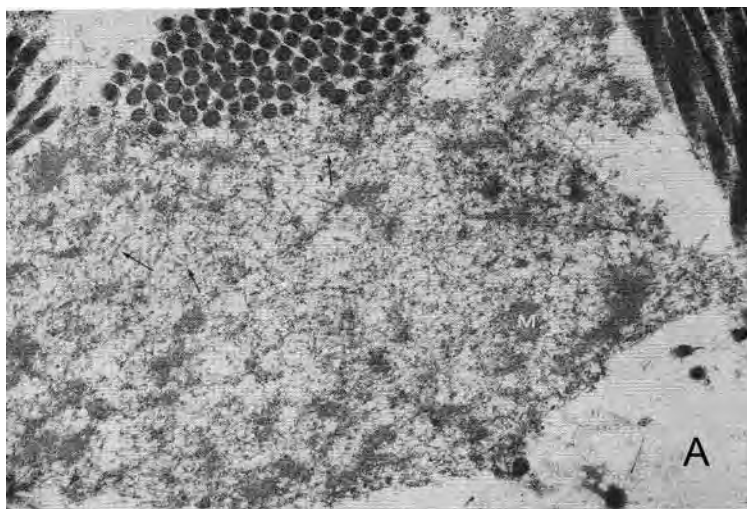


Fig. 37. Acrosclerotic scleroderma [18], continued. Fig. A: Broad elastic fibre in reticular dermis. Broad elastic fibre appears as fine net-works of threads and pieces of homogenous matrix (M). Arrows point at indistinct microfibrils. The figure represents degraded elastic fibre in scleroderma lesion. × 15,000. Fig. B: Sclerosing area in reticular dermis. Numerous microfibrils in bundle (E). Intermingling with thin collagen fibrils (C). Elastic microfibrils and collagen fibrils are probably formed. × 15,000.

Lupus erythematosus

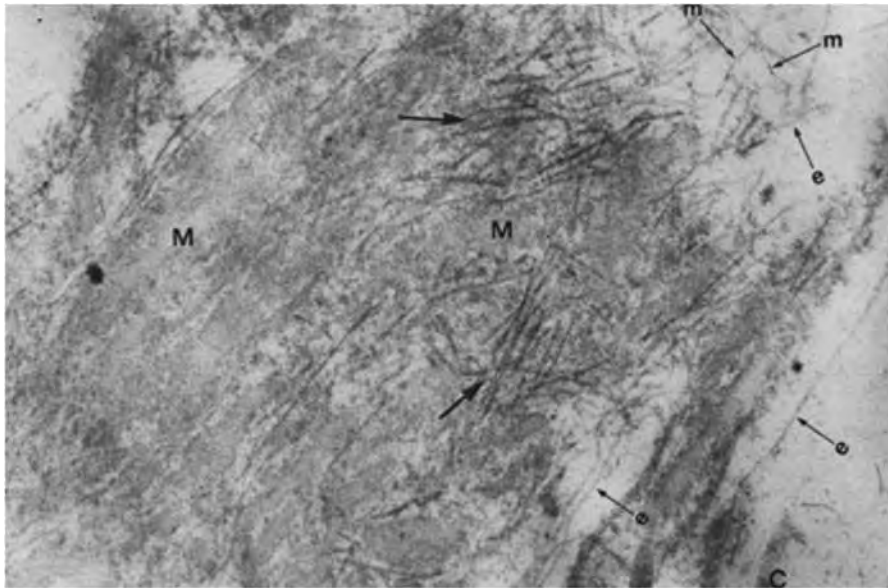


Fig. 38. Needle-form elastic microfibrils in lupus erythematosus [19]. Needle-form microfibrils are also found in the eruptions of morphea and the other autoimmune disorders. M: Elastic fibre matrix. Thick arrows: Needle-form elastic microfibrils. e: Normal elastic microfibrils. m: Glycosaminoglycan-figure. $\times 20,000$.

Inheritance-dependent disorders

Disseminated connective tissue nevi

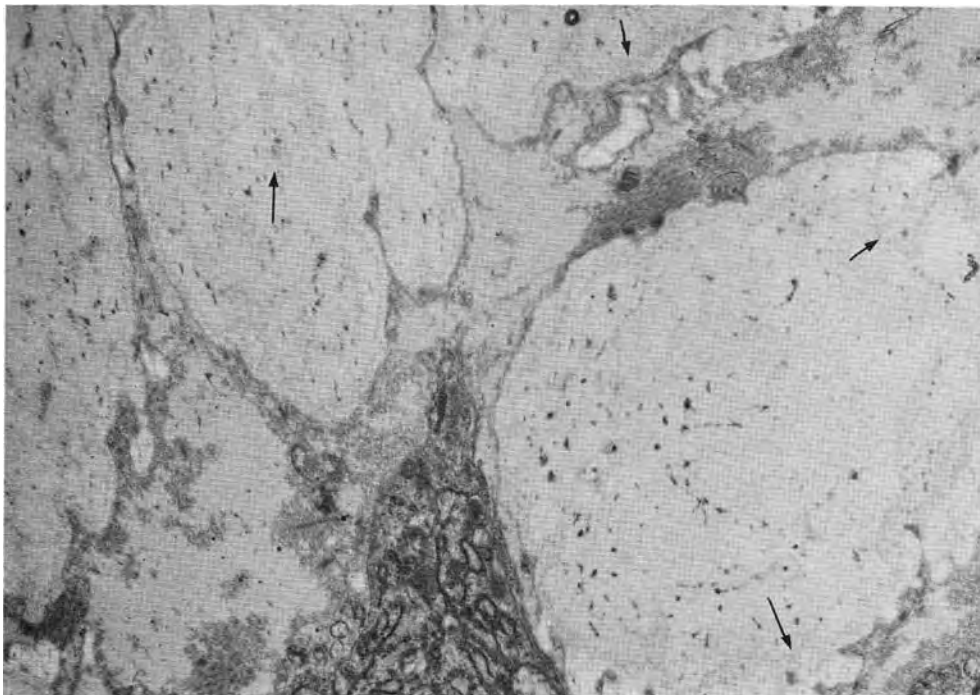


Fig. 39. Disseminated connective tissue nevi [20]. Broad elastic fibres from right forearm. Broad elastic fibres are large homogeneous with dots and thin stripes (Arrows). No clear figures of the internal stripes. Microfibrils are not seen on the matrix surface. $\times 4,000$.

Juvenile elastoma [21]

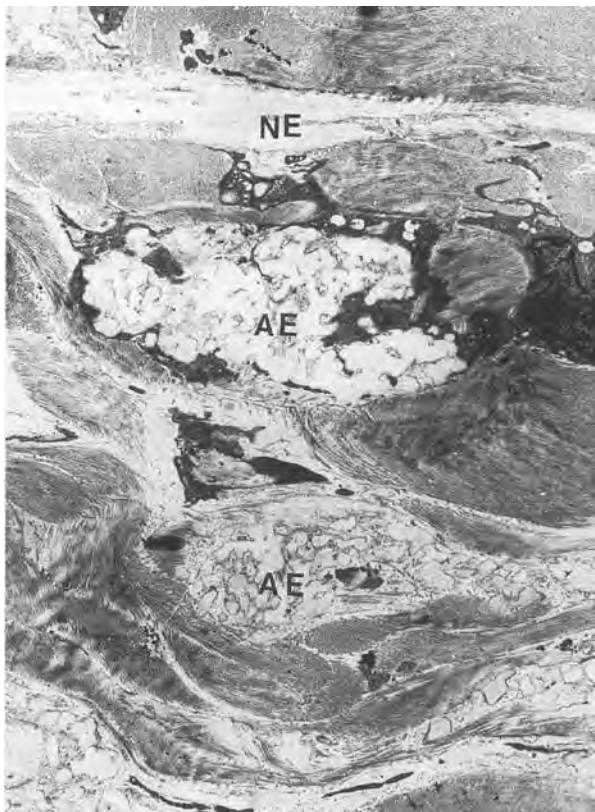


Fig. 40. Juvenile elastoma [14]. Altered broad elastic fibres show lucent homogeneous matrix (AE) lay side by side with normal broad elastic fibres (NE). Collagen fibrils in bundles are seen unchanged. $\times 2,600$. Details appear in the next slides. The ultrastructure of elastic system fibre in Disseminated connective tissue naevi, Juvenile elastoma and Osteogenesis imperfecta Type I presents similar ultrastructural changes.

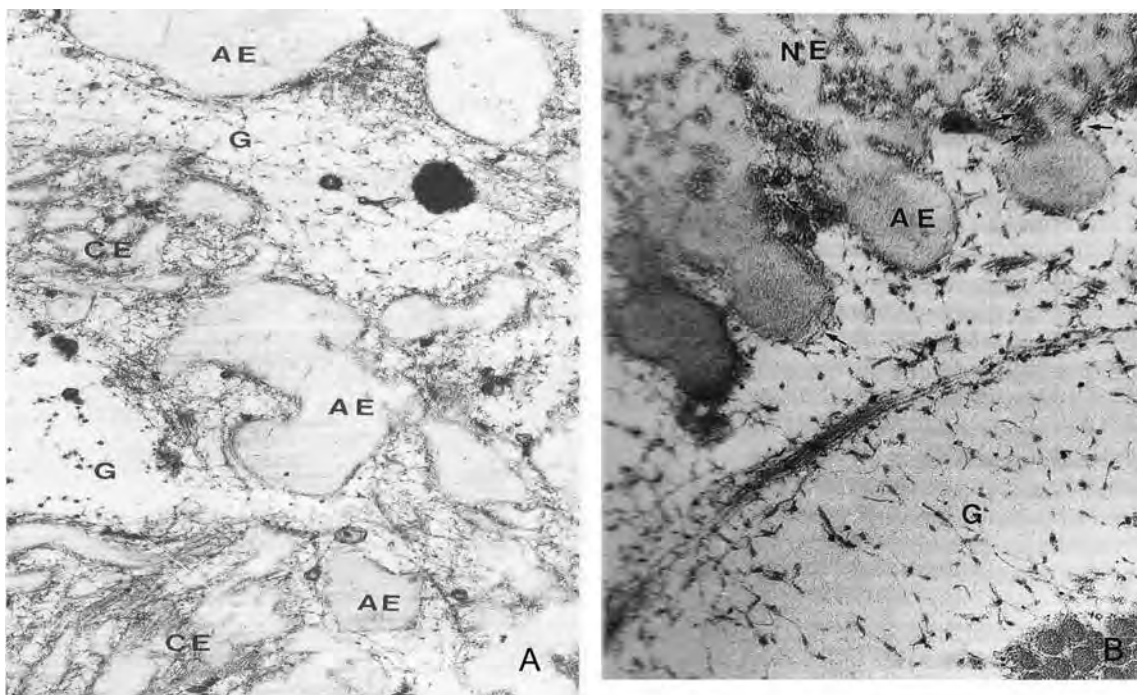


Fig. 41. Details of broad elastic fibres of juvenile elastoma. A) Broad elastic fibres with lucent matrix without microfibrils (AE). Glycosaminoglycan figures in the interfibrillar space. B) Round protrudes of lucent homogeneous matrix (AE) from normal elastic fibre. Left: $\times 5,000$. Right: $\times 10,000$.

Inherited hypermobile disorders

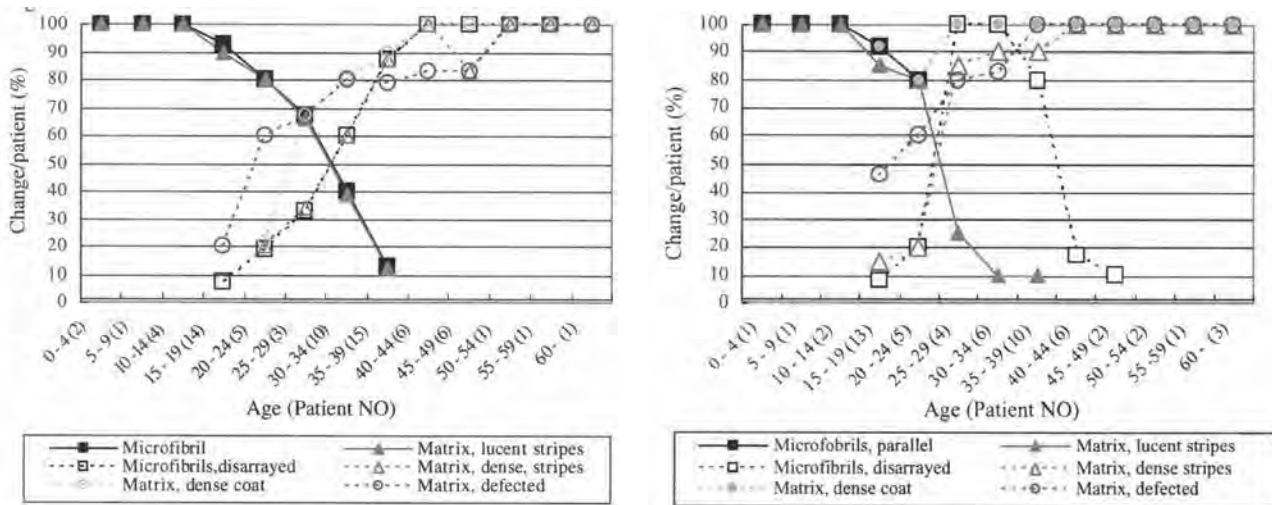


Fig. 42. Degeneration of dermal elastic fibres in Ehlers-Danlos syndrome and Hypermobile syndrome [5]. Ultrastructural changes of 4 age-patterns are the same as those found in normal elastic fibre. A value over 70% is taken for positive finding. Infantile pattern seems to move adolescent pattern in age-period of 25–29 year in reticular dermis and 20–24 year-period in papillary dermis. Degeneration of elastic fibre seem to begin to appear at 15–19 year-period in both dermis and increase over 70% of elastic fibre at 25–29 year-period in reticular dermis and 20–24 year-period in papillary dermis. Degenerate elastic fibres higher than 80% are found in 35–39 year-period in reticular dermis and 25–30 year period in papillary dermis. Senile pattern probably begins in 50–54 age-pattern in reticular dermis and 40–44 year-period in papillary dermis. Transforming age between adolescent and adult pattern is unclear. Degeneration of elastic fibre begins a year-period (5 years) earlier in papillary dermis. It seems that patients with Ehlers-Danlos syndrome and Hypermobile syndrome start aging of elastic fibre a year-period (5 years) earlier than normal (Fig. 10). Sol-exposure stimulates degeneration of elastic fibre, probably a year-period (5 years) earlier in papillary dermis than normal.

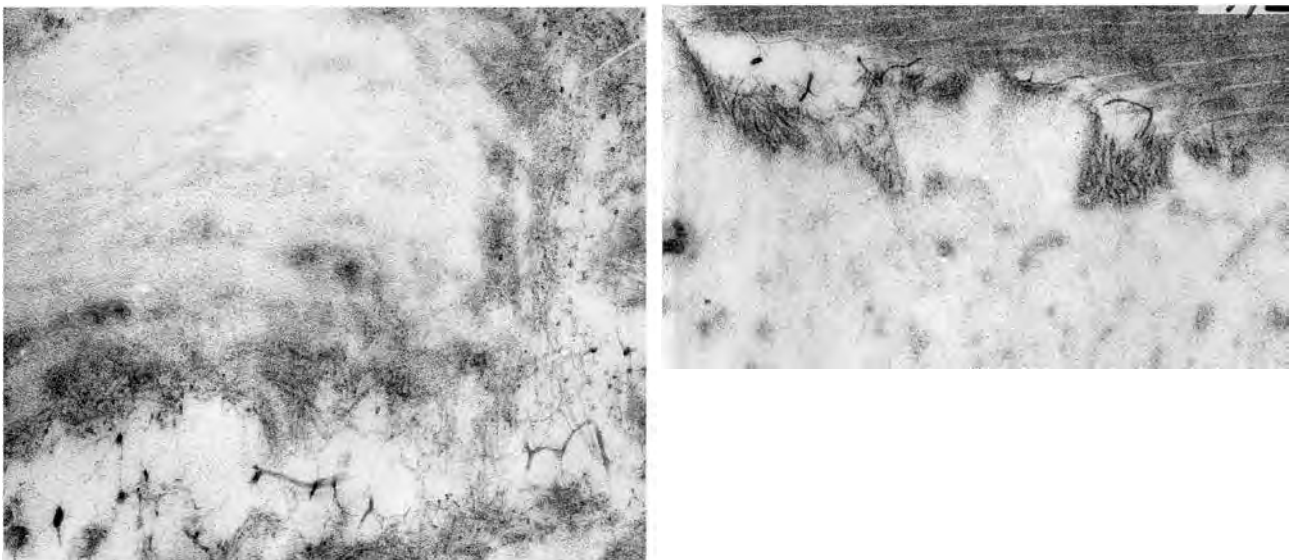


Fig. 43. Marfan syndrome [5]. Left: Infantile pattern. 18-year-old female. Broad elastic fibre in the papillary dermis of elbow [5]. Numerous distinct microfibrils, thick surface coat and glycosaminoglycan-figures on the matrix surface. Internal stripes of matrix are indistinct. Broad elastic fibres in the reticular dermis show identical ultrastructure. $\times 40,000$. Right: Adolescence pattern in a 33-year-old woman. Broad elastic fibre in reticular dermis shows distinct microfibrils in indentations and thick surface coat on the matrix. Internal stripes are blurry. Glycosaminoglycan figure in the vicinity of the matrix. $\times 40,000$.

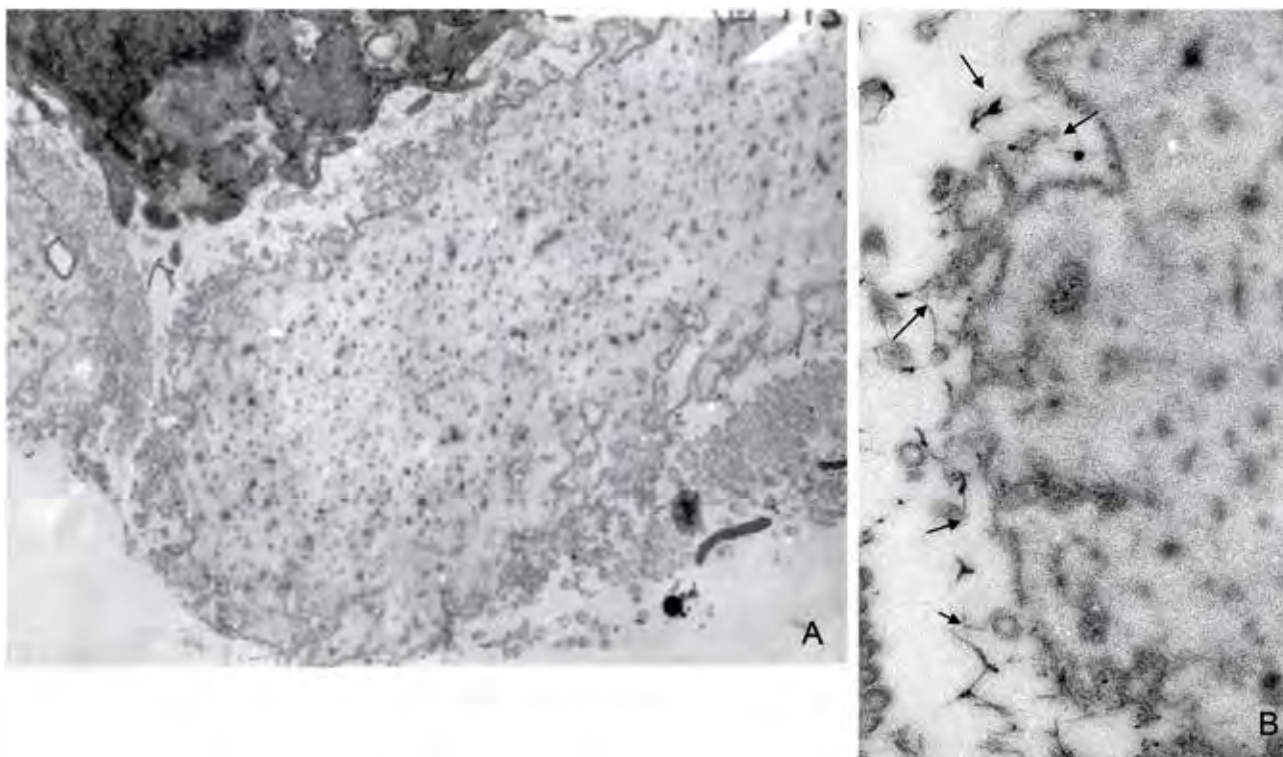


Fig. 44. Marfan syndrome. Adult pattern [5]. Broad elastic fibre in the reticular dermis of elbow in a 35-year-old woman. Fig. A shows numerous indentations like moth-eaten figure on the matrix surface. Dense surface coat of the matrix without microfibrils, dense spot-like internal stripes. $\times 5,000$. Fig. B shows details. Arrows point at glycosaminoglycan figures close to thick surface coat of the indented matrix. No microfibrils are found. $\times 40,000$.

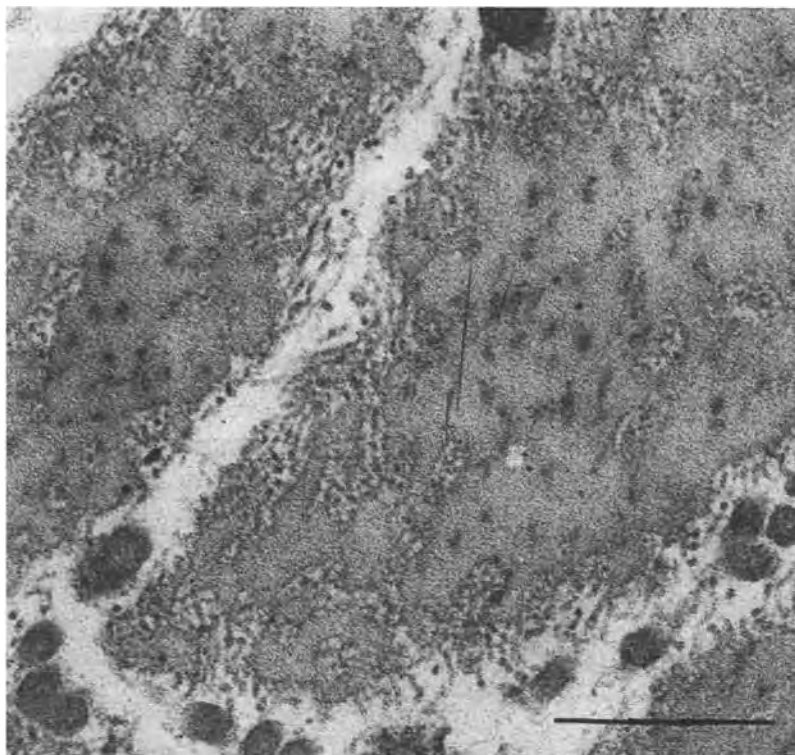


Fig. 45. Osteogenesis imperfecta, Type I. Infantile pattern [5]. Broad elastic fibre in the reticular dermis in a 4-year-old girl. Broad elastic fibre shows numerous wavy microfibrils on the irregular surface of matrix, while no surface coat of matrix is seen. Internal stripes are spot-form and dense. Papillary dermis of this patient shows identical ultrastructure. $\times 20,000$. Scale indicates $0.5 \mu\text{m}$.

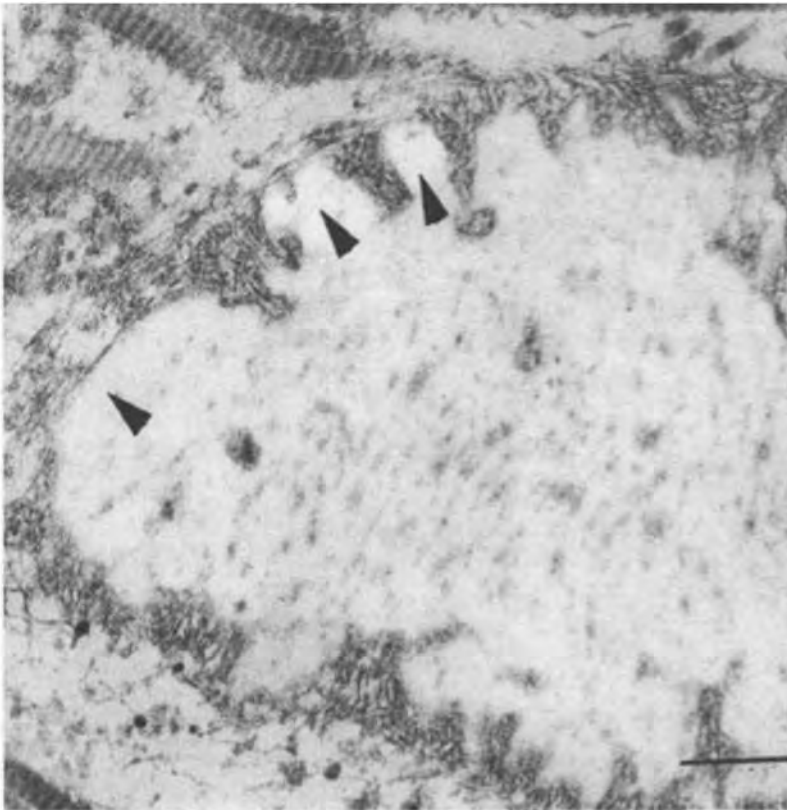


Fig. 46. Osteogenesis imperfecta, Type I. Adolescent pattern [5]. Broad elastic fibre of the reticular dermis of elbow in a 26-year-old woman. Broad elastic fibre shows indentations with microfibrils on the matrix surface. Matrix surface is not covered by microfibrils and internal stripes are thin and indistinct. Periphery of the matrix shows round lucent areas, supposedly bulges in an early phase of protrudes (arrow-heads). Glycosaminoglycan figures are seen in the interfibrous space. Similar ultrastructure is seen in the papillary dermis. $\times 10,000$. Scale indicates 0.5 μm .

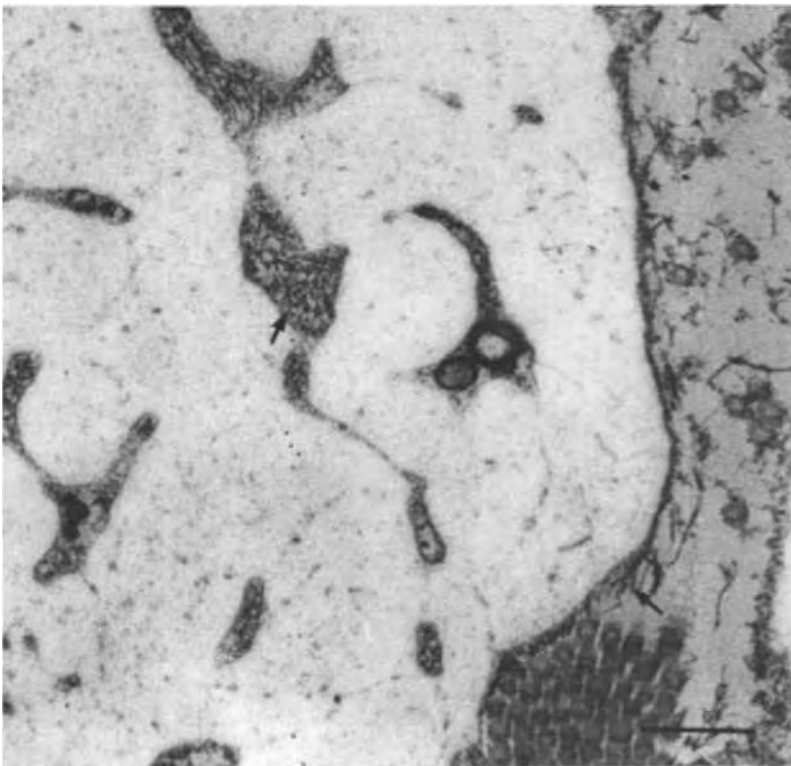


Fig. 47. Osteogenesis imperfecta. Type I. Adult pattern [5]. Broad elastic fibre in the reticular dermis of elbow in a 37-year-old woman. The matrix shows large round bulges with thin indistinct internal stripes. The matrix surface is covered by dense coat and scarce microfibrils (arrows). $\times 20,000$. Scale indicates 0.5 μm .

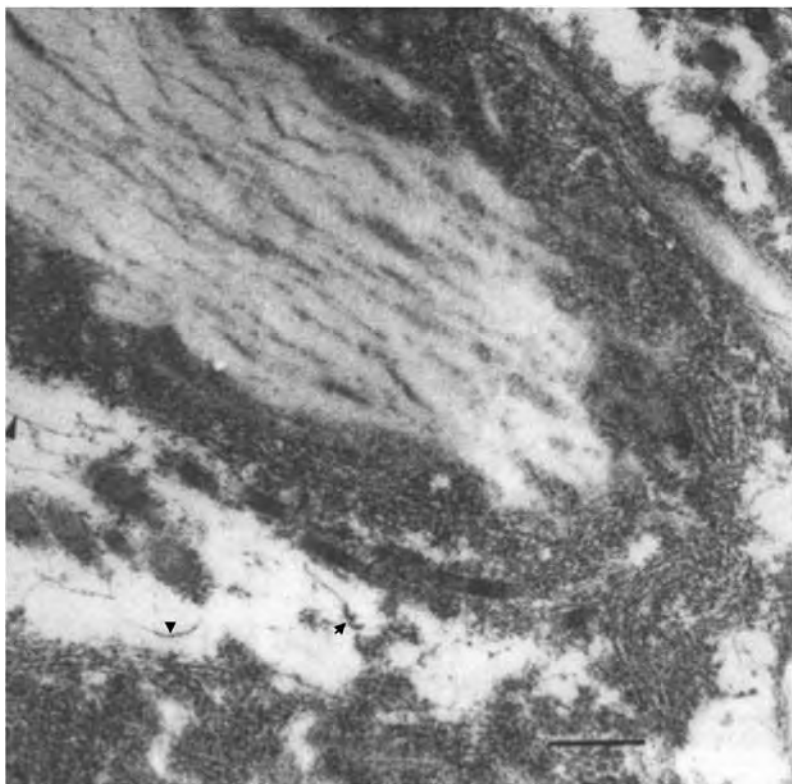


Fig. 48. Homocysteinuria. Infantile pattern [5]. Broad elastic fibre of the papillary dermis in the elbow of a 15-year-old female. Broad elastic fibre shows matrix with dense internal stripes and the matrix surface is covered by a thick layer of numerous microfibrils. Glycosaminoglycan figures are in the vicinity of the fibre (arrow-heads). $\times 20,000$. Scale indicates $0.5 \mu\text{m}$.

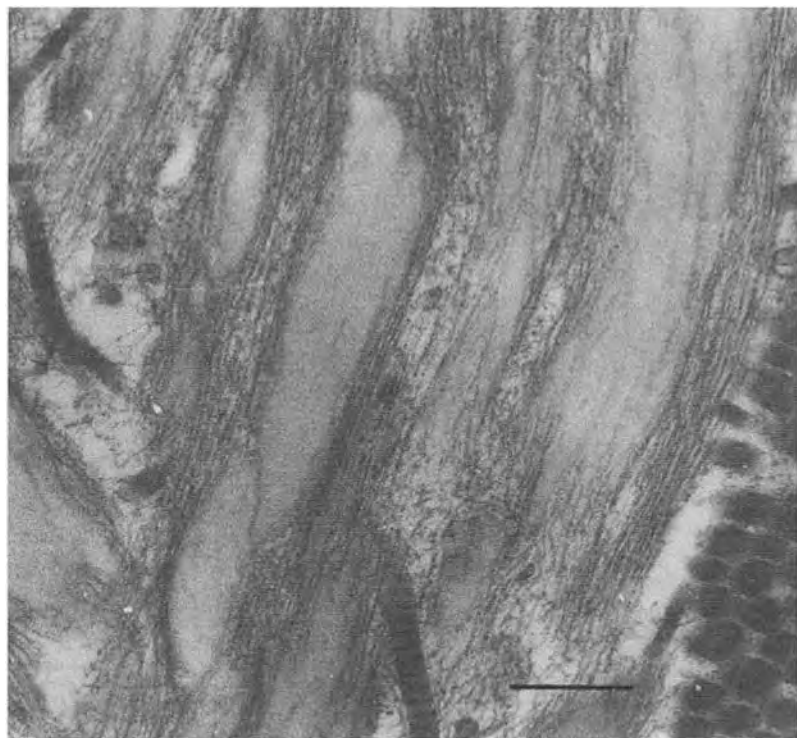


Fig. 49. Homocysteinuria. Infantile pattern [5]. Broad elastic fibre in the reticular dermis in a 15-year-old female. The fibre shows lucent matrix with indistinct internal stripes. The matrix is covered by numerous straight microfibrils in a parallel array. $\times 20,000$. Scale indicates $0.5 \mu\text{m}$.

II. Collagen fibrils

Overview	
• Ultrastructure	Figures 1–3
• Collagen types in normal dermis	Figures 4–11
• Calcification	Figure 12
• Luse body	Figure 13
• Degradation	
- Twisting	Figures 14–15
- Degradation by collagenolytic factors	Figures 16–17
- Collagen aggregate	
» Experiments	Figures 18–20
» Disorders, instances	Figures 21–26
• Dermatoses	
- Diabetes	Figure 27
- Papular mucinosis	Figure 28
- Necrobiosis lipoidica	Figure 29
- Spontaneous keloid	Figure 30
- Morphoea	Figures 31–33
- Acrosclerotic scleroderma	Figures 34–37
- Atrophoderma Passini	Figures 38–39
- Linear atrophy	Figures 40–41
• Inherited dermatoses	
- Ehlers-Danlos syndrome	
» Relation of hypermobility to thicknesses of collagen fibrils and ratio of collagen type I/III	Figure 42
» Collagen fibrils in EDS type II	Figures 43–45A
» EDS type III	Figure 45B
» EDS type VI	Figure 46
» EDS type VIII	Figure 47
- Marfan syndrome	Figure 48
- Osteogenesis imperfecta, Type I	Figure 49
- Pseudoxanthoma elasticum	Figures 50–52
- Shagreen patch	Figure 53
- Disseminated connective tissue nevi	Figure 54
- Systemic amyloidosis	Figure 55
- Cutis gyrate	Figure 56
- Angiofibroma, Burneville-Pringle	Figure 57

Ultrastructure

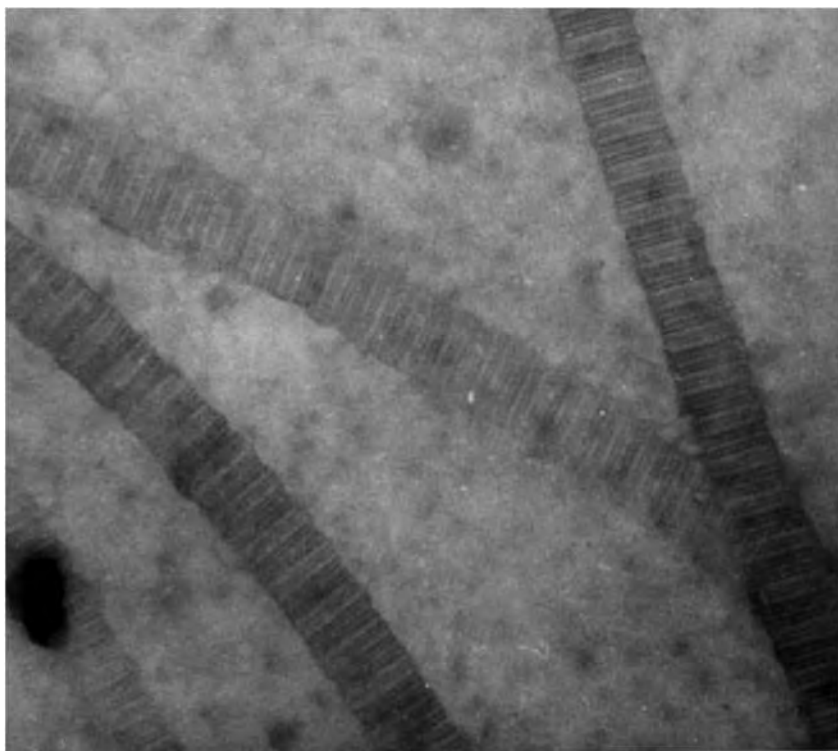


Fig. 1. Collagen fibrils of normal human skin. Collagen fibrils are straight non-branched fibrils. A collagen fibril is around 60 nm in thickness with cross-bands. Axial periodicity of 60 nm, by which collagen fibrils can be identified in dermis. Cross-bands are stained by periodic acid-silver proteinate (Thierry) or periodic acid-reduced silver. Thickness is varied among body areas as shown in Fig. 2. Fig. 1. shows unfixed collagen fibrils isolated from human dermis, and stained by phosphotungstic acid. $\times 20,000$.

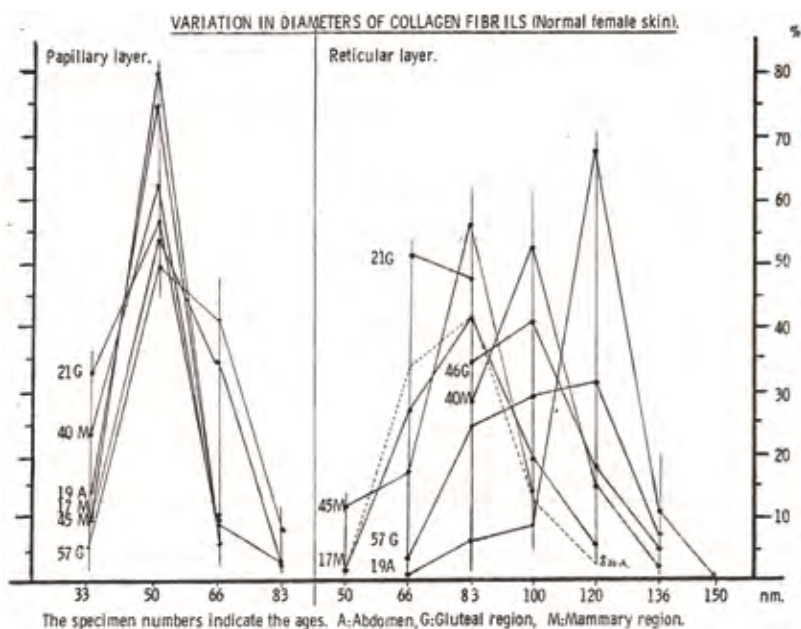


Fig. 2. Distribution of thicknesses of dermal collagen fibrils in some body areas. A: Abdomen, G: Gluteal region, M: Mammary region. Numbers indicate ages. Papillary dermis show monomodal distribution in a range of 33–80 nm with a sharp spike at 50 nm. Reticular dermis shows monomodal distribution in a range of 20–150 nm with a slow and sharp spikes. [Unpublished]

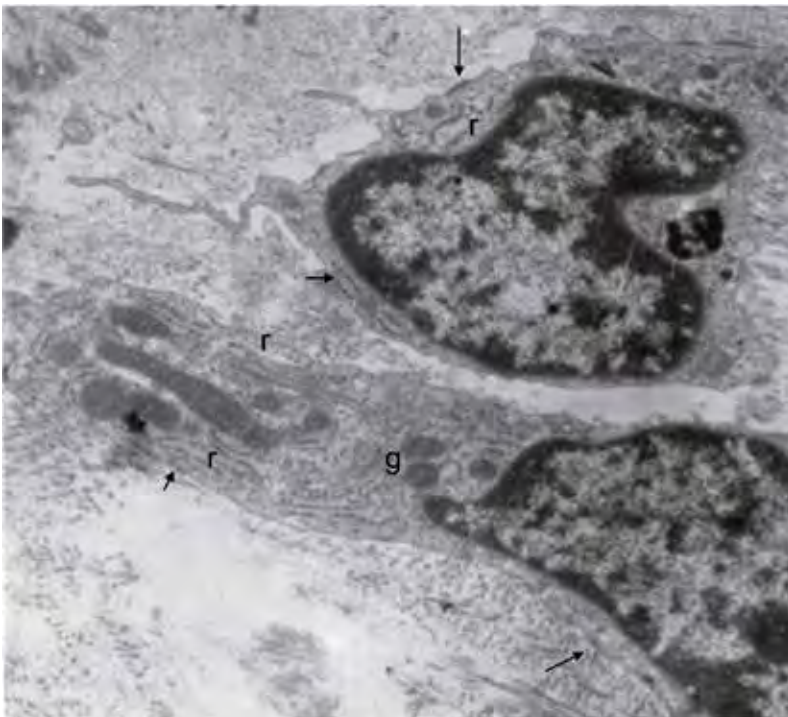


Fig. 3. Fibroblasts synthesize and secrete collagen by ribosomes of granular endoplasmic reticulum (r). Collagen is transported through the cisterna of the reticulum and secrets in the extracellular space. Collagen aggregates and form collagen fibrils in the extracellular space, close to the cell surface (arrows). Collagen fibrils thicker than 10 nm shows characteristic axial periodicity. The fibrils can be identified as collagen fibrils. Turn-over rate is said to be around 5 years for collagen fibrils in normal dermis. G: Golgi apparatus. $\times 5,000$. [Unpublished]

Types I, III, V, VI collagen in normal dermis

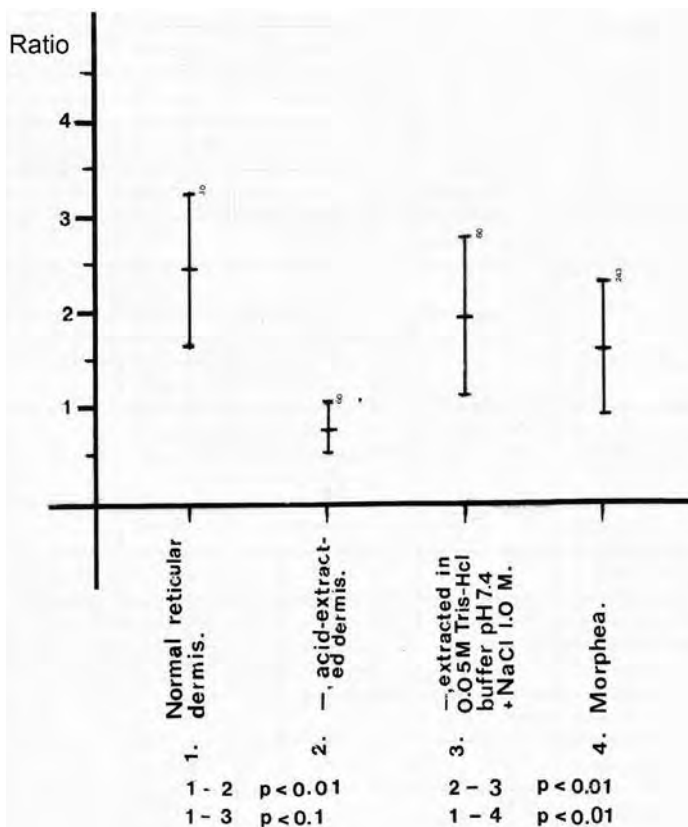


Fig. 4. Collagen fibrils in dermis composed of type I and type III collagen. Ratio of type I and III (I/III) is different among collagen fibril thickness, thinner fibrils in low I/III seen in the perivascular area and thick fibrils are high I/III in reticular dermis. The table shows the column of reticular dermis shows high ratio of I/III. Collagen is extracted by acid but mild by Tris buffer pH 7.4. Morphea shows lower ratio than normal. [Unpublished]

Collagen types in dermis

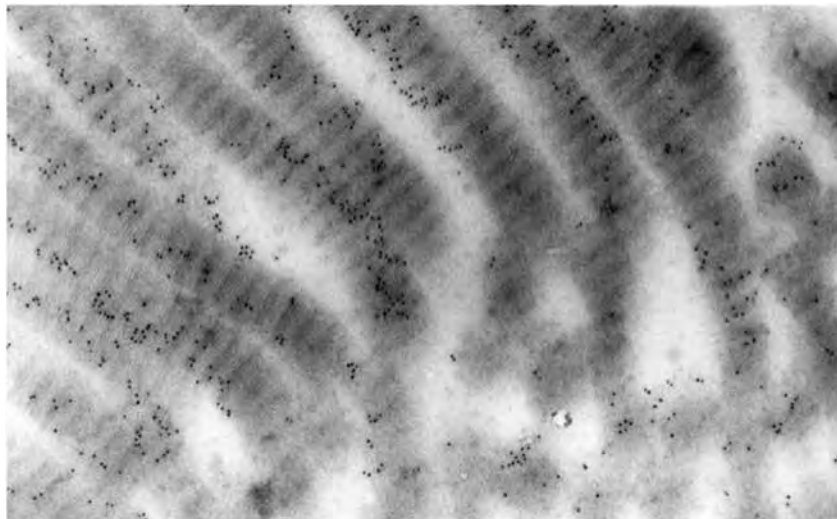


Fig. 5. Collagen type V in collagen fibrils in reticular dermis of normal human. Collagen type V is located on the cross bands of the fibrils [1]. $\times 20,000$. Techniques for the embedding and staining appear in Appendix.

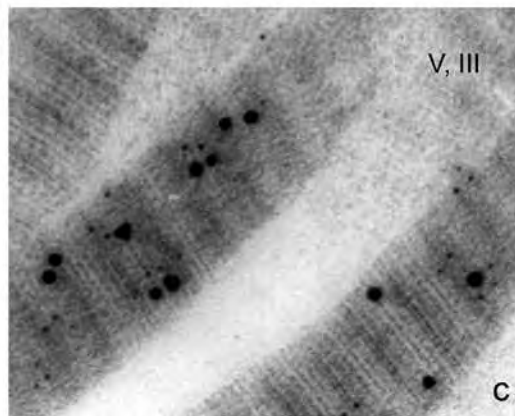
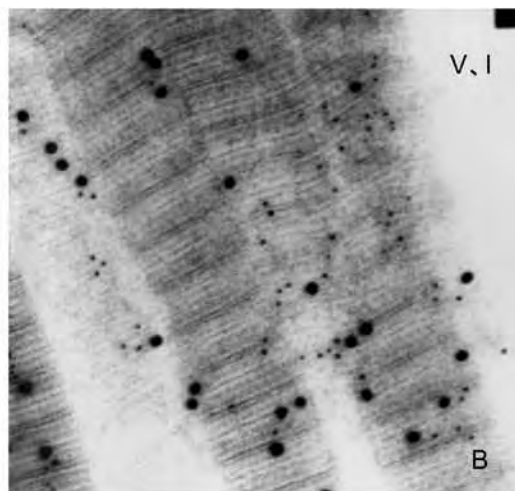
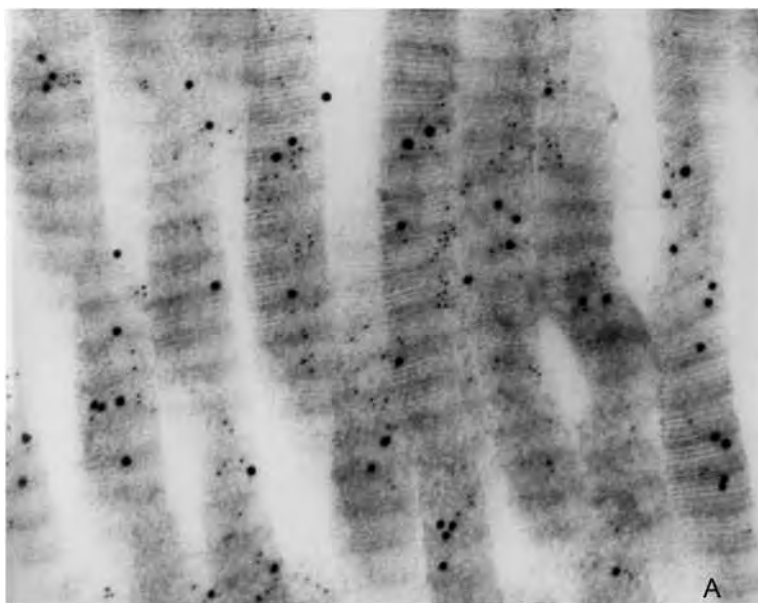


Fig. 6. Collagen molecules types V, I and type III are construct collagen fibrils [1]. These collagen molecules are demonstrated by immune electron microscopy. Gold particles for both types appear on the cross bands. (The techniques appear in the Appendix.) Left: shows collagen types V and I demonstrated by 5 nm and 10 nm gold particles, respectively. $\times 40,000$. Right: high resolution pictures. Type V collagen by 5 nm and type I (upper) and III (lower) by 10 nm gold particles. $\times 60,000$.

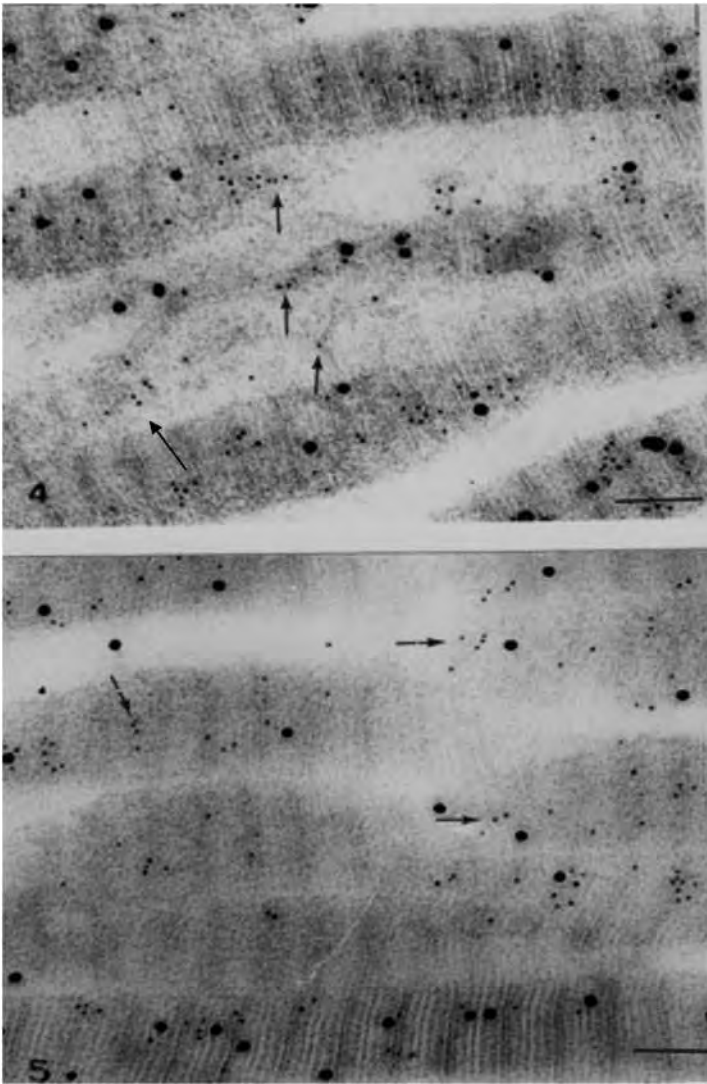


Fig. 7. Collagen fibrils from normal human dermis pretreated by 1 M citrate buffer (pH 3.5). Shown by the same techniques as Fig. 5. Upper picture shows type V collagen by 5 nm gold and type I by 10 nm gold. Lower picture shows type V collagen by 5 nm gold and type III by 10 nm gold. Type I and III collagen are extracted and type V collagen remains in the fibrils. $\times 50,000$. Seemingly, citrate buffer interferes with binding of type V collagen to type I or III and removes types I and III collagen from the collagen fibrils, while type V collagen remains in the fibrils. Type V collagen binds collagen types I and III in the collagen fibrils.

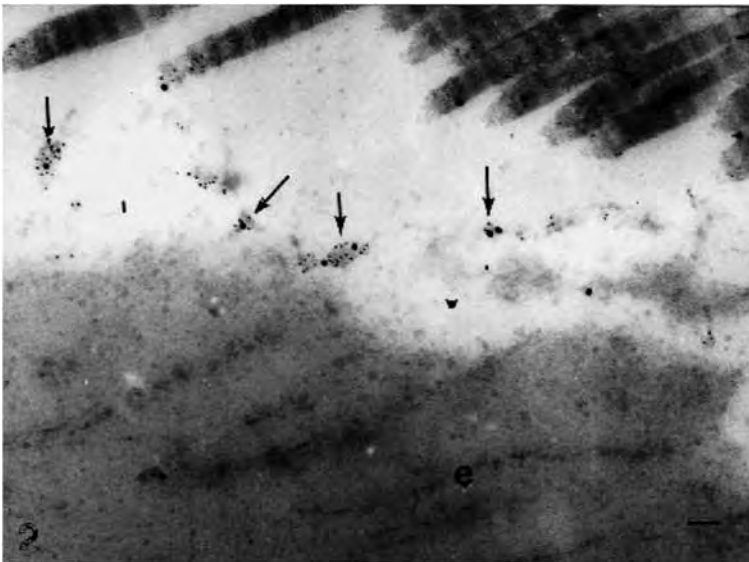


Fig. 8. Collagen types V and VI in the interfibrillar space [1]. Surface and internal stripes of elastic matrix are marked by 5 nm gold (Type V collagen). Type VI collagen (10 nm gold particles). Filaments of glycosaminoglycan figure in the interfibrillar space are marked by 5 and 10 nm gold (arrows). Type VI collagen is core protein of ground substance and form net-works in the stroma. Type VI collagen binds glycosaminoglycan and type V collagen. e: elastic fibre. $\times 33,000$.

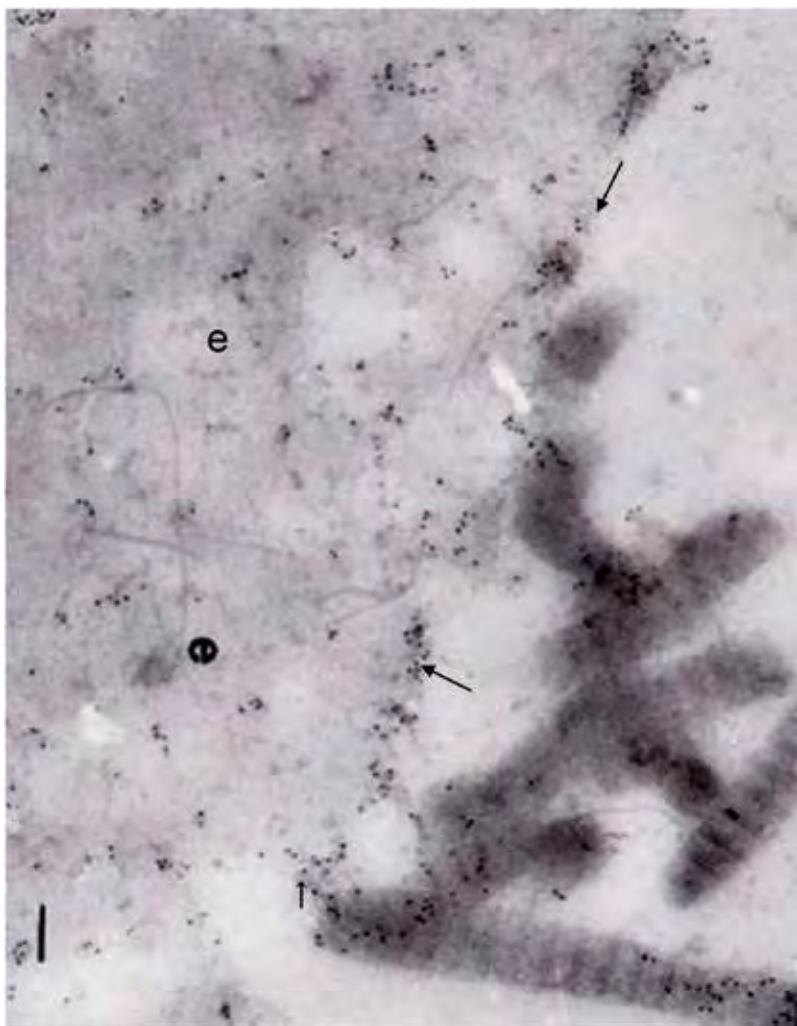


Fig. 9. Type V collagen on the surface of elastic fibre [1]. Normal human dermis, treated in 1M citrate buffer, pH 4. Type V collagen is marked by 5 nm gold particles. (Techniques are described in Appendix). Surface and inside of elastic matrix show type V collagen. e: elastic fibre matrix. Two arrows point at matrix surface. × 20,000.

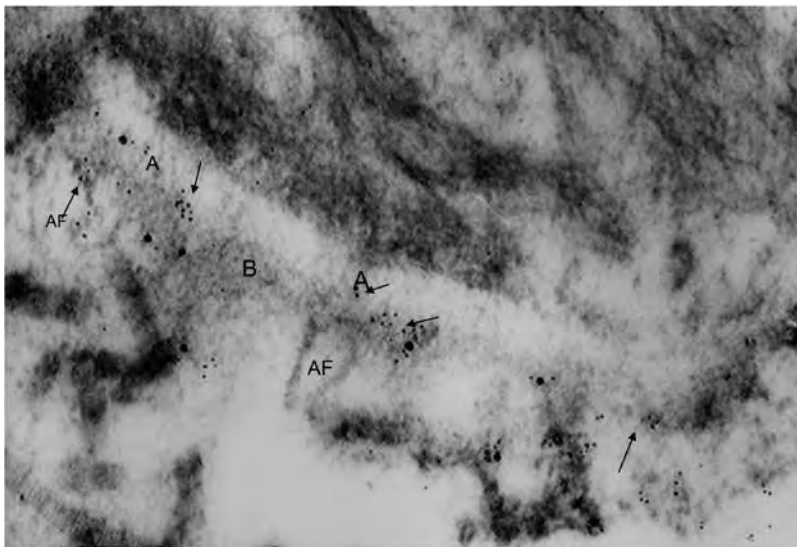


Fig. 10. Types V and VI collagen in dermoepidermal junction (5 nm gold for collagen types V and 10 nm gold for type VI collagen) [1]. Type V collagen (5 nm gold particles) is located on basal lamina, where anchoring filaments and anchoring fibrils (A) join to basal lamina (arrows). Type VI collagen (10 nm gold particles) is on the basal lamina. B: basal lamina, A: anchoring filaments, AF: anchoring fibrils. × 20,000.

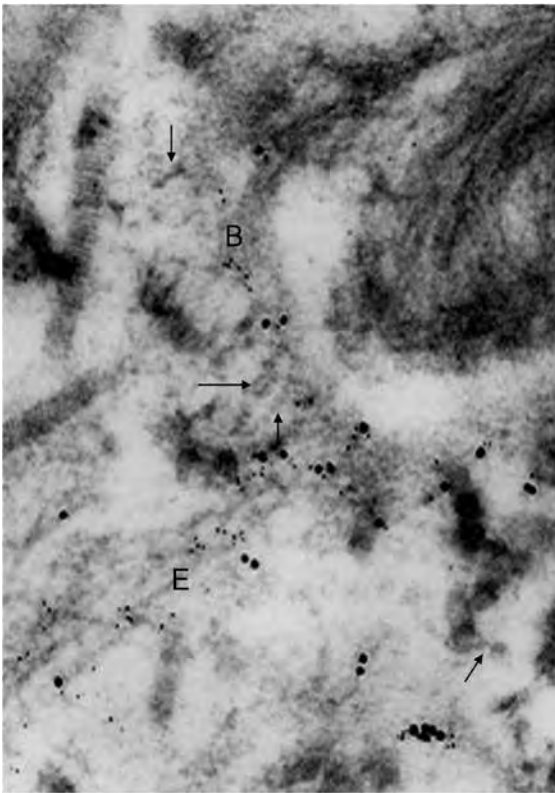


Fig. 11. Dermoepidermal junction. Type V collagen is marked by 5 nm gold and type VI collagen by 10 nm gold. Type V collagen is seen on the elastic microfibrils and the dermal aspect of basal lamina. Type VI collagen is on the basal lamina. E: elastic microfibrils, B: basal lamina, arrows: anchoring fibrils. $\times 33,000$.

Calcification

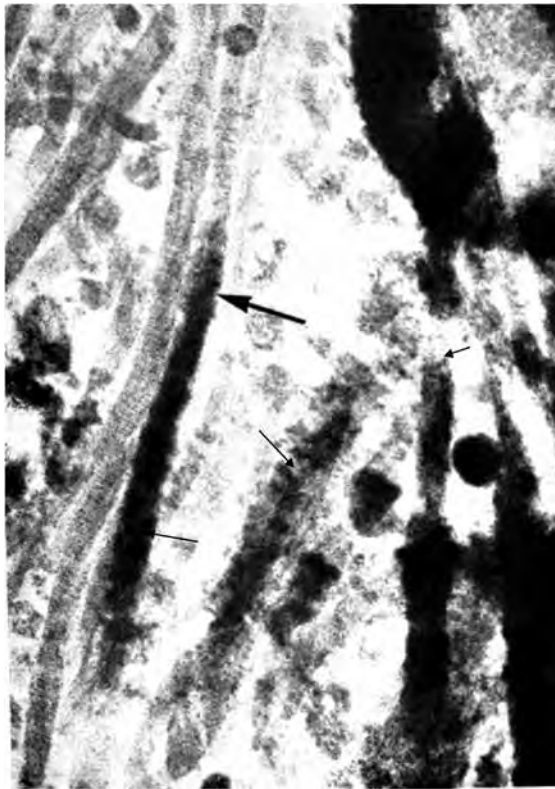


Fig. 12. Calcification of collagen fibrils. Gastric arterial wall of the patient of Pseudoxanthoma Elasticum [4]. Needle form crystals of calcium apatite appear along to procollagen (thick and thin arrows). $\times 20,000$.

Luse body

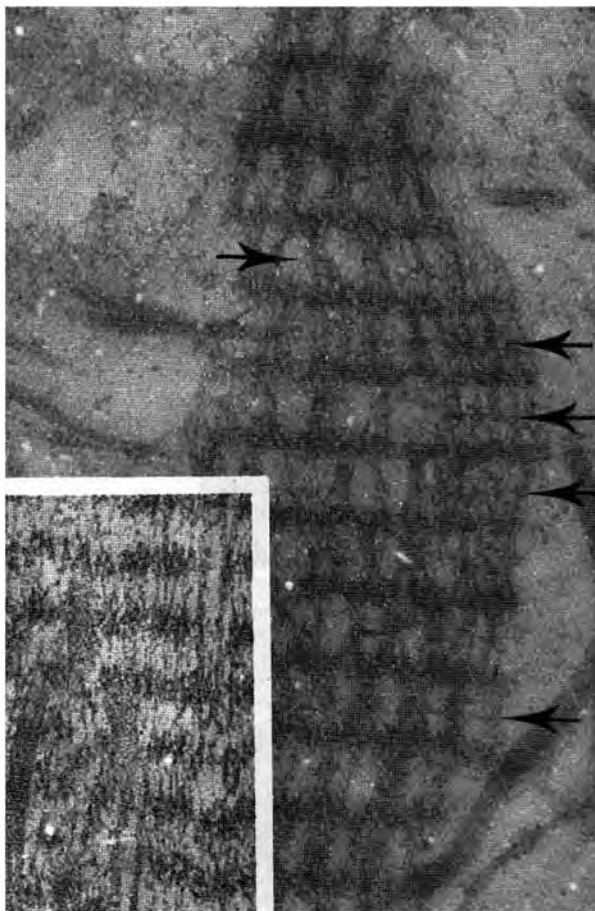


Fig. 13. Luse body [2]. Variants of normal collagen fibrils. Luse body in endoneurium of peripheral nerve in dermis. Inset shows collagen aggregate for comparison. Luse body was first detected in the endoneurium of acustics tumour. The body is a spindle-shaped filament mass with cross bands and small knobs (arrows) [2]. Own experiments show Luse body is collagenous, because of susceptibility for clostridial collagenase but the body is not stained by immunoglobulins to collagen types I, III, V. $\times 60,000$. For comparison, inset presents collagen aggregate in pathological dermis. [Fig. 18]. Structures resemble each other, but collagen aggregate is different on the filamentous structure between cross-bands, i.e. unparallel array of filaments with knobs in Luse body. $\times 60,000$.

Degradation

Twisting, experiments

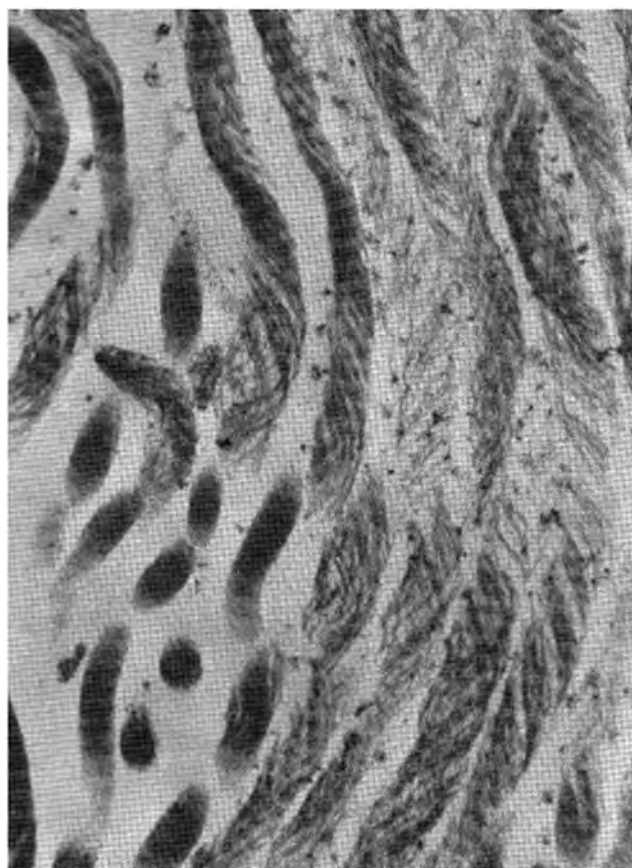


Fig. 14. Twisting of normal collagen fibrils. Longitudinal section. Experimental visualisation of twisting. Collagen fibrils of normal human dermis are incubated in citrate buffer pH 3.1 for 24 hours and prepared for routine electron microscopy [4]. Collagen fibrils are unwound and reveal twisting of procollagen in the fibrils. Angle in twisting is clockwise about 30 degrees. Twisted collagen fibrils are found in the inherited disorders, at about 15 degree of twisted angle. The twisted collagen fibrils in dermis are the sign for inherited malformation of collagen fibril [12, 19]. $\times 40,000$.

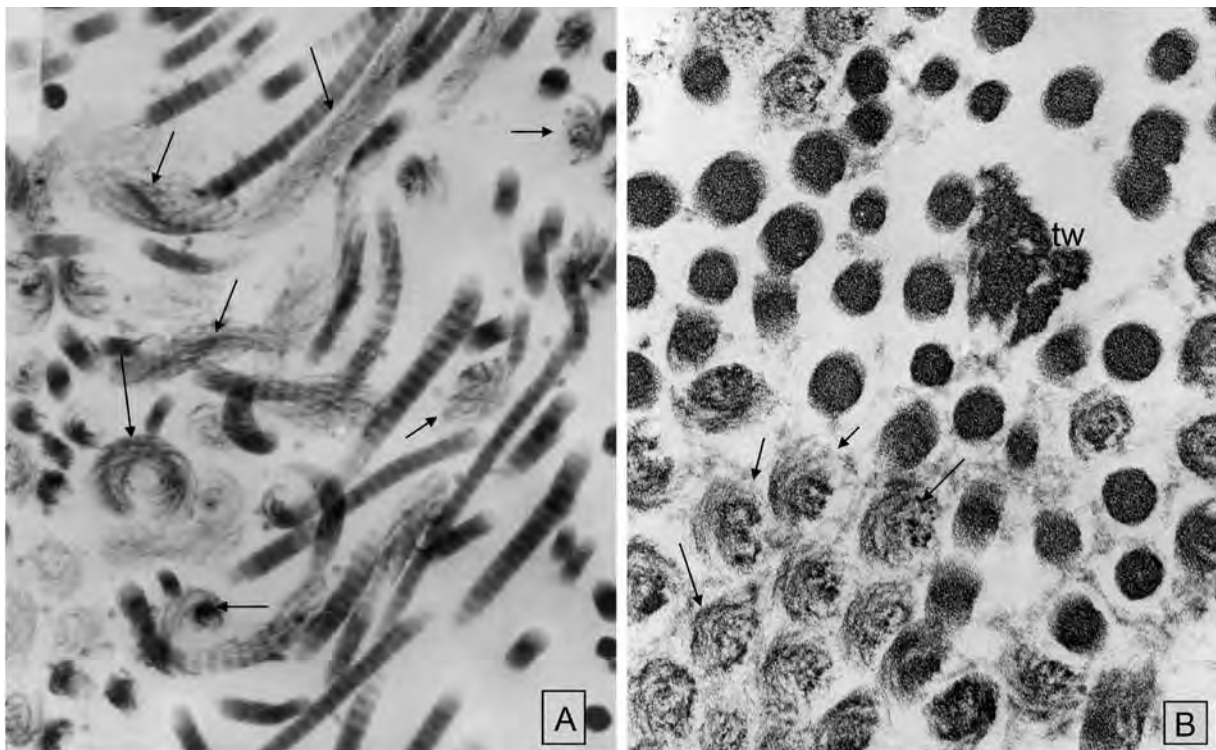


Fig. 15. Ehlers-Danlos syndrome. Unwound collagen fibrils after citrate buffer treatment. Longitudinal (A) and cross (B) section. The collagen fibrils are unwound and appear like rope and vortex (arrows). But a flower-like cut surface of twisted collagen fibril (tw) shows no clear vortex figure. $\times 20,000$.

Degradation by collagenolytic factors

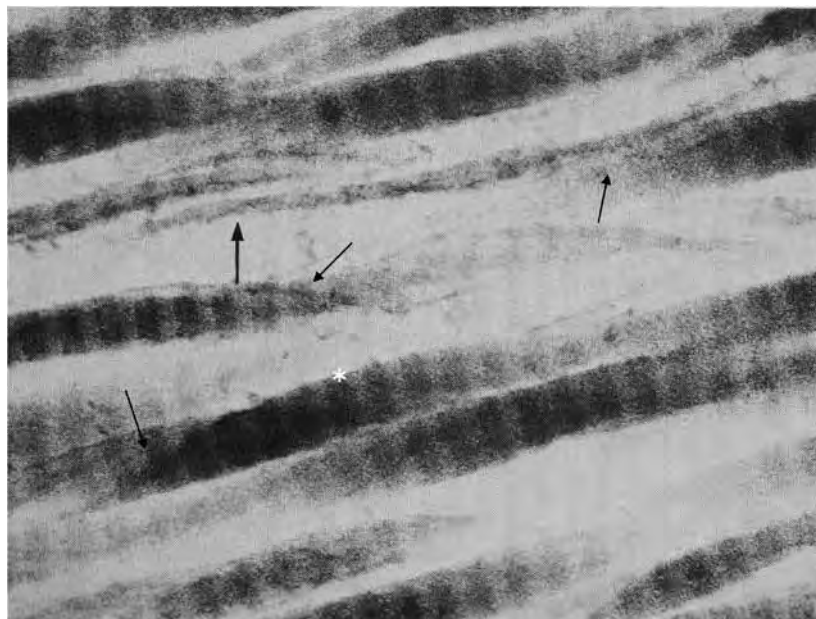


Fig. 16. Collagenolytic factor in the used culture media of myofibroblast [4]. Fresh dermis is incubated in the used media of cell culture of myofibroblast, Tris-HCl buffer pH 7.6 for 24 hours at 37°C. The collagen fibrils show tapered end (arrow) and twisting (*). $\times 20,000$.

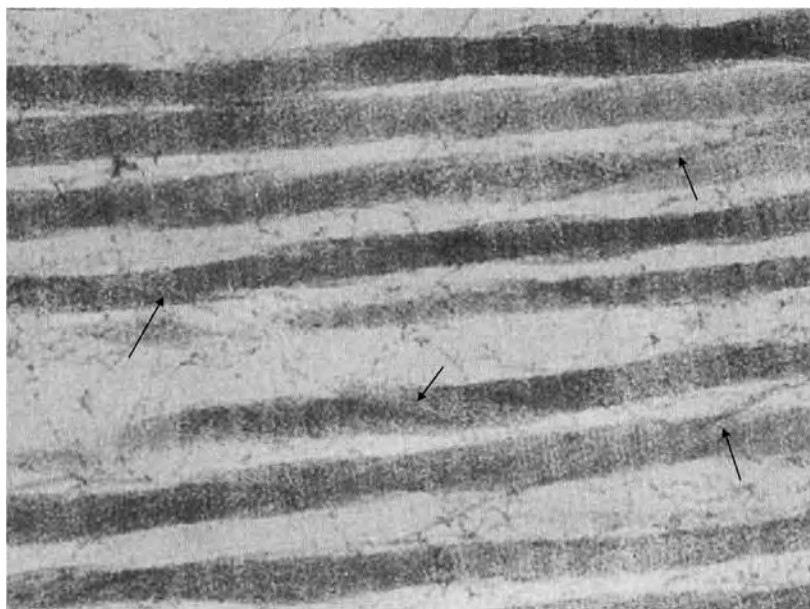


Fig. 17. Experimental degradation of collagen fibrils by clostridial collagenase. After 6 hours incubation of clostridial collagenase pH 7.6 [4]. Twist and tapered ends of collagen fibrils appear after 6 h incubation. $\times 20,000$.

Collagen aggregate, a sign for degradation: Experiments

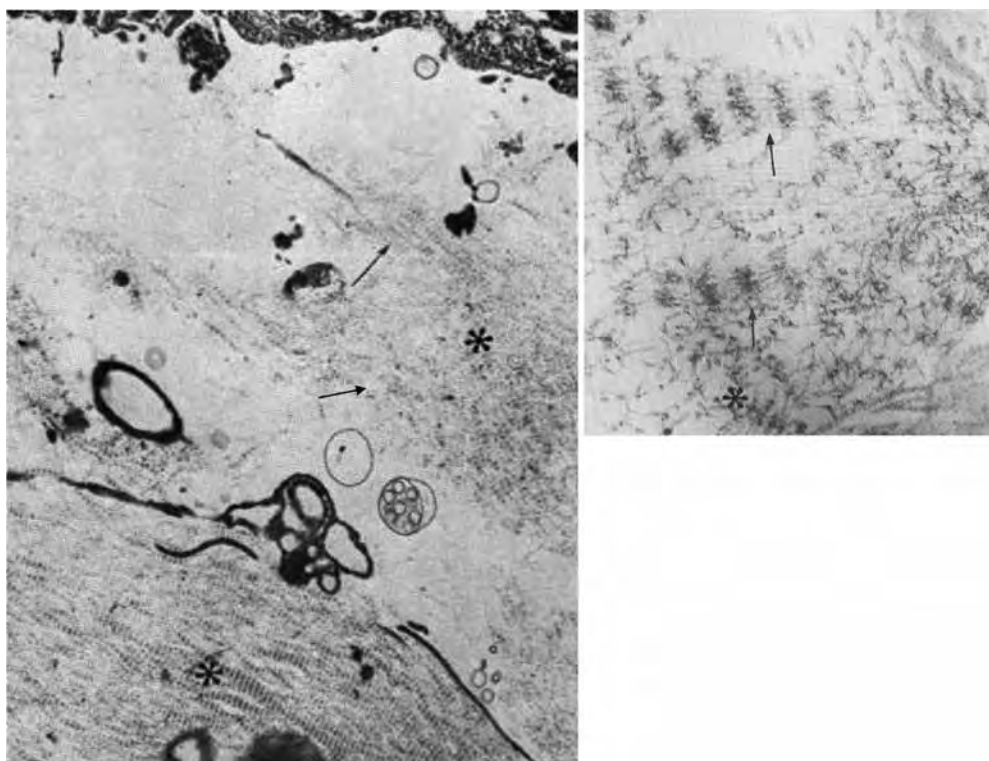


Fig. 18. Collagen aggregate [3, 4]. Left: Fresh normal dermis, incubated in clostridial collagenase, pH 6.8 for 6 hours. Collagen fibrils are degraded and appear as cross-banded filaments (asterisks). Threads are final product by the degradation (arrow). $\times 2,000$. Right: Collagen aggregate in high resolution. Arrows point at degraded collagen fibrils, collagen aggregates. Threads (asterisk) are end-product seen by electron microscope. $\times 20,000$. Collagen aggregate seems to be the figure of inter-mediate product of collagen fibril degradation by cellular collagenase.

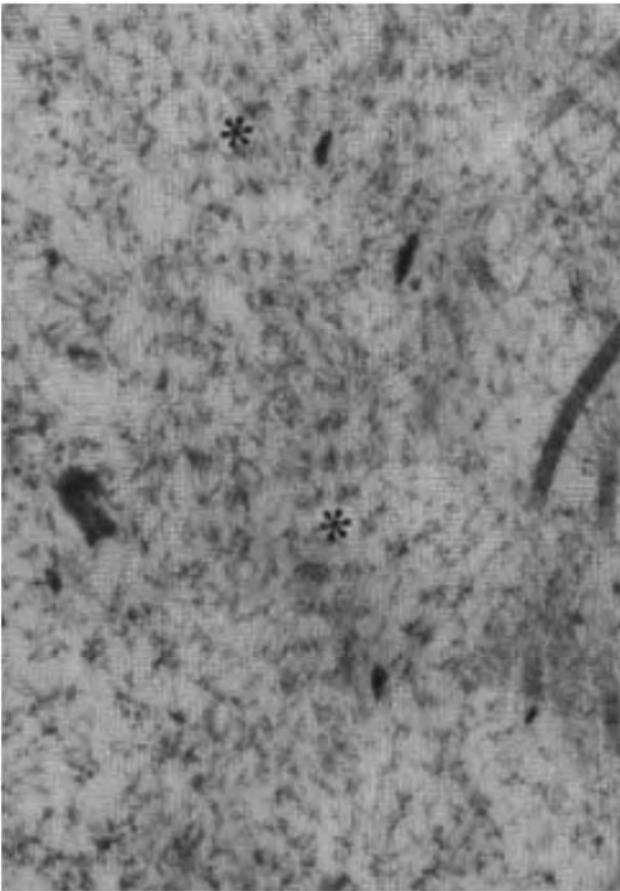


Fig. 19. Fresh dermis incubated in the used media of human myofibroblast culture [4]. Collagen aggregate (asterisk) and threads after degradation of fresh collagen fibrils by the used culture media. The finding indicates that the culture media contains collagenolytic material. $\times 20,000$. Used culture media is prepared from cell culture of human myofibroblast. Used media is accumulated, spun at 45,000 rpm and then ammonium sulfate is added in the supernatant. The precipitant is dialysed in distilled water, frozen and dried. The obtained powder is dissolved in 10 mg/1 ml in Hanks balanced salt solution pH 7.2 or Tris-Hcl pH 7.6. Fresh skin specimen is incubated for 24 hours.

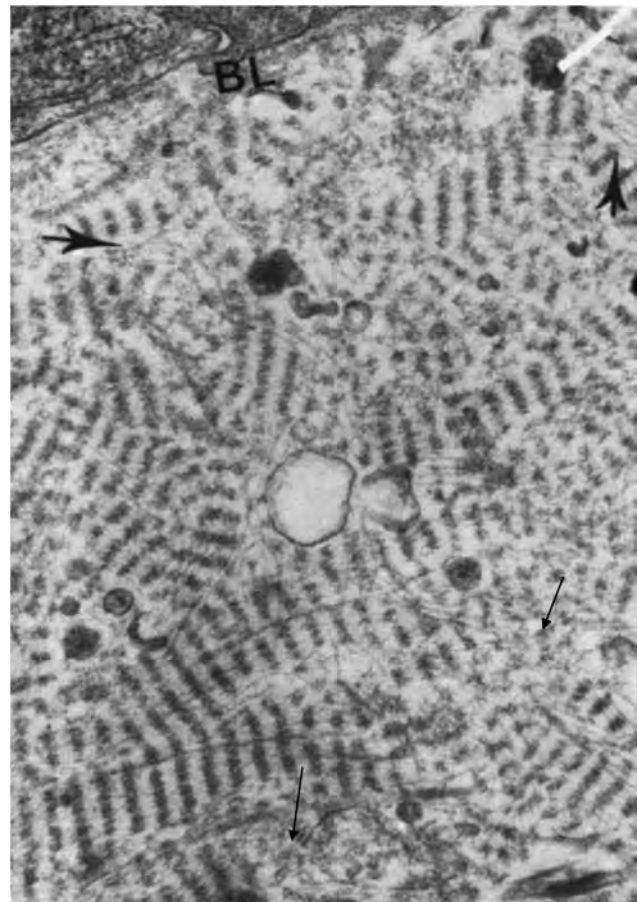


Fig. 20. Organ culture of human dermis for 10 days [5]. Dermis is filled of collagen aggregate. Thick and thin arrows point at threads, terminal product of degradation. Collagen aggregate is intermediate product of degradation. Myofibroblasts start to grow on 7th day after the culture begins. The finding indicates that the culture media contains collagenolytic factor. $\times 20,000$. For culture technique see Appendix.

Collagen aggregate in disorders

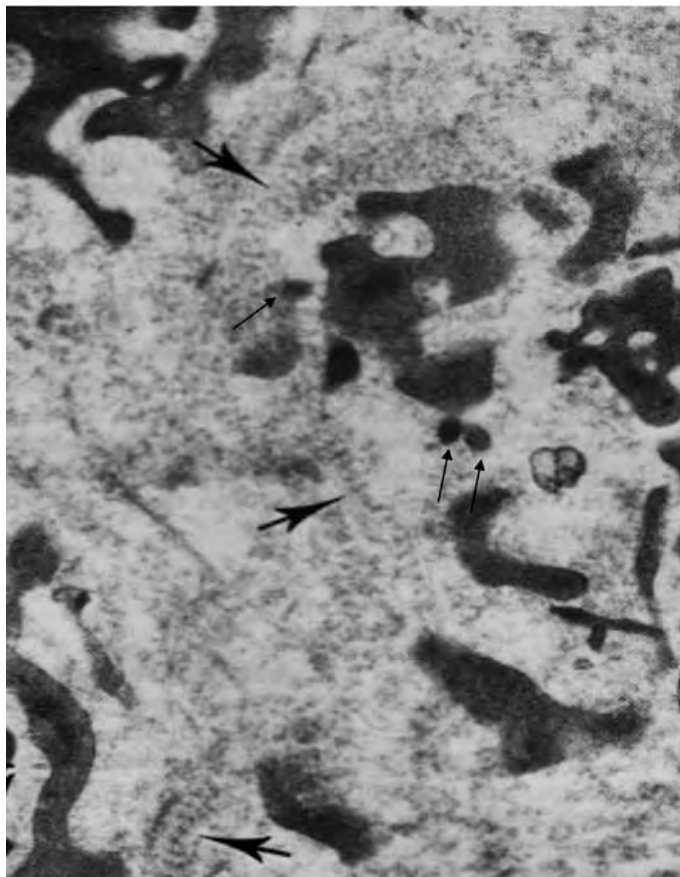


Fig. 21. Collagen aggregate in primary syphilitic chancre [unpublished]. Thick arrows point at collagen aggregate. Thin arrows point at Treponema pallidum. × 5,000. [Unpublished]

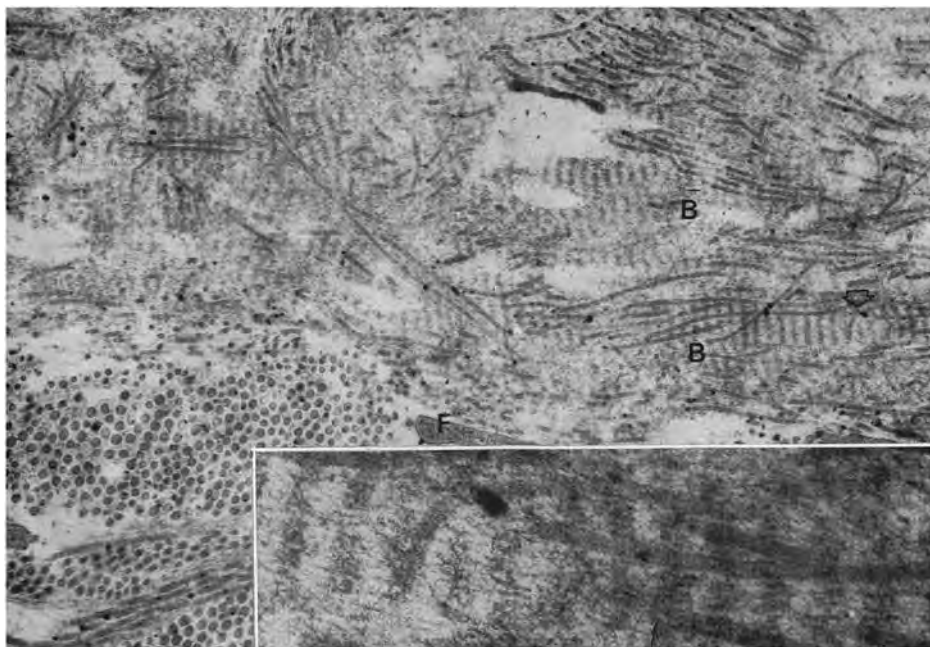


Fig. 22. Acrosclerotic scleroderma [6, 7]. Dermis contains collagen aggregate (B). × 5,000. Inset shows collagen aggregate in high resolution. × 20,000. It seems that normal collagen fibrils are degraded before sclerodermic collagen fibrils develop.

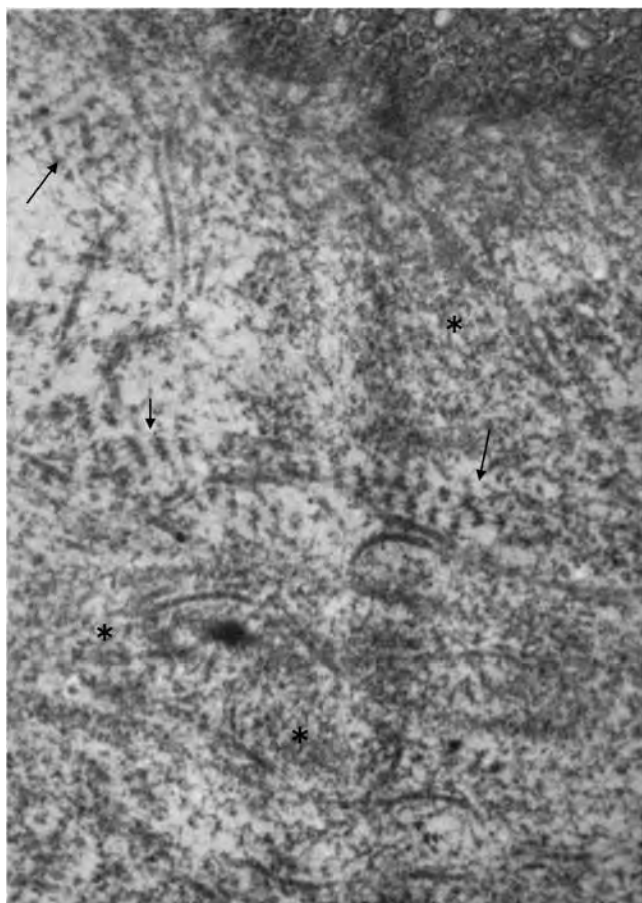


Fig. 23. Collagen aggregate in the lesion of lilac ring of morphoea [9]. Arrows point at the collagen aggregate. Asterisks-marked threads and amorphous material is final products by degradation. $\times 10,000$.

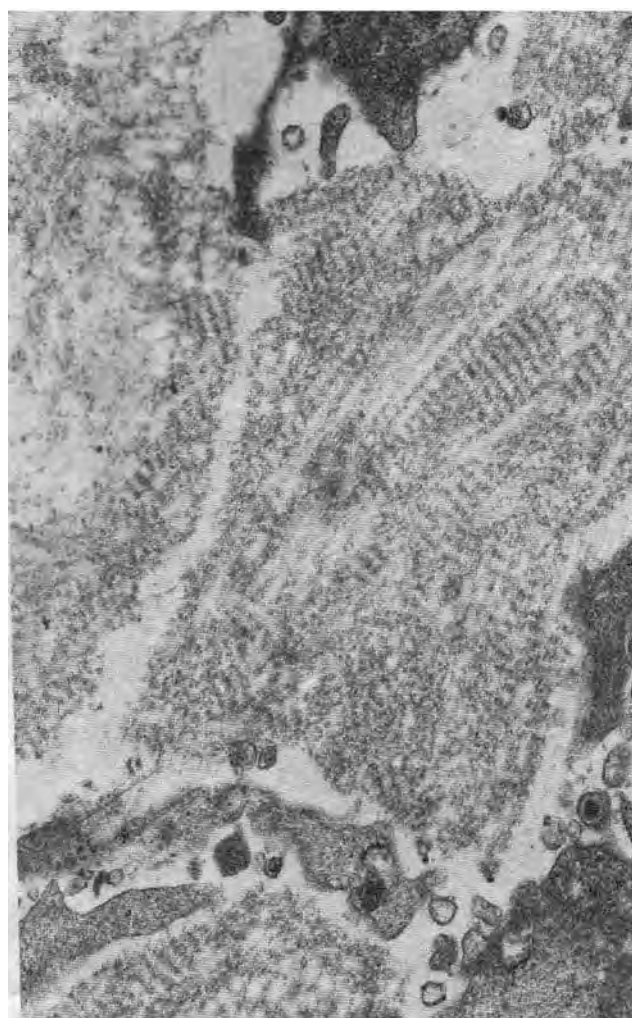


Fig. 24. Myeloid leukemia. Collagen aggregate in the dermis of the lesion. $\times 10,000$. [Unpublished]

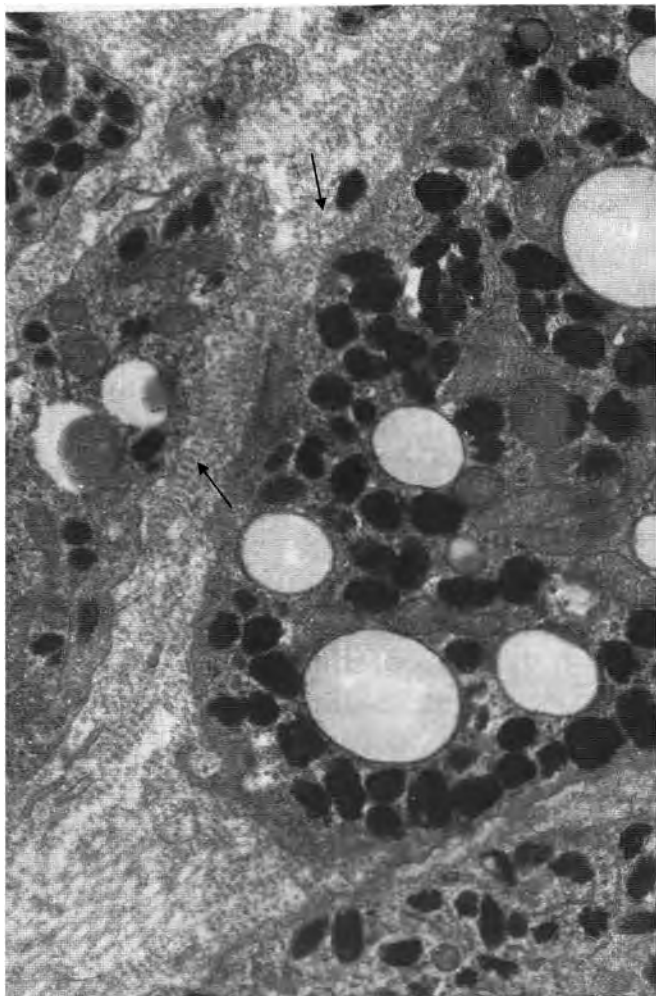


Fig. 25. Malignant melanoma. Collagen aggregate between melanoma cells (arrows). $\times 9,000$. [Unpublished]

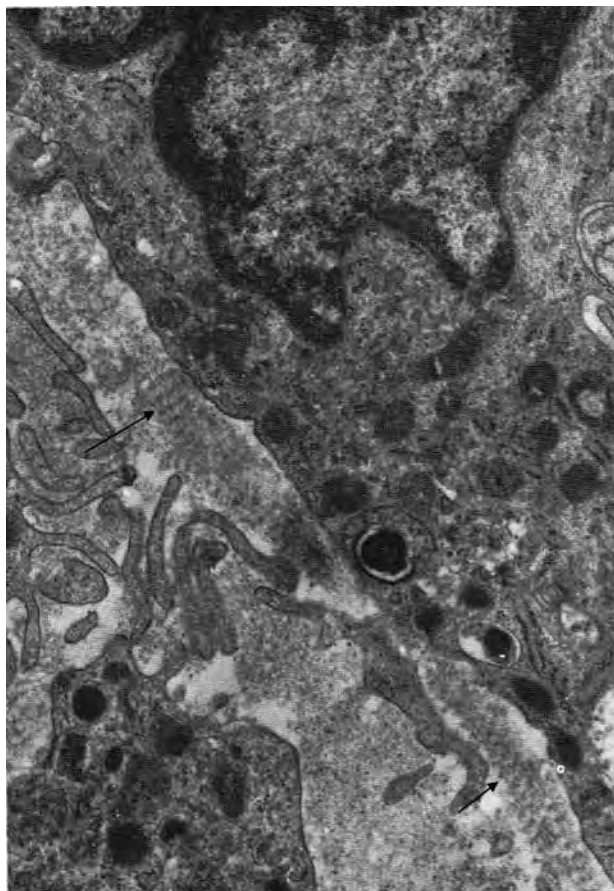


Fig. 26. Mastocytosis. Collagen aggregate close to mast cells (arrows) in the papular lesion. The finding indicates collagenolytic factor from mast cell. $\times 15,000$. The above demonstrated results of the experiments and the biopsy specimens indicate clearly that mesenchymal cells in dermis secrete collagenolytic factor and disintegrate collagen fibrils. [Unpublished]

Dermatoses

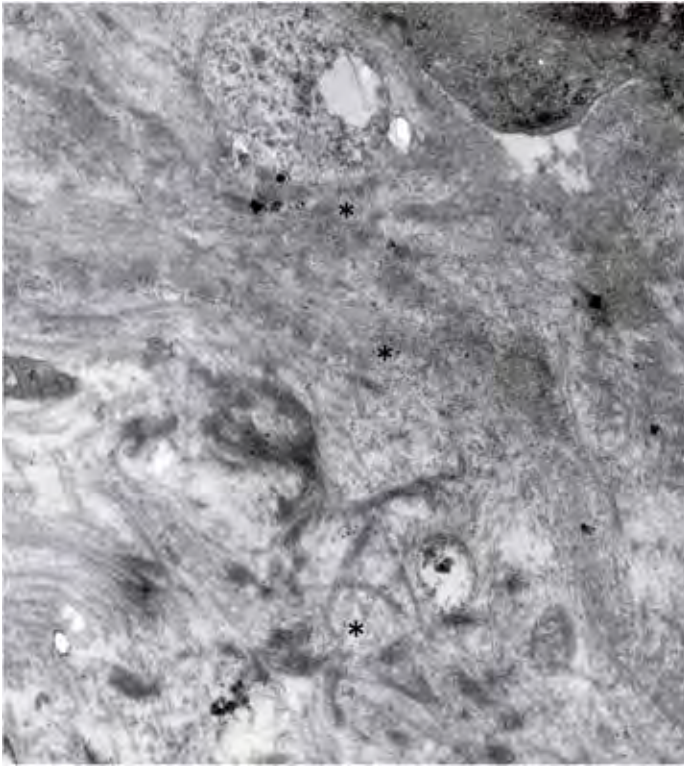


Fig. 27. Dermis around diabetic blister [8]. Dissociated collagen fibrils and amorphous material (asterisk). $\times 5,000$.

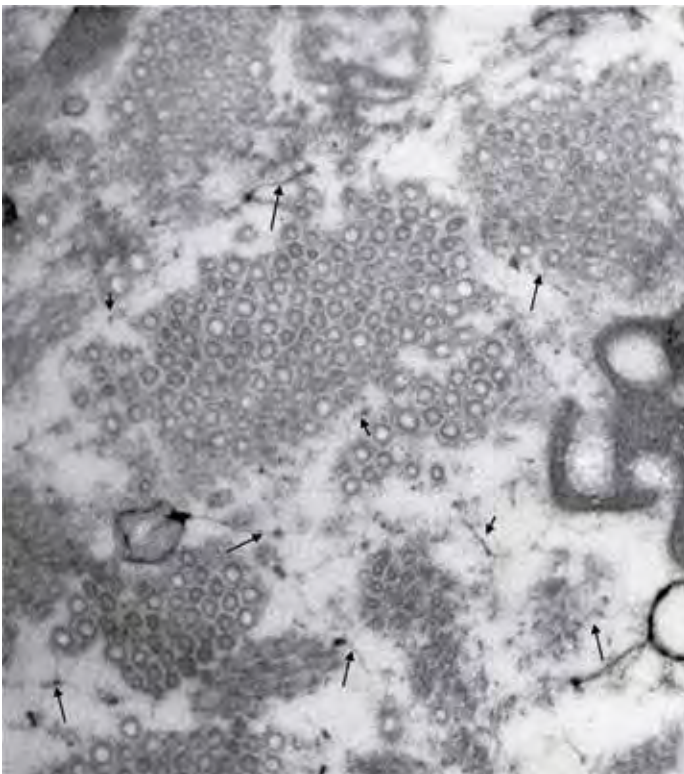


Fig. 28. Papular mucinosis of Steigleder. Collagen fibrils show various thickness, irregular margins and surrounding amorphous material. The figures indicate collagen fibril degradation. Glycosaminoglycan figures in the interfibrillar space (arrows). $\times 5,000$. [Unpublished]



Fig. 29. Necrobiosis lipoidica diabetorum [8]. Collagen fibrils present anomalies in thickness, shape and arrangement. Curled shape suggests increased twisting. The array of the fibrils in the bundle is abnormal. Amorphous material in the stroma may be degradation product (arrows). $\times 5,000$.

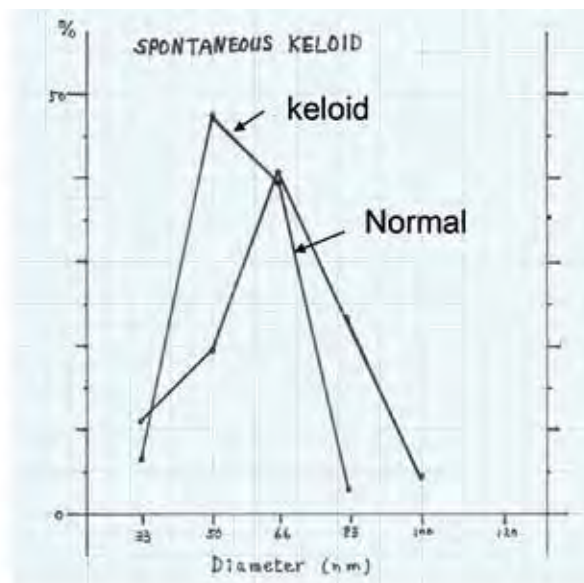


Fig. 30. Spontaneous keloid. Collagen fibrils in the lesion are straight. The fibrils are thinner than normal and arranged in distorted array. Graph to the right shows thickness distribution compared with normal reticular dermis. $\times 10,000$. [Unpublished]

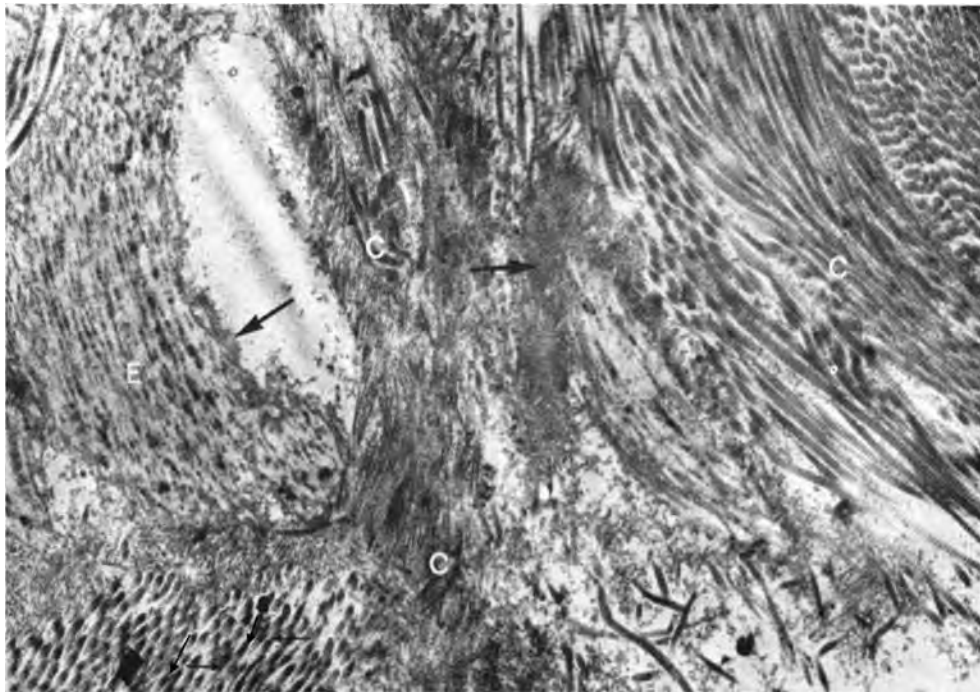


Fig. 31. Morphoea [9]. Pronounced changes of collagen fibrils in thickness, shape and arrangement (C). Two small arrow-pointed areas (lower-left of the micrograph) show bifurcated collagen fibrils (Fig. 32). E: elastic fibres (thick arrows).



Fig. 32. Collagen fibrils in inflammatory zone of morphoea [9]. Collagen fibrils are varied in thickness, 30–100 nm, and show bifurcation (arrows). Axial periodicity is normal. $\times 15,000$.

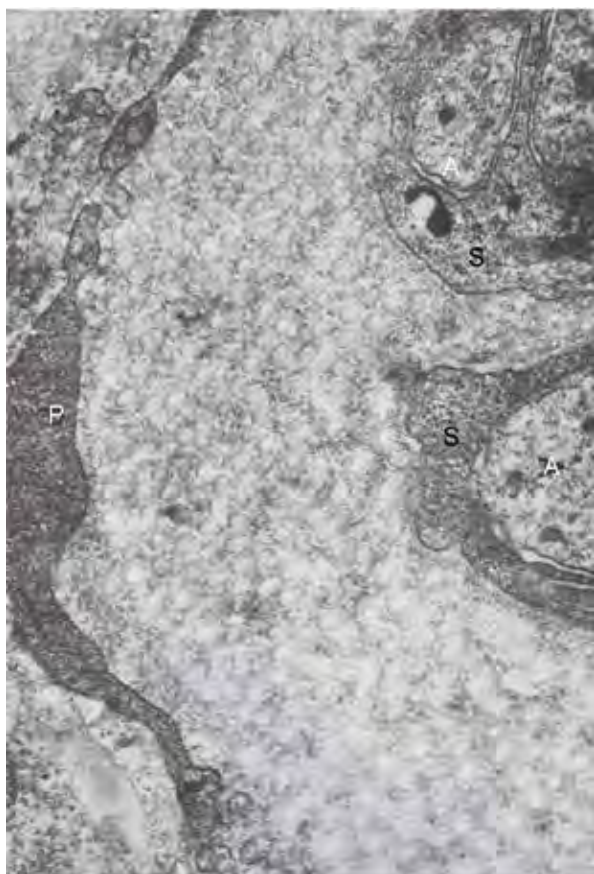


Fig. 33. Collagen fibrils of endoneurium in morphoea show thickness variation [9]. P: perineural cell. Basal lamina is interrupted. A: axon. $\times 20,000$.

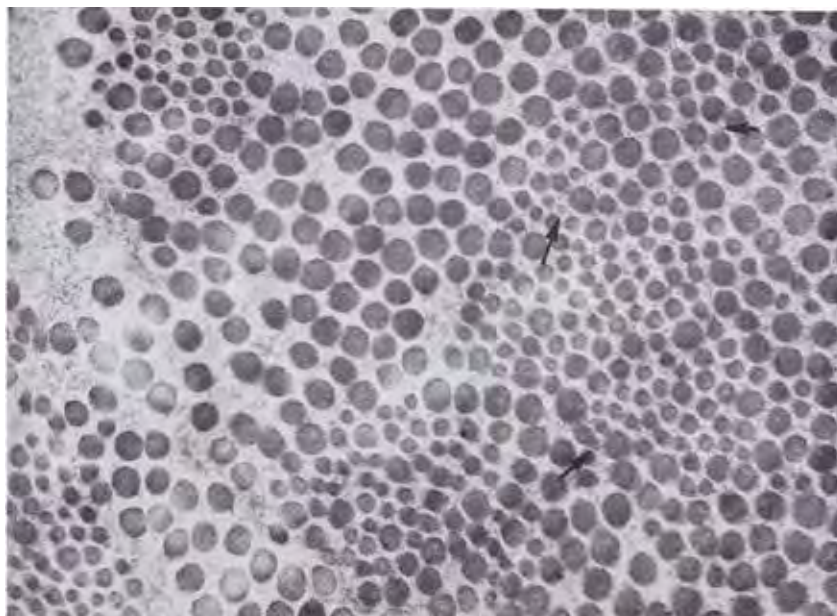


Fig. 34. Acrosclerotic scleroderma, sclerosing lesion. Cross-cut section [6, 7]. Collagen fibrils are packed compact and present round cut-surfaces of various thicknesses. Variation of the thicknesses is wide and show bimodal distribution (shown in Fig. 35). The fibrils with small diameter are new and under development. Arrows pointed at glycosaminoglycans between collagen fibrils. $\times 20,000$.

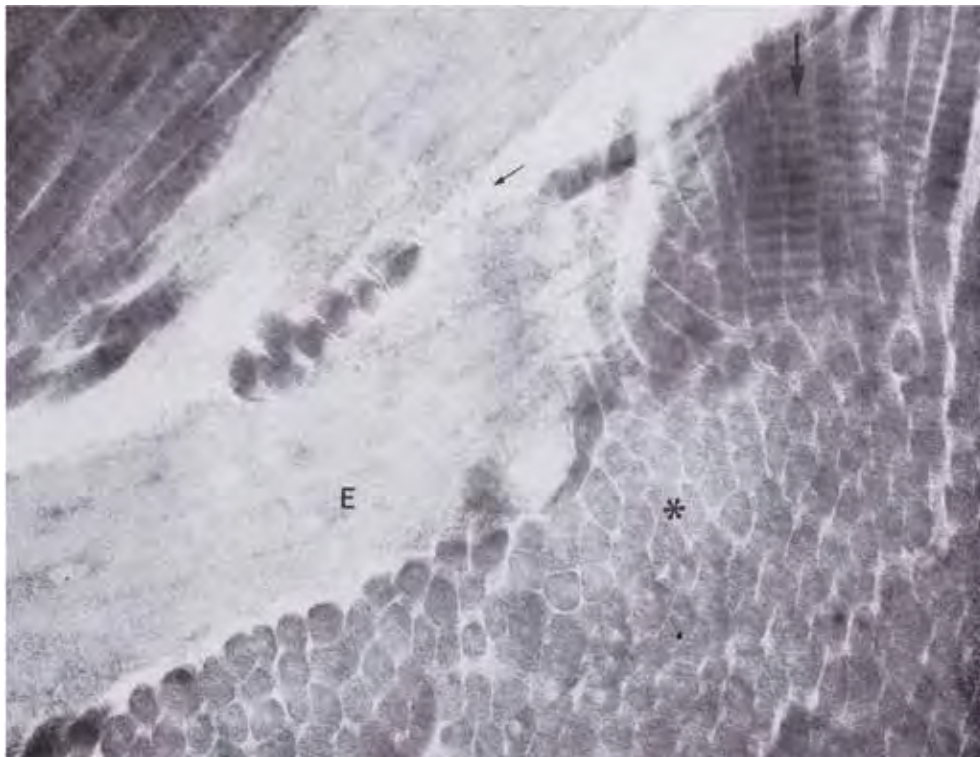


Fig. 35. Acrosclerotic scleroderma. Sclerotic area [9]. Collagen fibrils are compactly packed in a bundle. Some collagen fibrils show polyagonal cut-surface (asterisk). E: elastic fibre. $\times 20,000$.

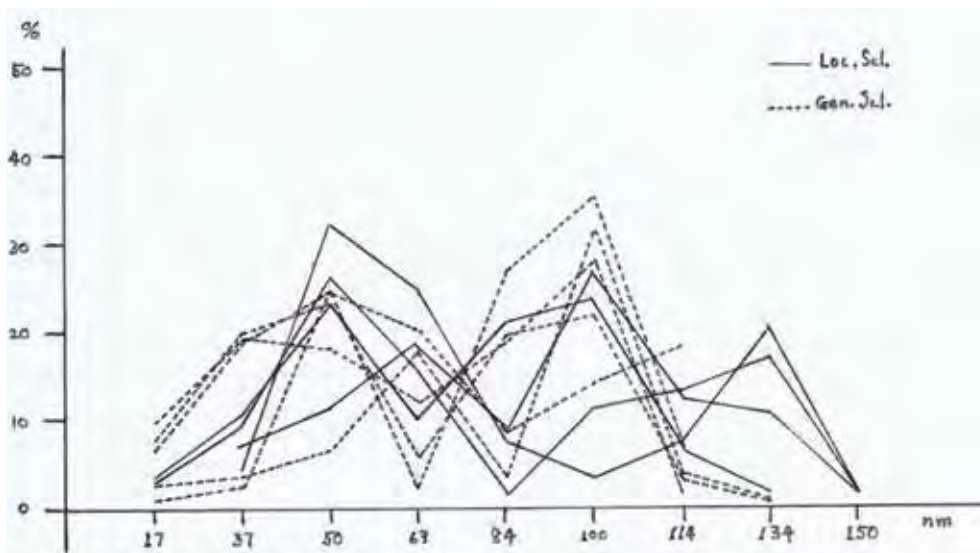


Fig. 36. Bimodal distribution of various thicknesses of collagen fibrils in generalized scleroderma (acrosclerotic) and localized scleroderma morphoea [7, 9]. Two spikes are at 50 nm in thinner fibrils and at 100 or 134 nm in thicker fibrils.

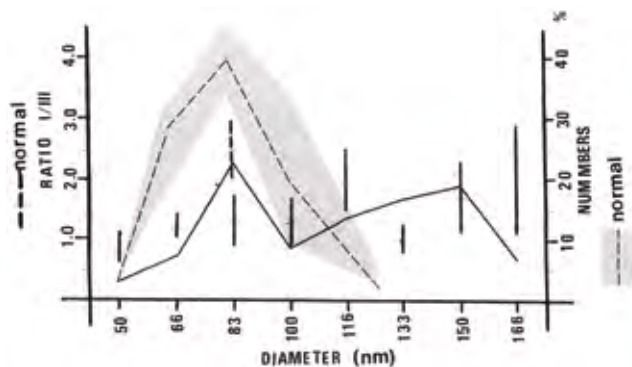


Fig. 37. Acrosclerotic scleroderma [6, 7]. Figure shows relation of bimodal distribution and ratio collagen I/III in the sclerotic lesion, in comparison to the distribution of thickness and ratio I/III in normal reticular dermis. Normal dermis presents a peak at 83 nm and ratio I/III 2.0–3.0 (broken lines and two arrows), while sclerotic lesion presents bimodal distribution and the lower values of I/III (less than 2.0).

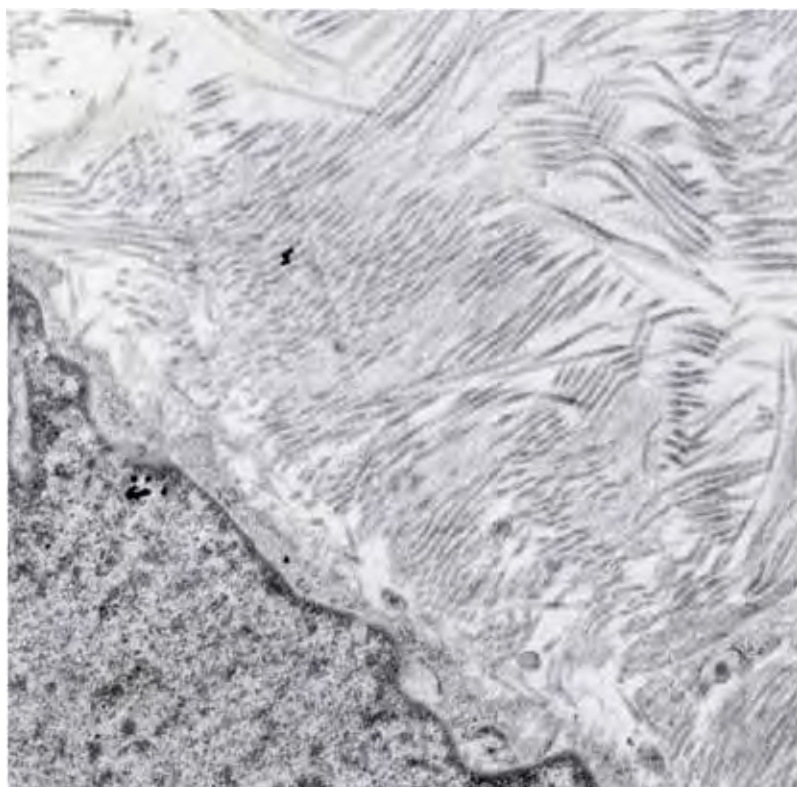


Fig. 38. Atrophoderma Passini. Atrophic lesion in the reticular dermis. Collagen fibrils are thin and show an irregular array. No twisted collagen fibrils are found. Distribution of the collagen fibrils is presented in Fig. 39 [unpublished data]. $\times 5,000$. [Unpublished]

Kollagenfibrildiameter i atrophoderma Passini

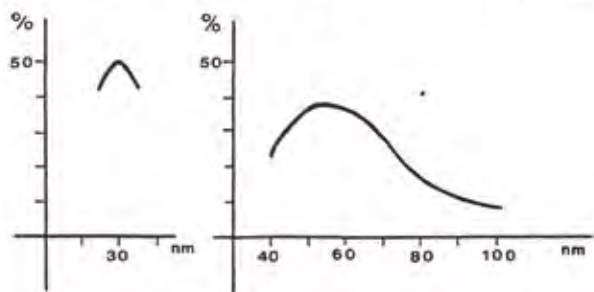


Fig. 39. Atrophoderma Passini. Distribution of various thickness of collagen fibrils in the lesion. In papillary dermis, distribution is normal, while the lesion in the reticular dermis reveals monomodal distribution with a slow peak at about 50 nm (thinner than normal), if compared with normal peak of 60–70 nm. No twisted collagen fibrils are found (indicating no inherited change of collagen fibrils).

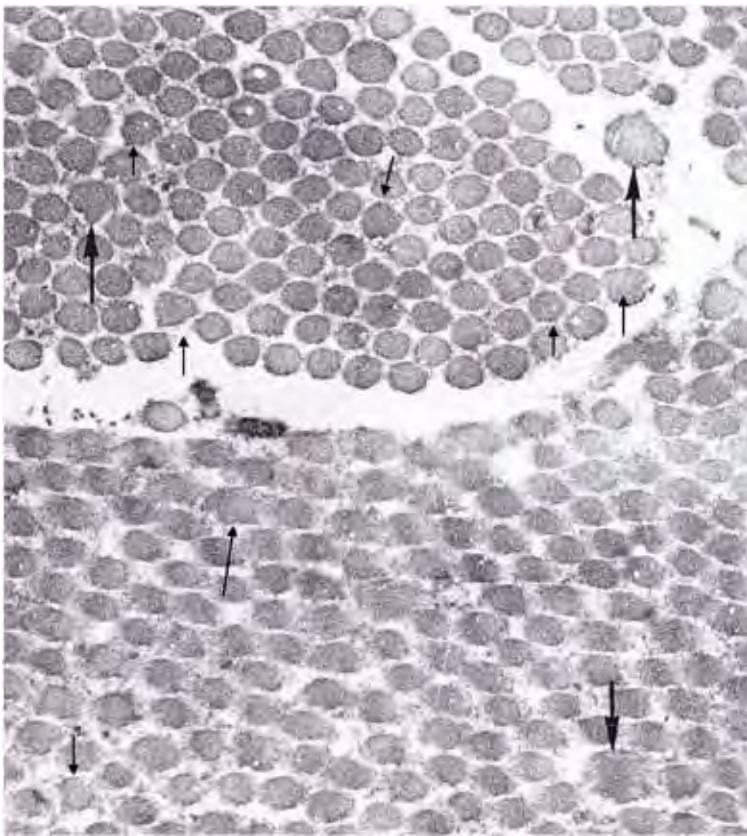


Fig. 40. Linear atrophy [10]. A 16-year-old female patient. Linear atrophic lesion on her legs and arms for 6 years duration. No obvious changes of redness and sclerosis are noticed. Note that the numbers of twisted collagen fibrils are admixed in the bundle [19]. Thin and thick arrows point at some examples. The findings imply heritable nature of the atrophy (figures of inherited dermatoses). $\times 20,000$. Distribution of thickness appears in the following figure (Fig. 41).

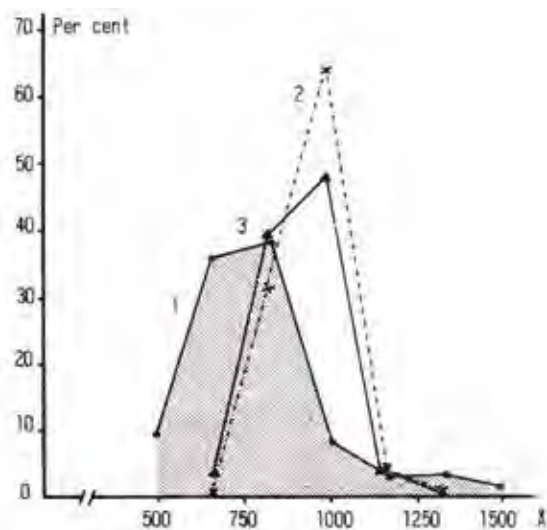


Fig. 5. Diameter of collagen fibrils in the reticular dermis. 1. Atrophic areas ($n=1\ 174$, mean= $783\ \text{Å}$, SD= $190\ \text{Å}$). 2. Perilesional control ($n=759$, mean= $950\ \text{Å}$, SD= $93\ \text{Å}$). 3. Regional control ($n=660$, mean= $930\ \text{Å}$, SD= $122\ \text{Å}$).

Fig. 41. Linear atrophy [10]. Distribution of thickness of collagen fibrils in the atrophic area (See Fig. 40). 1. Lesion ($n=1174$, mean= $783\ \text{Å}$, SD= $190\ \text{Å}$). 2. Perilesional area. 3. Normal area in the same part of the body.

Inherited Dermatoses

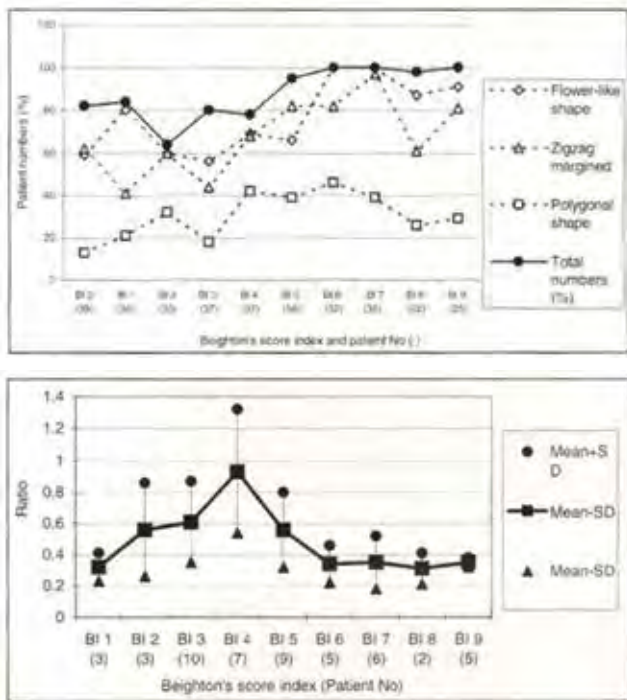


Fig. 42. Ehlers-Danlos syndrome (EDS). Hypermobile syndrome (HS) [11, 12]. EDS consists of 10 clinical variants, based on clinical symptoms, joint hypermobility, skin laxity and bruising. Severity of joint hypermobility is expressed by “Beighton’s score index” (BI) in 9 degrees. BI higher than 5 is diagnosed EDS and BI 3 and 4, HS. BI 1 and 2 is considered neither HS nor EDS. Dermal collagen fibrils in EDS and HS present characteristic ultrastructure, i.e. “twisted collagen fibrils” (TCF). TCF reveal increased twisting in longitudinal cut-surface (clockwise at 15°) and irregular cross cut-surfaces as seen polygonal, zig-zag margined and flower-like cut-surfaces. TCF is found in the dermis of all clinical variants, even BI 1 and 2. Normal family members show also TCF. (Upper table). Ratio of collagen type I/III is higher than 0.4 for EDS. The ratio is not followed well with BI (lower table). It seems that type I collagen is reduced in EDS.

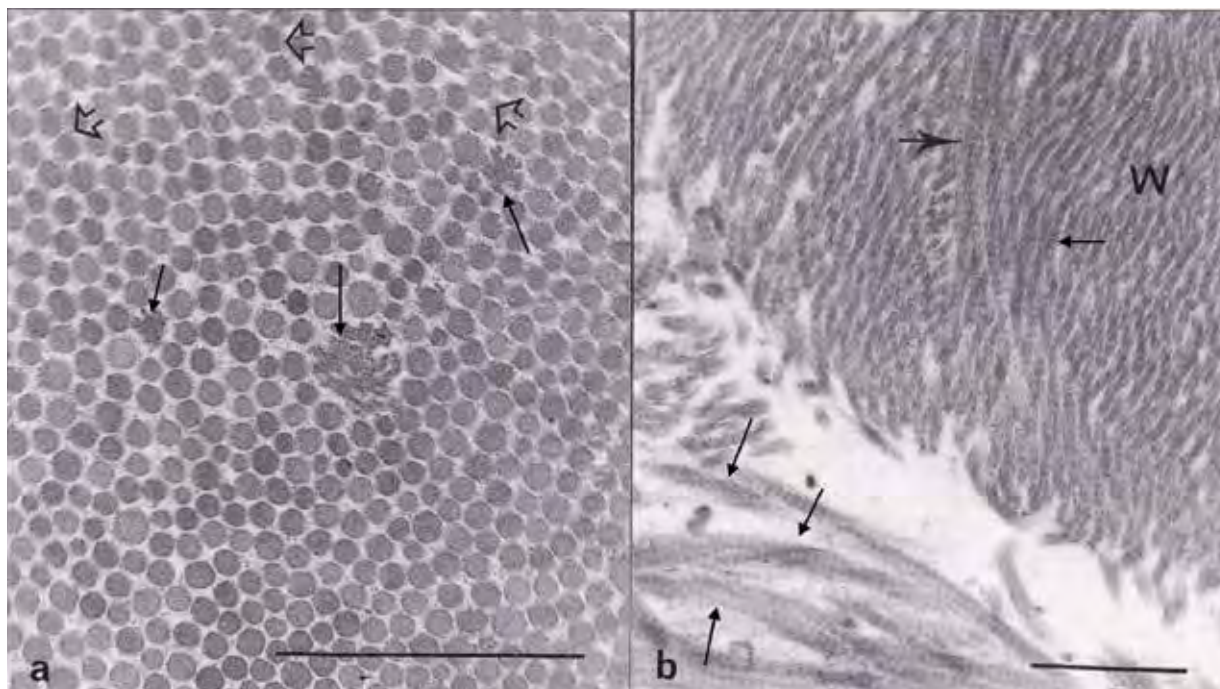


Fig. 43. Ehlers-Danlos syndrome, mitis type II [12]. Collagen fibrils show disarray and twisted fibrils. Thick and thin arrows point at some examples of twisted collagen fibrils. Scales bars: 0.1 μm. Figure a shows different thickness and whirl-form disarray (3) and framed arrows show the direction of the whirl. Figure b shows wavy collagen fibrils (w). Some of the twisted collagen fibrils are marked by thick and thin arrows. a: × 40,000. b: × 20,000.

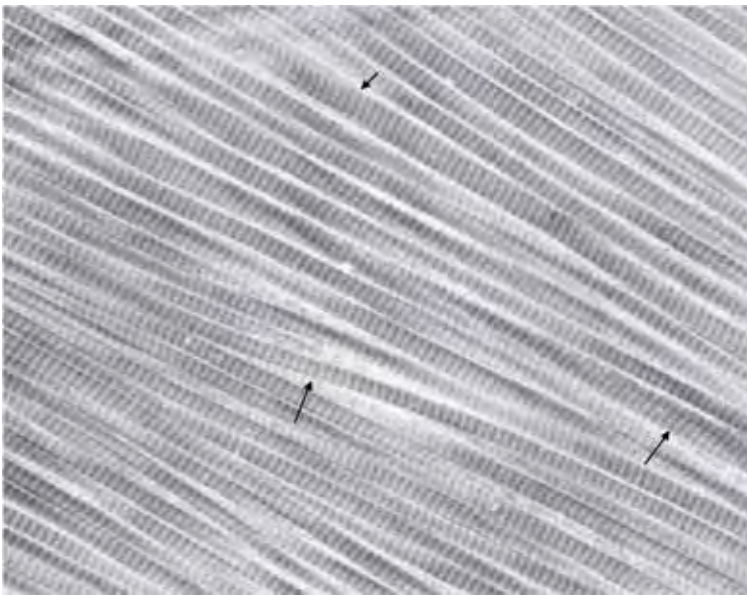


Fig. 44. Ehlers-Danlos syndrome, mitis type II [12]. Dermal collagen fibrils in longitudinal section. The collagen fibrils are straight. Note the thickness variation and the many twisted fibrils. Arrows points at some examples. $\times 10,000$.

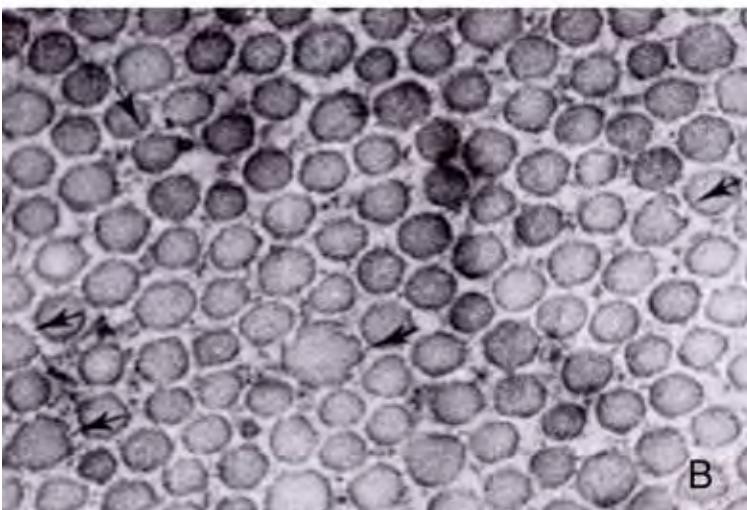
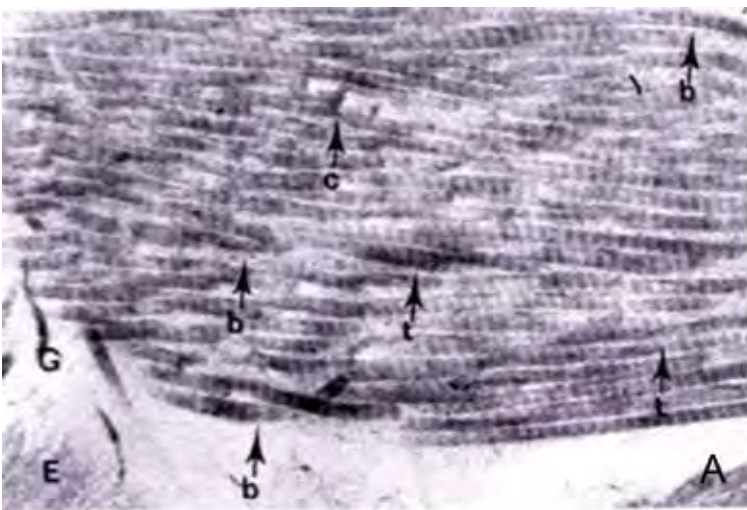


Fig. 45. Ehlers-Danlos syndrome, A. Mitis type II [11]. Arrows with b and c show examples of bent and curled shapes and arrow t for twisted collagen fibrils. E: elastic fibre, G: glycosaminoglycans. $\times 15,000$. B: Benign hypermobile type III. Collagen fibrils point zig-zag margins. Arrows point at irregular margins of twisted collagen fibrils. $\times 20,000$.

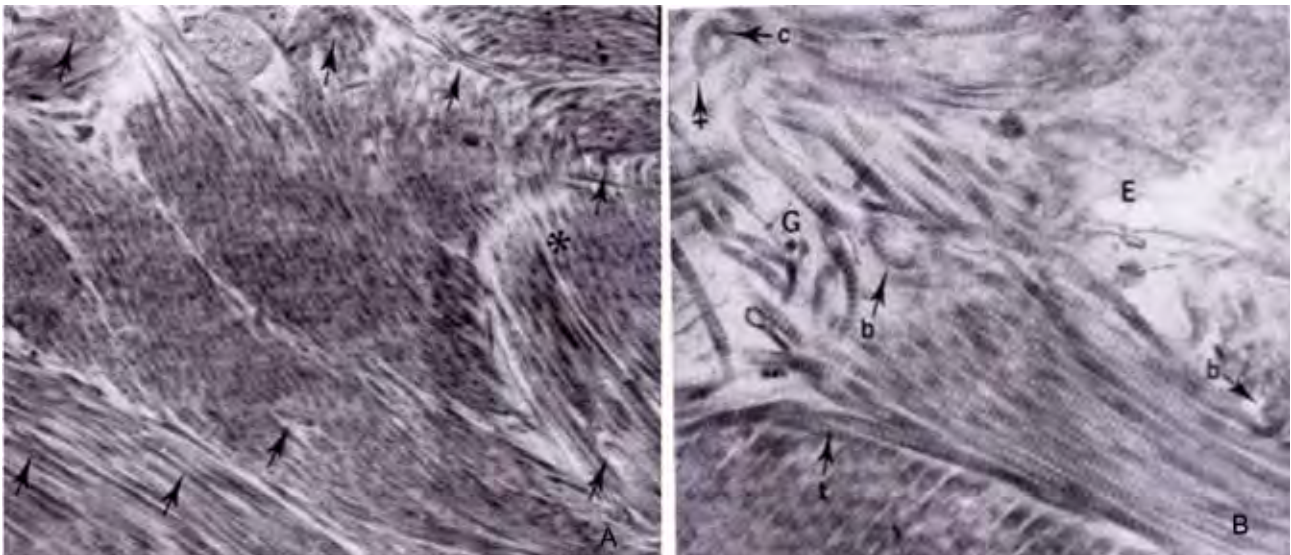


Fig. 46. Ehlers-Danlos syndrome, ocular type VI [11]. A: Arrows point at twisted collagen fibrils. $\times 5,000$. B: Arrows with b and c point at strongly curled and bent shapes. Arrows with t point at twisted collagen fibrils. An arrow with cross points at split end of a collagen fibril. E: elastic fibre. $\times 10,000$.

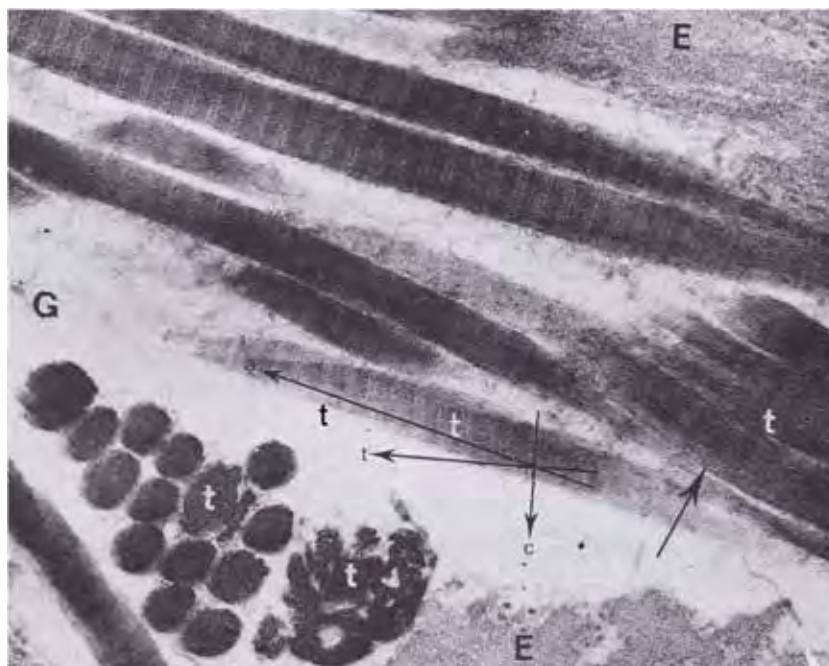


Fig. 47. Ehlers-Danlos syndrome, Periodontitis type VIII [11]. Showing twisting of the fibrils in longitudinal section and flower-like cut-surface. Arrow a indicates fibril axis, arrow c level of cross bands and arrow t the twisted direction. The level (c) incline to the fibril axis (a) at 15 degrees. E: elastic fibre, G: glycosaminoglycan filaments. $\times 20,000$.

Marfan syndrome

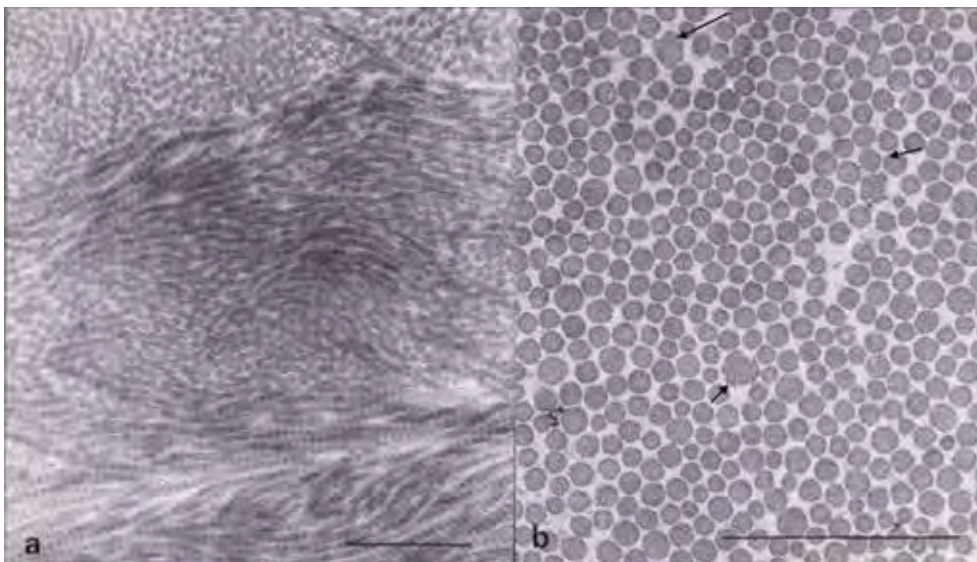


Fig. 48. Dermis of Marfan syndrome [12]. a: Slightly varied thickness and disarray of collagen fibrils. b: varied thickness and twisted collagen fibrils (arrows). a: $\times 20,000$, b: $\times 40,000$. Scale bars indicate $1 \mu\text{m}$.

Osteogenesis imperfecta, type i

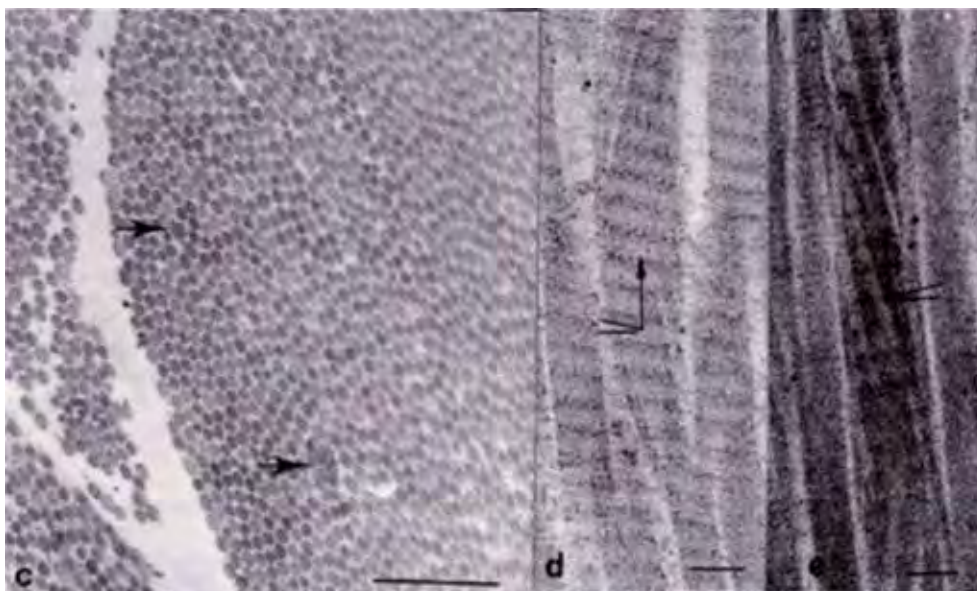


Fig. 49. Dermis of Osteogenesis imperfecta, type 1 [12]. c: Collagen fibrils shows slight variation of thickness and twisted collagen fibrils (arrows). $\times 20,000$. d. Long section of collagen fibrils show thick twisted collagen fibrils showing cross band inclined at approximately 15° to the fibril axis. Arrows indicate fibril axis. $\times 80,000$. Scale bars in the pictures indicate $0.1 \mu\text{m}$.

Pseudoxanthoma elasticum

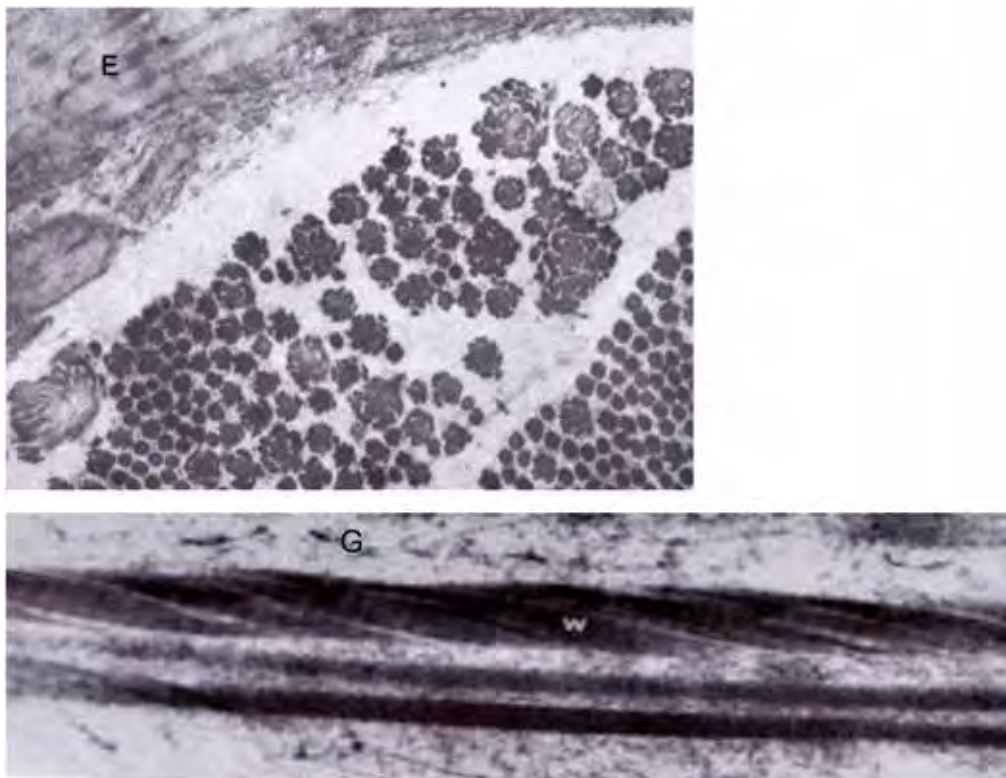


Fig. 50. Pseudoxanthoma elasticum. Twisted collagen fibrils in the lesion of dermis [13]. Flower-like cut surfaces in the upper picture and twisted shape (W) in longitudinal section in the lower picture. E: elastic fibre, G: glycosaminoglycan filaments. × 20,000.



Fig. 51. Pseudoxanthoma elasticum. Collagen fibrils found in a operation scar. Twisted fibrils are unwound and split off thinner fibrils (arrows) [14]. × 20,000.

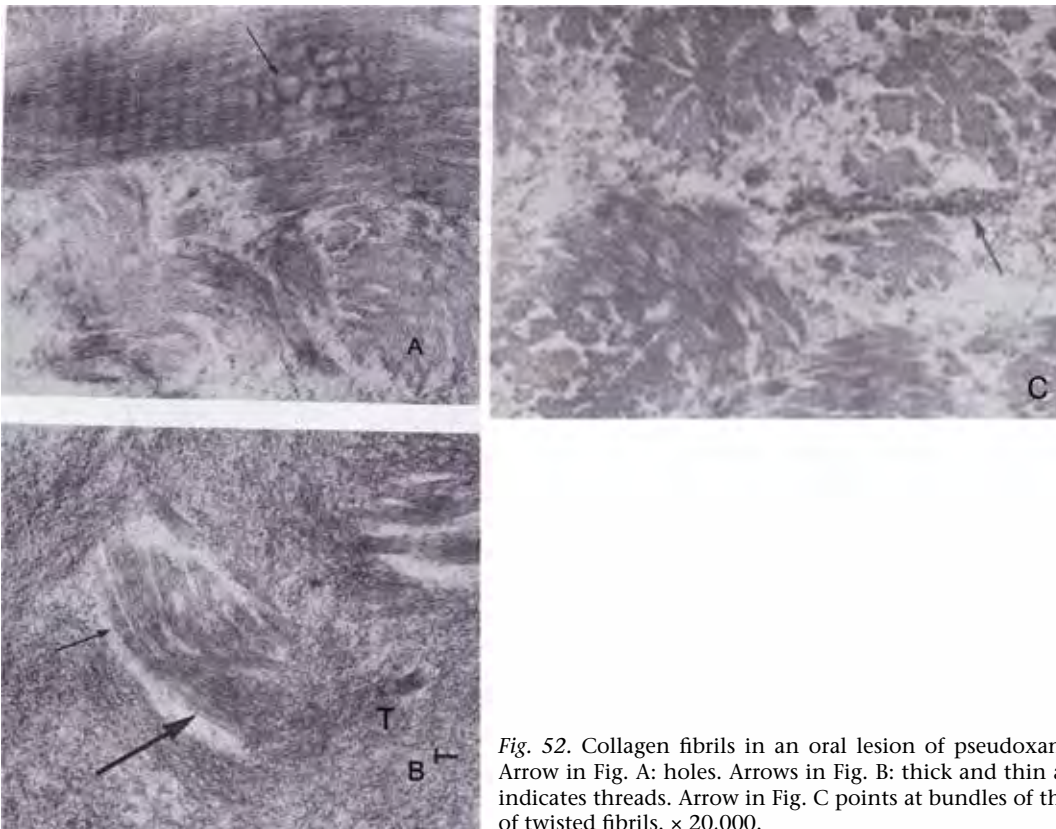


Fig. 52. Collagen fibrils in an oral lesion of pseudoxanthoma elasticum [15]. Arrow in Fig. A: holes. Arrows in Fig. B: thick and thin arrows twisted fibrils. T indicates threads. Arrow in Fig. C points at bundles of threads and large flowers of twisted fibrils. $\times 20,000$.

Shaqreen patch

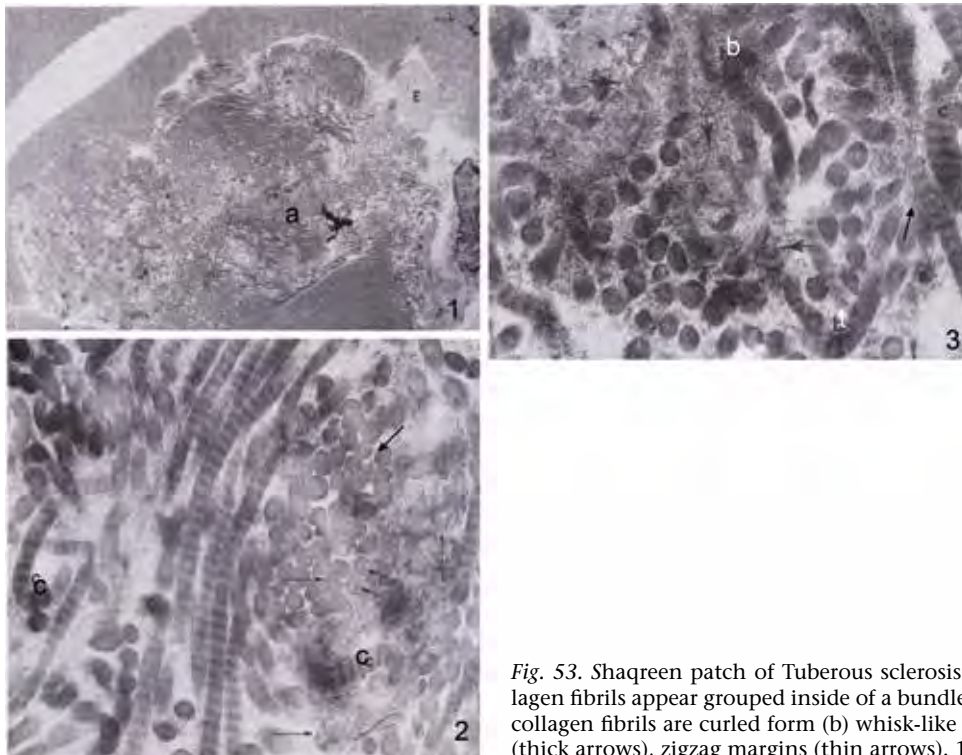


Fig. 53. Shaqreen patch of Tuberous sclerosis [16]. Picture 1: Abnormal collagen fibrils appear grouped inside of a bundle (a). Picture 2 and 3: Abnormal collagen fibrils are curled form (b) whisk-like ends (c), filaments and threads (thick arrows), zigzag margins (thin arrows). 1: $\times 1,500$. 2, 3: $\times 20,000$.

Disseminated connective tissue naevi

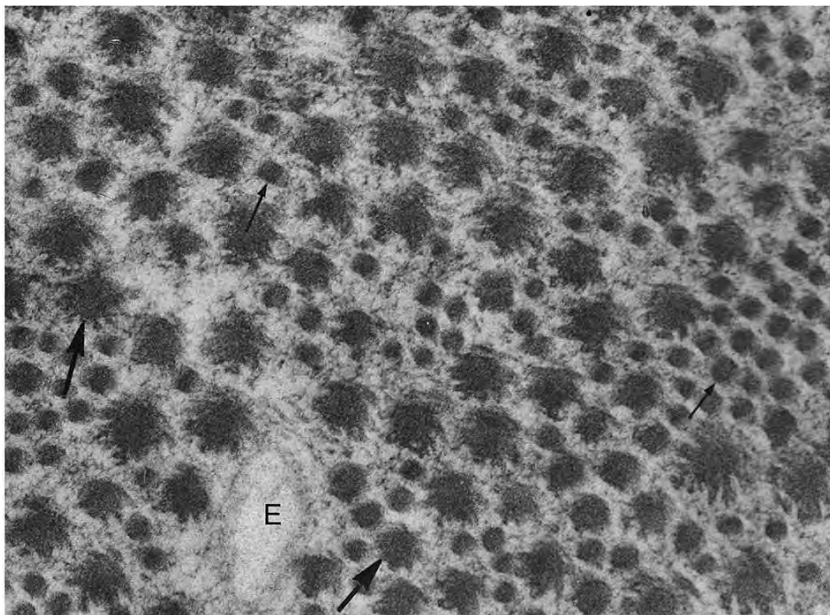


Fig. 54. Disseminated connective tissue naevi. Twisted collagen fibrils [17]. Collagen fibrils in cross section show flower-like cut-surface. Thick arrows point at some examples of twisted fibrils. Thin arrows point at normal shaped collagen fibrils. E: elastic fibre. × 20,000.

Systemic amyloidosis

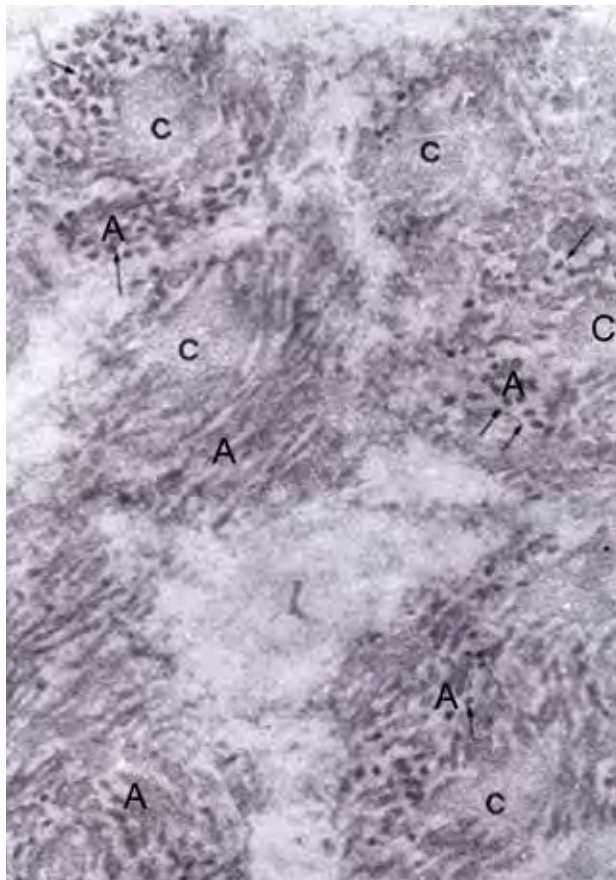


Fig. 55. Systemic amyloidosis [18]. Amyloid fibrils and collagen fibrils. Amyloid fibrils (A) and large twisted collagen fibrils (C) are intermingled, but they show no binding. × 40,000.

Cutis gyrata

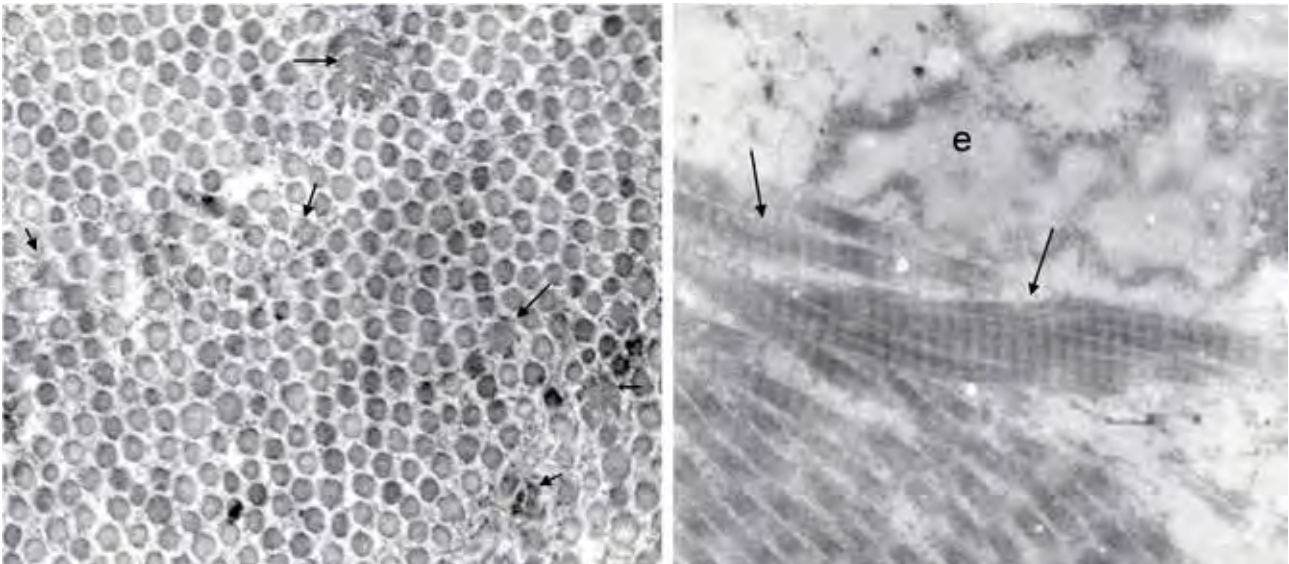


Fig. 56. *Cutis gyrata*. To the left, cross section. To the right, longitudinal section. Dermal lesion contains twisted collagen fibrils in thick and thin forms (Arrows). E: Elastic fibre. $\times 20,000$. [Unpublished]

Angiofibroma, Burneville-Pringle

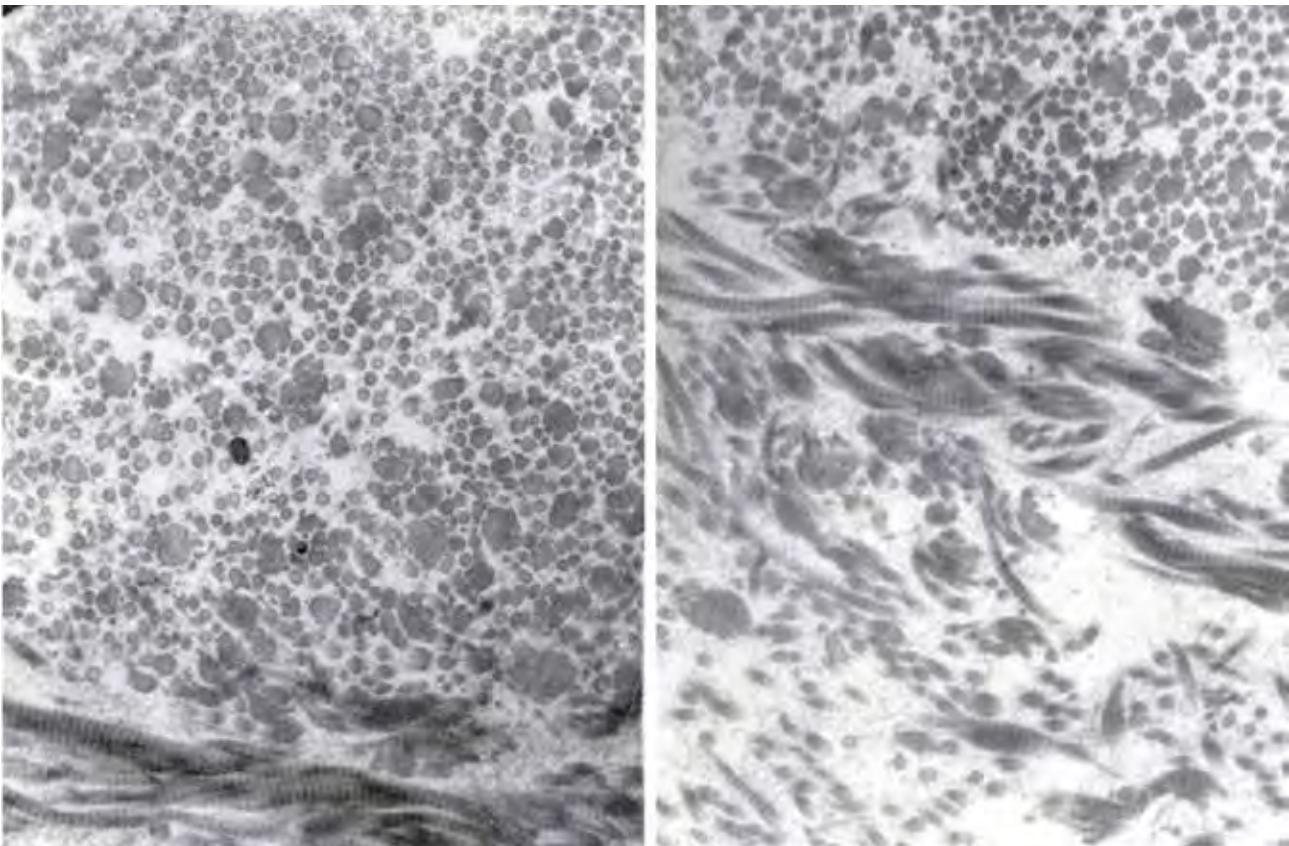


Fig. 57. Bournville-Pringle's phacomatosis. Specimen is biopsied in the lesion of angiofibroma. Large twisted collagen fibrils are numerous. $\times 5,000$. [Unpublished]

III. Ground substance

Overview	
• Fixation – Introductory remarks	Table I
• Ultrastructure	Figures 1–3
• Supplements in the fixatives	Figures 4–6
• Histochemistry	Figures 7–9
• Protein core of ground substance	Figure 10
• Pretibial localized myxoedema	Figures 11–13
• Scleromyxoedema	Figure 14
• Papular mucinosis	Figures 15
• Lupus erythematosus	Figures 16–17
• Morphoea	Figures 18–19
• Fibrodysplasia ossificans progressiva	Figure 20–21
• Basal cell carcinoma	Figure 22

Fixation of specimens for ground substance

Table I. Glycosaminoglycans (GAG) and some fixatives

GAG in fixed umbilical cord	Hexosamine/mg dried defatted tissue, µg Mean ± SD
Frozen dried, unfixed tissue	15.74±3.31
6% glutaraldehyde solution	
Plain	11.78±1.52
With 1% cetylpyridinium chloride	12.81±2.81
With 10% sucrose	12.75±2.23
With 7% sucrose	13.29±1.82

Personal communication.

Fixation of good preservation of ultrastructure and glycosaminoglycan (GAG) for the ultrastructural study of dermis. Fixation for ultrastructure study should concern good preservation of ultrastructure and GAG. Preservation of ultrastructure is estimated by double layer of cell membrane. Common fixative, 6% glutaraldehyde solution in cacodylate buffer (or phosphate buffer) pH 7.3 is the best for ultrastructure, alternative 4% paraformaldehyde in phosphate-buffered saline at pH 7.3 for immunochemical stain. For GAG preservation some GAG precipitation chemicals are added for test. Sucrose suppresses dissolving GAG from tissue and isotonic concentration of 7.5% show no ultrastructural damage. As shown in the table, GAG is preserved in tissue fairly good in 7.5% sucrose solution. Cetylpyridinium chloride, alcian blue and unfixed freeze-dry tissue are tested (see Table and following slides). Supplement of sucrose 7.5% in common glutaraldehyde fixative gives fairly good results for the purpose. Wash solution after the fixation is also supplemented by sucrose before dehydration in 70% ethanol. [Unpublished]

Ultrastructure after sucrose-supplemented glutaraldehyde fixation

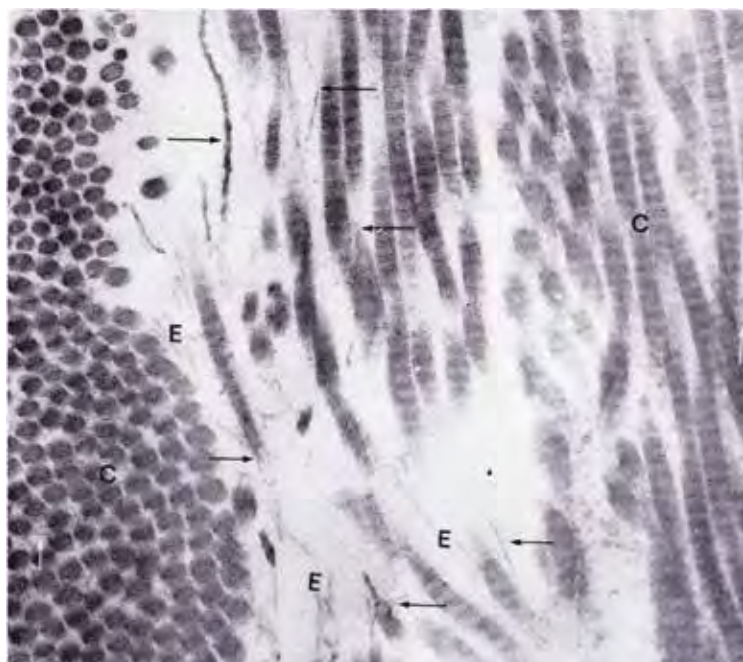


Fig. 1. Ground substance in the interfibrous space of reticular dermis after routine staining of uranyl acetate and lead citrate [1]. Ground substance appears filamentous of different sizes in normal dermis (arrows). The specimen is fixed in 6% glutaraldehyde solution of phosphate-buffered saline pH 7.3 with 7.5% sucrose. Ultrathin sections of epoxy resin are stained in uranyl acetate and lead citrate. E: elastic fibril, C: collagen fibrils. × 2,000.



Fig. 2. Ground substance in the vicinity of elastic fibre in reticular dermis after routine stain [1]. Ground substance in filament shape. The filaments are varied in thickness and join each other forming rough net-works. E: elastic fibre and microfibrils, C: collagen fibrils. Thick and thin arrows point at filamentous ground substance. $\times 20,000$.

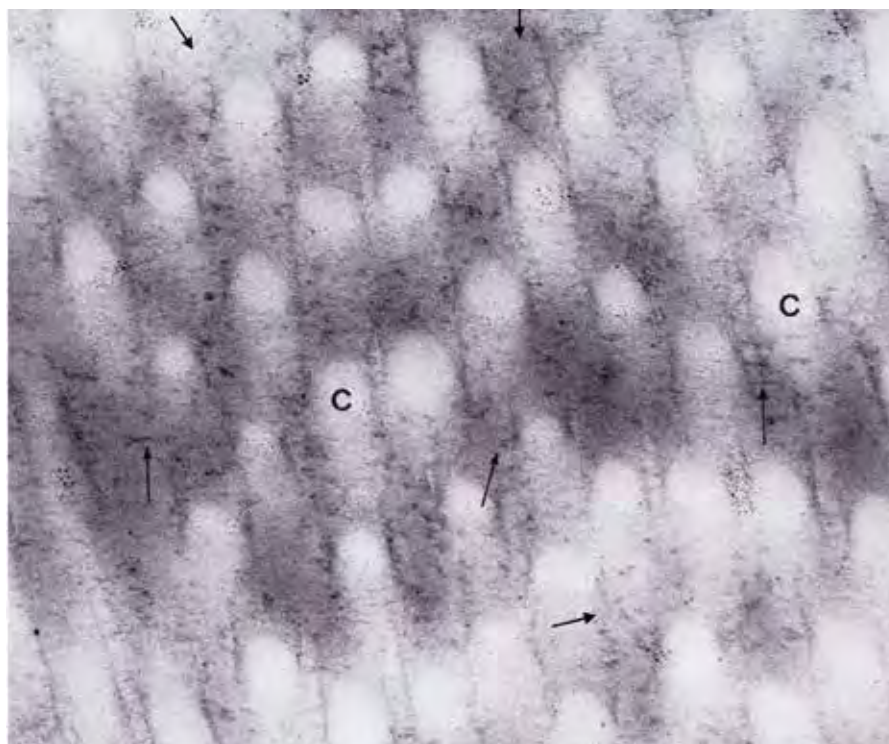


Fig. 3. Glucosaminoglycan (GAG) in the bundle of collagen fibrils in reticular dermis [1]. GAG appears in short filaments on the surface of collagen fibrils (c and arrows). $\times 20,000$.

Supplements in fixative alter the shape of ground substance

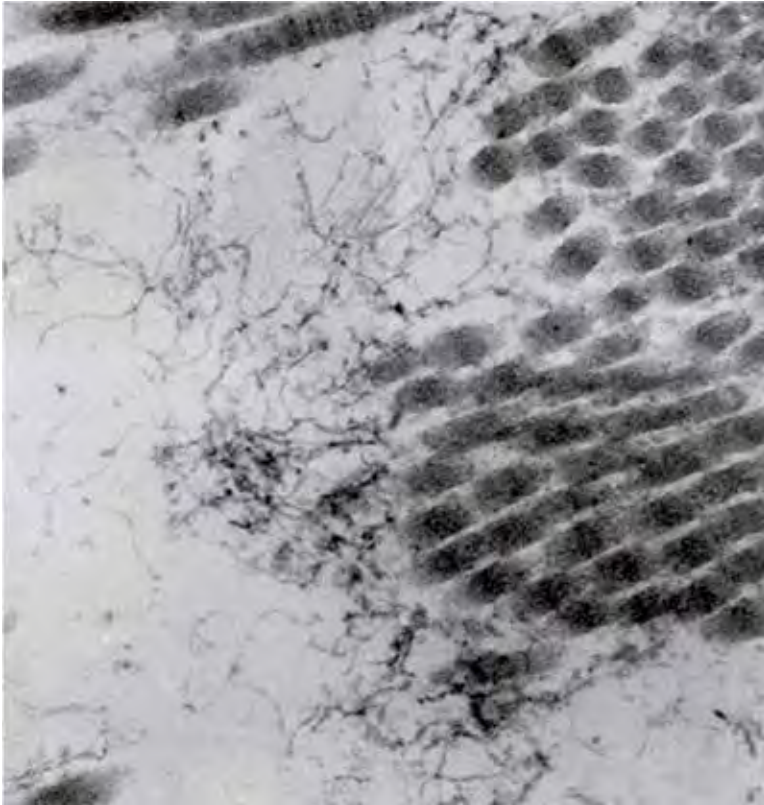


Fig. 4. Cetyl pyridinium chloride of the supplement for preservation of glycosaminoglycan in tissue [1]. Glutaraldehyde fixative, supplemented of cetylpyridinium chloride (CPC). CPC is in common use for biochemistry. Tissue is from myxoedema lesion after glutaraldehyde fixative with CPC after uranyl and lead citrate stain. Ground substance reveals filamentous shape. $\times 20,000$.

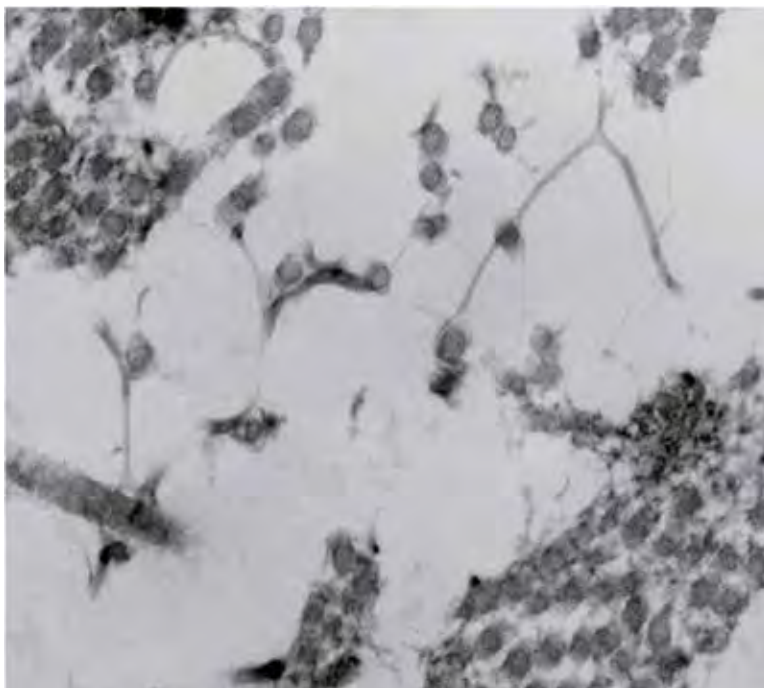


Fig. 5. Myxoedematous dermis fixed in glutaraldehyde fixative supplemented with 1% alcian blue [1]. Alcian blue is a precipitate and gives contrast on GAG. Ground substance appears as thick and thin straight filaments. $\times 20,000$.

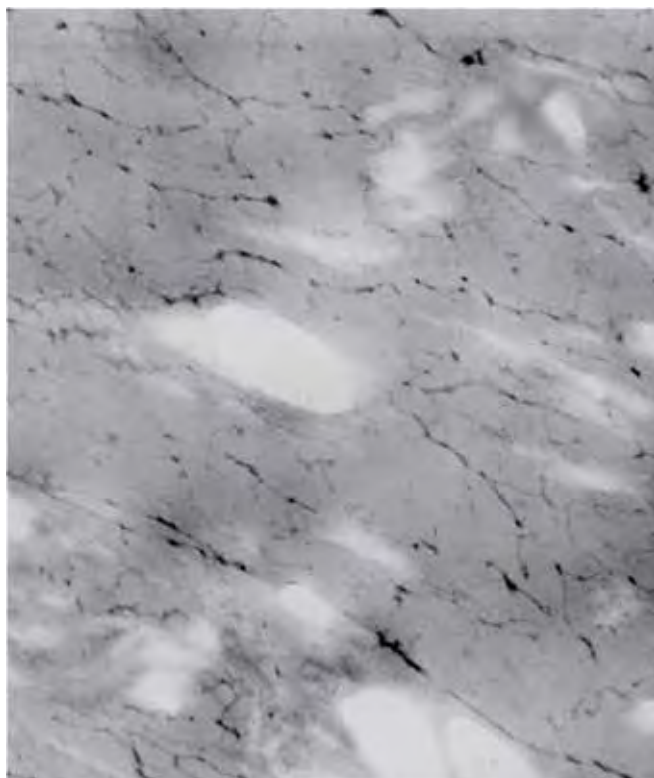


Fig. 6. Myxoedematous dermis is freeze-dried and embedded in epoxy resin. Stained by lead citrate, only [1]. Glucosaminoglycan reveals filamentous net-works with small dots. Collagen fibrils are unstained. $\times 20,000$.

Histochemistry



Fig. 7. Myxoedematous dermis (lead subacetate stain) [1]. Localized myxoedema, fixed in routine glutaraldehyde fixative with 7.5% sucrose. Ultrathin section of epoxy-resin is stained with 17% lead subacetate. Lead subacetate is known to precipitate glycosaminoglycan *in vitro*. Dots and filaments of ground substance figure are stained by lead subacetate. Dots are intensively stained, indicating high content of GAG in dots. Collagen fibrils (C) are unstained. $\times 20,000$.

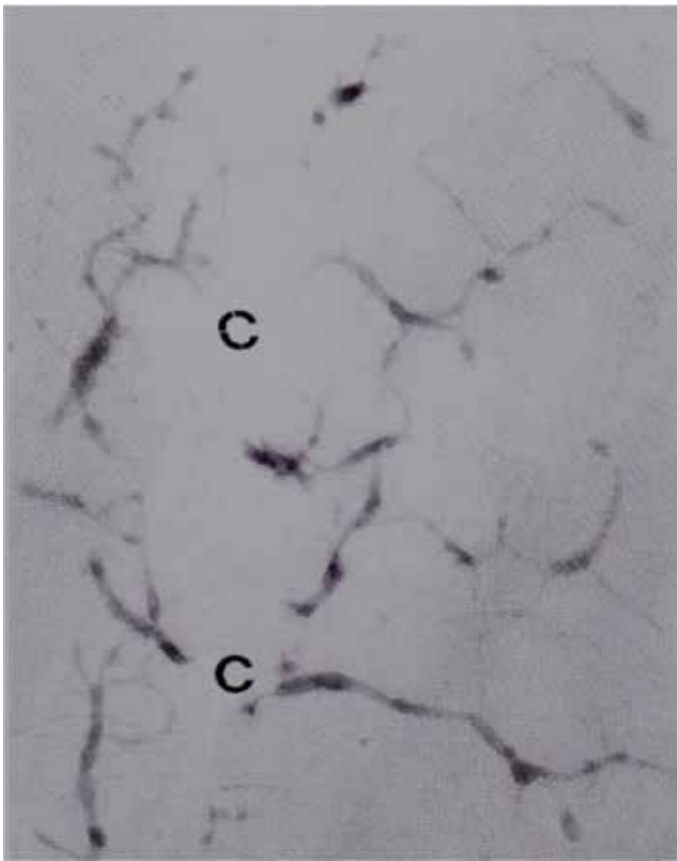


Fig. 8. Localized myxoedema [2] (ruthenium red stain). Fixed in the glutaraldehyde fixative with 7.5% sucrose. Epoxyresin-sections are stained by 0.5% ruthenium red [2]. Ruthenium red stains mast cell granules as well as glucosaminoglycan. The figure of ground substance, “filaments and spots” is stained by ruthenium red, while collagen fibrils (C) are unstained. $\times 20,000$.

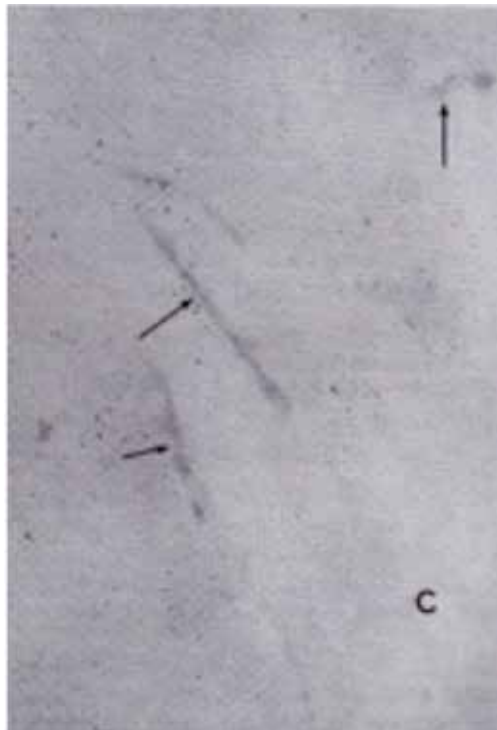
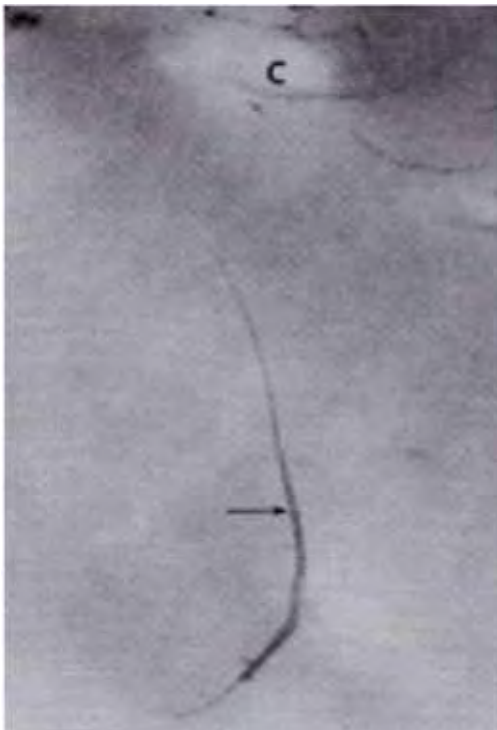


Fig. 9. Hyaluronidase influence on ground substance of normal dermis [1]. The specimens of normal dermis is fixed in sucrose-containing glutaraldehyde fixative. Ultrathin epoxy resin-sections are incubated in testicular hyaluronidase (Sigma) 3 mg (about 1,100 i.u.) in 0.1 mol phosphate buffer pH 7.1, at 37°C for 6 hours. The ultrathin sections are then stained by lead citrate. Left: Before hyaluronidase influence. Right: After the influence by testicular hyaluronidase (Sigma), filamentous figure reduced contrast and lost sharp figure. $\times 50,000$.

Protein core of ground substance

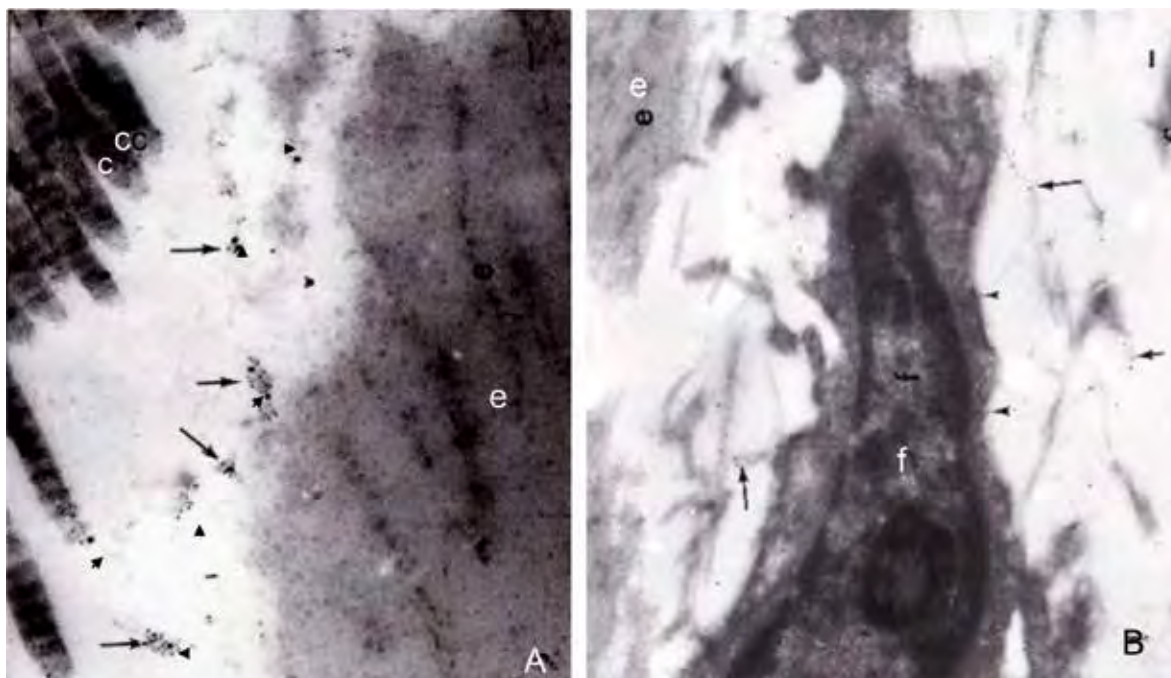


Fig. 10 A and B. Collagen types V and VI in ground substance [3]. Immune electron microscopy. Type V collagen by 5 nm gold particles (thick arrow) and type VI collagen by 10 nm gold particles (arrow-heads). Glycosaminoglycan filaments contain type V and VI collagen. Type VI collagen is filamentous (core protein of ground substance), join each other and form networks in the interfibrous space and associate to glycosaminoglycan. Type V collagen binds to type VI collagen, fibres and cells. e: elastic fibre, f: fibroblast. A: $\times 20,000$. B: $10,000$.

Pretibial localized myxoedema. Glycosaminoglycan and proteoglycan

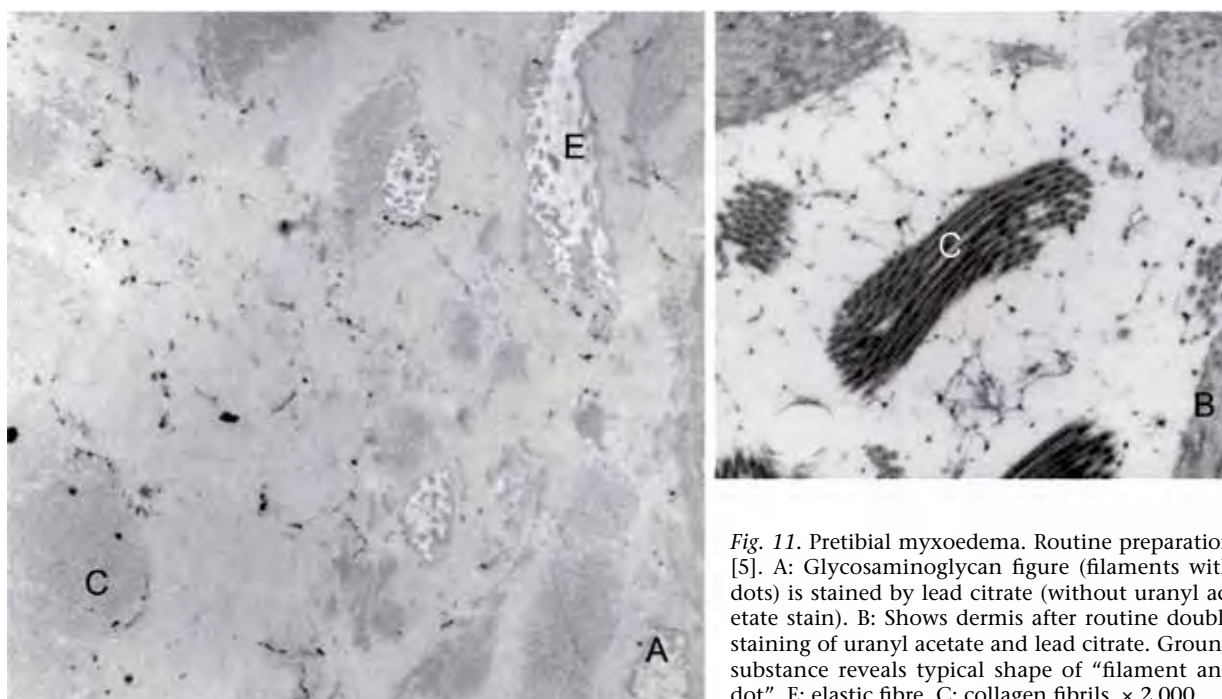


Fig. 11. Pretibial myxoedema. Routine preparation [5]. A: Glycosaminoglycan figure (filaments with dots) is stained by lead citrate (without uranyl acetate stain). B: Shows dermis after routine double staining of uranyl acetate and lead citrate. Ground substance reveals typical shape of "filament and dot". E: elastic fibre, C: collagen fibrils. $\times 2,000$.

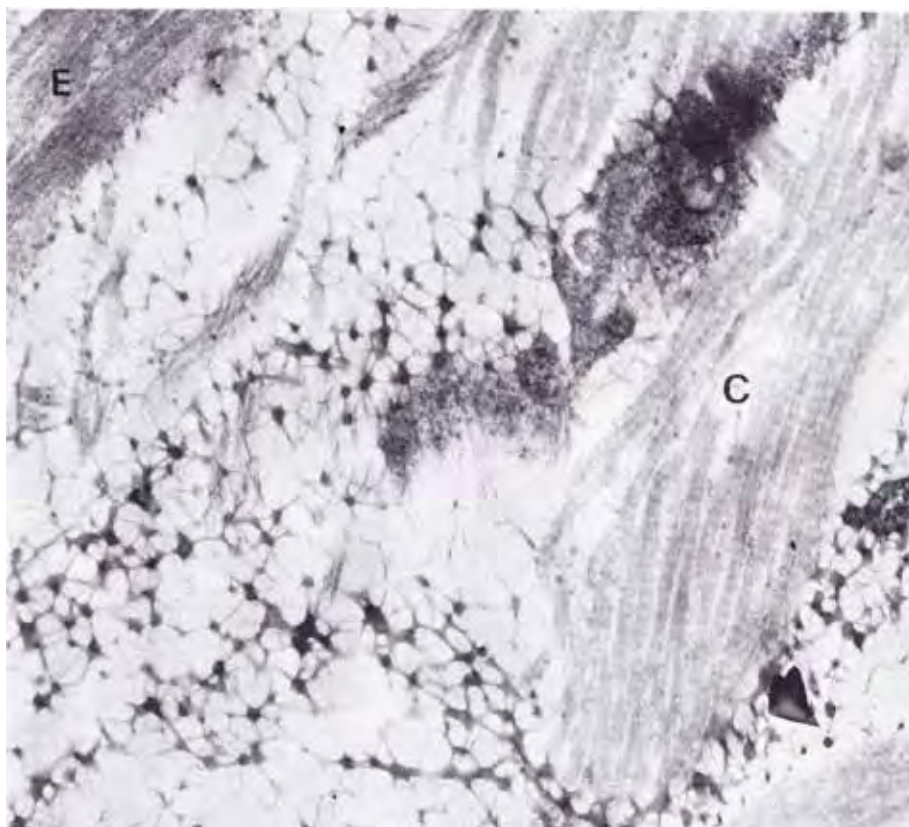


Fig. 12. Pretibial myxoedema [5]. Ground substance is a complex of glycosaminoglycan (GAG) and type VI collagen in various ratio. Ground substance presents characteristic figure “filaments and dots” in the interfibrous space. However, the figure is varied in size and shape. Dots seem to express rich content of GAG and filaments are more collagenous. GAG-rich ground substance is shown in the interfibrous space of dermis. Ground substance appears as “dots and filaments” in the interfibrillar space. C: collagen fibrils. × 20,000.



Fig. 13. Pretibial myxoedema [5]. The surface of broad elastic fibre is covered by dense coat and dots of glycosaminoglycan (A). Dense large dots and faint filaments are around elastic fibre. Thin arrows points at elastic microfibrils. E: matrix of the broad elastic fibre. × 20,000.

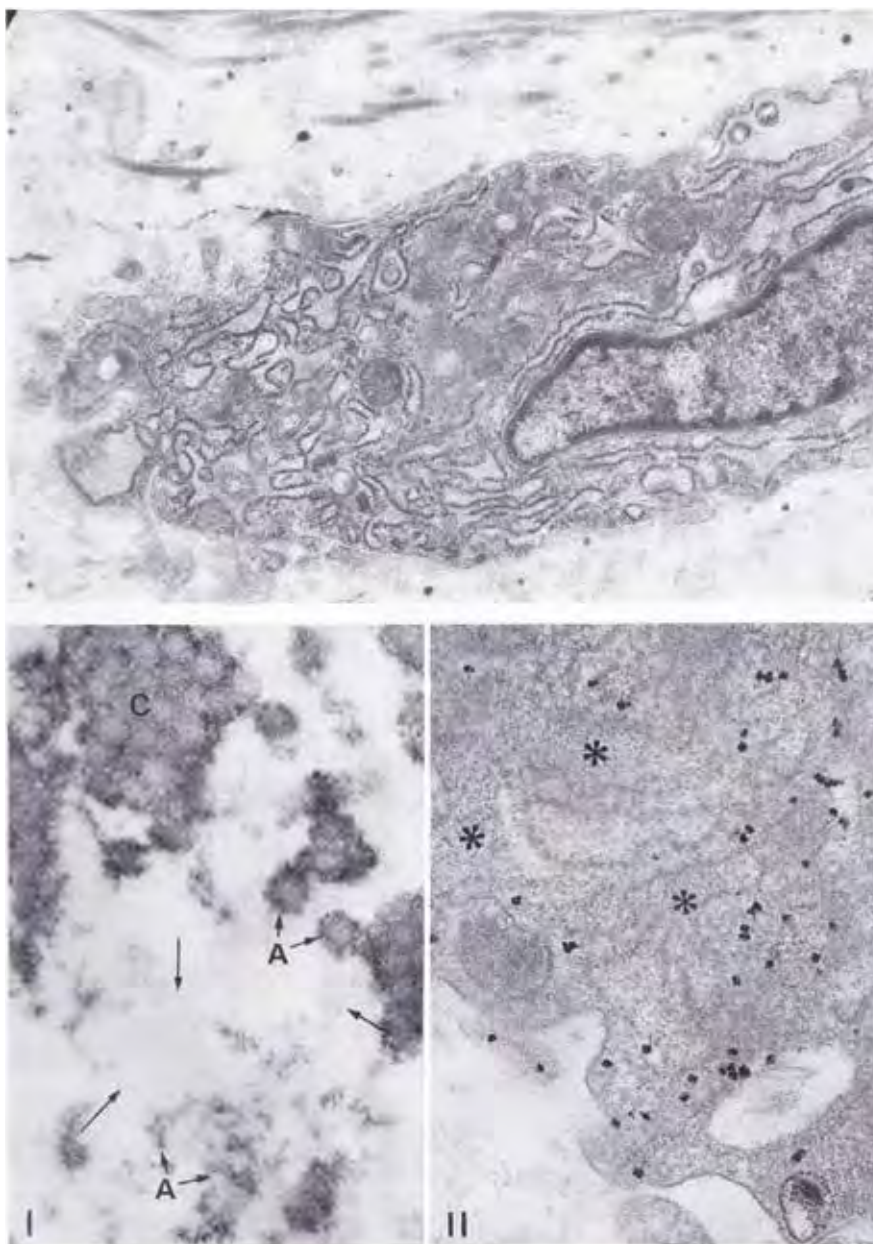


Fig. 14. Scleromyxoedema. Glycosaminoglycan (GAG) and proteoglycan in myxoedematous dermis [6]. Proteoglycan is demonstrated by periodic acid oxidation followed by silver proteinate [4] or by silver methenamine [5] staining. Upper picture shows proteoglycan demonstrated by routine method. No GAG figure is seen in the dilated cisterna of fibroblasts. GAG filaments are in the space around fibroblast. Granular endoplasmic reticula show dense granules of ribosomes. $\times 20,000$. Lower-left picture (I) shows thick silver stain covering over collagen fibrils, while GAG filaments are unstained in the interfibrillar space. $\times 60,000$. Lower right picture (II) shows after periodic acid silver proteinate stain [3]. Fibroblast in details. Cisterna is dilated (asterisks) and contain fine silver granules and dense dots of silver. $\times 60,000$.

Papular mucinosis

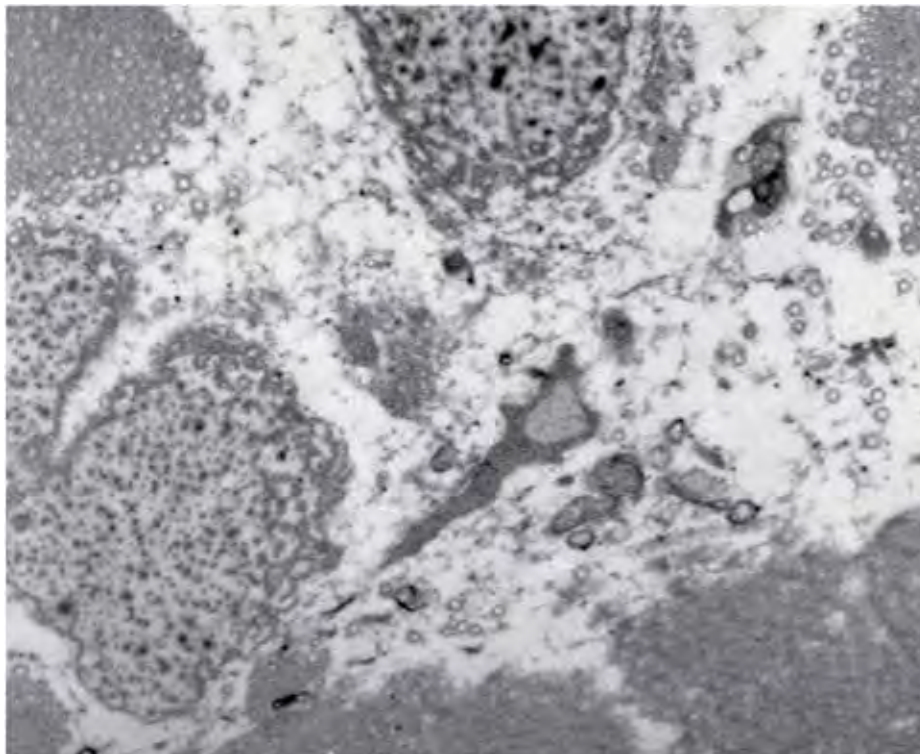


Fig. 15. Papular mucinosis of Steigleder. Glycosaminoglycan (filaments and dots) in the interfibrous space. Elastic fibre show senile pattern. $\times 10,000$. [Unpublished]

Lupus erythematosus

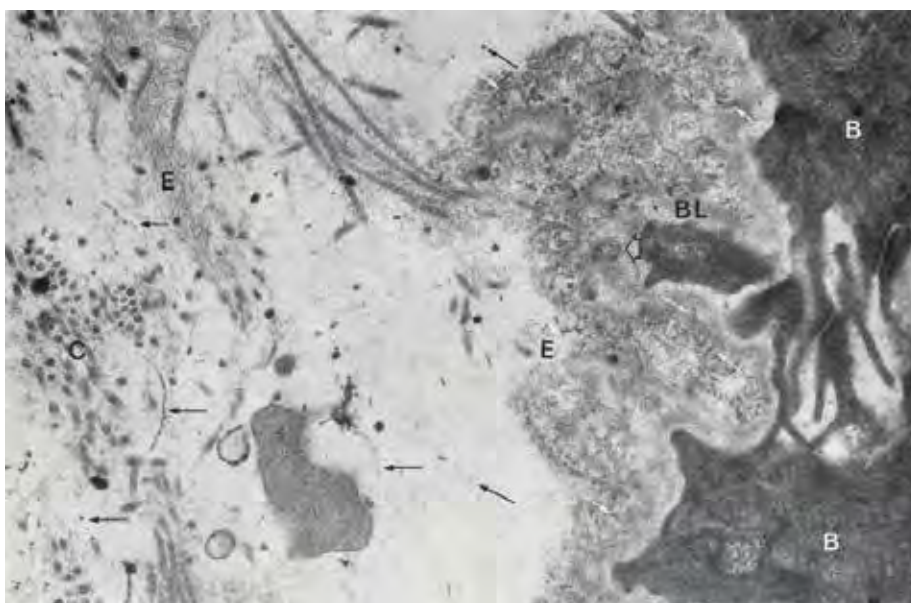


Fig. 16. Lupus erythematosus [7]. The dermis shows glycosaminoglycan in the wide interfibrous space. Arrows point at some examples. C: collagen fibrils, E: elastic fibre, BL: basal lamina, B: basal cells. $\times 7,500$.

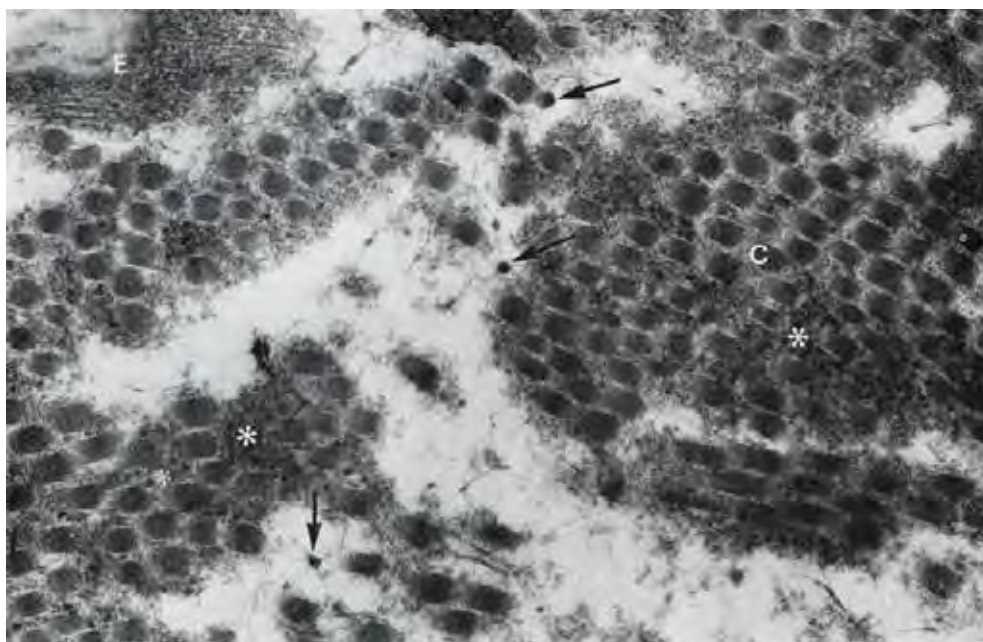


Fig. 17. Lupus erythematosus [7]. Reticular dermis in the lesion. Glycosaminoglycan are numerous between collagen fibril bundles (C) and in the collagen fibril bundles (asterisks). $\times 15,000$.

Morphoea

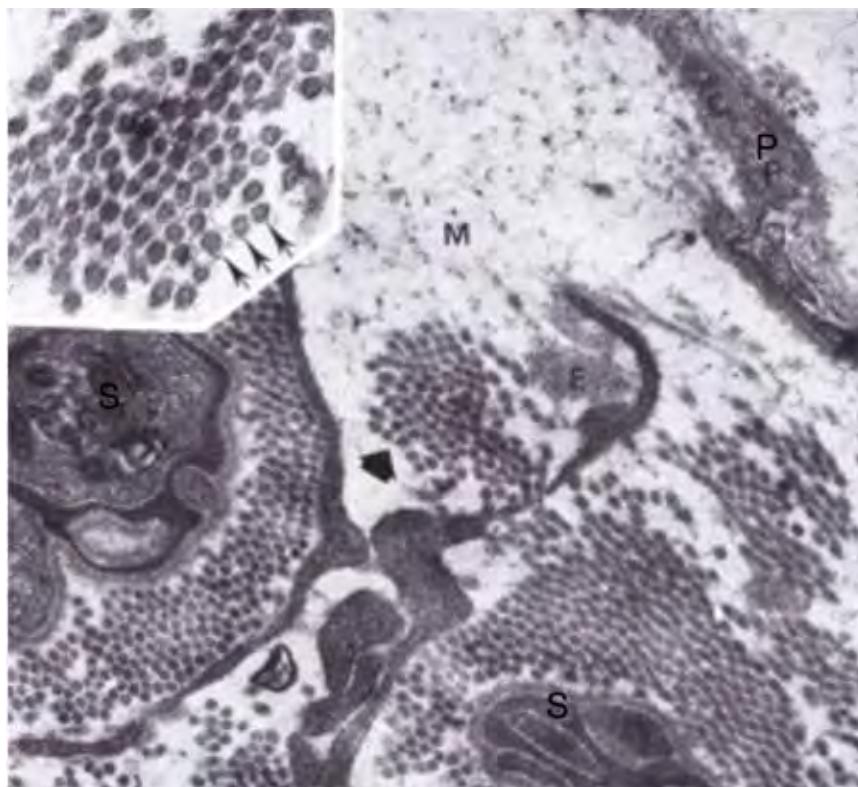


Fig. 18. Morphoea. Ground substance increased in perineurium (M). Collagen fibrils are degraded. A wide arrow-pointed area is shown in the inset. Collagen fibrils show glycosaminoglycan filaments on the surface (arrows). P: Pericyte, S: Schwann cells. $\times 25,800$. Inset $\times 51,600$. [Unpublished]

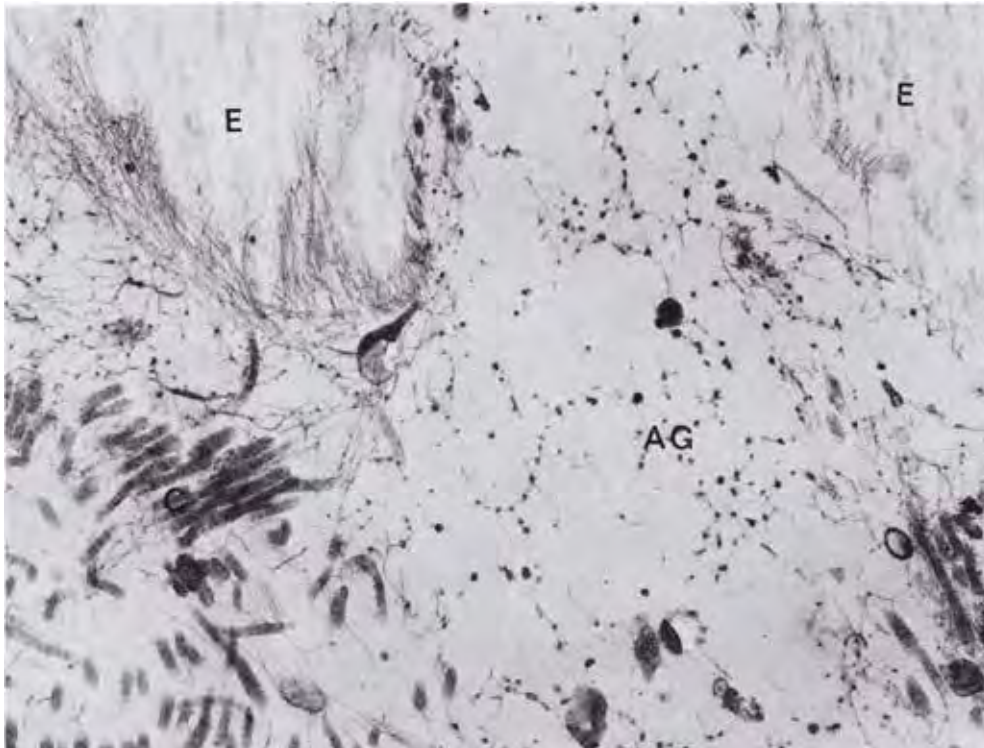


Fig. 19. Morphoea [8]. Glycosaminoglycan show many dots in the interfibrillar space. E: elastic fibre, C: collagen fibrils, AG: glycosaminoglycan. $\times 7,000$.

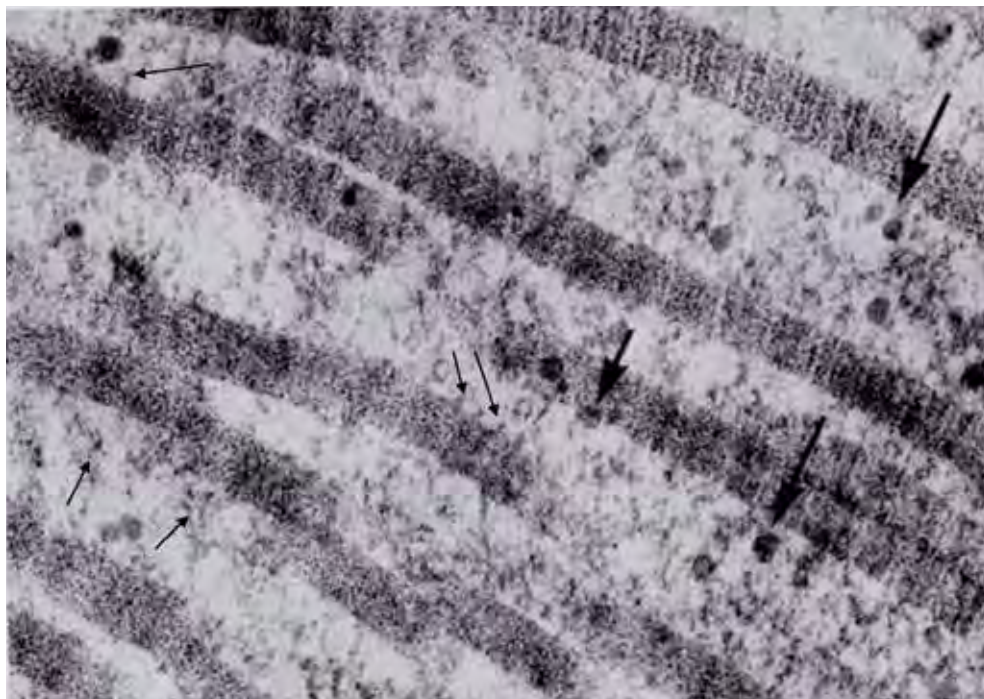


Fig. 20. Scleromyxoedema [6]. Thick arrows point at some examples of glycosaminoglycan (dots) between collagen fibrils. Thin arrows show examples of thin filaments on the collagen fibril surface. $\times 30,000$.

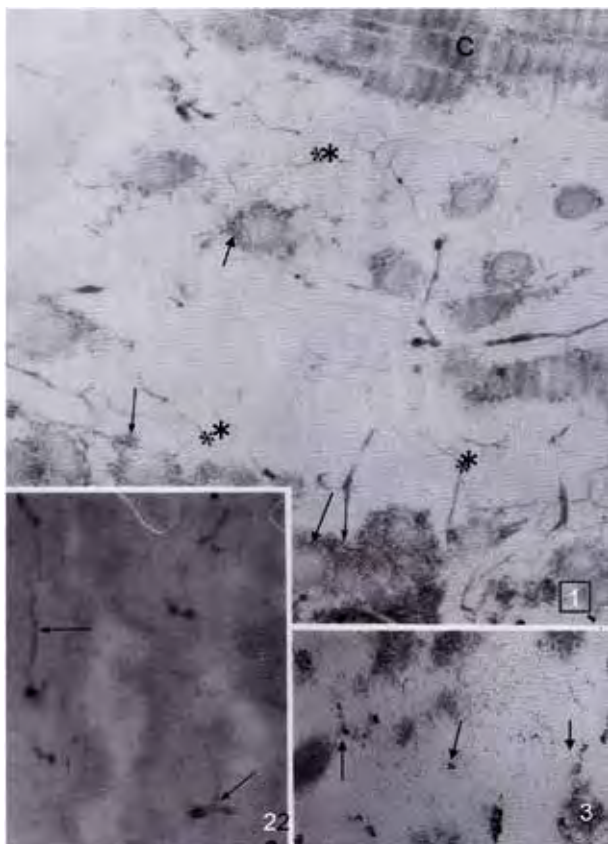


Fig. 21. Fibrodysplasia ossificans progressiva [9]. Fig. 1: Glycosaminoglycan (GAG) (*) and proteoglycan (arrows). Fig. 2: Glycosaminoglycan stained by ruthenium red (arrows). Staining confirm GAG in the interfibrous space. Fig. 3: Arrows pointed at dots after routine stain of uranyl acetate and lead citrate. $\times 20,000$.

Basal cell carcinoma

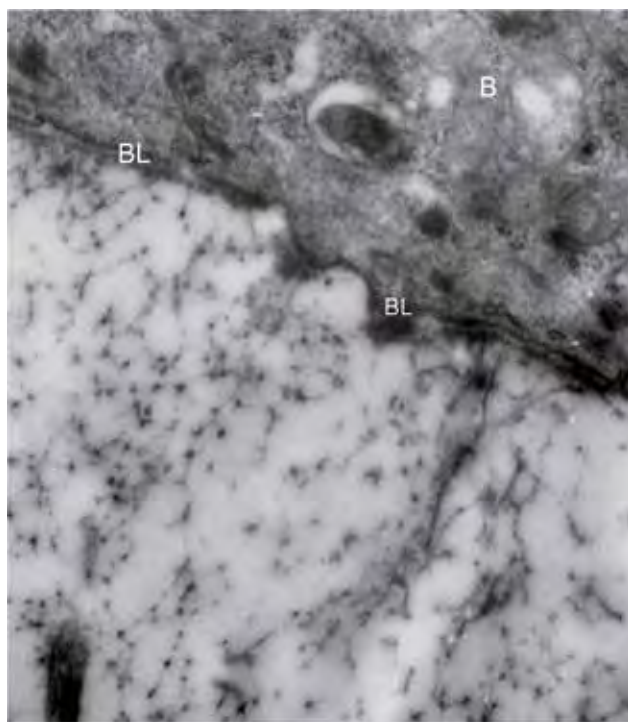


Fig. 22. Basal cell carcinoma [10]. Myxoedematous stroma, outside of the cancer nest. Numerous glycosaminoglycan (dots and filaments) indicate myxoedematous stroma. BL: basal lamina in fragments on the basalioma cell membrane, B: cell of basal cell carcinoma. $\times 15,000$.

IV. Junction

Overview	
• Ultrastructure	Figures 1–4
• Junction in nerve and vessel	Figures 5–7
• Histochemistry	Figures 8–14, Table I
• Collagen types	Figure 15–18
• Formation	
- Fetal skin	Figure 19
- Formation. Organ culture	Figures 20–28
- Formation. Cell culture	Figures 29–33
• Dermoepidermal junction in dermatoses	
- Classification	Table II, Figures 34–35
- Penetration	Figures 36–38
- Dermoepidermal separation	
» Epidermal separation	Figures 39–49
» Subepidermal separation, real type	Figures 50–55
» Subepidermal searation, false type	Figures 56–63
» Dermolytic separation	Figures 64–65
- Produktive change	
» Disorders	Figures 66–74
- Basal cell carcinoma	Figures 75–81
- Squamous cell carcinoma	Figures 82–85
- Miscellaneous	
» Mucin	Figure 86
» Amyloid	Figures 87–88
» Hyalin	Figures 89–90
» Filamentous body	Figures 91–92

Ultrastructure

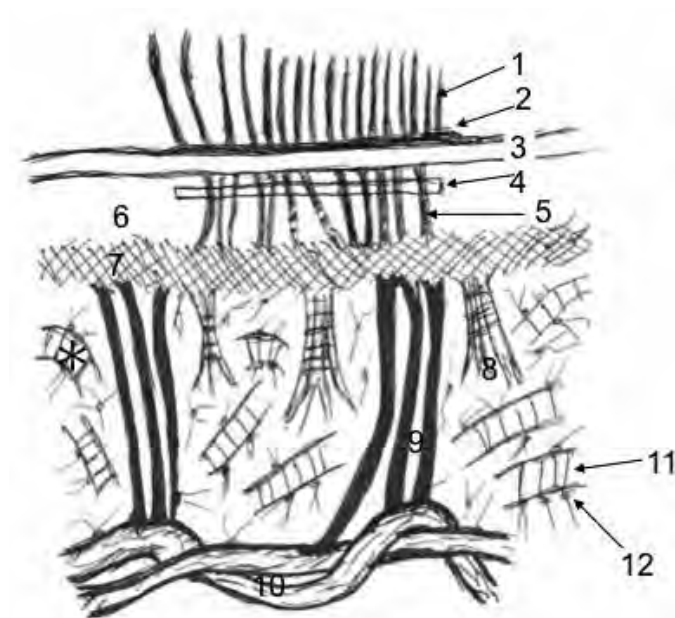


Fig. 1. Terminology of ultrastructural components. 1) Tonofilaments. 2) Attachment plaque. 3) Cell membrane. 4) Junction plate. 5) Anchoring filaments. 6) Subepidermal space (Lamina lucida). 7) Basal lamina (Lamina densa). 8) Anchoring fibril. 9) Ascending rami of elastic microfibril. 10) Subpapillary plexus of elastic fibre. 11) Collagen fibrils. 12) Glycosaminoglycan.

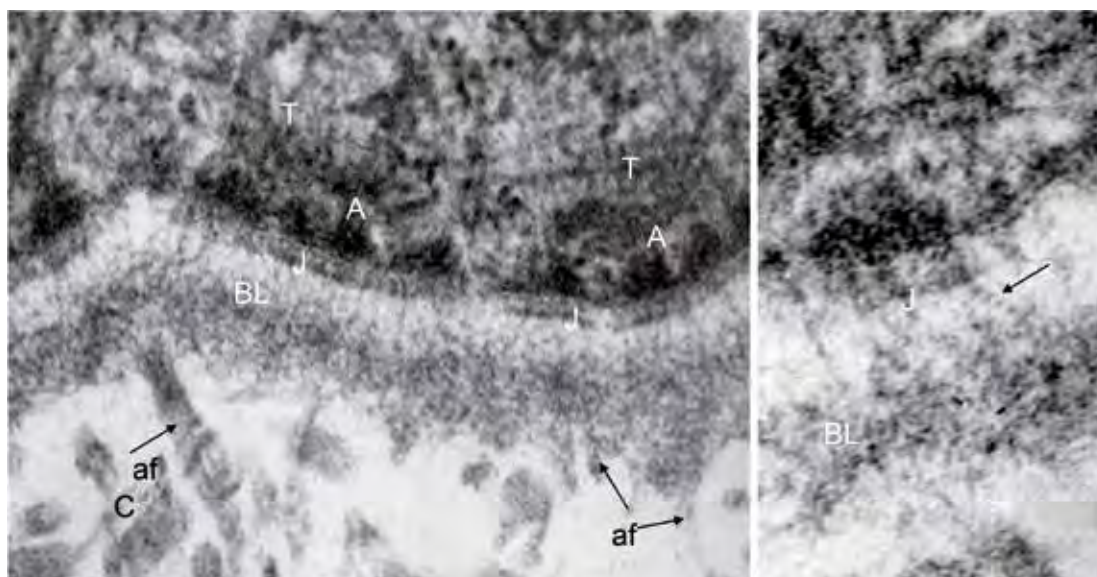


Fig. 2. Hemidesmosomes, basal lamina and anchoring filaments [1, 2, 3]. Left: Tonofilaments (T) terminate on inner cell membrane and form attachment plaque (A) and junction plate (J). Anchoring filaments extend upwards from basal lamina (BL) to attachment plaque (A) through junction plate (J). Anchoring fibrils (arrow af). Collagen fibril (C). $\times 40,000$. Right: A hemidesmosome and anchoring filaments. Arrow points at cross bands of anchoring filaments. BL shows filamentous structure inside of anchoring filaments. Basal lamina shows filamentous structure inside. $\times 60,000$.

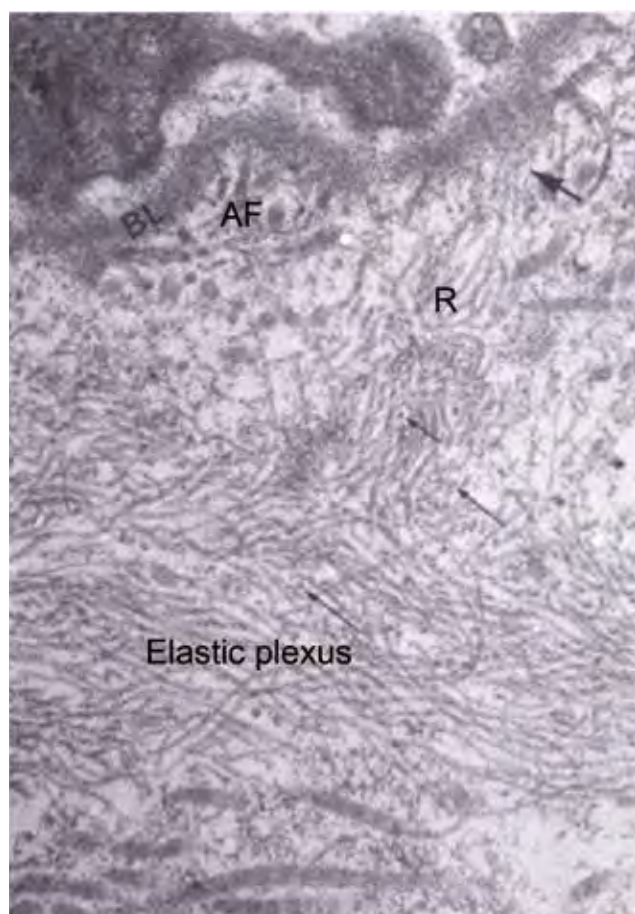


Fig. 3. Dermoepidermal junction [3, 4]. Elastic microfibrils of ascending rami (R), (thin arrows) from subpapillary elastic plexus fuse to basal lamina (BL) (thick arrow). Anchoring fibrils (AF) extended from BL into dermis and end free in the uppermost dermis $\times 15,000$. Schematic explanation (see Fig. 1) [1–3, 6].

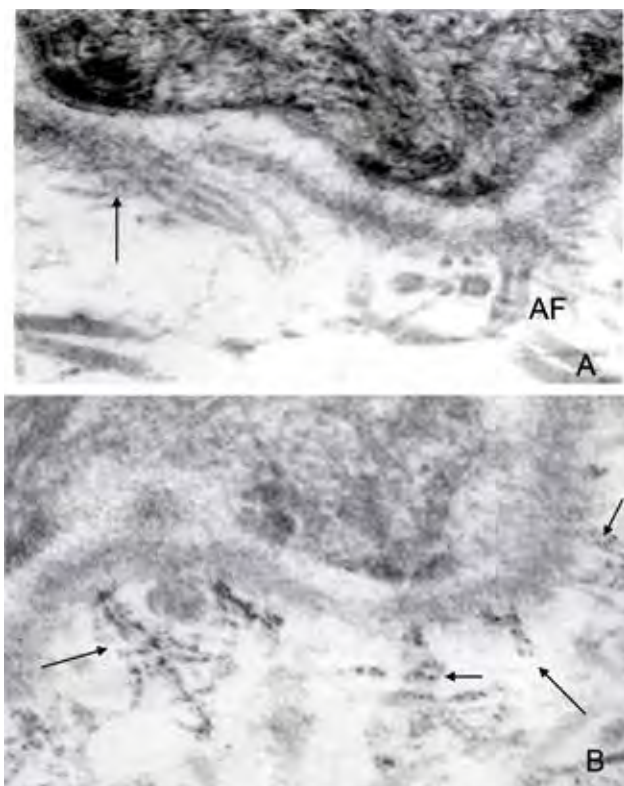


Fig. 4. Elastic microfibril anchoring and anchoring fibrils [3, 5]. A. Elastic microfibrils fuse to basal lamina (arrow). Anchoring fibrils (AF) show distinct cross bands, $\times 20,000$. B. Cross bands of AF and threads in the basal lamina are stained by periodic acid-silver proteinate (arrows). No counter-stain. Positive stain indicate proteoglycan content in the structure. $\times 20,000$.

Junction in nerve and vessel

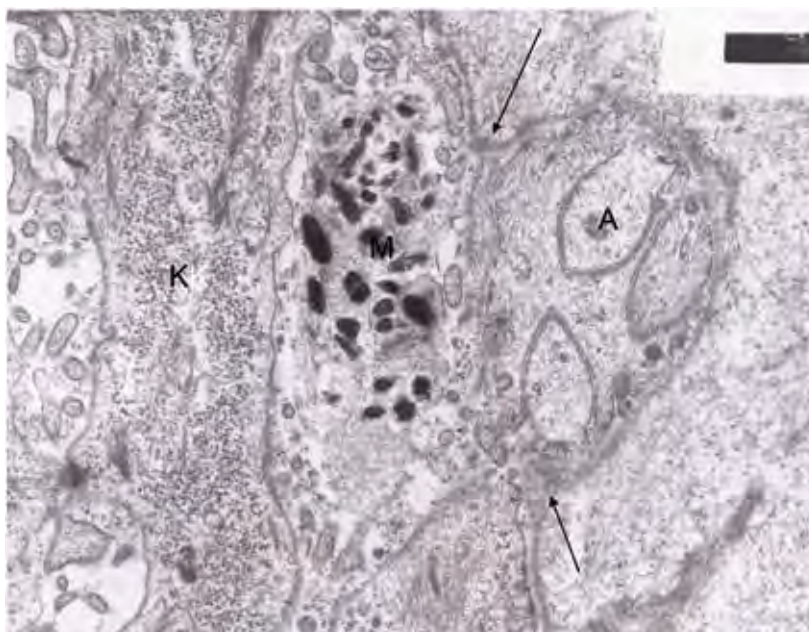


Fig. 5. Basal lamina of Schwann cell fuses to basal lamina of epidermis (arrows). Axon faces directly to melanocyte [3]. M: melanocyte, A: axon, K: keratinocyte. $\times 10,000$.



Fig. 6. Basal lamina of peripheral nerve [3]. Schwann cells and pericytes are surrounded by basal lamina. Elastic microfibril anchoring of basal lamina and anchoring fibrils are scarcely recognized. a: axon, $\times 5,000$.

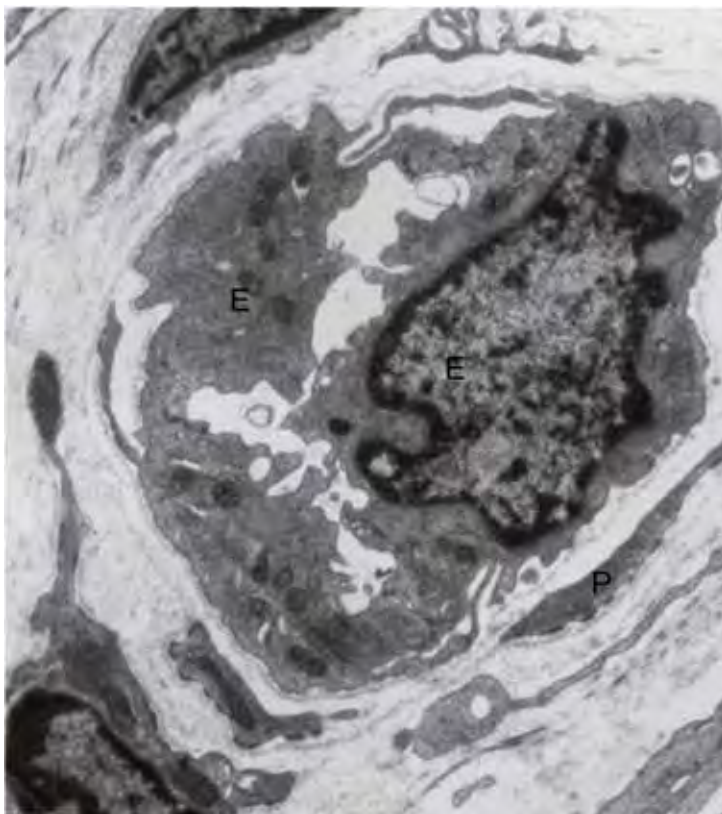


Fig. 7. Blood vessel. Pericyte (P) shows basal lamina only on the dermal aspect [3]. Mesenchymal cell tissues, such as vessel, nerve, smooth muscle and fat cells also produce basal lamina and these tissues anchor with connective tissue. However, hemi-desmosomes, anchoring filaments, anchoring fibrils and elastic fibril anchoring are hardly found. Endothelial cell (E), $\times 5,000$.

Histochemistry



Fig. 8. Effect of clostridial collagenase on junction and dermal connective tissue [7]. Clostridial collagenase (Sigma) influences normal fresh skin for 6 hours. Epidermis (E) is preserved (seen in the right-upper corner of the picture). Junction structure and collagen fibrils are dissolved. Dermis is filled by collagen aggregate (asterisks). See Section II. Collagen. $\times 2,000$.

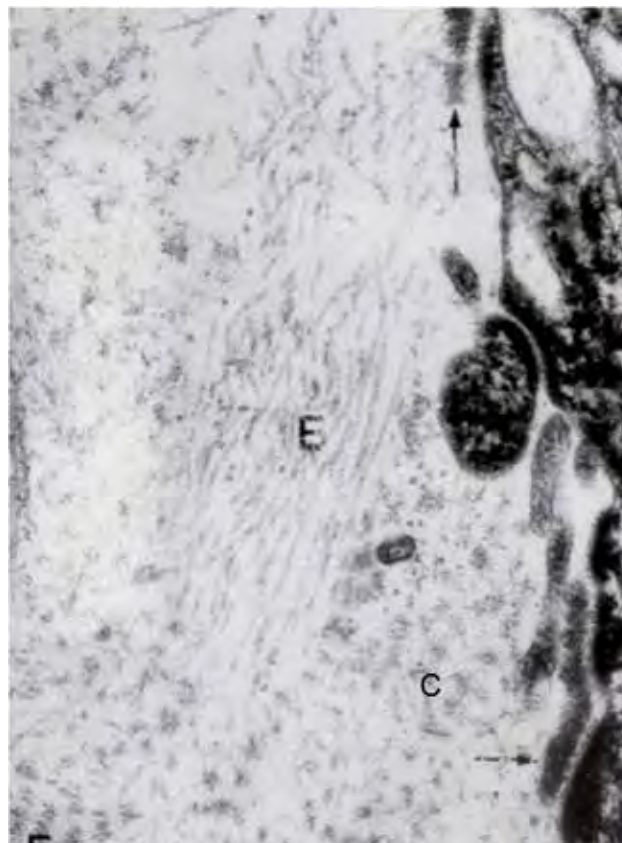


Fig. 9. Influence by clostridial collagenase in details (uppermost area of the former picture). Collagen fibrils appear as filamentous aggregate of collagen (collagen aggregate) (C). Elastic microfibrils are intact (E). Basal lamina is almost disappeared. Rest of basal lamina is pointed by arrows. $\times 20,000$.

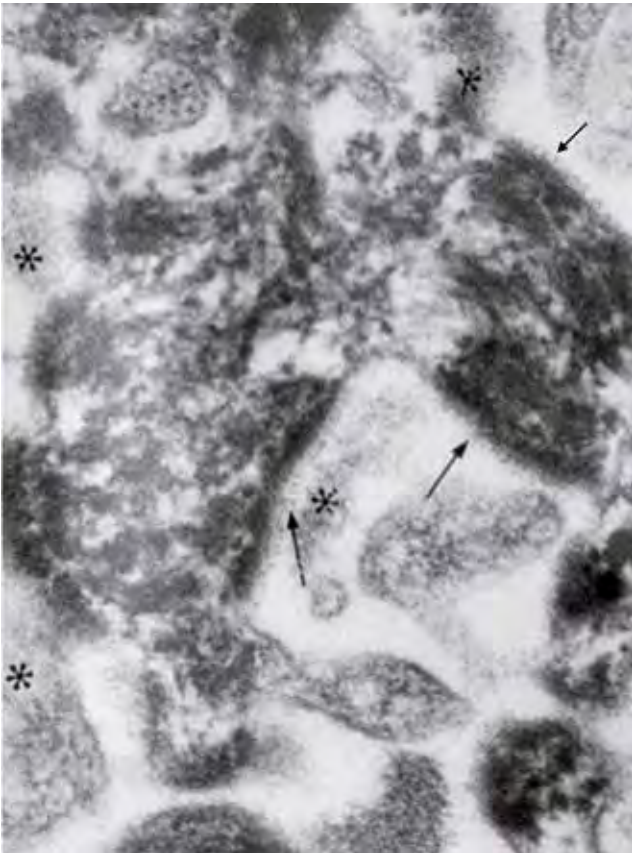


Fig. 10. Influence by clostridial collagenase. Hemidesmosomes are left intact (arrows). Basal lamina, junction plate and anchoring filaments are removed. Asterisk points rest of basal lamina. $\times 20,000$.

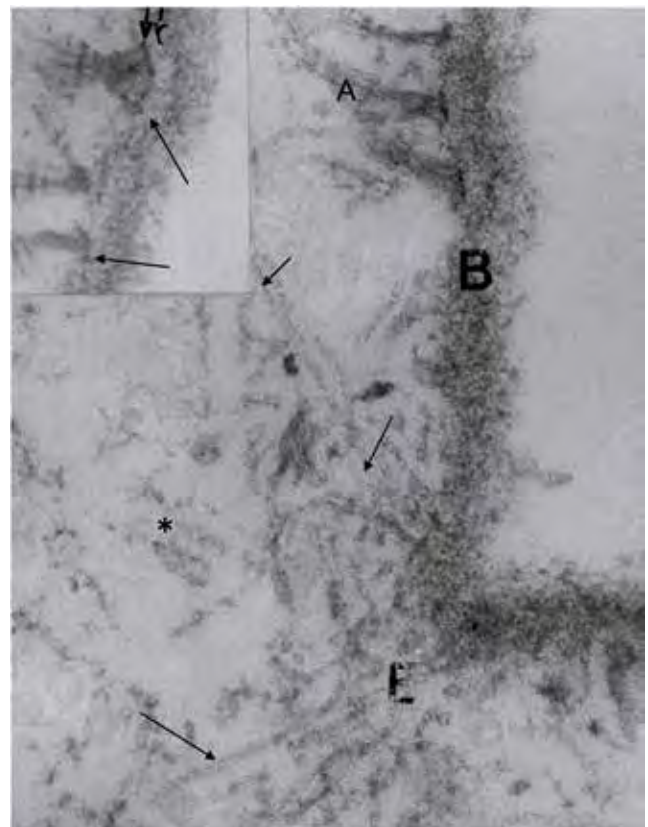


Fig. 11. The junction after the influence by the used culture media [7]. Culture media from 2-day-old cell culture of myofibroblast of human dermis. (See Section II. Collagen). Basal lamina (B), anchoring fibrils (A) and elastic microfibrils (arrows) are left intact. Collagen fibrils are removed. Collagen aggregate (asterisk), $\times 20,000$. Inset shows a clear zone between basal lamina and anchoring fibril (arrows). $\times 40,000$.



Fig. 12. Pancreatic elastase on normal skin piece for 6 hours [7]. Elastic matrix and basal lamina is dissolved. Collagen fibrils (C) and elastic microfibrils are unaffected (arrow). Details appear in Fig. 13. $\times 2,000$.

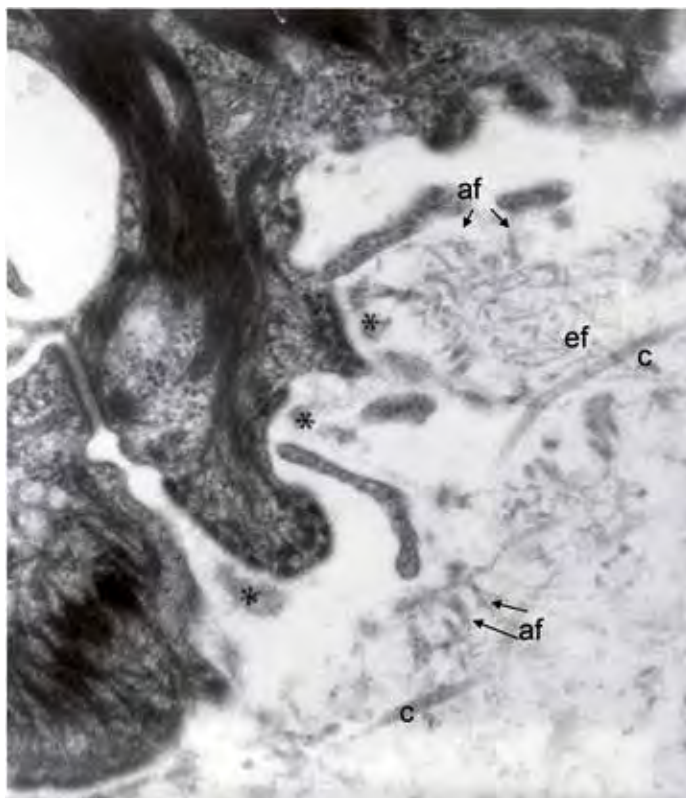


Fig. 13. Pancreatic elastase influences dermoepidermal junction [7]. Basal lamina and anchoring filaments disappear, while collagen fibrils (c), anchoring fibrils (arrow, af), elastic microfibrils (ef) and hemidesmosomes are intact. $\times 10,000$.



Fig. 14. Dermoepidermal junction after influence by dithioerythritol for 6 hours [7–10]. Basal lamina and anchoring filaments are influenced (arrows) but anchoring fibrils and collagen fibrils are intact. × 20,000. Inset shows intact anchoring fibrils and disintegrated basal lamina (B). × 40,000.

Table I. Susceptibility of enzymes and chemicals of junction components
Experimental degradation of normal dermo–epidermal junction

	Clostridial collagenase	Cellular collagenase ^a	Elastase	Dithioerythritol
Junction plates	+	–	–	+
Anchoring filaments	+	+	+	+
Basal lamina	+	(+)	+	+
Anchoring fibrils	+	–	–	+
Collagen fibrils	+	–	–	–
Elastic fibrils	–	–	–	+
Elastic matrix	–	+	+	–

^aCrude enzyme separated from used culture medium of skin.

+: degraded; (+): basal lamina is separated from anchoring fibrils. Lamina itself is not influenced; –; not degraded.

Collagen types of junction structure

Basal lamina and anchoring filaments are composed of type IV collagen [11] and kallinin, a variant of laminin [12], and anchoring fibrils contain type VII collagen and proteoglycan.[3,4, 5].

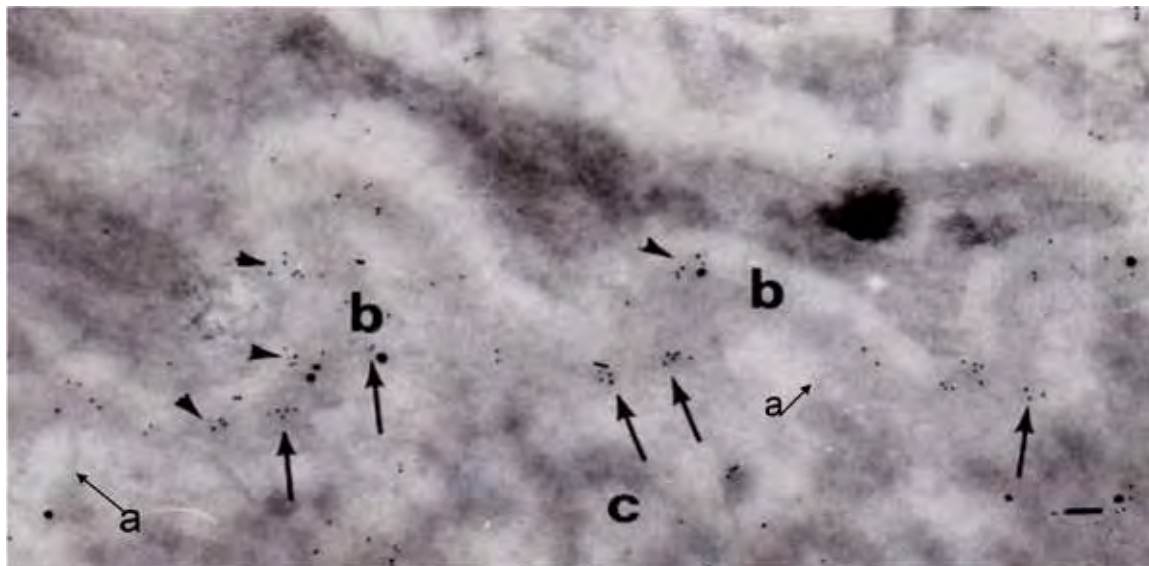


Fig. 15. Collagen types V and VI in the junction [12]. Collagen type V, 5 nm gold particles (arrow-heads). Collagen type VI collagen 10 nm gold particles (arrows). Anchoring fibrils (arrows a), basal lamina (b), collagen fibrils (c). × 10,000. See details in Figs 16, 17.

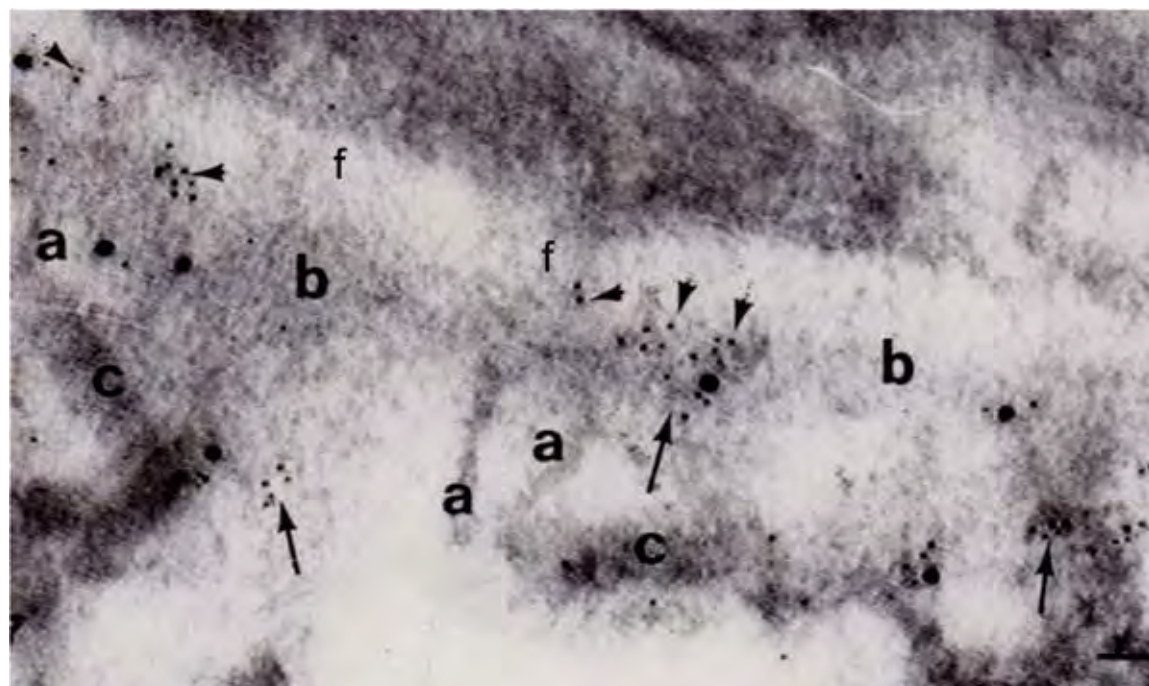


Fig. 16. Dermoepidermal junction. Collagen Types V and VI. Collagen type V, 5 nm gold particles (arrow-heads). Collagen type VI 10 nm gold particles (arrows). Anchoring filament (f), anchoring fibrils (a), basal lamina (b), collagen fibrils (c). × 33,000.

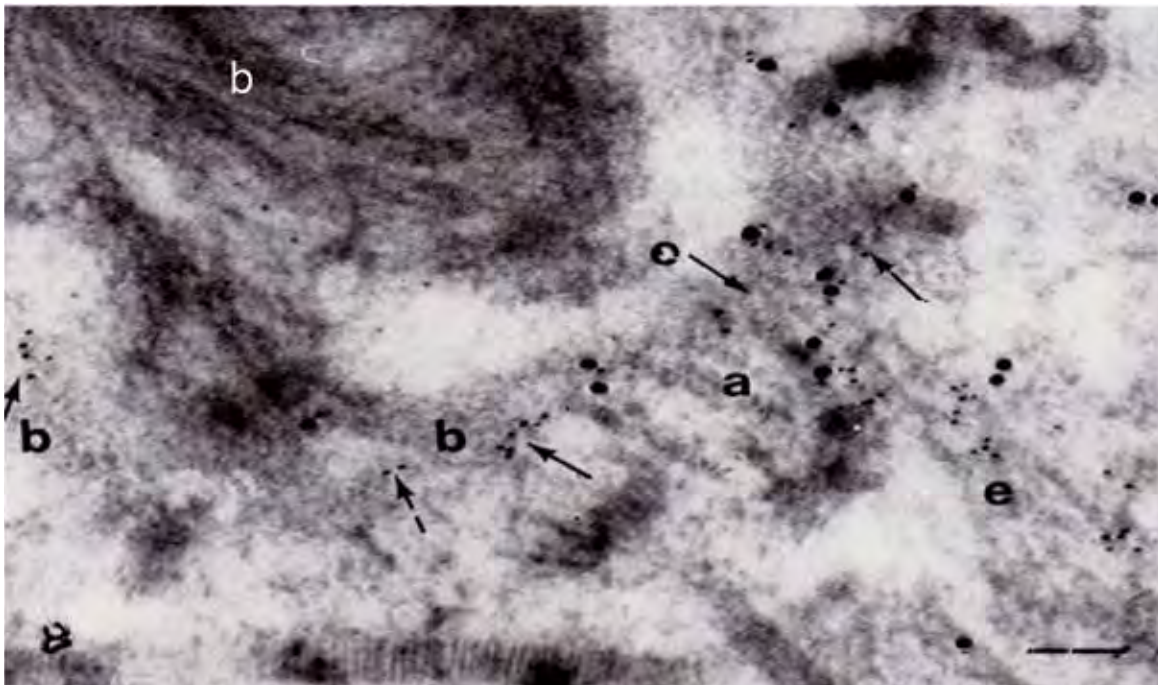


Fig. 17. Dermoepidermal junction. Collagen type V and collagen type VI (continued). Collagen type V, 5 nm gold particle. Collagen type VI, 10 nm gold particle. Anchoring fibril (a), basal lamina (b), elastic microfibrils (e). $\times 33,000$.

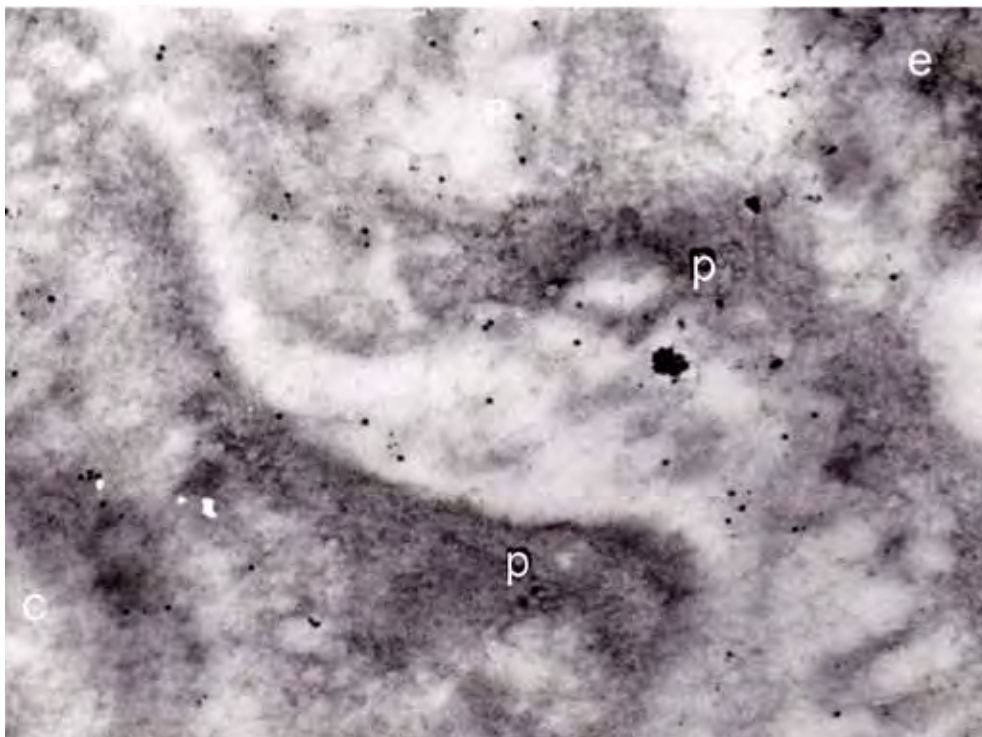


Fig. 18. Vascular wall. Collagen types IV and V. Collagen type IV, 5 nm gold particle. Collagen type V, 10 nm gold particle. Type IV collagen in the basal lamina and type V collagen on the surface and in the space. Endothelial cell (e), pericyte (p), collagen fibrils (c). $\times 20,000$.

*Formation of dermoepidermal junction
Fetal skin [8]*

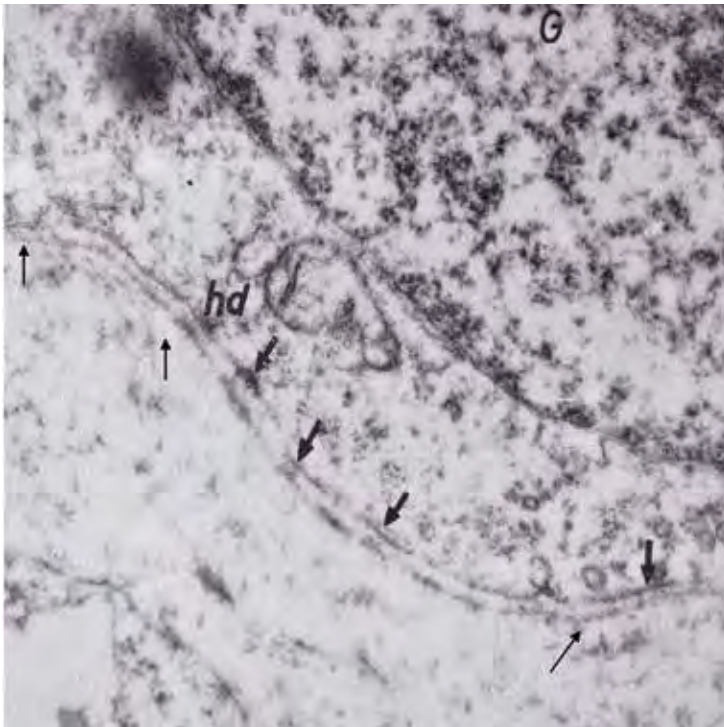


Fig. 19. Incomplete dermoepidermal junction in 12-week-old foster [8]. Hemidesmosomes (arrows and hd). Keratinocyte in germinative cell layer (G). Basal lamina is uneven in thickness, thicker on the opposed site of hemidesmosomes (arrows). Anchoring filaments extend to basal lamina from thickened cell membrane. Anchoring fibrils are scarcely seen, and extend from basal lamina (thin arrows) to dermis. × 10,000.

*Formation of dermoepidermal junction
Experimental formation in organ culture of skin graft. [Unpublished Figs 20–28] [28–30].*



Fig. 20. Organ culture of skin at 8 hours. Formation of dermoepidermal junction is experimentally studied by organ culture of normal skin. Dermoepidermal junction in the mother piece. Keratinocytes lost hemidesmosomes and retract cytoplasm. Basal lamina of the mother piece is on the dermal surface. Subepidermal space is dilated like a pocket (arrows). × 10,000.

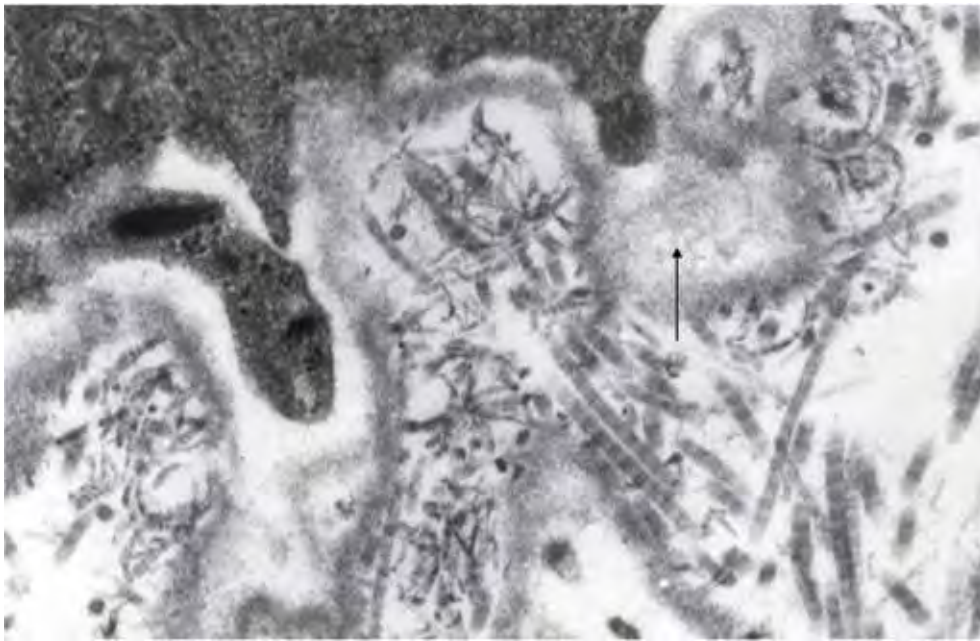


Fig. 21. Organ culture of normal skin for 12 hours. Basal lamina is thickened. Hemidesmosomes are bury. Arrow indicated are basal lamina cut tangentially. Anchoring fibrils are distinct and increased in number. $\times 10,000$.

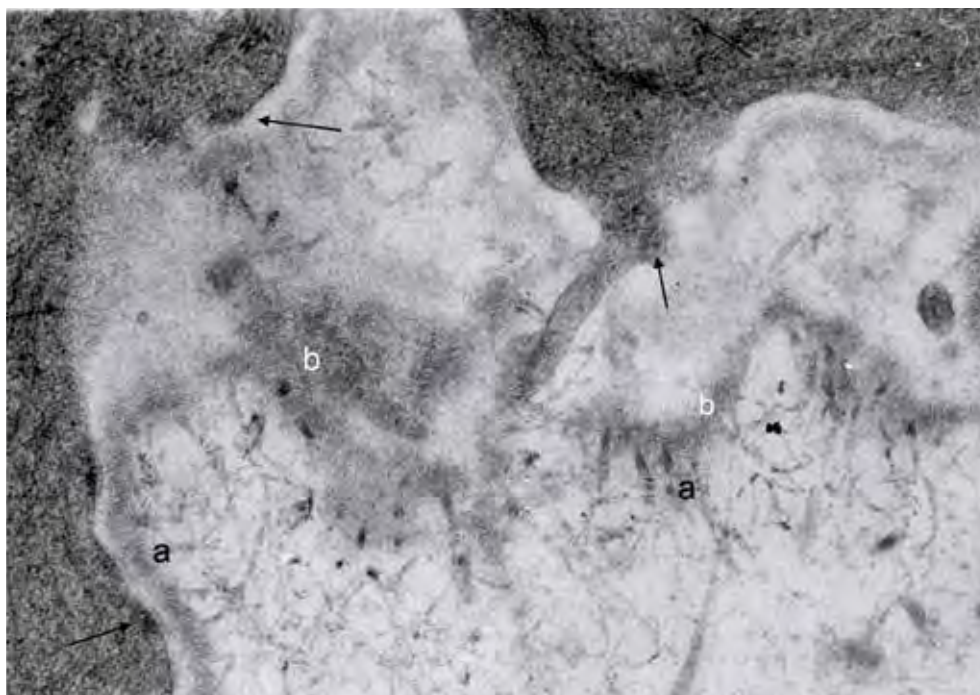


Fig. 22. Organ culture of skin graft, one day old. Keratinocytes form hemidesmosomes and basal lamina with anchoring filaments (arrows). Anchoring fibrils are scarce. Basal lamina (b) of the mother piece are distinct and show many distinct anchoring fibrils (a). $\times 20,000$.



Fig. 23. Organ culture of normal skin after 48 hours. Basal lamina grows perpendicularly into the dermis and forms numerous distinct anchoring fibrils (arrows). Dermal collagen fibrils are disintegrated (C) and show “collagen aggregate”. K: keratinocytes. × 10,000.

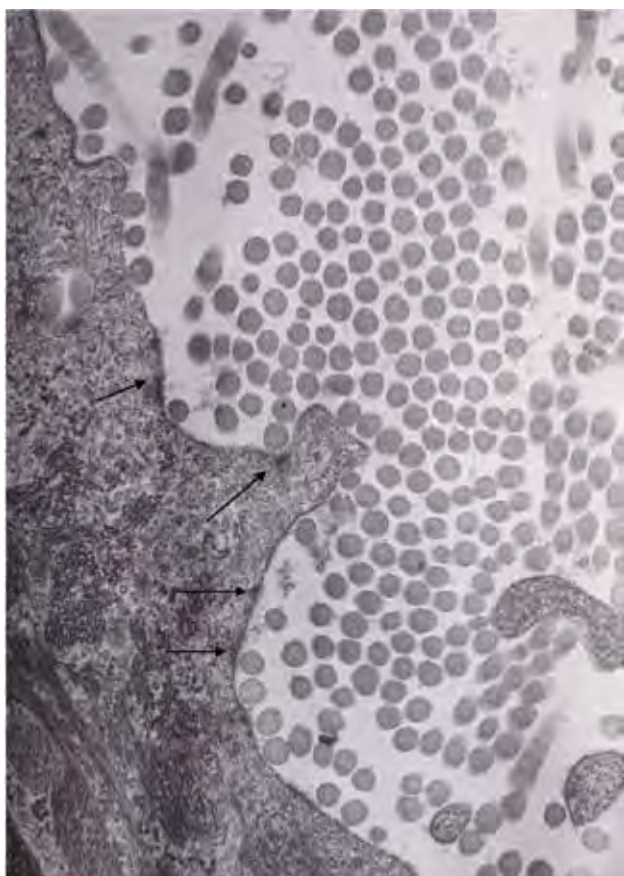


Fig. 24. Organ culture of normal skin. Out-growth of new keratinocytes grow over the cut-edge of dermis and cover the dermal cut-surface of the mother piece. Culture for 8 hours. Keratinocyte are facing on the collagen fibrils of the mother piece and shows new hemidesmosomes (arrows). Basal lamina is not formed. × 20,000.

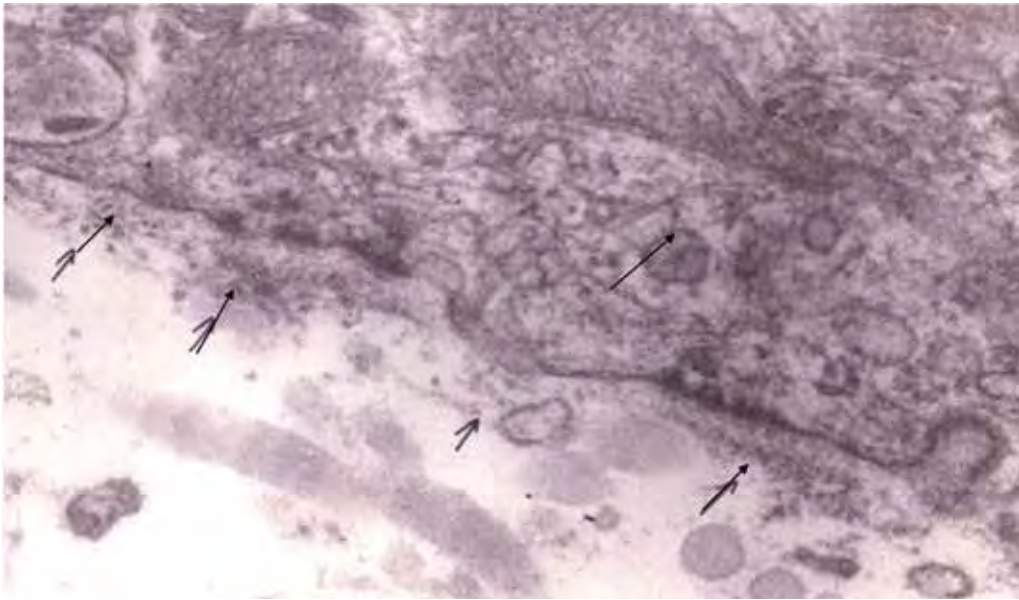


Fig. 25. Keratinocytes in organ culture, one day old. The out-growth over cut-surface of the mother piece. Under the outgrowth, the keratinocytes form hemidesmosomes and anchoring filaments. Basal lamina is formed in short stretch covering the cell surface of hemidesmosomes. No anchoring fibrils are developed. No connection of basal lamina to the underlying collagen fibrils. Arrows show new basal lamina. $\times 20,000$.

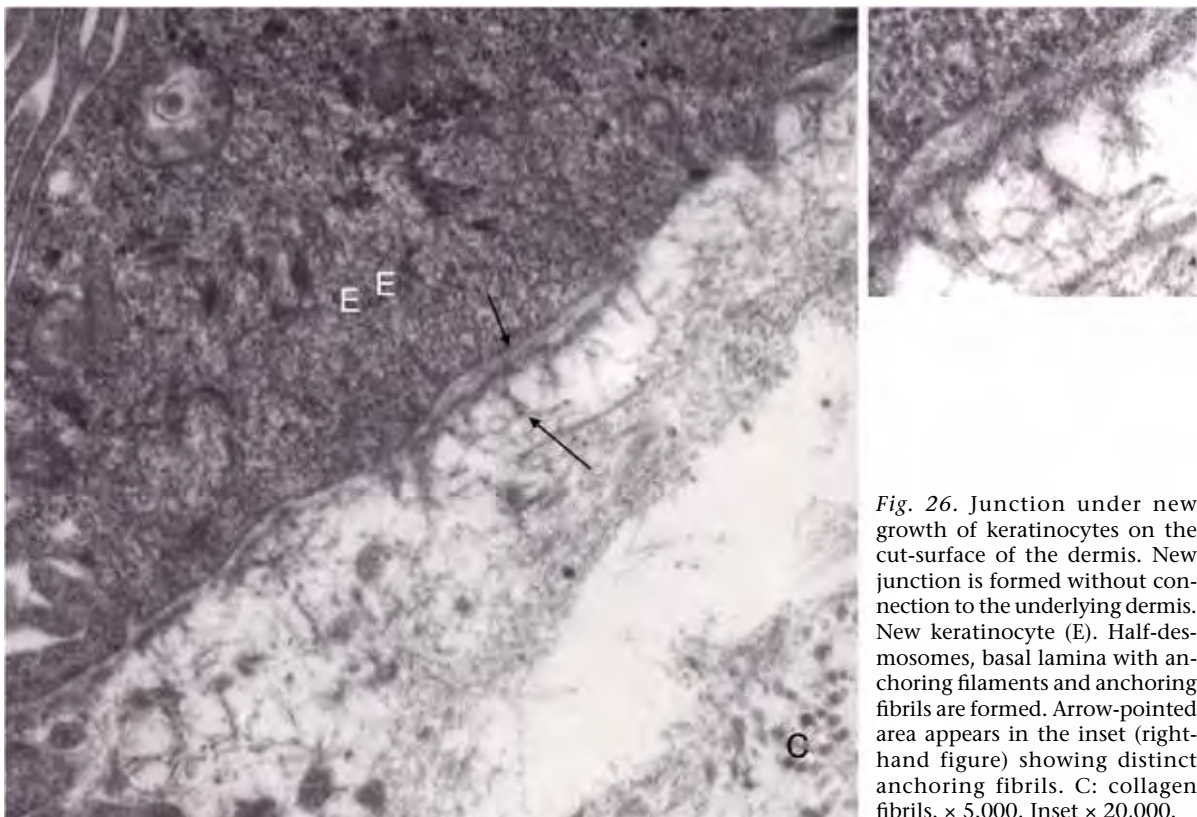


Fig. 26. Junction under new growth of keratinocytes on the cut-surface of the dermis. New junction is formed without connection to the underlying dermis. New keratinocyte (E). Half-desmosomes, basal lamina with anchoring filaments and anchoring fibrils are formed. Arrow-pointed area appears in the inset (right-hand figure) showing distinct anchoring fibrils. C: collagen fibrils. $\times 5,000$. Inset $\times 20,000$.



Fig. 27. Newly grown keratinocyte on the elastic fibre in the dermis of the mother piece. Hemidesmosomes of the new keratinocyte join directly to matrix of elastic fibre (e). Arrows shows the junction of hemidesmosomes to elastic matrix without basal lamina. $\times 20,000$.

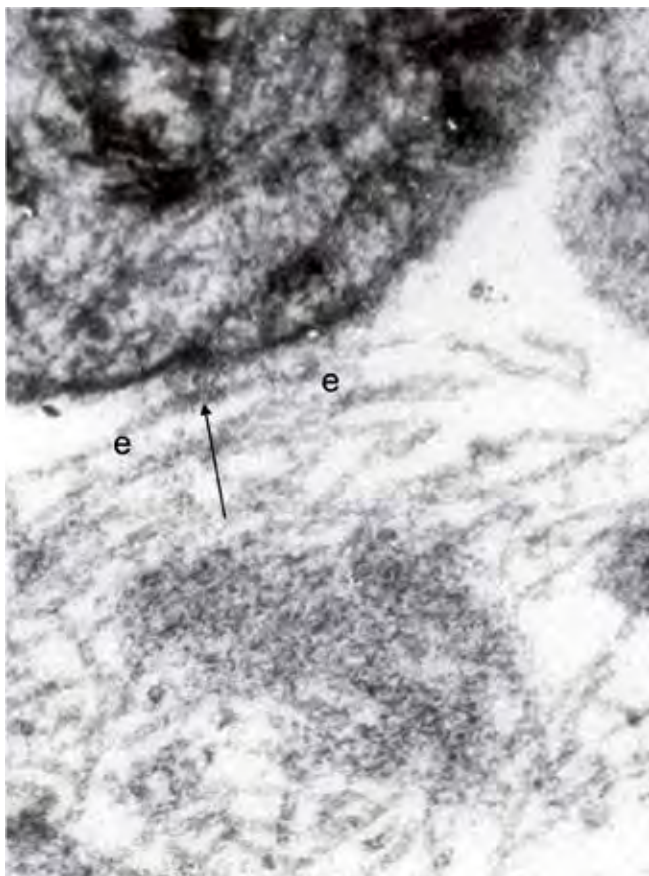


Fig. 28. Filamentous connection of hemidesmosomes to elastic microfibrils without basal lamina (arrow). e: elastic microfibrils. $\times 40,000$. These findings in the culture imply that half-desmosome has significant role for construction of junction structure (See also the junction of cancer tissue).

Cell culture of human keratinocyte
Membranous growth of human keratinocyte

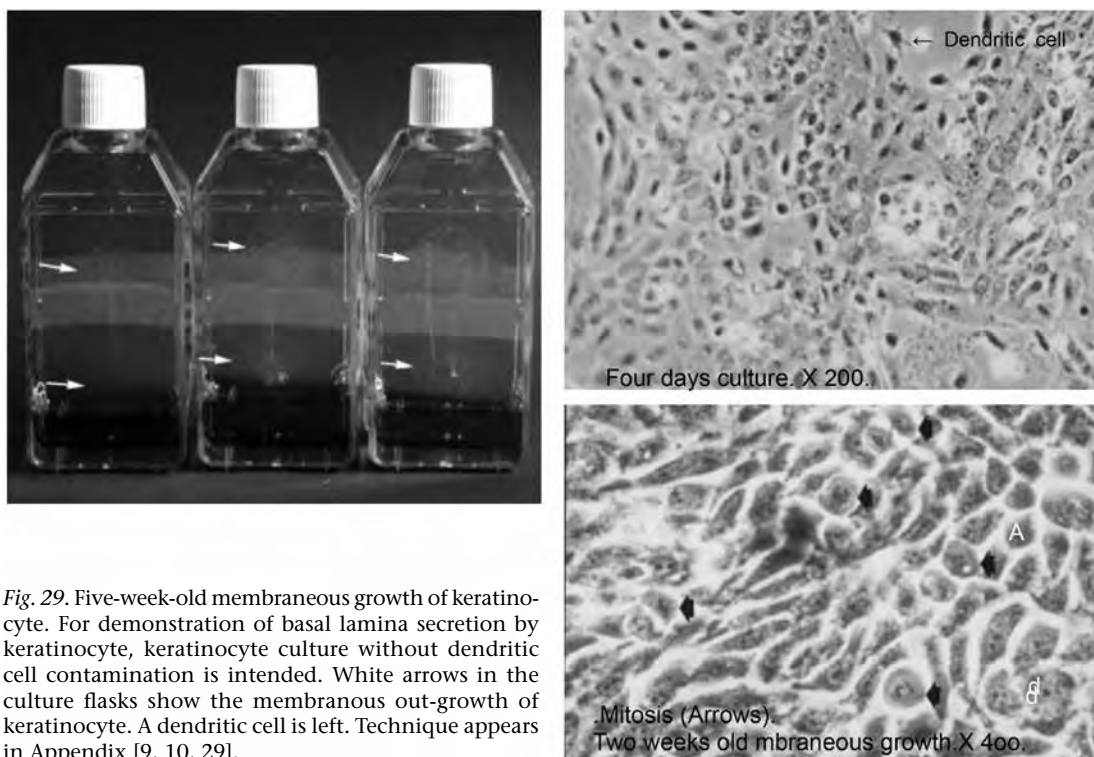


Fig. 29. Five-week-old membranous growth of keratinocyte. For demonstration of basal lamina secretion by keratinocyte, keratinocyte culture without dendritic cell contamination is intended. White arrows in the culture flasks show the membranous out-growth of keratinocyte. A dendritic cell is left. Technique appears in Appendix [9, 10, 29].

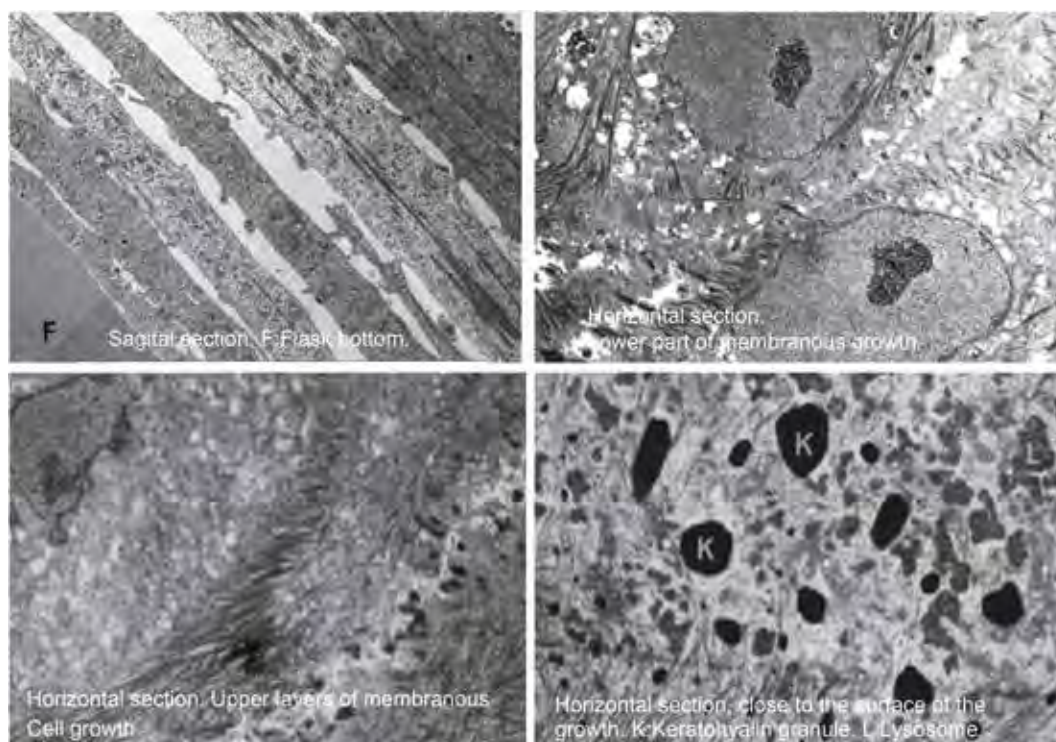


Fig. 30. Membranous growth of keratinocytes. Direct magnification: 5,000.

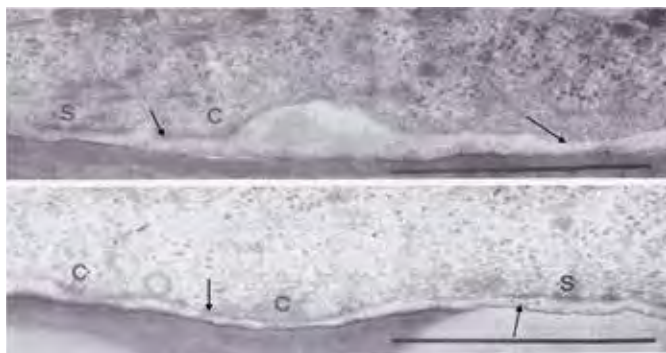


Fig. 31. Cell culture of human keratinocyte for 7 days [11]. Bottom of Falcon culture flask is coated by fixed film of human type I collagen. Localized thickenings of cell membrane (C), hemidesmosomes (S). Thread-like material to the collagen film is anchoring filaments (arrows). Bar indicates 1.0 µm.

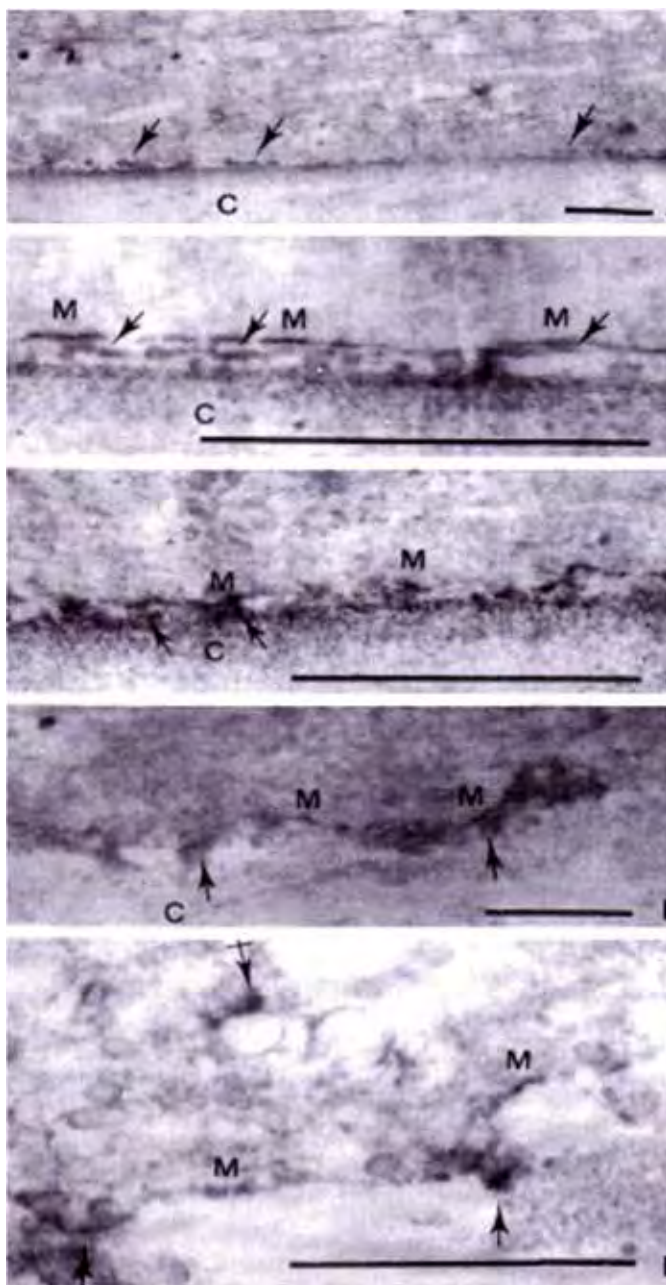


Fig. 32. Seven-day culture of keratinocyte in a Falcon flask. Keratinocytes grow on the film of type I collagen [11]. The cell growth is stained by antiserum to type IV collagen and visualized by peroxidase-antiperoxidase reaction. M indicates thick cell membrane (Hemidesmosome). Arrows point type IV collagen on cell surface. C points at fixed collagen film on flask bottom. Bars indicate 1 µm.

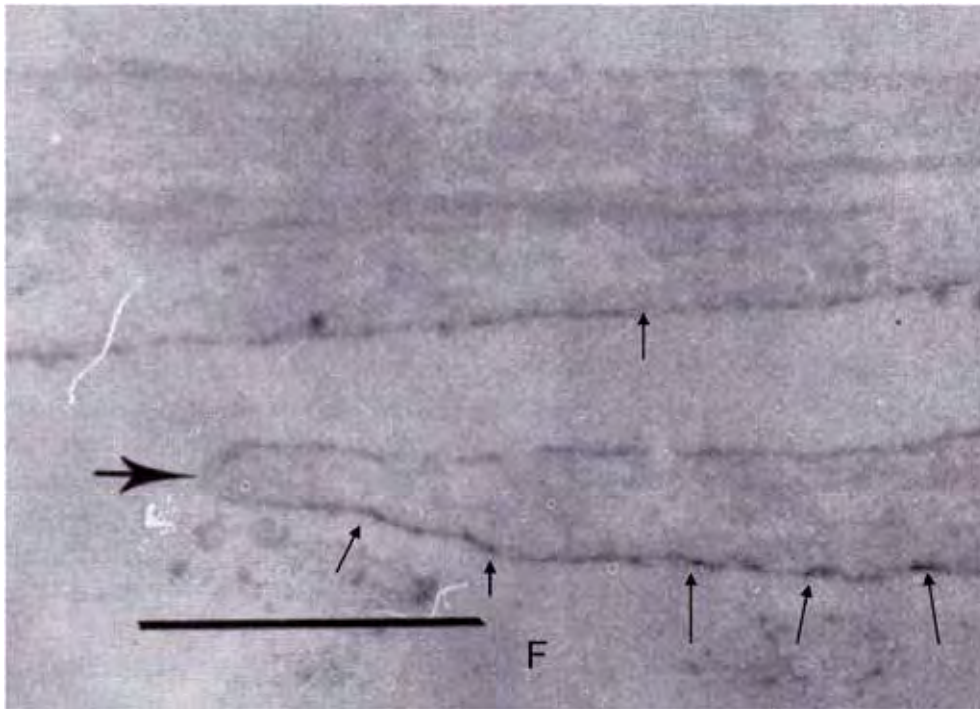


Fig. 33. Two-week-old cell culture of keratinocyte, stained by immunoglobulin to type IV collagen and visualized by peroxidase-antiperoxidase stain. No counter-stain [11]. Dense cell surface facing to the flask bottom (thin arrows). Thick arrow shows edge of newly grown keratinocyte. Positive staining represents that type IV collagen is produced by keratinocytes. F: bottom of Falcon flask. Bar indicates 1.0 μm.

Dermoepidermal junction in dermatoses

Classification of the change

PATHOLOGY OF DERMO-EPIDERMAL JUNCTION	
<u>Destructive changes</u>	
1.	Dermoepidermal separation
1.1.	Intraepidermal separation Spongiotic S., Infrabasal (Acantholytic) S. Transbasal S.
1.2.	Subepidermal separation
1.3.	Sublaminal (Dermolytic) separation
2.	Interruption of basal lamina From epidermis. From dermis
<u>Productive changes</u>	
1.	Thickenings of basal lamina Diffuse type. Uneven type
2.	Multiple layers of basal lamina
3.	Globus of anchoring fibrils
4.	Abnormal precipitants Amyloid. Immune products. Proteoglycans

Table II. The classification of the changes in drawing appear in Figs. 34, 35.

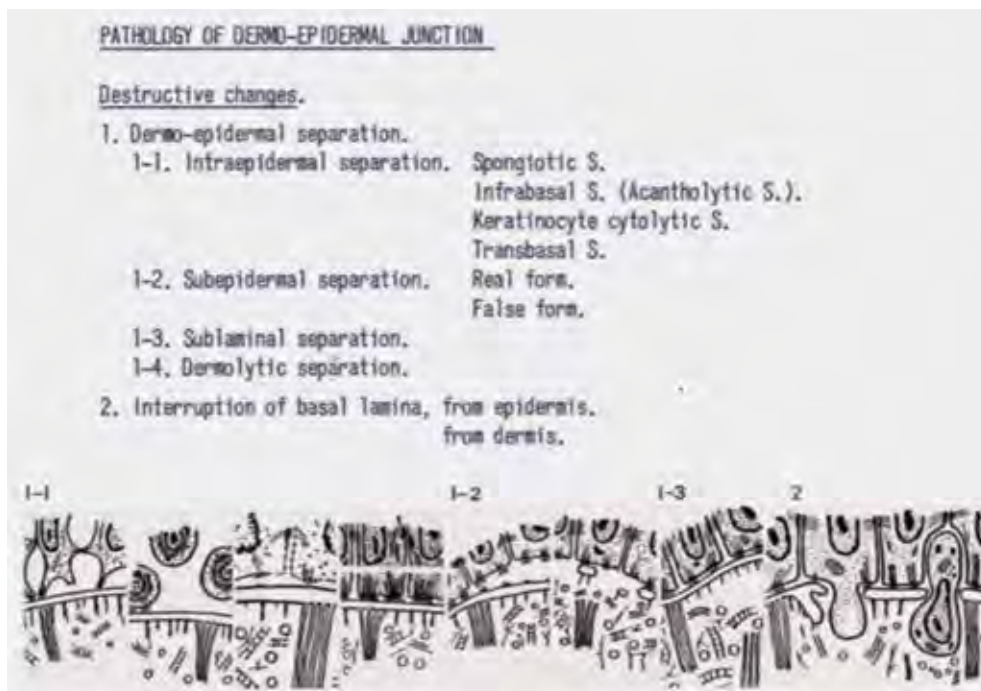


Fig. 34. Pathology of dermoepidermal junction [4].

Productive changes.

1. Multiple layers of basal lamina. (Irregularly wide subepidermal spaces.)
2. Thickening of basal lamina, diffuse and uneven.
3. Globus of anchoring fibrils.
4. Abnormal precipitants. Amyloid.^c Immune products.^a Proteoglycans.^d



Fig. 35. Pathology of dermoepidermal junction. Continued from Table II.

Penetration

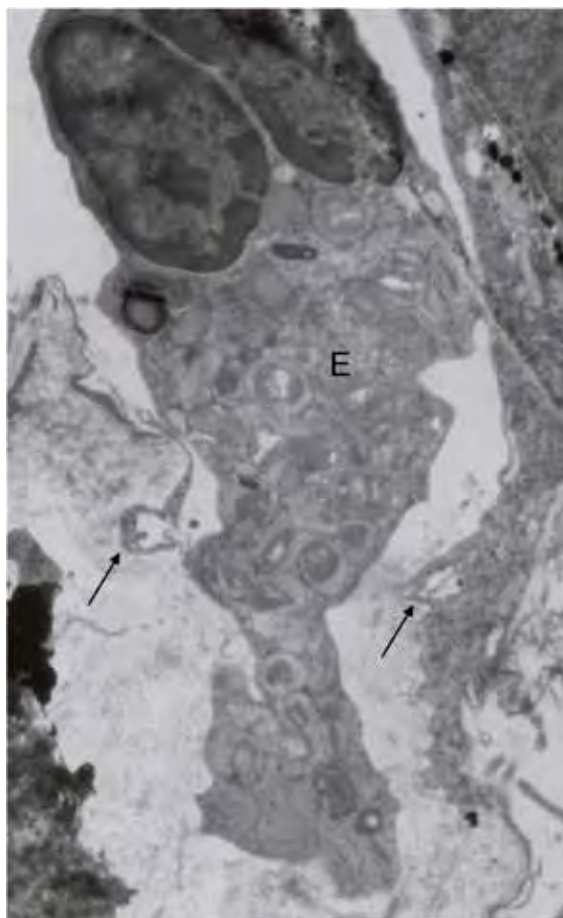


Fig. 36. Penetration of junction without visible destruction junction, Macropage, Langerhans cell, eosinophile granulocyte, filamentous body (Civatt) and cancer cells pass through the junction without any structural damage of the junction. This figure shows the junction in Incontinentia pigmenti. An eosinophile granulocyte penetrate through the junction. The two arrows point at the edges of basal lamina. $\times 5,000$. [Unpublished]

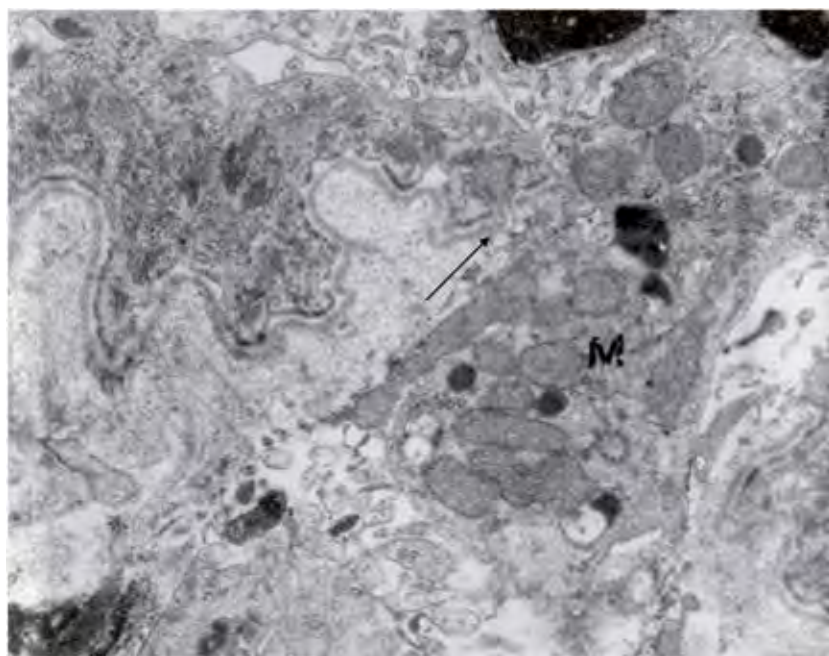


Fig. 37. Erythema multiforme. A macrophage (M) penetrates through the junction. Arrow points at the edge of basal lamina. $\times 5,000$. [Unpublished]

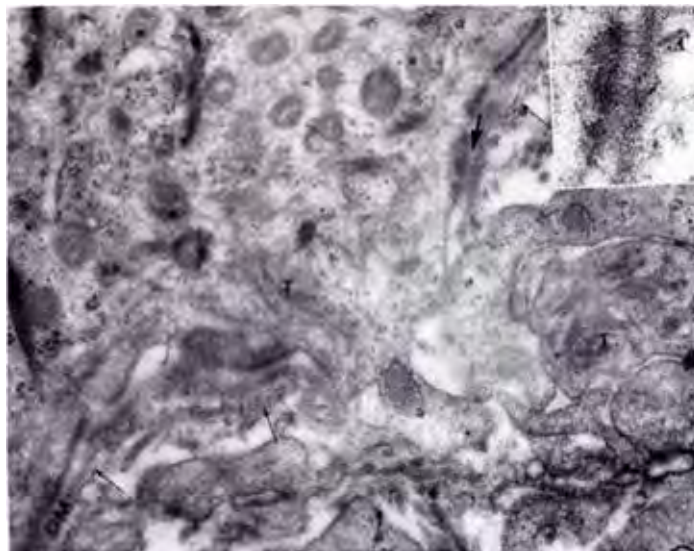


Fig. 38. Basal cell carcinoma. A carcinoma cell protrudes cytoplasm into the dermis [23]. The area with thick arrow shows basal lamina and semidesmosome connection (inset). Anchoring fibrils are indistinct (thin arrows). Tonofilaments in cancer cells (T). Basal lamina (DM). $\times 40,000$. [Unpublished]

Dermo-epidermal separation

The separation, seen blister in clinic, is epidermal, subepidermal and dermal by the separated level. The separation damages in the components of the junction structure. Individual bullous reveals characteristic figure of the damaged junction.

Epidermal separation

Epidermal blister occurs by spongiosis, acantholysis and cytolysis of keratinocyte. Junction structure is not damaged.

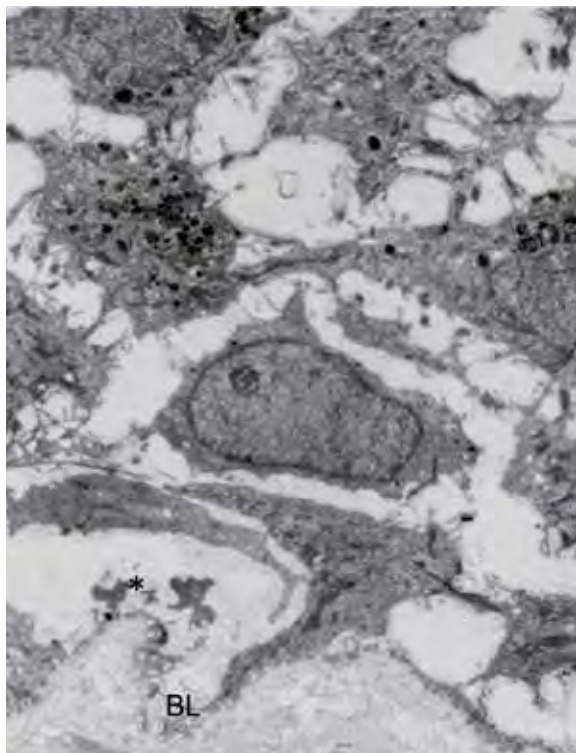


Fig. 39. Spongiotic blister of eczema. Junction structure and desmosomes are not injured. BL: basal lamina. $\times 2,000$. [Unpublished]

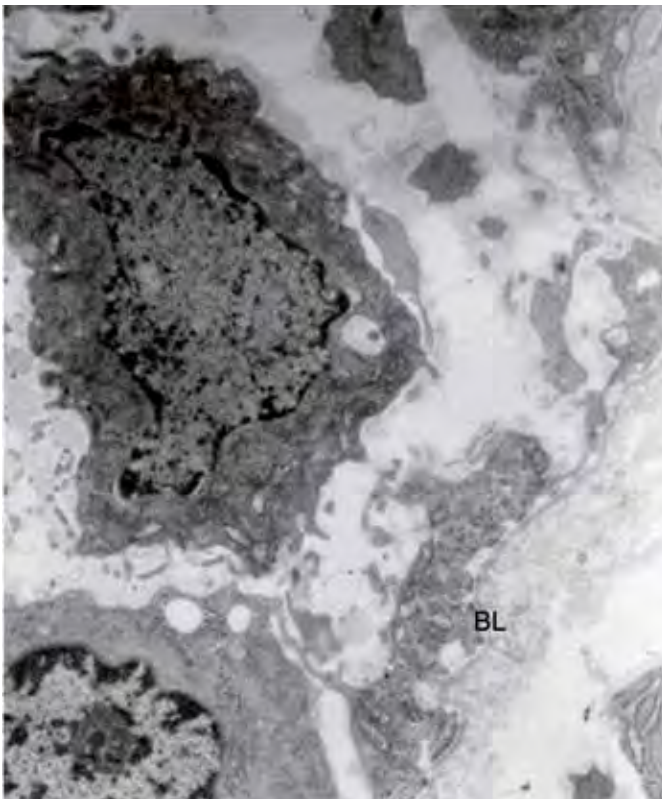


Fig. 40. Acantholytic blister. Pemphigus group reveals blister by altered desmosomes as seen defect of median line of desmosome. Desmosomes are separated at each sides and keratinocytes become free but the junction structure, hemidesmosomes, is intact. Basal cells release the keratinocytes in the upper layers of epidermis. The figure is the blister of pemphigus vulgaris. BL: basal lamina. $\times 2,000$. [Unpublished]

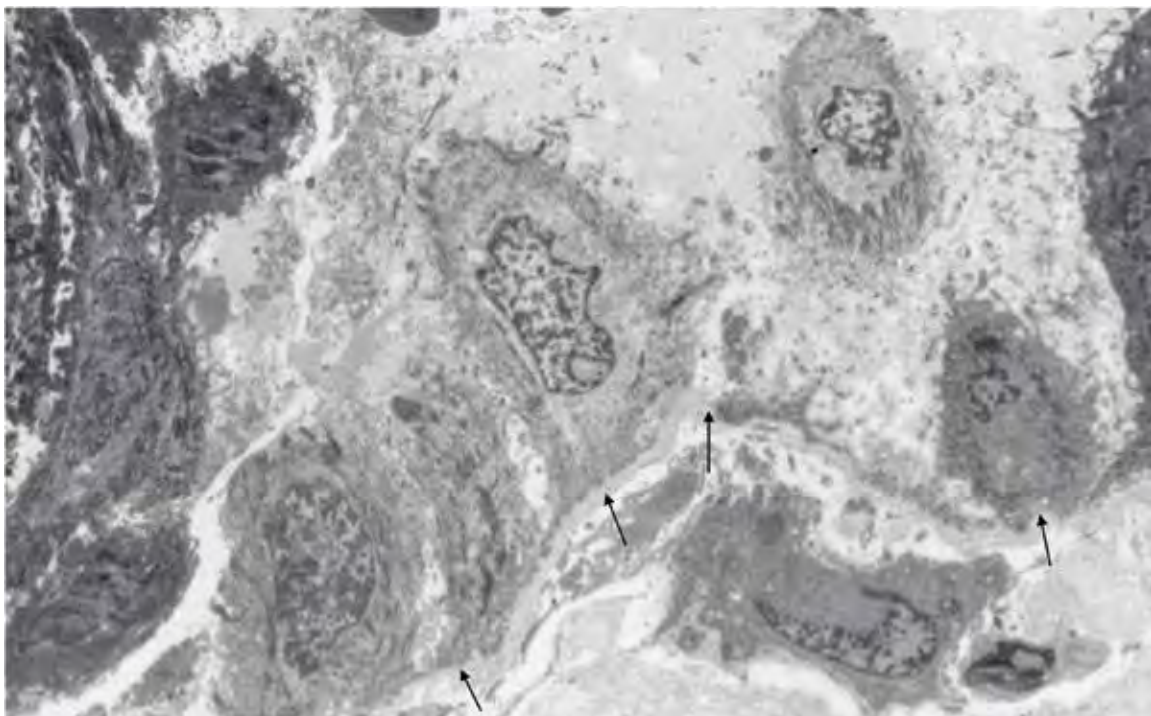


Fig. 41. Paraneoplastic pemphigus. Keratinocytes in the spinous cell layer are acantholytic and released from basal cells. Junction structure is preserved (arrows). $\times 3,000$. [Unpublished]

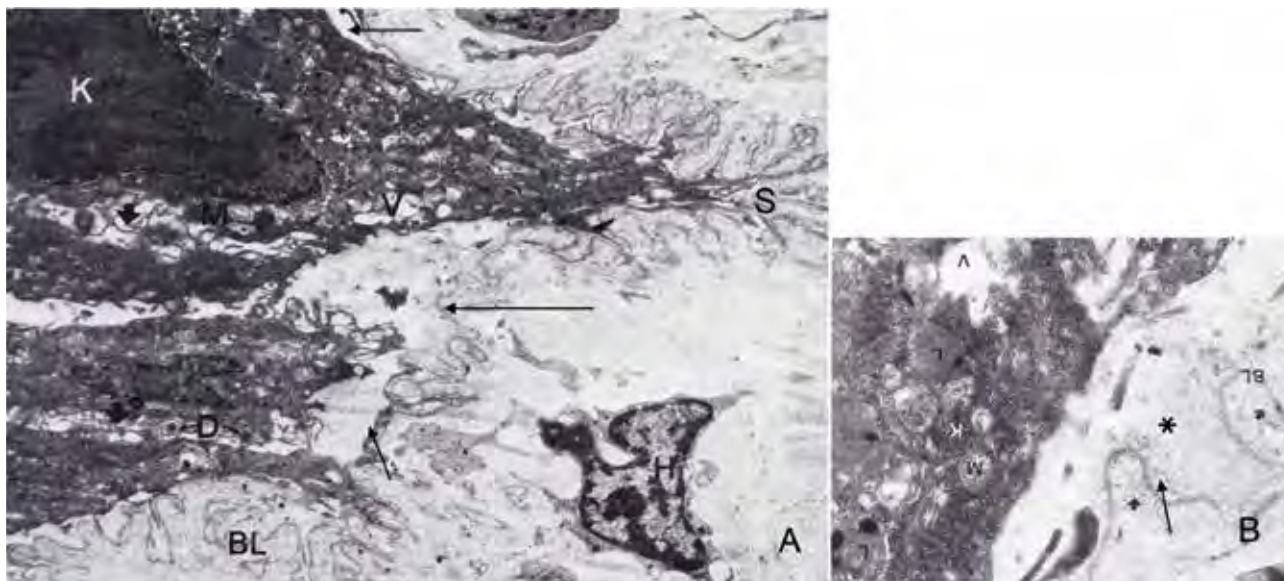


Fig. 42. Bullous acrodermatitis due to zinc deficiency [13]. Fig. A: Blister is located subepidermal. Basal keratinocytes are degenerated and released from basal lamina (arrows) and shows many slender pocket-like invaginations with narrow spaces (S). Fig. B: Separation in subepidermal space (asterisks). Arrow points at basal lamina. A. $\times 4,000$. B. $\times 20,000$.

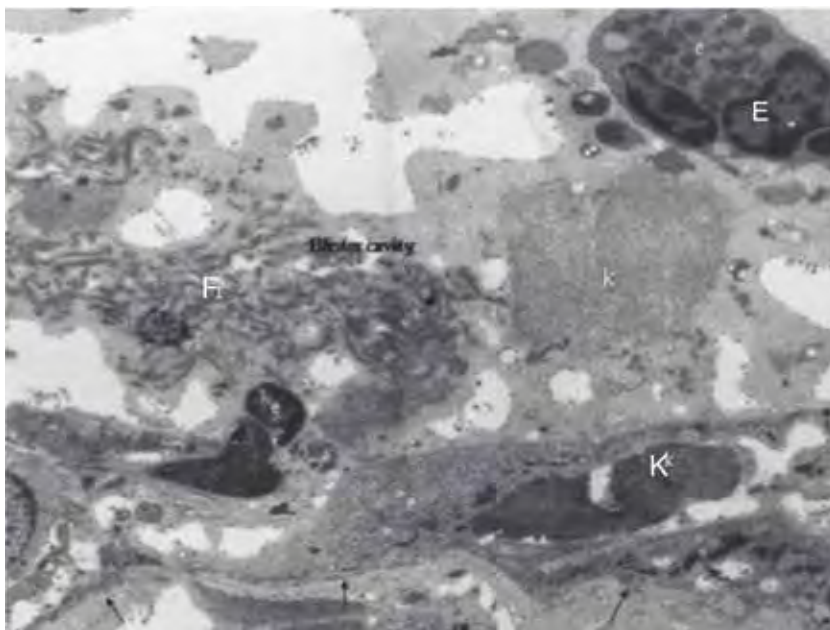


Fig. 43. Blister of incontinentia pigmenti. Basal cells and the junction is not affected. Basal lamina (arrows) is continued. Eosinophile granulocytes (E) and fibrin (F) in the blister cavity. Disintegrated keratinocytes (K). $\times 2,000$. [Unpublished]

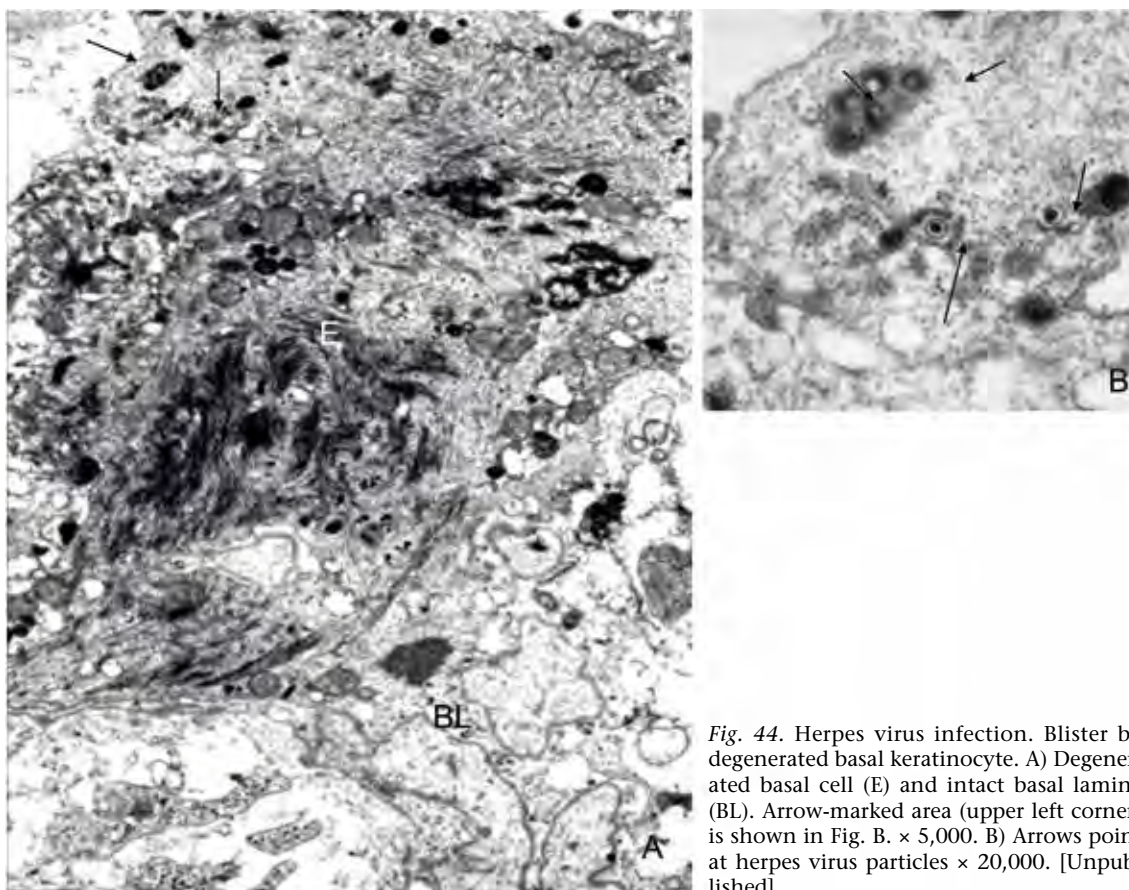


Fig. 44. Herpes virus infection. Blister by degenerated basal keratinocyte. A) Degenerated basal cell (E) and intact basal lamina (BL). Arrow-marked area (upper left corner) is shown in Fig. B. $\times 5,000$. B) Arrows point at herpes virus particles $\times 20,000$. [Unpublished]

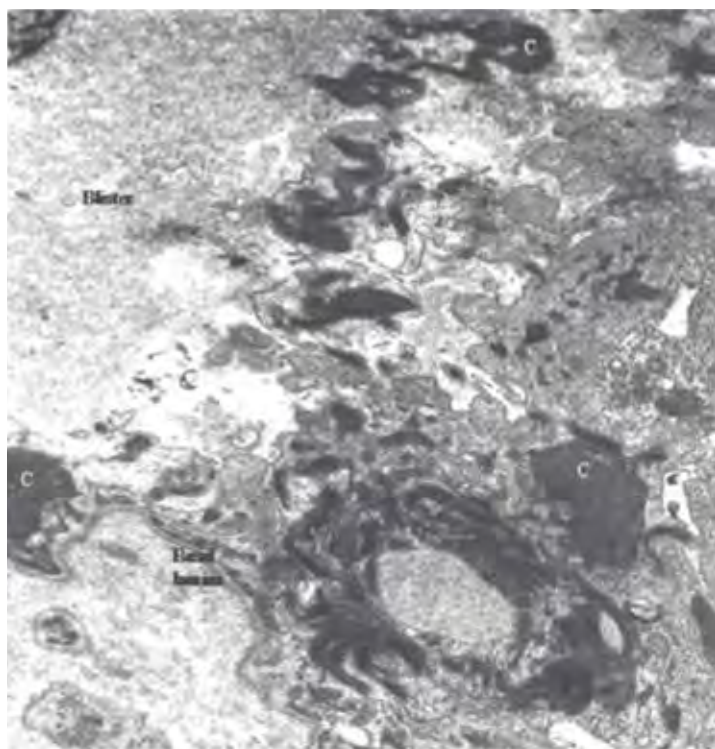


Fig. 45. Epidermolysis bullosa simplex, Dawling-Meara. Keratinocytes in basal and supra-basal cell layer are degenerated but basal cells are preserved and show characteristic conglomerate of tonofilaments (c). Junction structure is preserved. C: Characteristic conglomerate of tonofilament in basal cells. $\times 10,000$. [Unpublished]

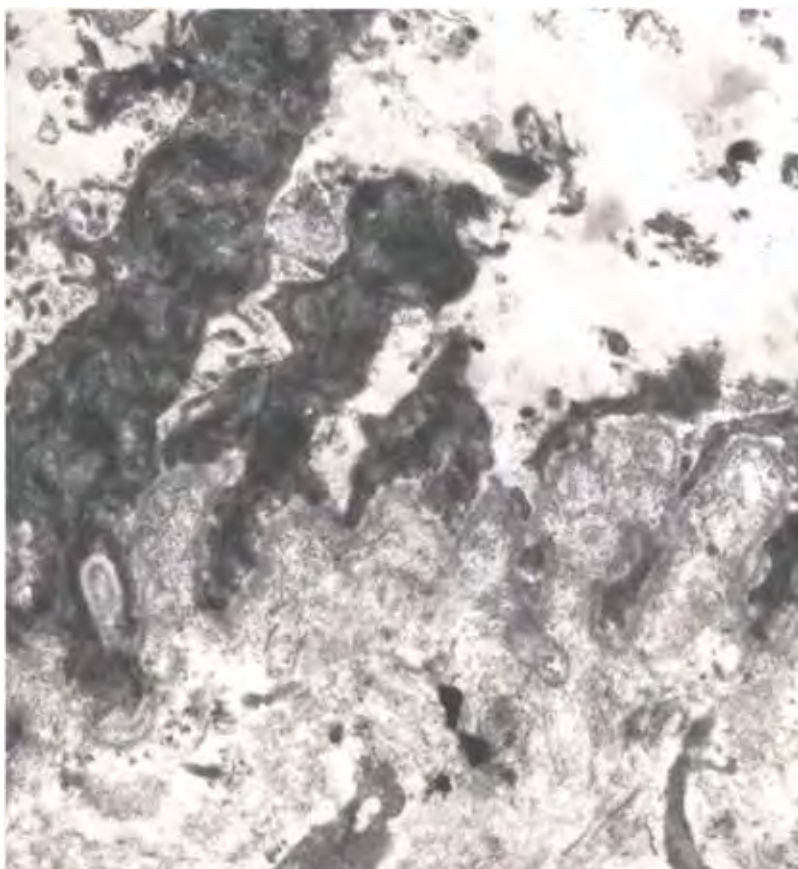


Fig. 46. Epidermolysis bullosa simplex (Köbner). Blister is formed in the epidermis. Blister is in the suprabasal cell layer. Basal keratinocytes show condensed cytoplasm but are not released from basal lamina. $\times 10,000$. [Unpublished]



Fig. 47. Bullous ichthyosiform erythroderma. Blister roof is basal keratinocytes and blister floor is covered by basal keratinocytes and basal lamina. $\times 2,000$. [Unpublished]

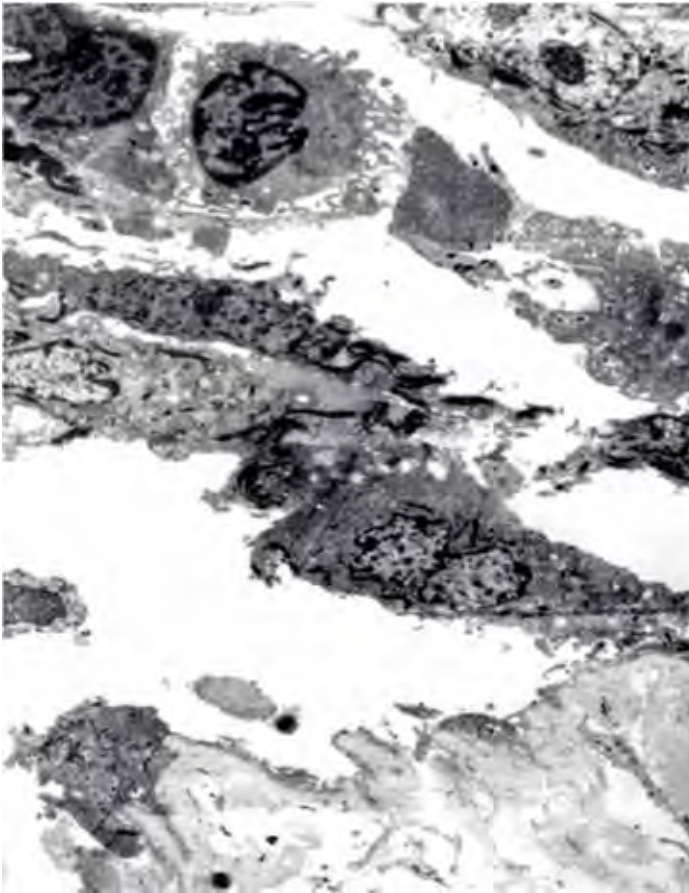


Fig. 48. Herpes gestationis. Blister locates in the epidermis. Basal cells are seen on the basal lamina. Basal lamina preserves the continuity. Keratinocytes of basal cell layer are seemingly degenerated. $\times 3,300$. [Unpublished]

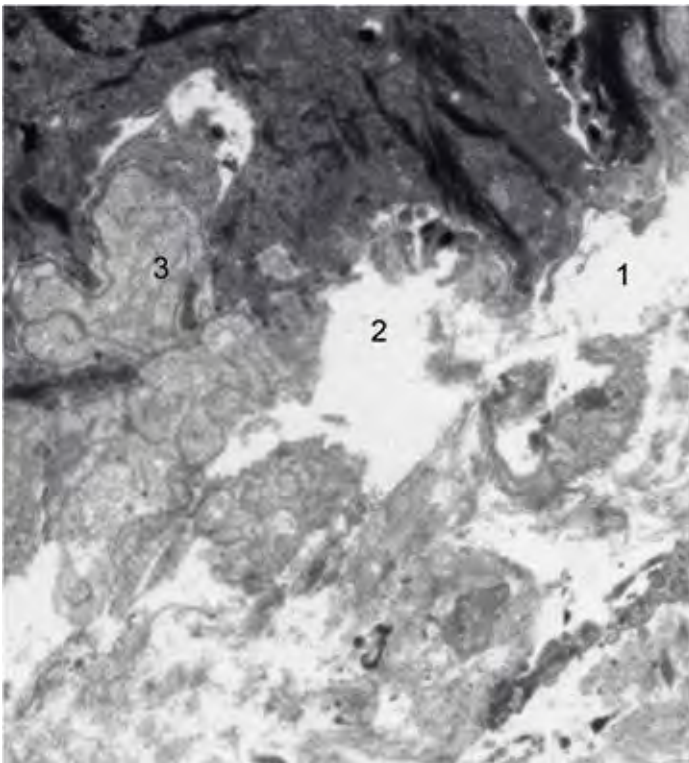


Fig. 49. Porphyria cutanea tarda chronica. Junction shows various shapes. It probably occurs after the long-standing change in the junction. Epidermis is separated from dermis, in sublaminal (1) and subepidermal (2). While productive pattern is seen as net-works of basal lamina (3). Keratinocytes of the blister show no changes. $\times 5,000$. [Unpublished]

Subepidermal separation. Real type

Real subepidermal separation are seen in blisters of epidermolysis bullosa junctionalis (inherited nature), bullous pemphigoid (immunologic reaction) [15] and suction blister (normal skin by mechanical force) [16, 17]

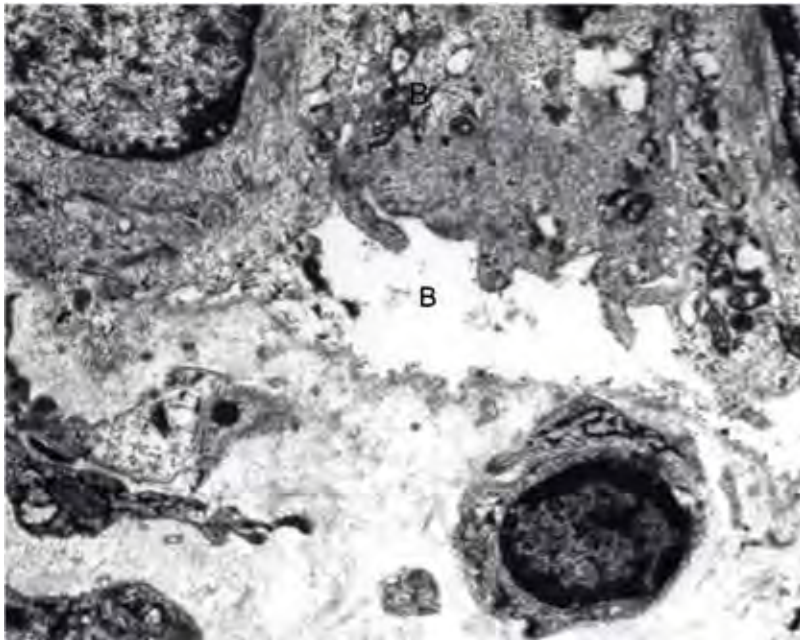


Fig. 50. Epidermolysis bullosa atrophicans junctionalis. Subepidermal blister of real type. Blister roof is the cell membrane of basal keratinocytes. Hemidesmosomes and anchoring filaments are not developed well. Detailed figure is shown in Fig. 53. Anchoring filaments are dubious. Blister floor is of basal lamina. B: blister cavity. x 5,000. [Unpublished]

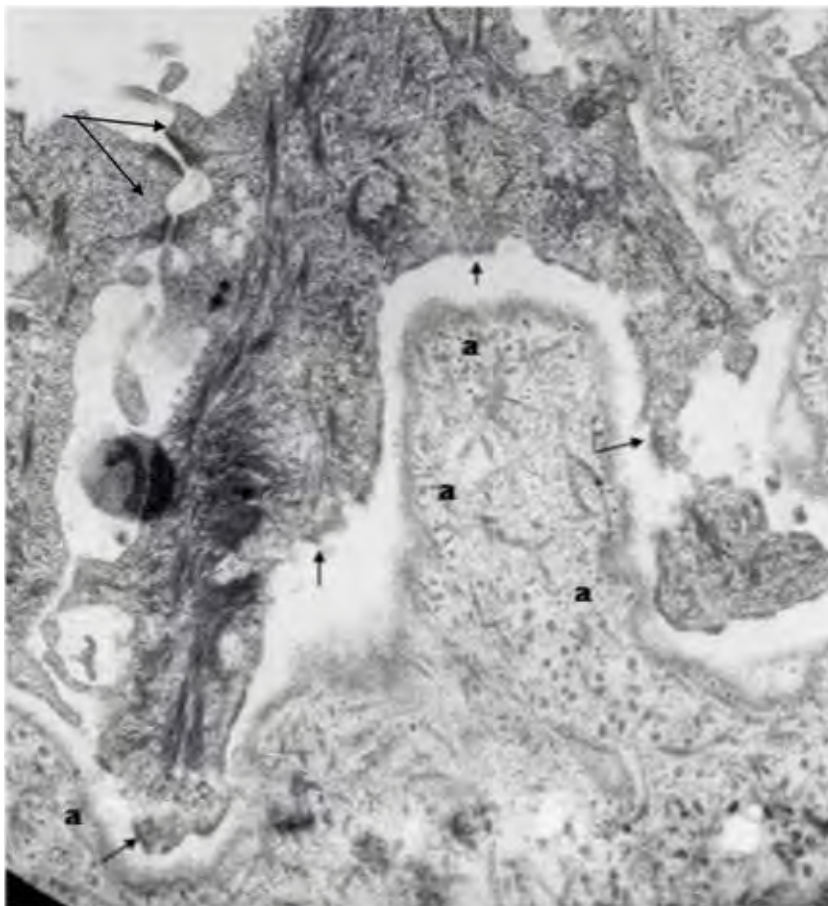


Fig. 51. Epidermolysis bullosa junctionalis (detailed figure of the junction). Epidermis is separated in subepidermal space. Cell membrane of basal keratinocyte is intact but hemidesmosomes are incomplete (arrows). Anchoring filaments are torn apart. Basal lamina is not interrupted and anchoring fibrils are thin indistinct. Desmosomes are also dissociated (thick arrow). Blister spreading test is positive. [Unpublished]

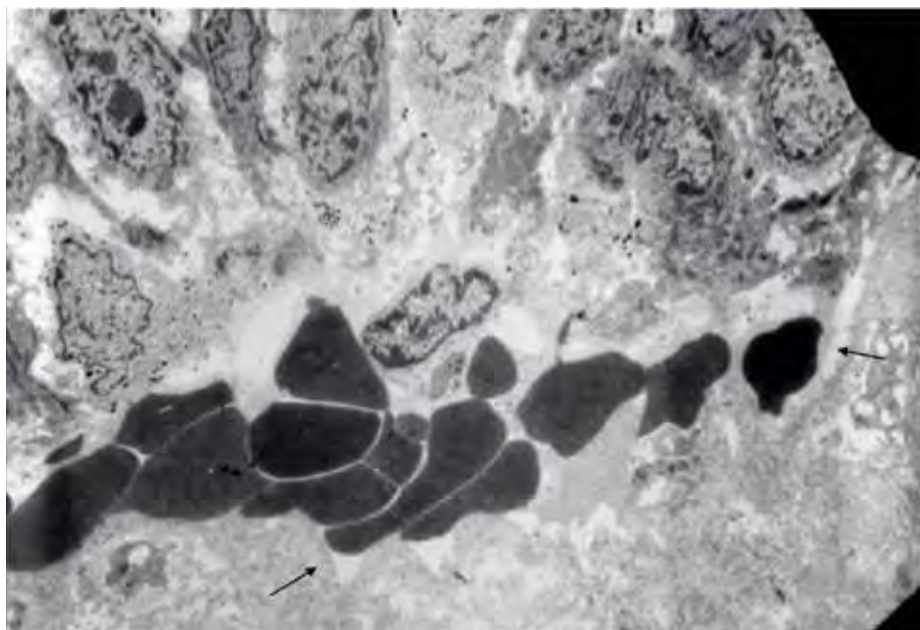


Fig. 52. Bullous pemphigoid [14]. Blister floor is of basal lamina and blister roof is of keratinocytes. Basal lamina (arrows) and cell membrane is preserved. The blister cavity contains erythrocytes. $\times 2,000$.

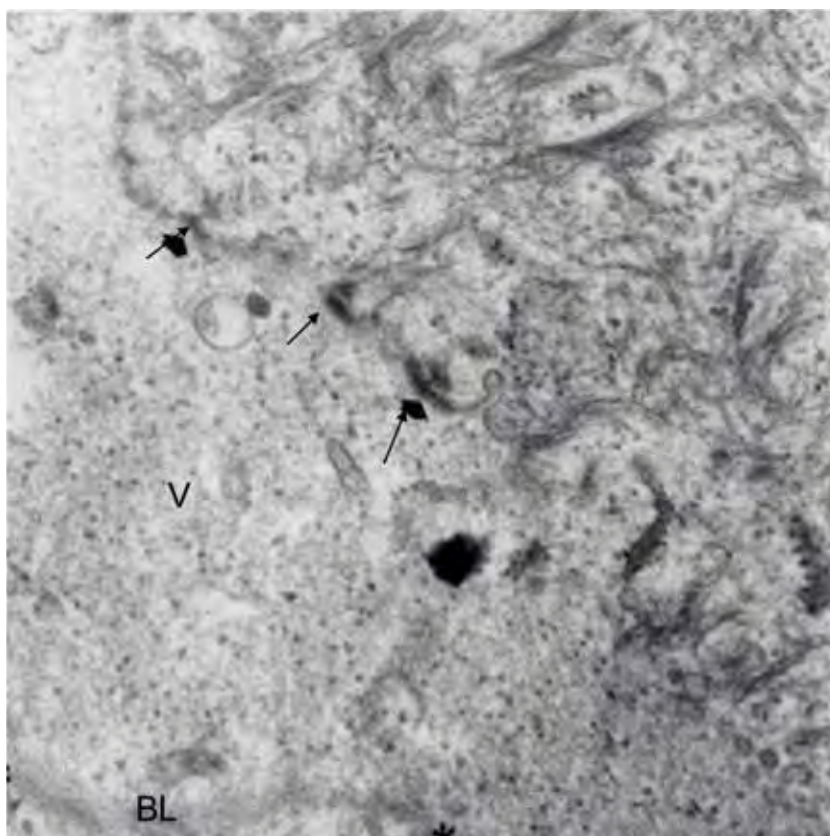


Fig. 53. Details of blister in bullous pemphigoid. Blister floor is of basal lamina (BL). Blister roof is cell membrane of keratinocytes in basal cell layer. Arrows point at hemidesmosomes. Anchoring filaments are torn apart. Blister cavity (V). $\times 20,000$.

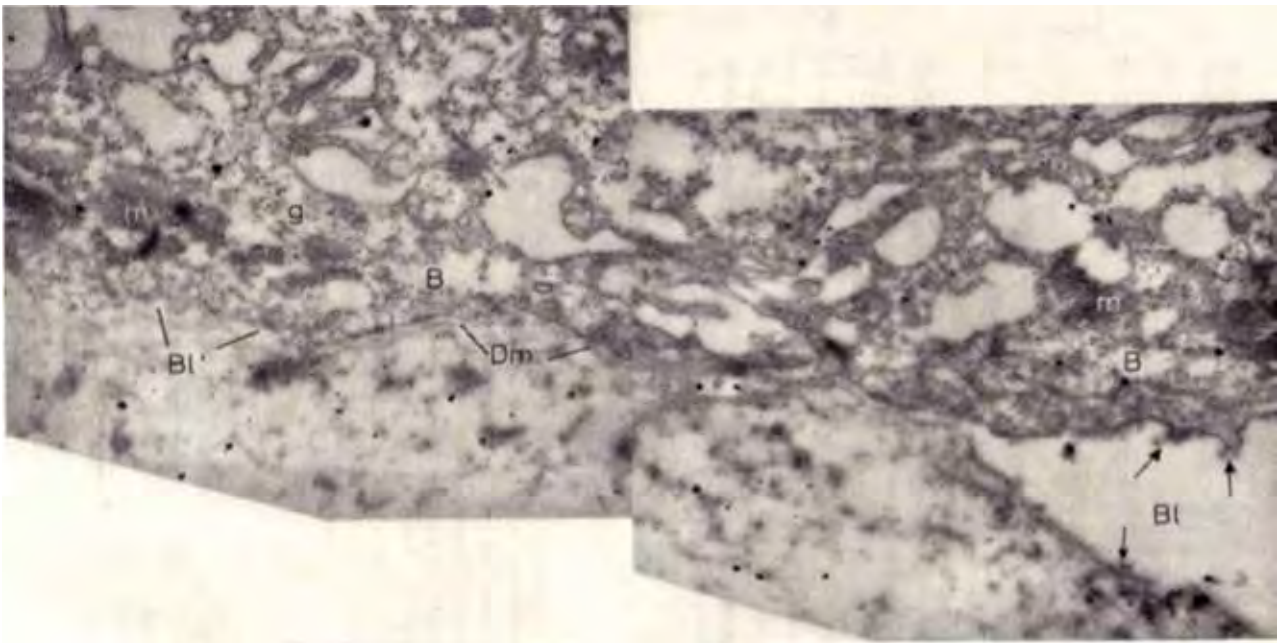


Fig. 54. Bullous pemphigoid. Blister edge after blister spreading test (Asboe-Hansen) [14]. Asterisk marks the spreading edge of the blister. Arrows point anchoring filaments torn apart. Dm: basal lamina, B: basal keratinocytes, Bl: blister cavity. $\times 10,000$. Dermo-epidermal separation is produced experimentally by suction on normal skin [15]. The separated sheath of epidermis can be applied for transplantation [16].

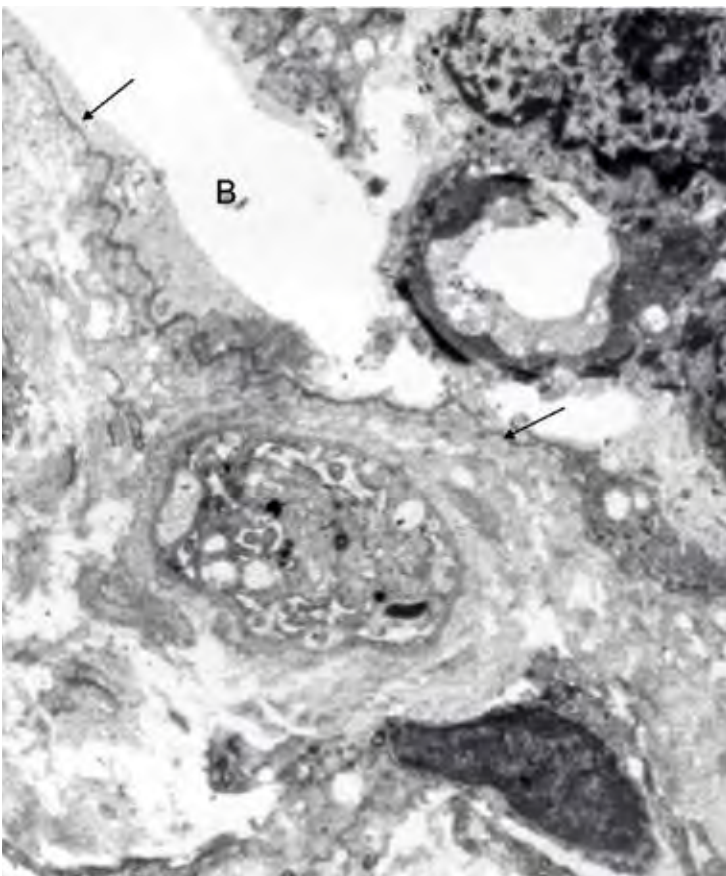


Fig. 55. Linear IgA disease. Blister floor is covered by basal lamina. Basal lamina (arrows) is dense and not interrupted. IgA precipitates on the basal lamina. B: blister cavity. $\times 10,000$. [Unpublished]

Subepidermal separation. False type

Separation occurs between basal cell membrane and basal lamina (Subepidermal space)

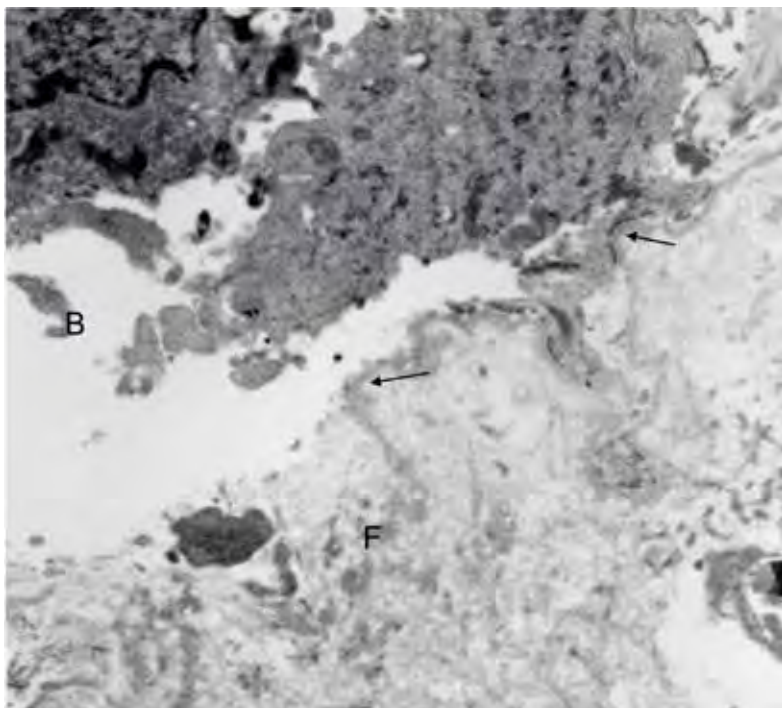


Fig. 56. Dermatitis herpetiformis. Blister is subepidermal. The blister edge reveals real subepidermal but in the middle part of the blister, basal lamina is fragmented (F). IgA precipitates on the basal lamina and fragments. Neutrophile granulocytes probably act for IgA-precipitated fragments. The blister becomes false variant of subepidermal blister. Blister cavity (B). $\times 10,000$. Neutrophiles do not appear in the picture. [Unpublished]

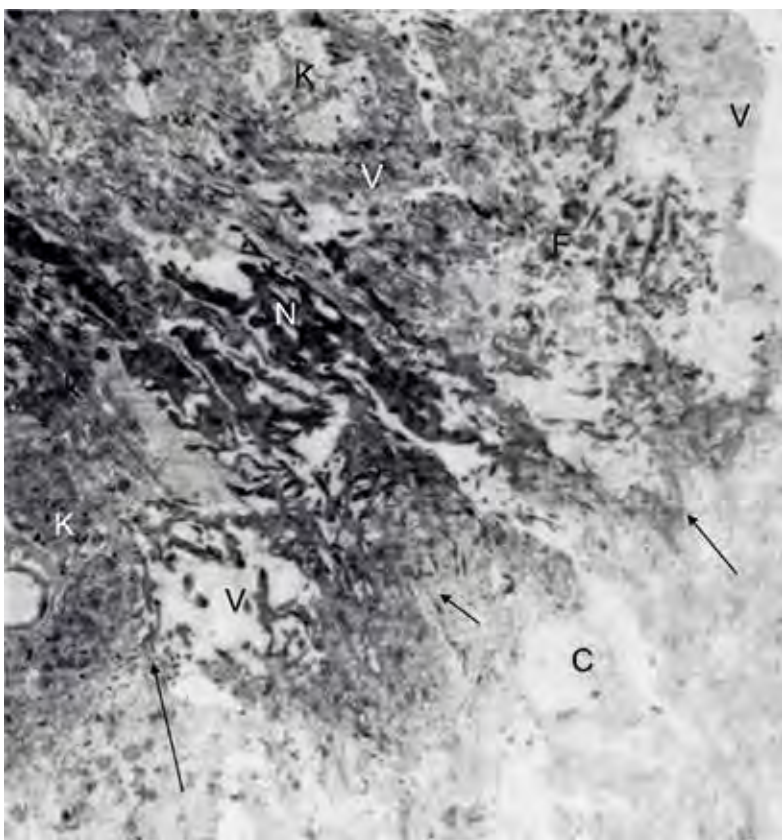


Fig. 57. Dermatitis herpetiformis. Middle part of the blister. Blister floor is dermal tissue (C) and fragments of basal lamina (arrows). Blister cavity (V) contains fibrin (F) and neutrophile granulocytes (N). K: keratinocyte. $\times 10,000$. [Unpublished]



Fig. 58. Epidermolysis bullosa dystrophica dominans albopapuloides of Passini. Blister edge. Blister roof is of basal lamina and blister floor is of dermis. Basal keratinocytes anchor basal lamina by hemidesmosomes and anchoring filaments. Basal lamina shows remnants of anchoring fibrils (arrows) and scarce elastic fibril anchoring. Fine filaments and spots adhere to the basal lamina of blister roof. $\times 10,000$.



Fig. 59. Epidermolysis bullosa dystrophica dominans. Details of blister roof. False subepidermal blister. Blister roof is junction structure consisting of basal lamina, anchoring filaments and hemidesmosomes. No distinct anchoring fibrils and no elastic fibril are found. $\times 10,000$.

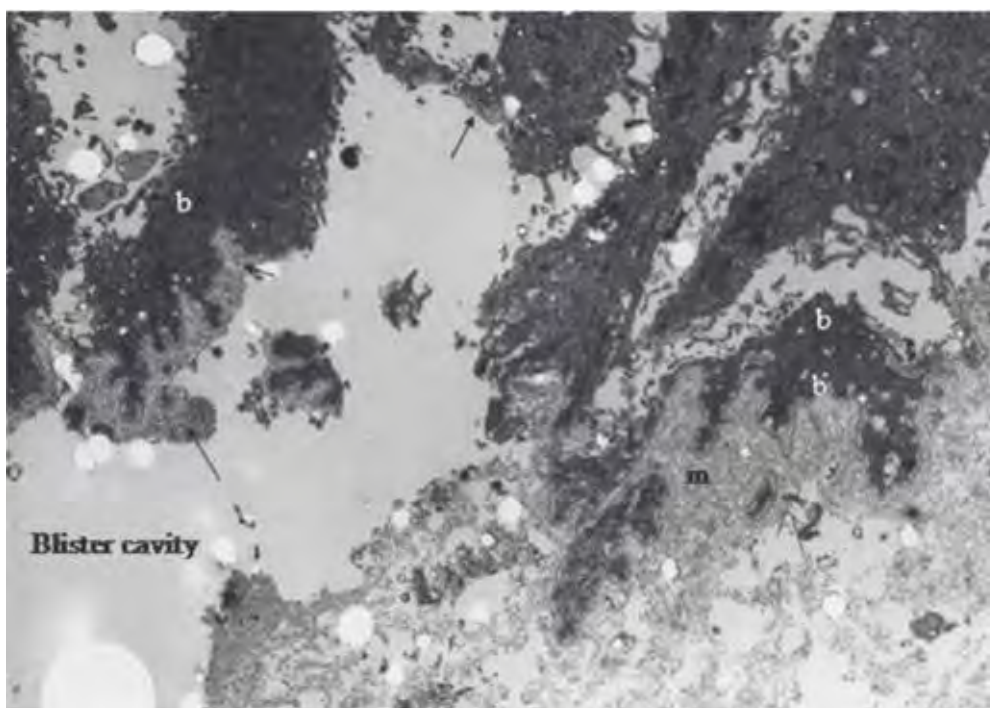


Fig. 60. Epidermolysis bullosa dystrophica recessiva [17]. False subepidermal blister. Blister roof is of basal lamina and remnants of dermis (arrows). Keratinocytes in the basal and suprabasal layers are separated from each other. The blister floor is dermis. On the edge of the blister, basal lamina forms meshes (m). $\times 1,600$.

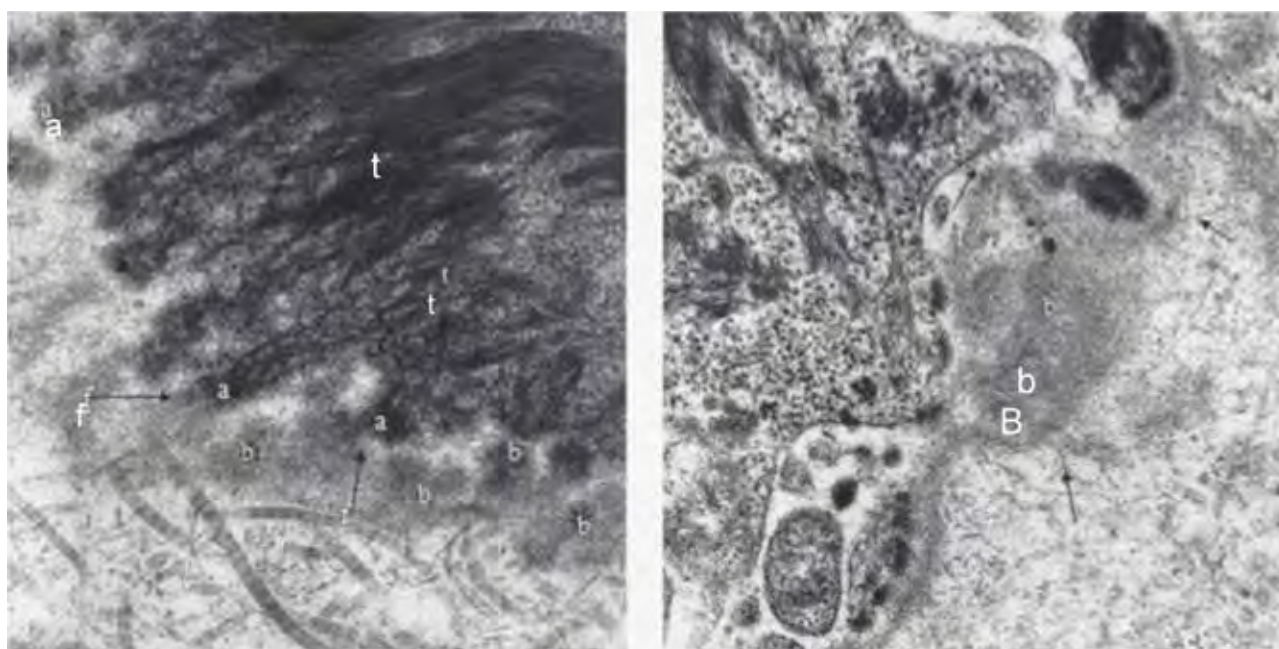


Fig. 61. Epidermolysis bullosa dystrophica recessiva, variant of Hallopeau-Siemens (Uninvolved skin) [17]. Both figures show irregular junction structure. Tonofilament-bundles are mesh-form (t) and attachment plaque is spot-formed (a). Basal lamina is varied in thickness (b), anchoring filaments (arrow f) and anchoring fibrils are thin (arrows). The changes are seen severer in the left hand picture. $\times 20,000$. Inherited factor seems to alter basal keratinocytes, especially keratinization.

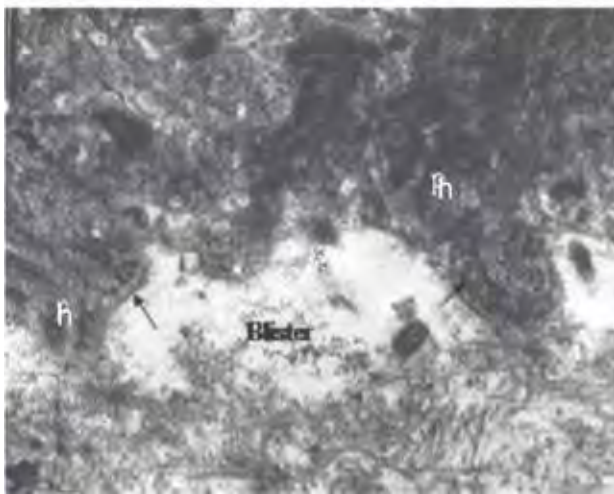
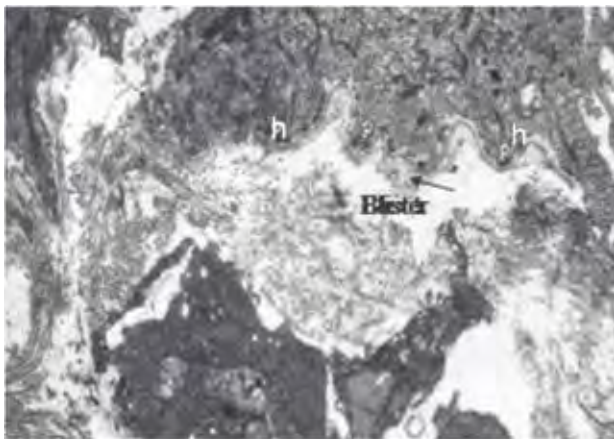


Fig. 62. Epidermolysis bullosa dystrophica recessiva. Small blisters under the junction, mimic to dominant variant. Upper: Blister roof is of basal lamina and remnants of dermal tissue (arrow). Most part of the blister roof resembles to dominant variant. Hemidesmosomes with anchoring filaments are seen spot-like (h). The blister floor is of dermis. $\times 10,000$. Lower: The blister roof is basal cells. Blister edge shows basal lamina without dermal remnants (arrows). In the middle of the blister, spot-form hemidesmosomes without basal lamina (h). Cell membrane of keratinocytes is facing directly the blister cavity without basal lamina nor hemidesmosomes. $\times 10,000$. [Unpublished]

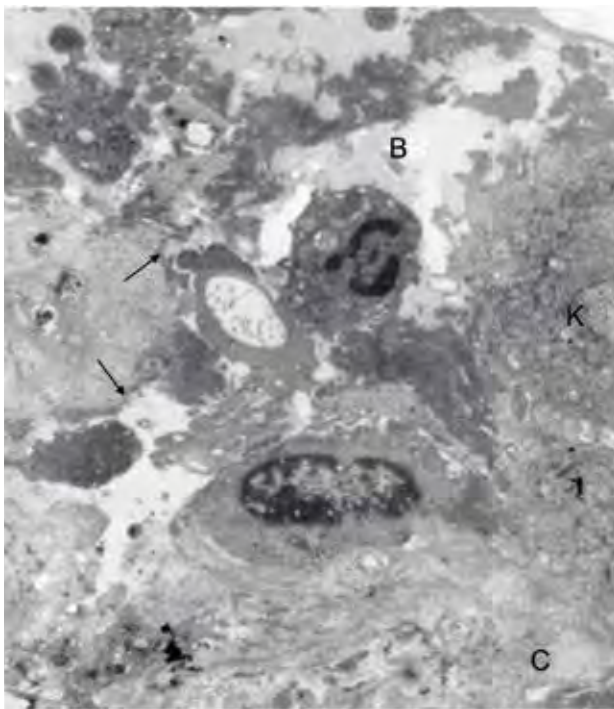


Fig. 63. Diabetic blister (false subepidermal blister). Blister floor is dermis or keratinocytes. Basal lamina is destroyed and not seen. Blister roof is epidermis. K: keratinocyte, B: blister cavity, C: corium, arrows: rest of basal lamina. $\times 5,000$. [Unpublished]

Dermolytic separation

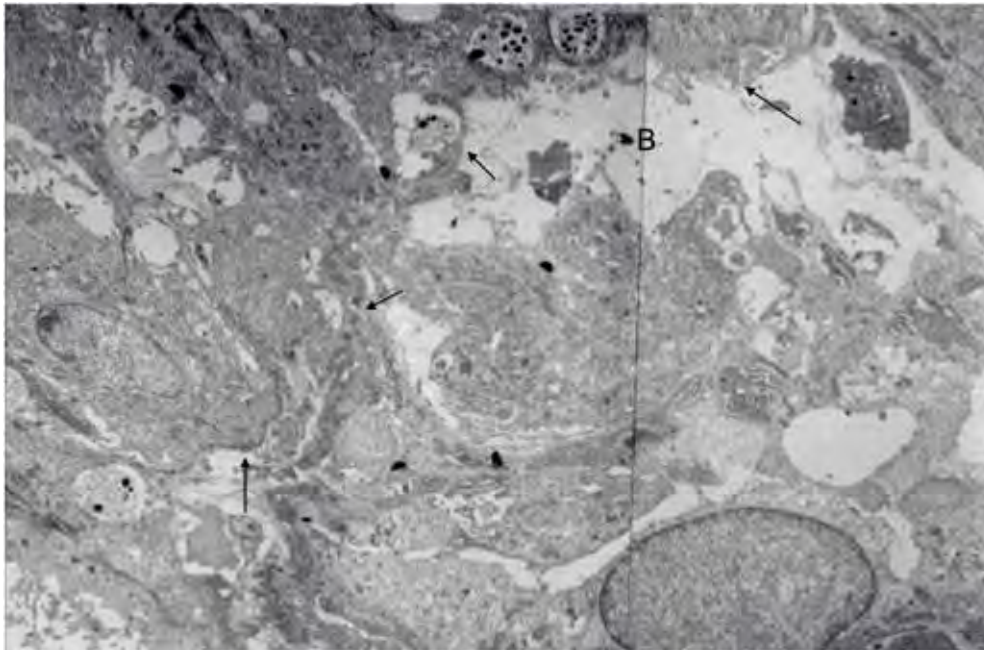


Fig. 64. Epidermolysis bullosa acquisita. Subpapillary dermis is damaged and form blister. Blister is seen under the junction. Arrows point at basal lamina. B: blister cavity. $\times 5,000$.

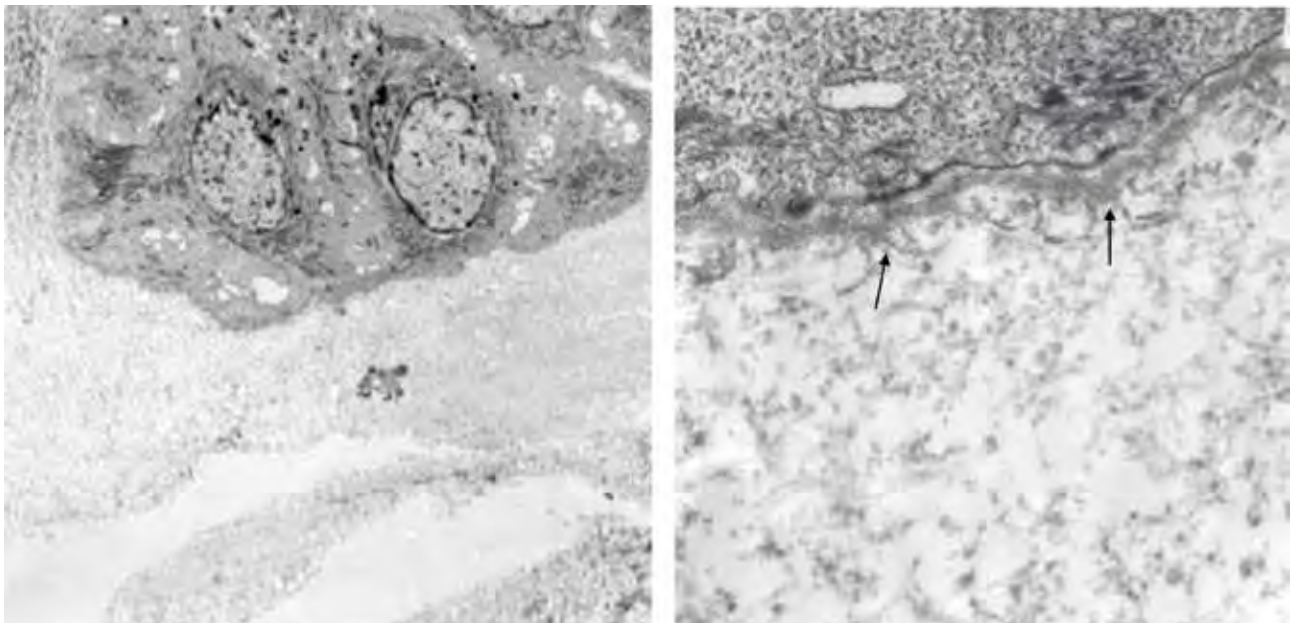


Fig. 65. Generalized morphea [18]. Blister in reticular dermis. The papillary dermis is damaged and form leak in the dermis. $\times 2,000$. Details of the junction is shown in the right-hand figure. Dermoepidermal junction is seen unchanged. Connective tissue in the papillary dermis is damaged. Blister locates under the junction. Arrows point at anchoring fibrils. $\times 20,000$.

*Productive changes of dermoepidermal junction
Disorders*

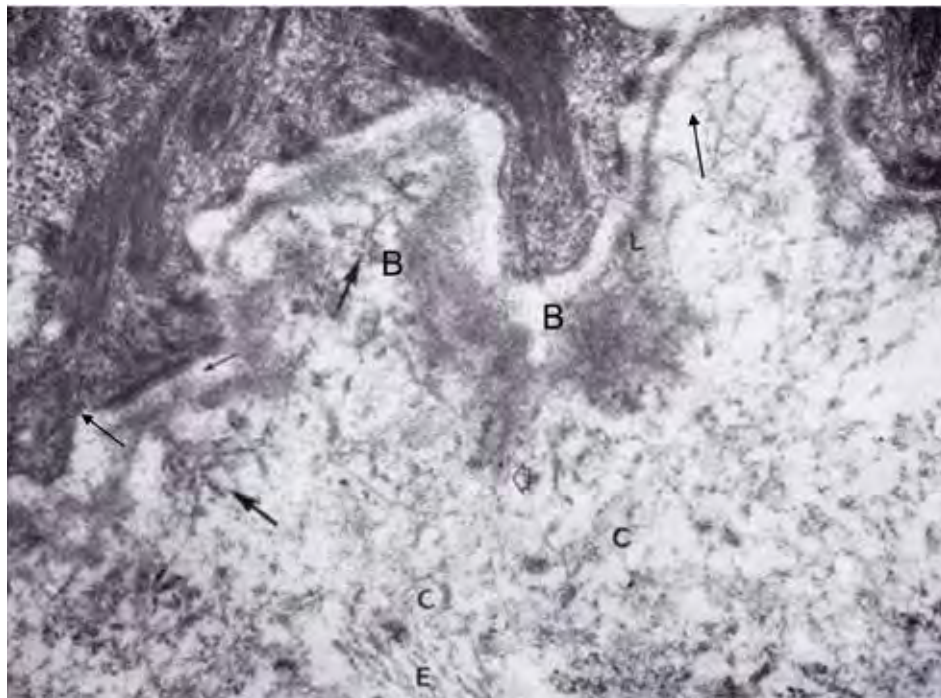


Fig. 66. Dermoepidermal junction in generalized scleroderma [19]. This picture shows localized thickening of basal lamina (B) and well developed anchoring fibrils in clumps (arrows). Collagen fibrils (C) are reduced [20]. Collagen fibrils in sublamina area is vanished. $\times 10,000$.

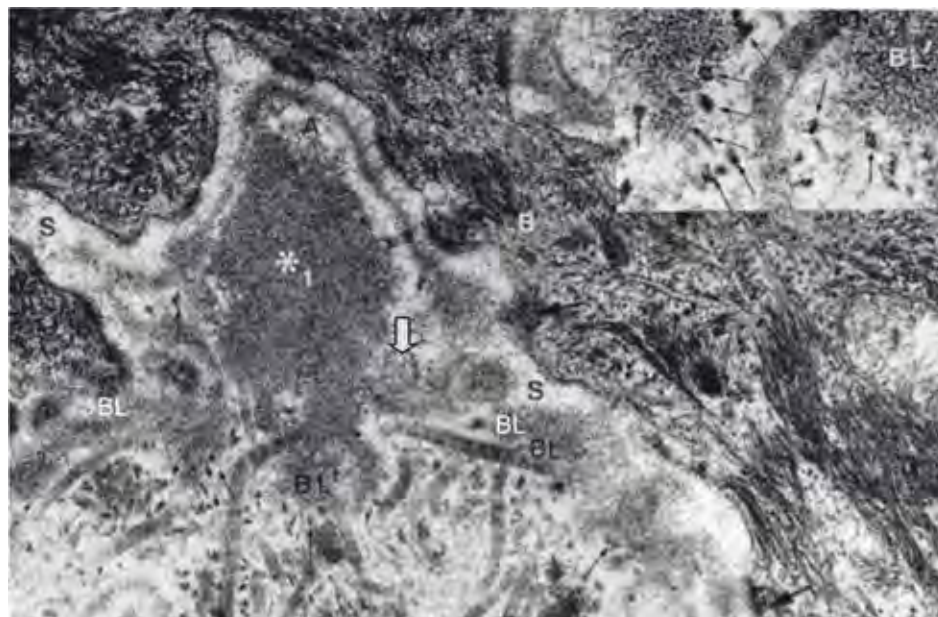


Fig. 67. Lupus erythematosus [20]. The junction components reveals enormous anomalies. Irregularly thickened basal lamina (BL), Asterisk 1 marked mass is thick basal lamina with crystalline figure. Mass of thin anchoring fibrils (A) are seen on the surface, subepidermal space (S). Anchoring fibrils are spot form as shown in the inset. Inset shows the area (A) in detail. Dense spot-form anchoring fibrils (thin arrows). A wide black arrow points at an oval particle of unknown nature. $\times 15,000$. $\times 30,000$ (inset).



Fig. 68. Lupus erythematosus [20]. Crystalline structure covers over the dense masses (Asterisks 2, 3). The masses seem to be basal lamina with immune reactant, because of anchoring fibrils on the surface (Arrows). Basal lamina is irregularly thick (BL). Hemidesmosomes are normal (thick arrow). Glycosaminoglycan (G). $\times 20,000$.

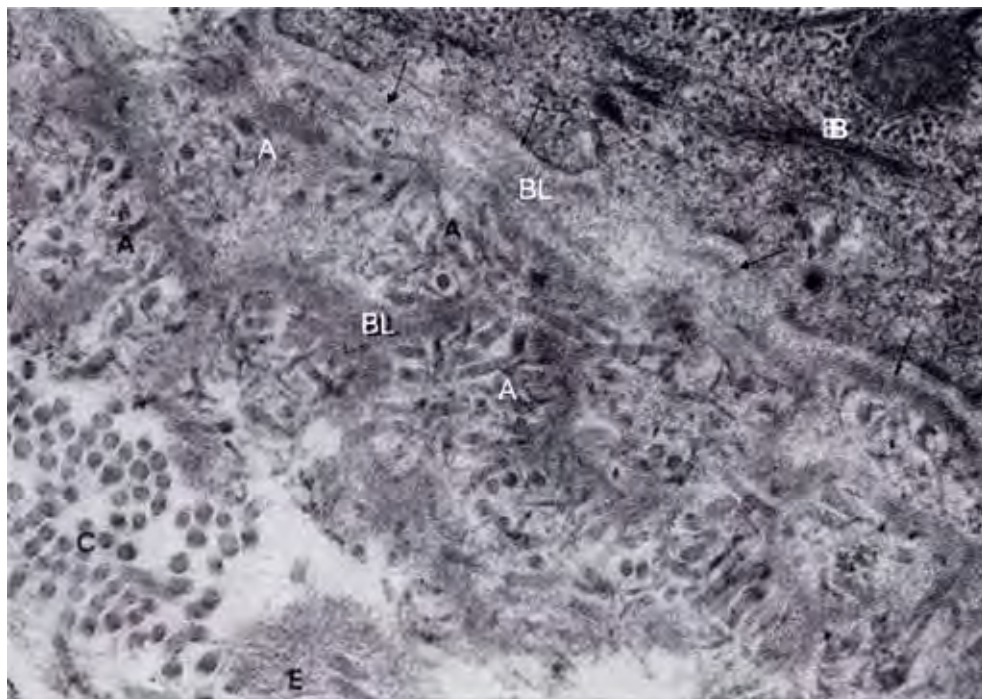


Fig. 69. Lupus erythematosus [21]. Basal lamina are 4-5 layers. The lowest basal lamina is thick distinct with well developed anchoring fibrils (BL), while the other layers of basal lamina on the epidermal side are thin indistinct (arrows) with anchoring fibrils (A). B: Keratinocyte. $\times 20,000$.

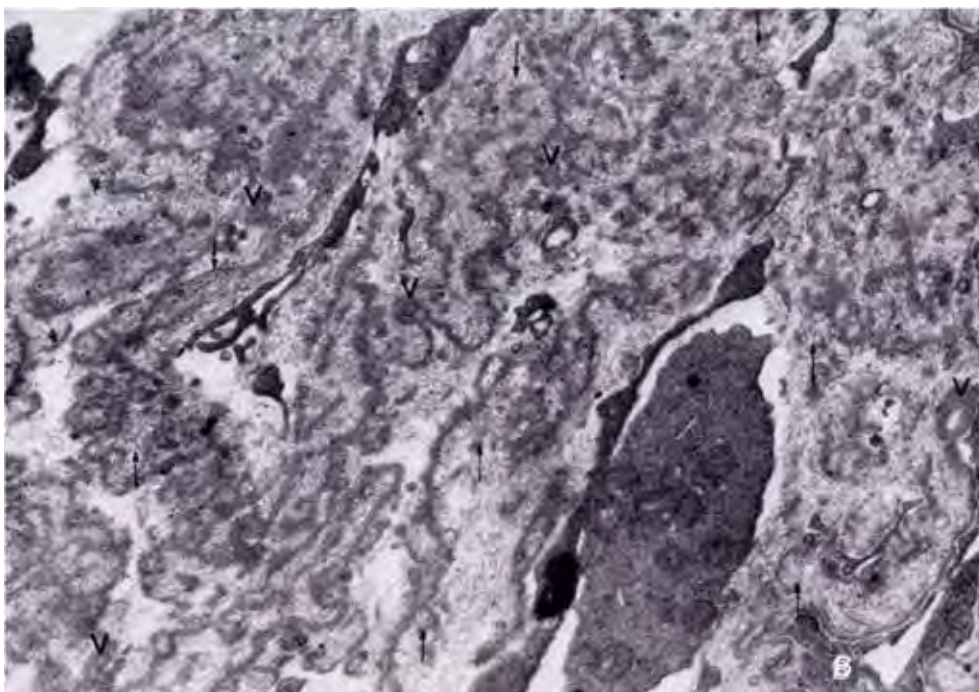


Fig. 70. Lupus erythematosus [21]. Enormous growth of basal lamina under the epidermis. Basal lamina forms irregular net-works in the dermis (v shows examples). Arrows point at mass of anchoring fibrils. Basal lamina under epidermis (B) is seen on the down right corner. $\times 2,100$.



Fig. 71. Lupus erythematosus [21]. Fragmented and band-shaped basal lamina with normal anchoring fibrils in the upper corium (arrows). Anchoring fibrils form conglomerates (BA-1). E: epidermis. Details in Figs 74, 75. $\times 2,000$.

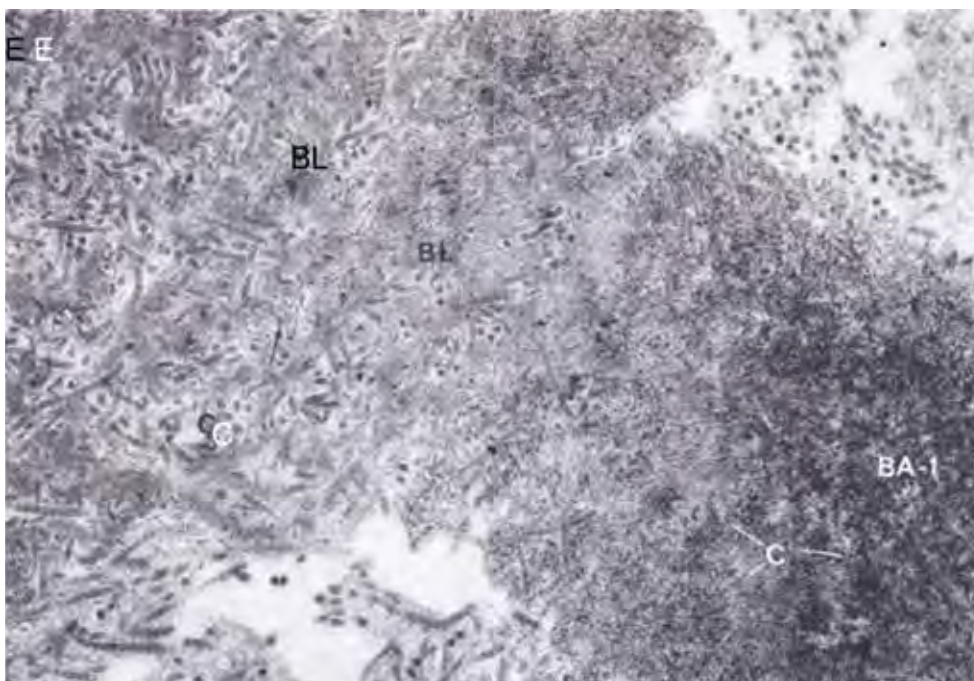


Fig. 72. Lupus erythematosus. Fragments and bands of basal lamina with normal anchoring fibrils (BL). BA-1 indicates conglomerate of abnormal anchoring fibrils, as shown in Fig. 71. Basal lamina and collagen fibrils (C). E: epidermis. $\times 5,000$. Details of BA-1 appears in Fig. 73.



Fig. 73. Conglomerate of thick anchoring fibrils (BA 1) and straight thin anchoring fibrils (BA 2) are continued to band-formed basal lamina (BL). Anchoring fibrils are in various shapes (thin arrows 1, 2, 3). Arrow 1: Normal shape; Arrow 2: non-banded; Arrow 3: grainy shape. Two insets on the left upper corner show enlarged picture of types 2 and 3 anchoring fibrils. $\times 30,000$. Inset. $\times 60,000$.

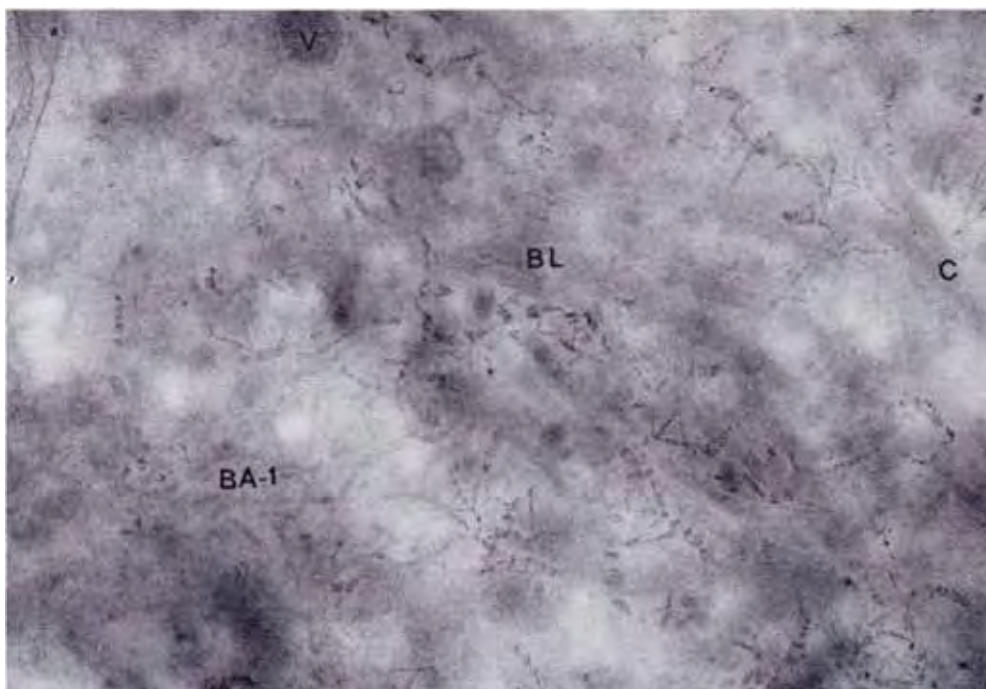


Fig. 74. Lupus erythmatosus. Invaded basal lamina and abnormal anchoring fibrils are stained by periodic acid-silver proteininate staining. Basal lamina (BL) and cross bands of anchoring fibrils are stained (BA-1). Collagen fibrils (C). × 10,000.

Basal cell and spinous cell carcinoma [22, 23]

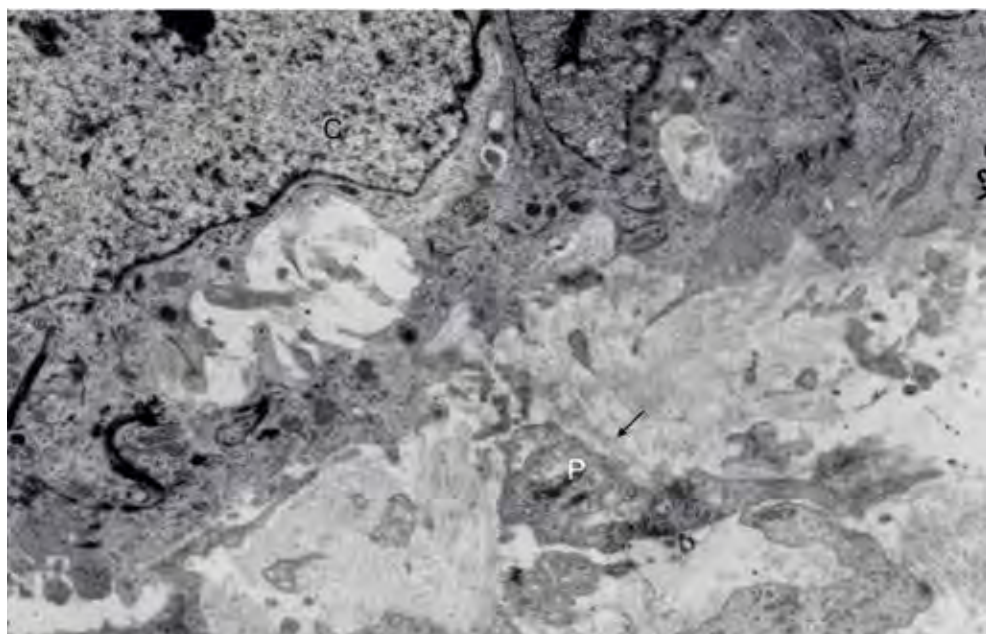


Fig. 75. Basal cell carcinoma. Invading zone. Cancer cell (C) protrudes cytoplasm (P) and form poor junction (arrow). × 10,000. See also Fig. 39.

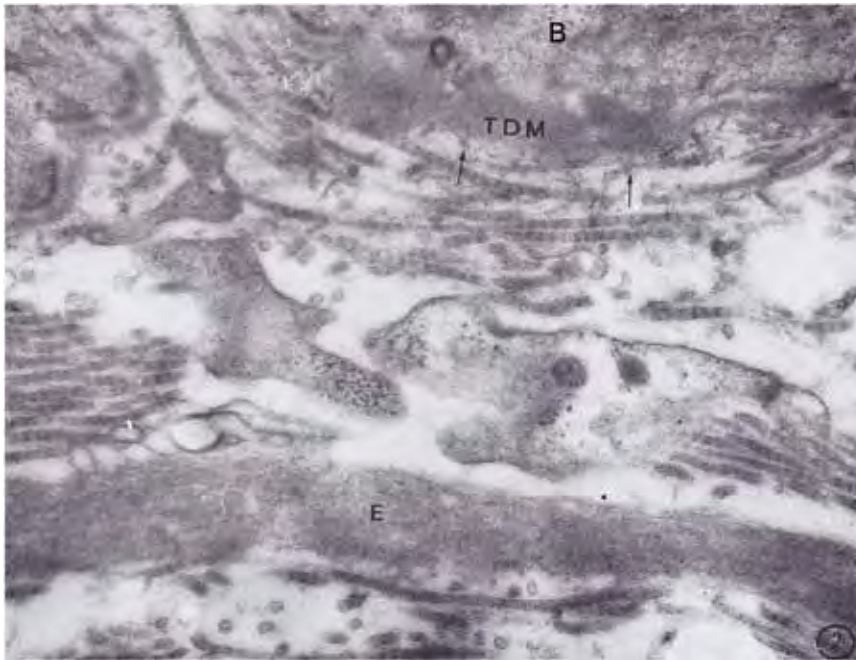


Fig. 76. Basal cell carcinoma (invading zone) [23]. Localized thickening of basal lamina (TDM) with few small anchoring fibrils on the dermal surface. B: carcinoma cell, E: elastic fibre. $\times 15,000$.



Fig. 77. Basal cell carcinoma (periphery of cancer invasion). Net-works of basal lamina (DM). Invading cytoplasm of cancer cell (C). Cytoplasmic protrudes invade into dermis. Basal lamina forms rough net-works with anchoring fibrils (A). Arrows point at poor hemidesmosomes. $\times 10,000$.

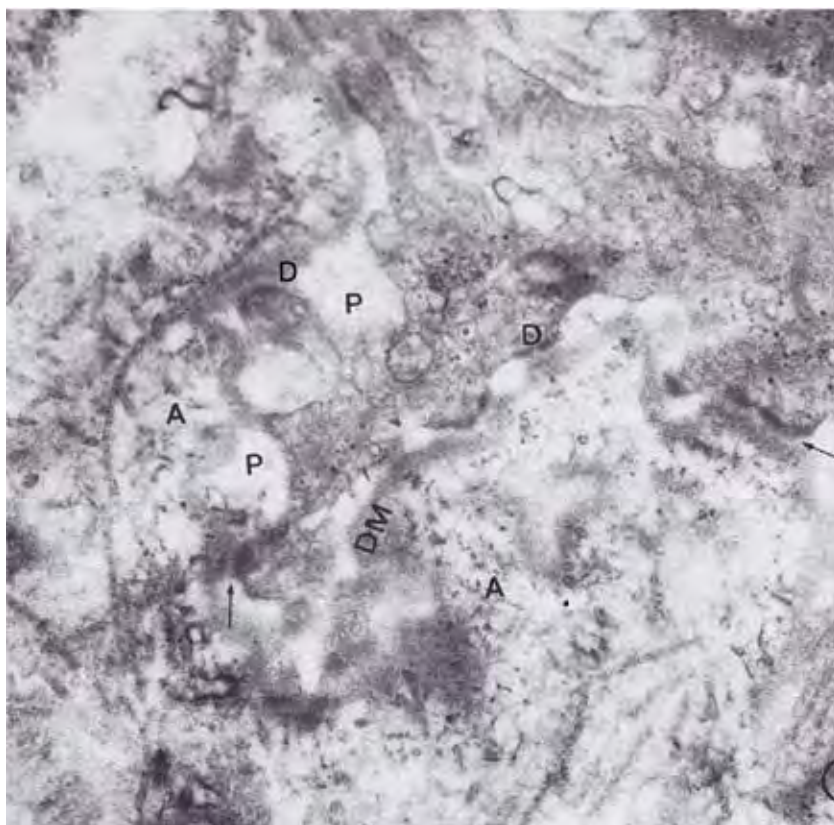


Fig. 78. Basal cell carcinoma. Invading cytoplasm of carcinoma cell. Basal lamina (DM) and widened subepidermal space (P) are irregular in width. Hemidesmosomes (D) are distinct. Anchoring fibrils are numerous (A). No collagen aggregate is noticed in the dermis of sublaminar area. $\times 20,000$.



Fig. 79. Basal cell carcinoma. Cancer cell nest. Fragments of basal lamina cover the cancer cell surface and are seen like surface coat of cancer cells. Half desmosomes and anchoring filaments are poor. Dermis is mucinous (M). Details appears in the following slides. $\times 2,000$.

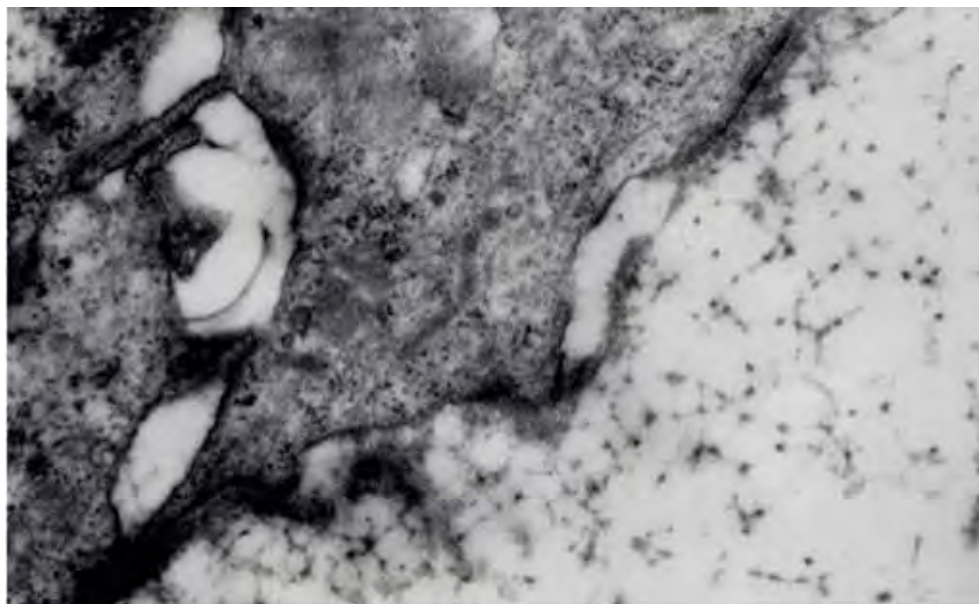


Fig. 80. Basal cell carcinoma. Abnormal junction and mucinous stroma. The components of the junction are not identified. Basal lamina covers partly over the cancer cell surface like cell coat. Hemidesmosomes are unclear. No anchoring filaments and anchoring fibrils are found. Dermis is filled of glycosaminoglycans. $\times 10,000$.

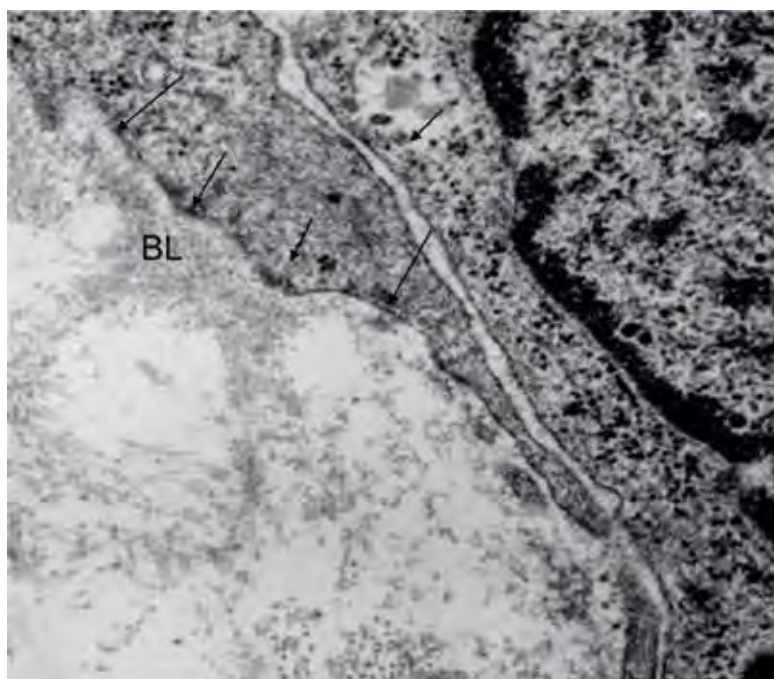


Fig. 81. Left: Basal carcinoma cells show incomplete hemidesmosomes (arrows) and basal lamina appears like cell coat (BL). Anchoring filaments and anchoring fibrils are not well identified. Right: Basal cell without junction structure. Basal lamina is wide diffuse band-form coat. No regular junction structure is developed. No collagen aggregate is found in the dermis around cancer nests. $\times 20,000$ (both Figs A and B).

Squamous cell carcinoma [24]

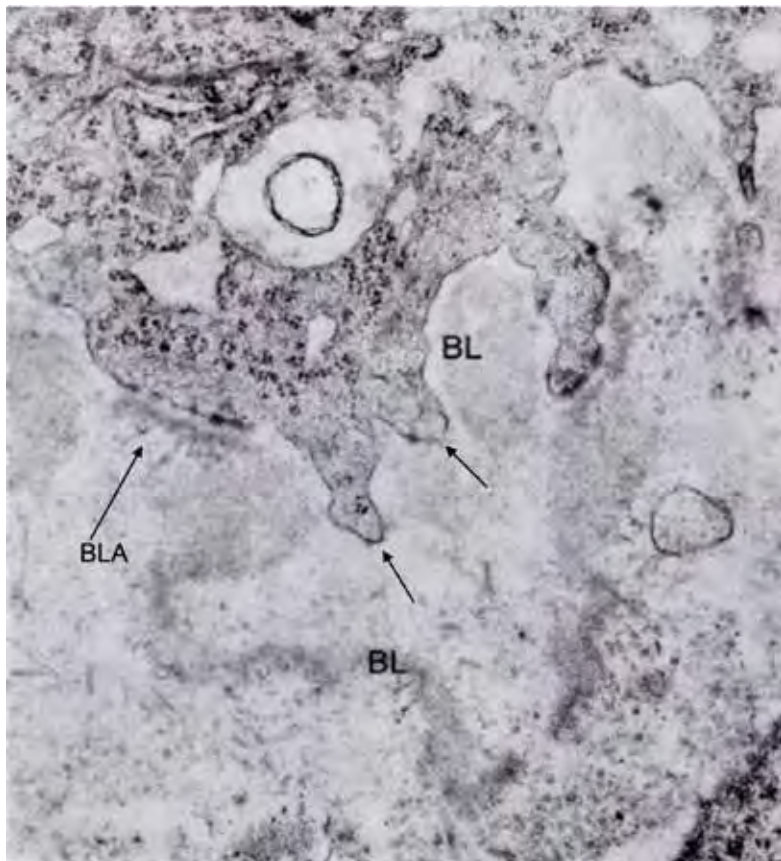


Fig. 82. Early stage of the invasion. Invaded cytoplasmic protrudes of cancer cell has poor hemidesmosomes (two arrows). Basal lamina (BL) is diffusely widened. When hemidesmosomes are formed in the surface of same cell, BL is also seen like band-form and form anchoring fibrils (arrow BLA). No collagen aggregate was seen in the dermis of the invading area. × 20,000.

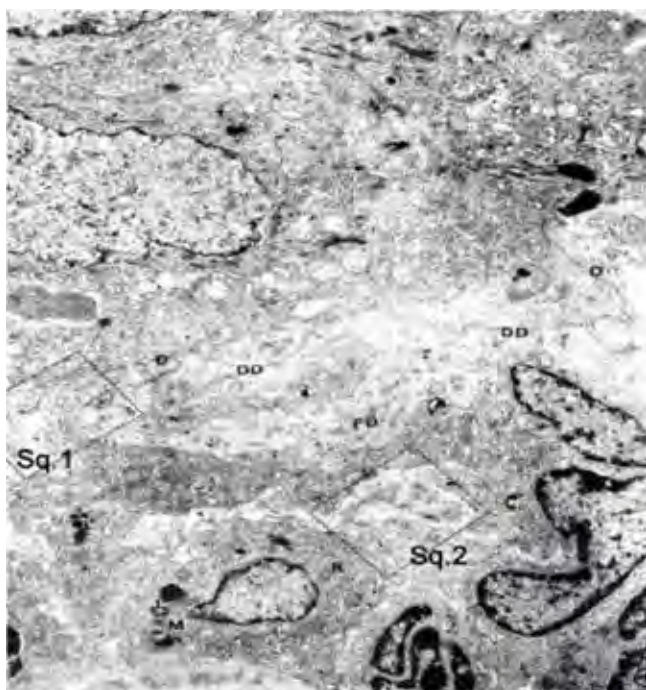


Fig. 83. Invasion of cancer cell into dermis through the junction. Square 1: Penetrating area. Square 2: New basal lamina among the infiltrated cells. × 5,000. Both squares appear in Fig. 84

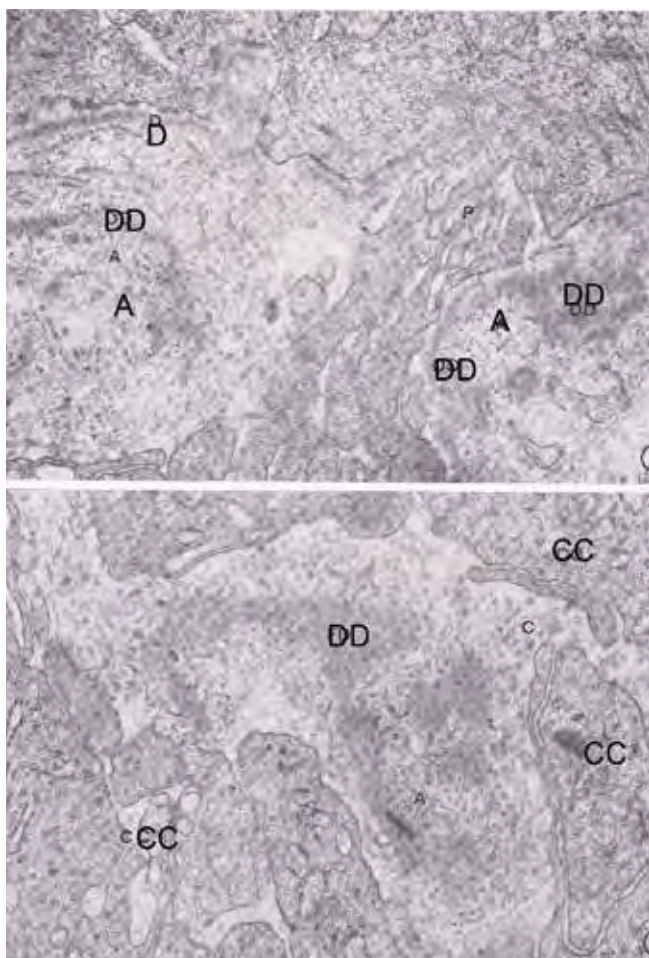


Fig. 84. Squamous cell carcinoma, enlarged figure of Fig. 85. The upper figure shows enlarged figure of square 1. Basal lamina is seen in ordinary form (D) and double layered (DD). Anchoring fibrils (A). $\times 20,000$. The lower figure shows enlarged figure of square 2. The picture shows dislocated basal lamina like fragments with numerous anchoring fibrils (DD) among the infiltrated cells (CC). $\times 20,000$.

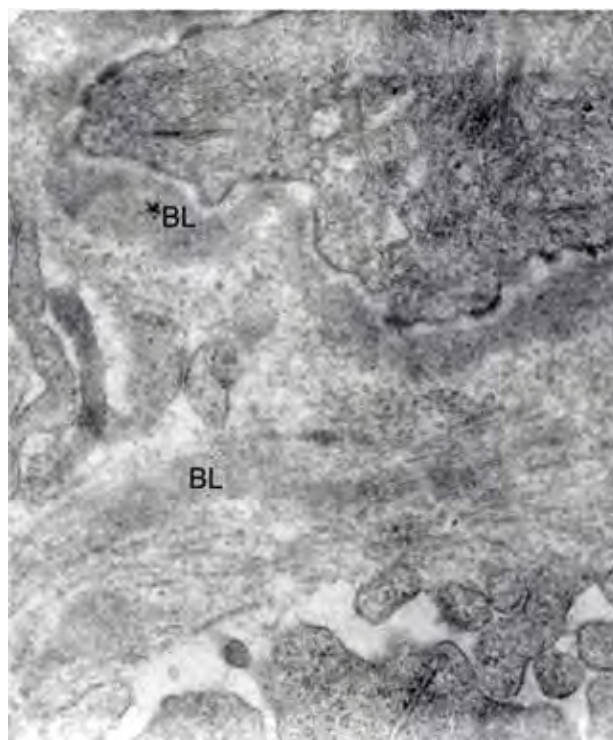


Fig. 85. Irregular basal lamina in squamous cell carcinoma. Hemidesmosomes and irregularly thickened basal lamina (BL) without anchoring fibrils are seen. Concerning the junction of basal cell carcinoma and squamous cell carcinoma, cancer cells of both type produce own specific junction. Basal cell carcinoma presents the junction-like diffuse, structure-less like cell coat, while squamous cell carcinoma forms own junction, along to the cancer cell surface. BL is thick. Anchoring fibrils are poor in both carcinoma. $\times 20,000$.

Miscellaneous: Mucin

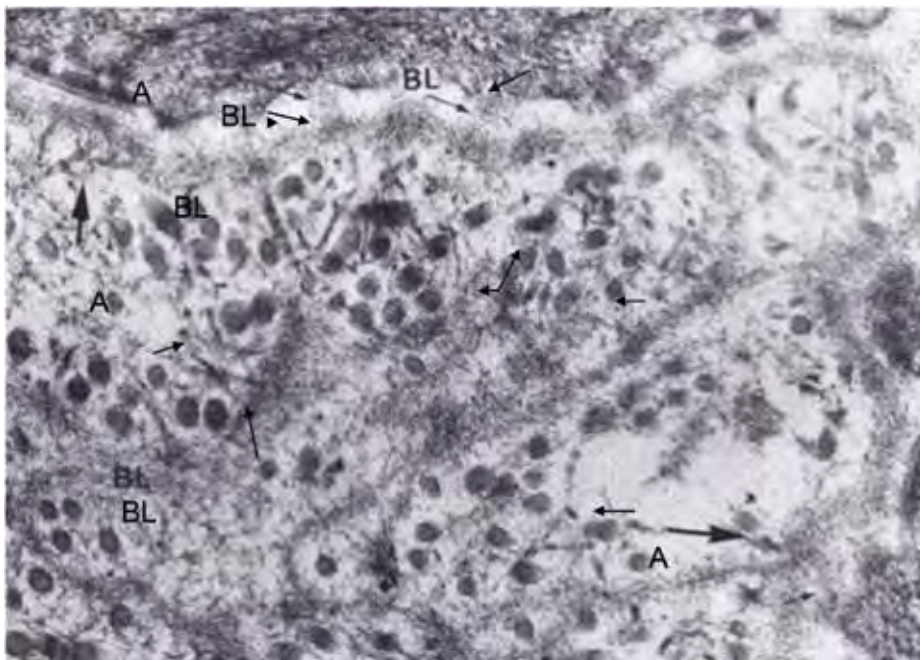


Fig. 86. Localized myxoedema [24]. Glycosaminoglycan appears as fine threads between collagen fibrils under basal lamina (BL) (thin arrows). BL appears varied in thickness. Anchoring filaments are seen like felt (thin arrow with BL). Anchoring fibrils are thin without distinct cross bands (thick arrow with A). × 20,000. See also Section for Ground substance.

Miscellaneous: Amyloid

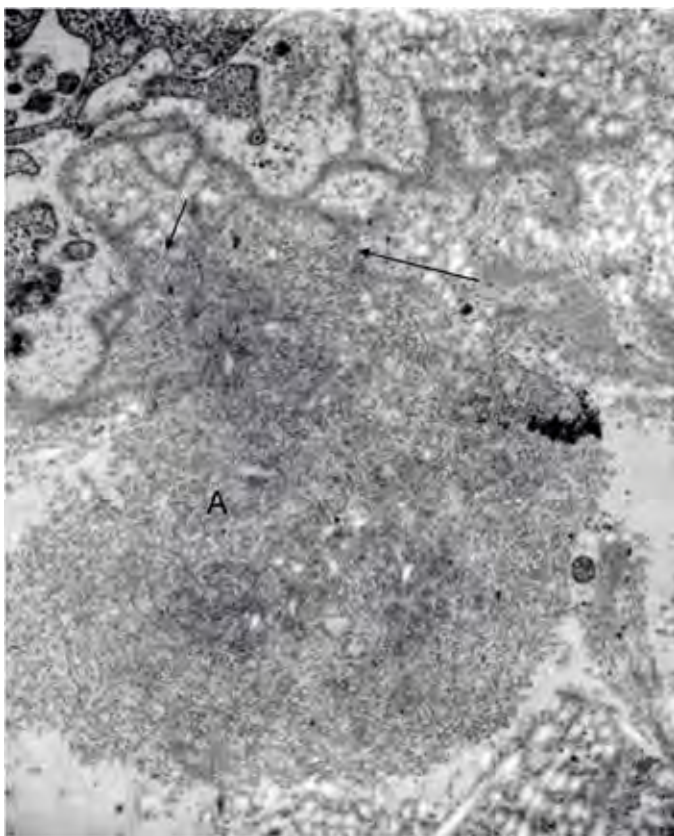


Fig. 87. Systemic amyloidosis [25]. Mass of amyloid (A) fuses to basal lamina of epidermis (arrows). It is presumed that biochemical components of amyloid, elastic matrix and basal lamina have some similarities. Details of amyloid filaments are seen in the Section of Collagen. × 5,000.



Fig. 88. Amyloid masses on the basal lamina of Schwann cell (S) and pericytes (P) in peripheral nerve. Arrows point at amyloid masses. A: axon. $\times 10,000$.

Miscellaneous : Hyalin



Fig. 89. Hyalinosis cutis et mucosa [26]. Vascular wall in dermis presents hyalin on the basal lamina of fibroblast. h: hyalin mass, b: basal lamina of pericyte, F: myofibroblast. Arrows: Supposedly calcium spot. Details of hyalin mass appear in the following figure. $\times 5,000$.

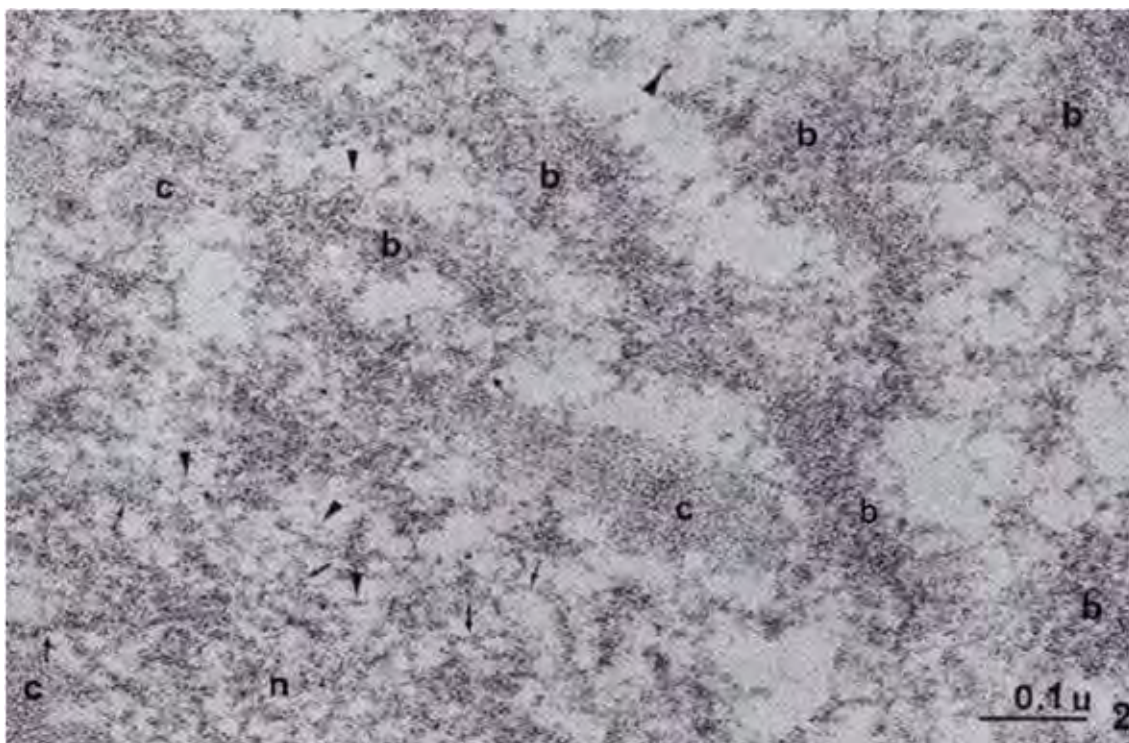


Fig. 90. Hyalinosis cutis (detail). High-powered figure shows hyalin filaments (h) in mesh (arrows). Hyalin filaments join basal lamina (b). Arrow-heads point to glycosaminoglycans. Collagen fibrils (c). $\times 15,000$.

Miscellaneous : Filamentous body (Civatt body) [22, 28]

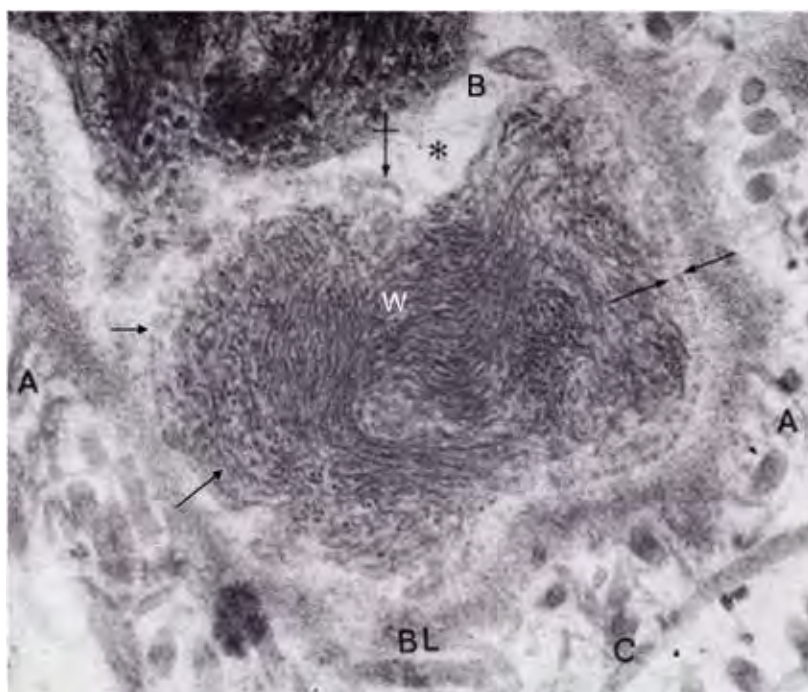


Fig. 91. Filamentous body (Civatt body) in subepidermal space. Filamentous body is eosinophilic and mass appear in whirl array (W). The body falls down into dermis through the junction. The body is described in morphea, lupus erythematosus [20, 27]. Probably the body is degenerated keratinocyte. BL: basal lamina, A: anchoring fibrils, B: intercellular space, C: collagen fibril. Arrows: cell membrane of basal cell. $\times 10,000$.

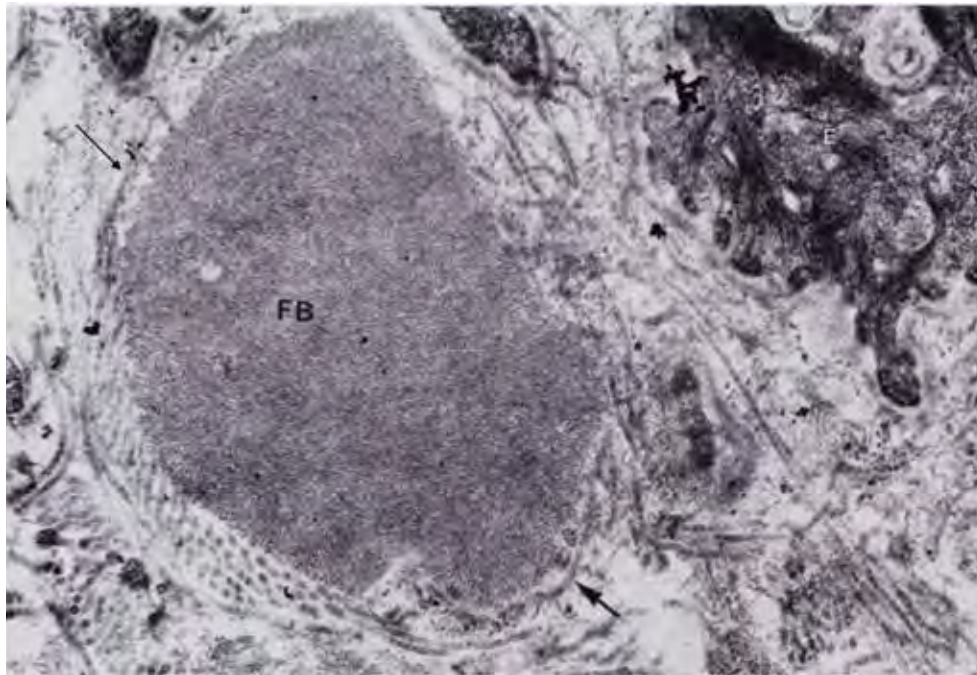


Fig. 92. Filamentous body (FB) in the papillary layer. Cell membrane and basal lamina is vanished. Arrows pointed at rests of the basal lamina on the body surface. E: epidermis. $\times 5,000$.

V. Mast cell

Overview	
• Ultrastructure	Figures 1–3
• Degranulation and regranulation	Figures 4–12
• Mast cells in dermatoses	
- Pretibial myxoedema	Figures 13–17
- Scleromyxoedema	Figure 18
- Morphoea	Figure 19
- Generalized scleroderma	Figure 20
- Fibrodysplasia ossificans progressiva	Figure 21
- Amyloidosis	Figures 22–23
- Basal cell carcinoma	Figures 24–30, Table I
- Squamous cell carcinoma	Figures 31–37

Ultrastructure [1]

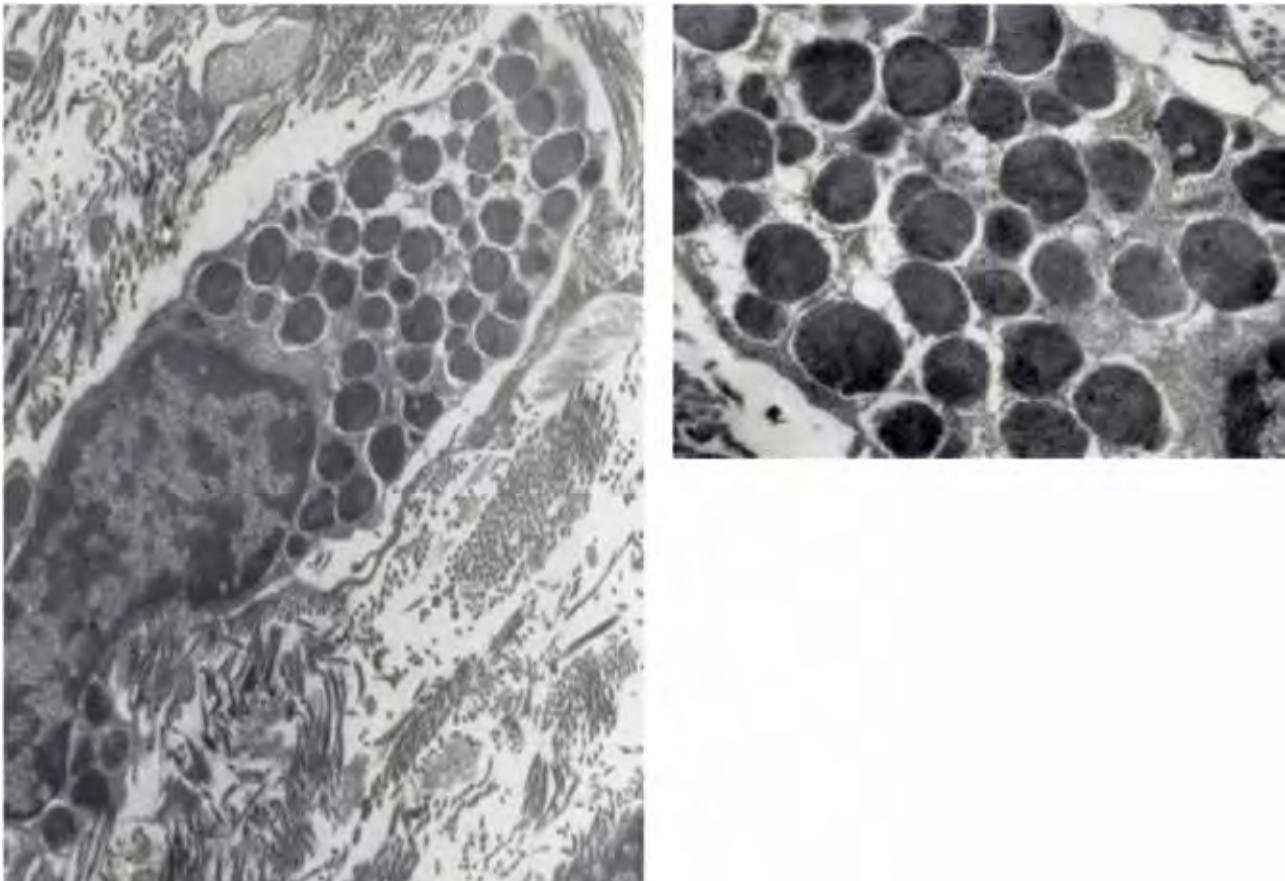


Fig. 1. Mast cell in normal dermis [1]. Mast cells are easily identified in histological section by metachromasia. In normal dermis, mast cells are found around hair follicle, vessel, nerve, gland. Figures show mast cell in normal dermis. The granule contains glycosaminoglycans, proteolytic enzymes, histamine and heparin, etc. Mast cell functions by the granule content. The granules are filled in the cell and reveal characteristic structure. A $\times 5,000$. B. $\times 20,000$.

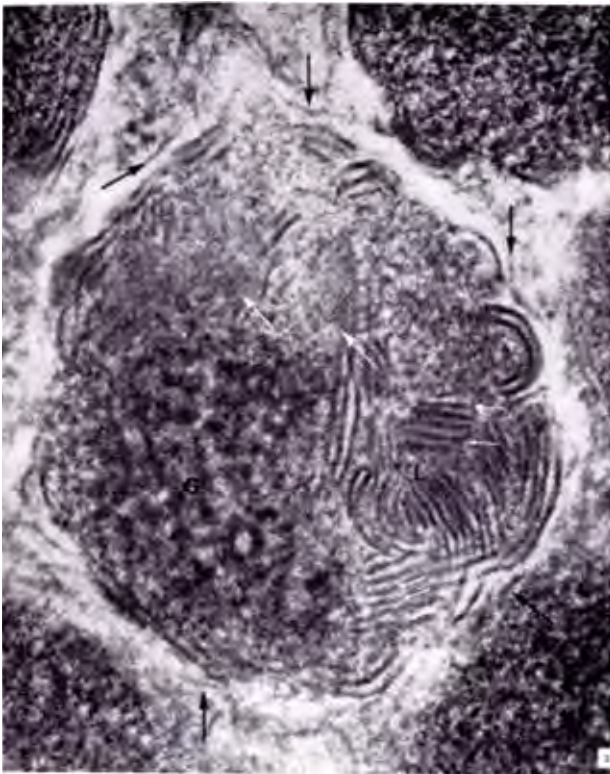


Fig. 2. Mature granule of mast cell [1]. A mature granule shows lamellar structure in parallel line and scroll and dense granular material with crystalline parallel lines (white arrows). Enclosing membrane is single layer, not distinct (black arrows). $\times 100,000$.

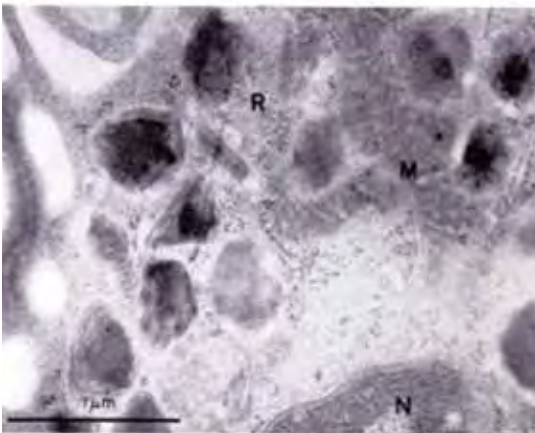
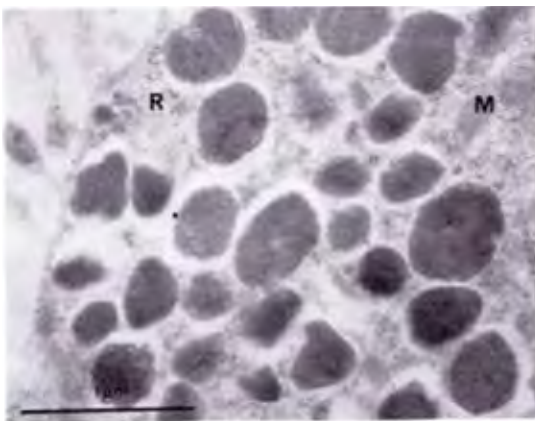


Fig. 3. Mast cell granules. Ruthenium red stain. Mast cell granules are contrasted by ruthenium red, and contrasted, indicating glycosaminoglycan content [2]. The upper figure shows diffuse stain in mast cell granules, contrasted by ruthenium red in ammoniac solution. The granules are contrasted diffusely. $\times 10,000$. Scale bar indicates 1 μm . The lower figure shows ruthenium red in acetic acid solution. The granular material is contrasted by ruthenium red, indicating a high content of glycosaminoglycan in the granular material. $\times 10,000$. Scale bar indicates 1 μm .

Degranulation and regranulation [3]



Fig. 4. Urticaria pigmentosa [1]. Mast cells degranulate by chemical and physical way, such as polymixine B, corticosteroid, histamine-liberator and a simple stroke on skin surface. Mast cells of urticaria pigmentosa are provoked degranulation by a stroke. The figure shows a mast cell in the eruption. The granules are mature and disintegrated leaving honeycomb structure in the cytoplasm (arrow-heads). The granules are also extruded in the extracellular space. Besides, mast cells show ordinary cell organelles, mitochondria (M), endoplasmic reticulum (R), intracytoplasmic filaments (F). × 5,000. Details are shown in the following slides.

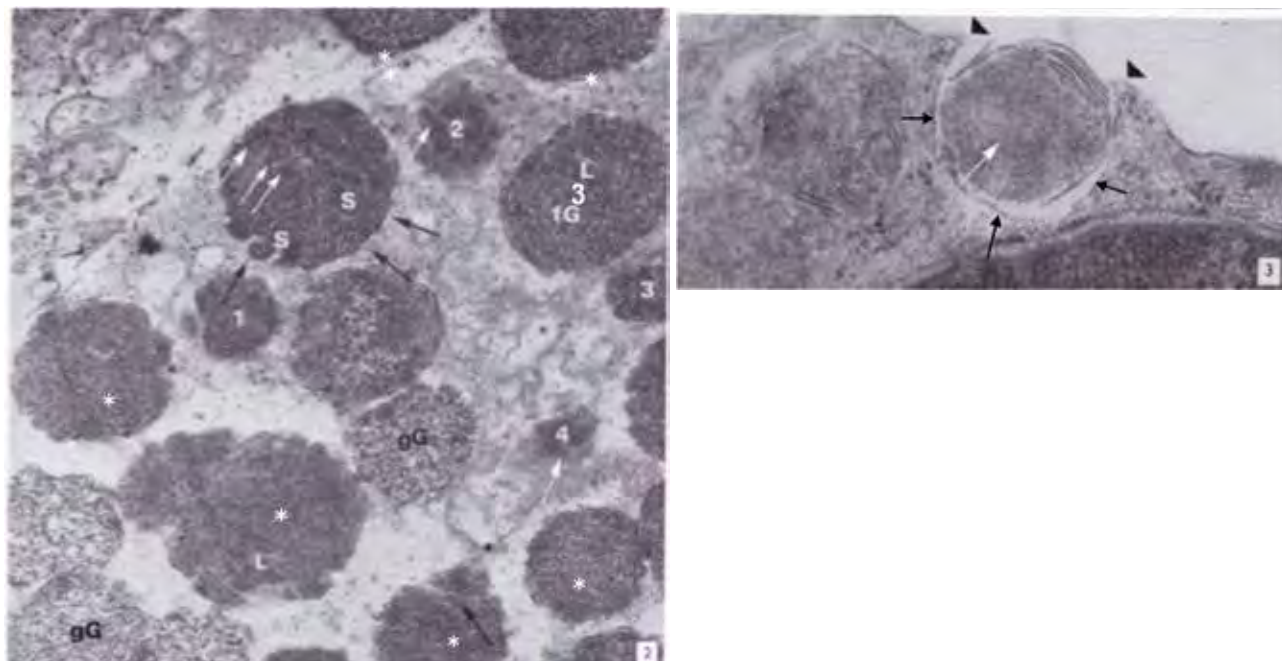


Fig. 5. Degranulation of mast cell, in urticaria pigmentosa. In details [1]. Left: Granules No.1-3; intracellular mature granules. No. 4. disintegrating granule. Granules marked by S and fG are extruding. Black arrows point at distinct enclosing membrane. gG: coarse granular content. White arrows point at indistinct crystalline figure. Granules (asterisks) are extracellularly. × 20,000. Right: A mature granule is extruding (white arrow). Arrow heads point at edges of cytoplasm. The enclosing membrane is distinct (thin arrows) and fuse to cell membrane. × 40,000.

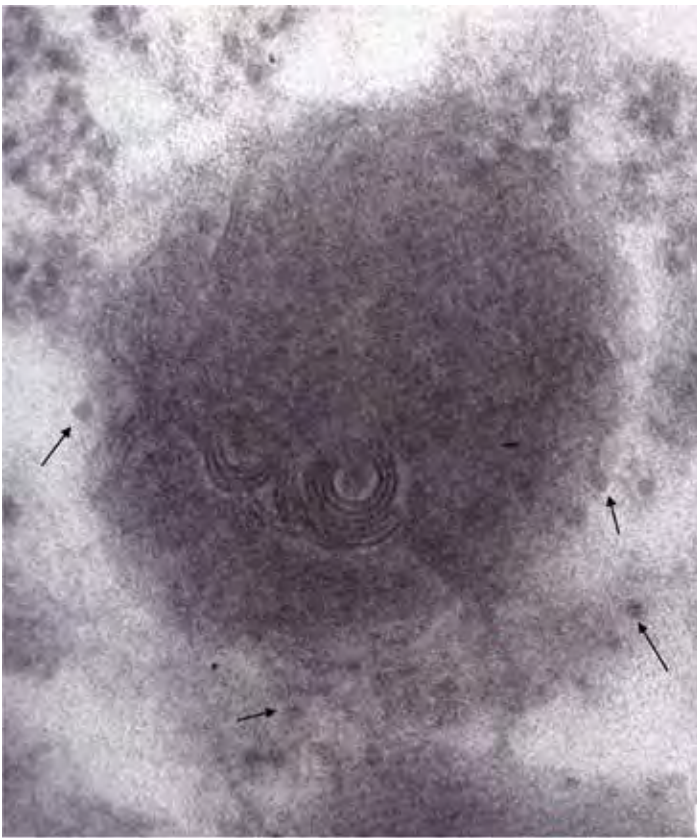


Fig. 6. A granule extruded in the extracellular space [1]. The granule shows scrolls and homogenous material. No enclosing membrane is seen. Arrows point at glycosaminoglycan figure. $\times 100,000$.

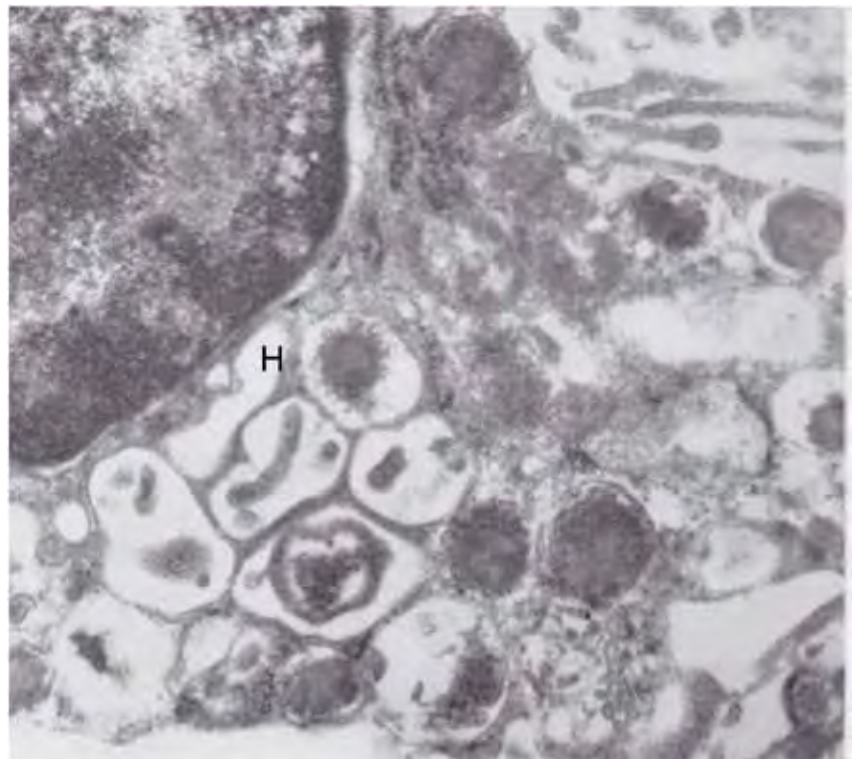


Fig. 7. Honey-comb structure [1]. The granule content is disintegrated and secreted in the extracellular space, leaving empty space in the cytoplasm. The structure left in the cytoplasm is called honeycomb structure (H). $\times 10,000$.

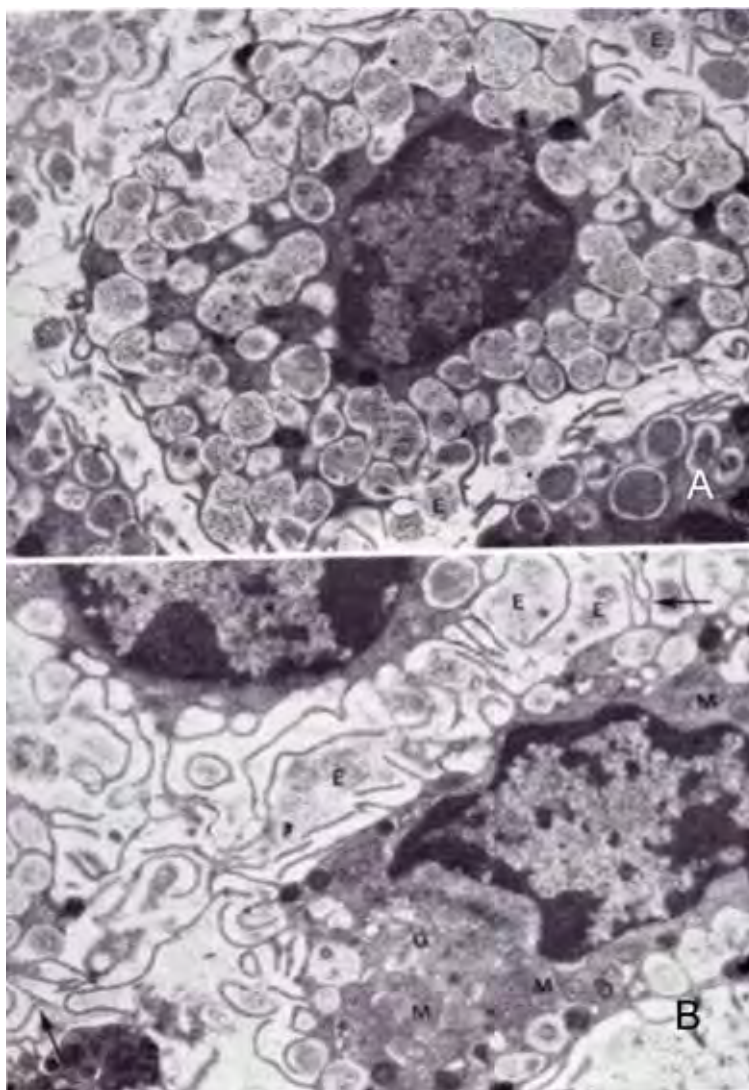


Fig. 8. Urticaria pigmentosa. Mast cell after a stroke by a blunt tool. A) Directly after a stroke. Degranulation of mast cells. The granules are disintegrated but still left in the cell. × 8,000. B) Around 5 minutes after a stroke. The granules are extruded and solved in the extracellular space. Numerous thin long villi are left on the cell surface. × 8,000.

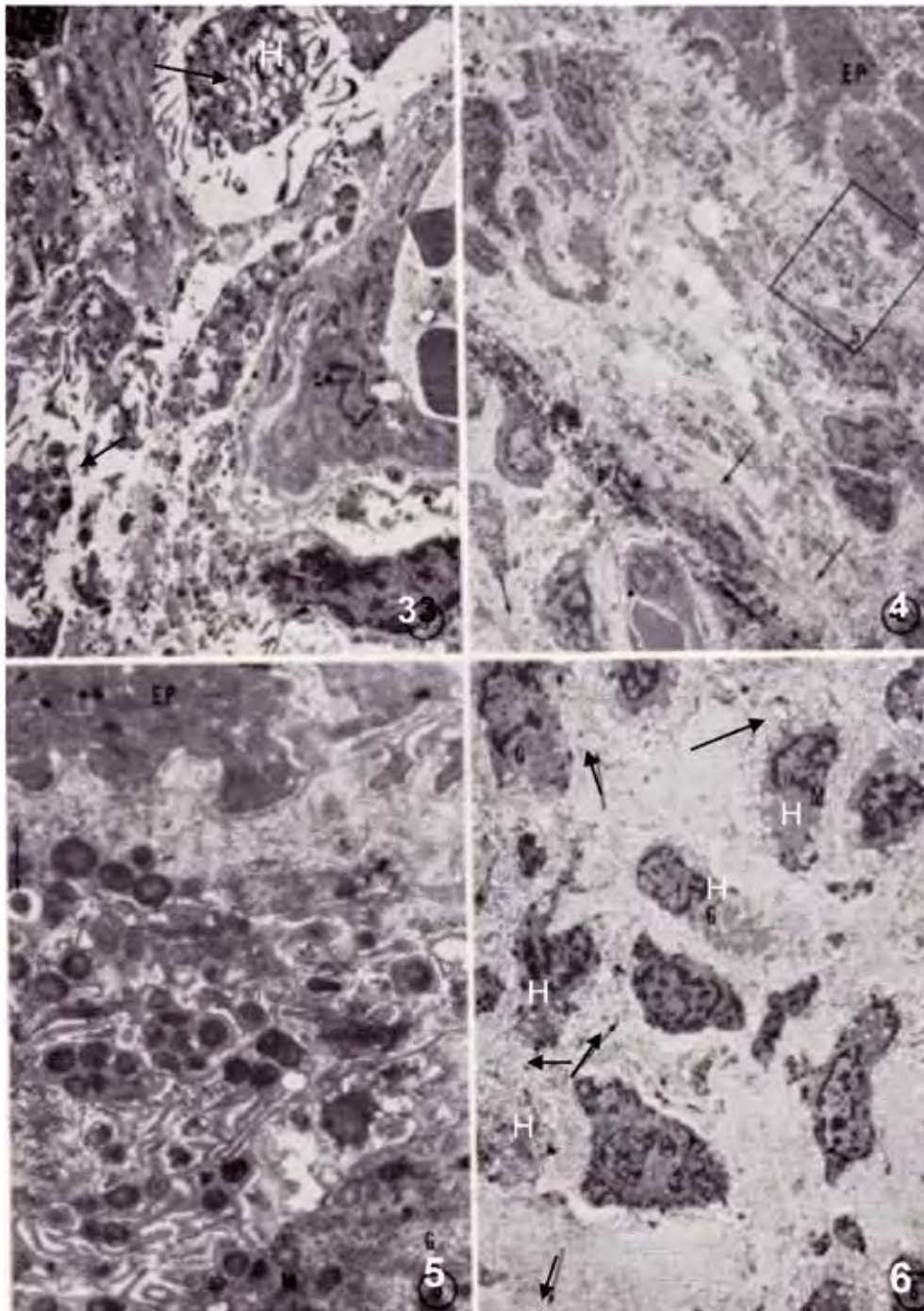


Fig. 9. De- and regranulation of mast cells of urticaria pigmentosa [3]. No. 3. shows mast cells at 30 second after a stroke. Granules in intra- and extra-cellular space. Honeycomb structure (H) and extruded granules are seen (arrows). Nos 4–6. Mast cells in different level of corium 1 minute after stroke. No. 4. Mast cells in the uppermost part of dermis show mild response. The squared area and arrow-pointed area show degranulation and long villi. No. 5 shows framed area of No. 4. The mast cells show intra- and extra-cellular granules and long villi. No. 6. shows mast cells in reticular dermis. The mast cells show honeycomb structure (H), disintegrating granules (g) and long villi (arrows). × 2,000. Nos 3, 5, 6. × 5,000, for No. 4. Continue to the next figure.

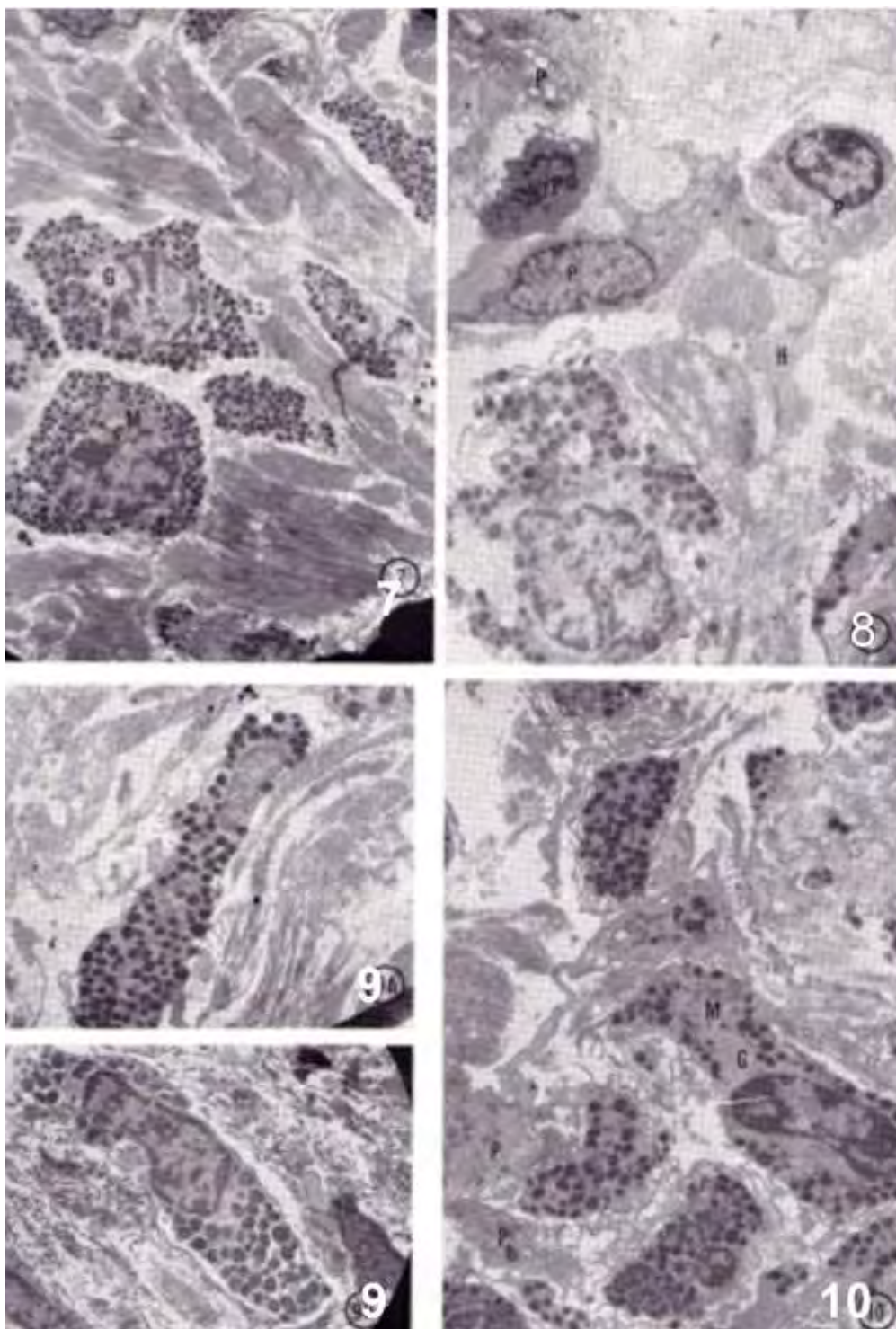


Fig. 10. No. 7. Mast cells in deep part of reticular dermis in urticaria pigmentosa. No degranulation is seen after a stroke. No. 8. Mast cells in the middle dermis at 2 minutes after a stroke. The mast cells show degranulation and villi. No. 9 upper. A mast cell in the middle dermis at 10 minutes after stroke. The cell shows mature granules, no degranulation and long villi. No. 9 lower shows a mast cell in normal dermis, for comparison. A mast cell shows mature granules and no villi. No. 10. Mast cell in middle dermis of urticaria pigmentosa, at 10 minutes after stroke. The mast cells with mature granules and villi. The cells seem to be regranulated. $\times 2,000$.

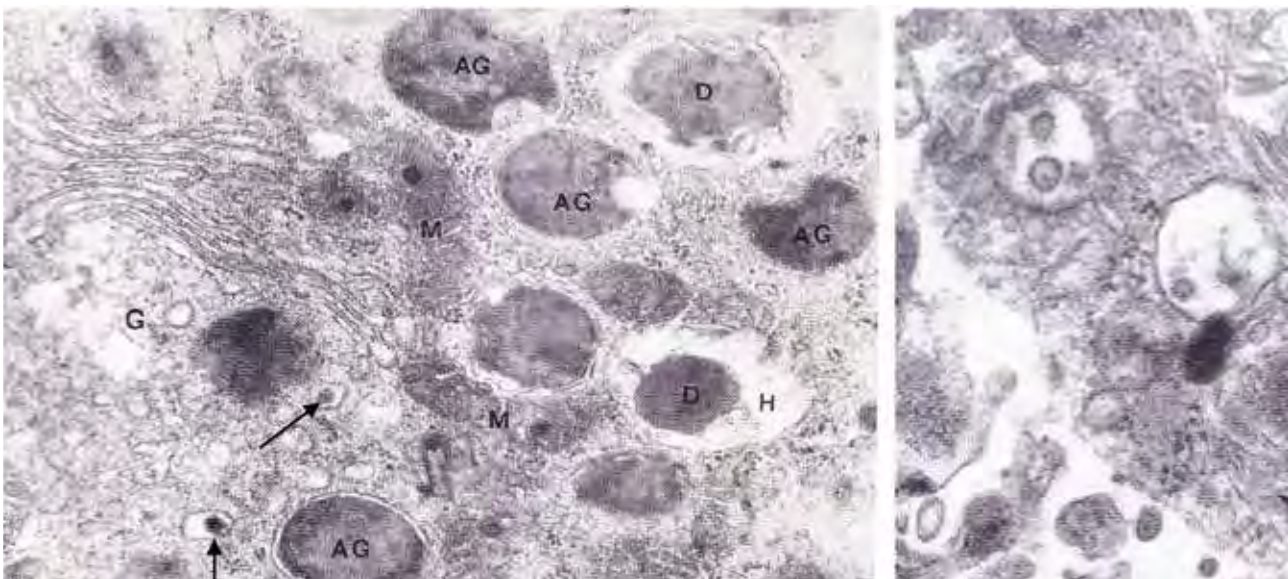


Fig. 11. Regranulation. Regranulation seems to begin earliest around 5 minutes after stroke. The regranulation begins to form progranules in Golgi apparatus (left-hand figure) and lamellar structure appears as stripes in an irregular array in the Granules (right-hand figure). Corticosteroid interferes on the development of mast cell granule. Numbers of the abnormal granule and degranulation are increased [4]. Progranules in a vesicle of Golgi zone (arrows). G: Golgi zone, AG: abnormal granules, D: disintegrating granules, H: honeycomb. $\times 20,000$. An immature granule in Golgi zone. The immature granule exhibits incomplete lamellar structure showing irregular array (large arrow) and fine crystalline structure (fine arrow). $\times 60,000$.

Time relapse for degranulation and regranulation

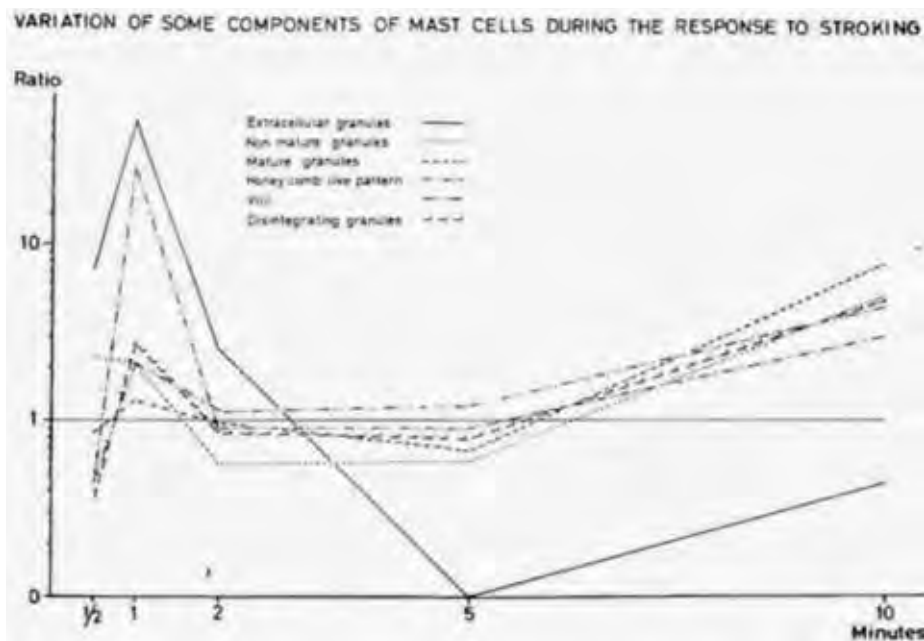


Fig. 12. Mast cell granules are counted in about $800 \mu^2$ area. It may be concluded that degranulation is closed almost 2 minutes after stroke and the granules in the extracellular space vanish in 5 minutes. Regranulation begins at about 5 minutes after stroke, and regranulation starts. Degranulation increased at 10 minutes after stroke. The mast cells show cytoplasm in same appearance as before stroke.

Mast cells in dermatoses

Pretibial myxoedema [5]. Mast cells present various figures as shown in Figs 13–16

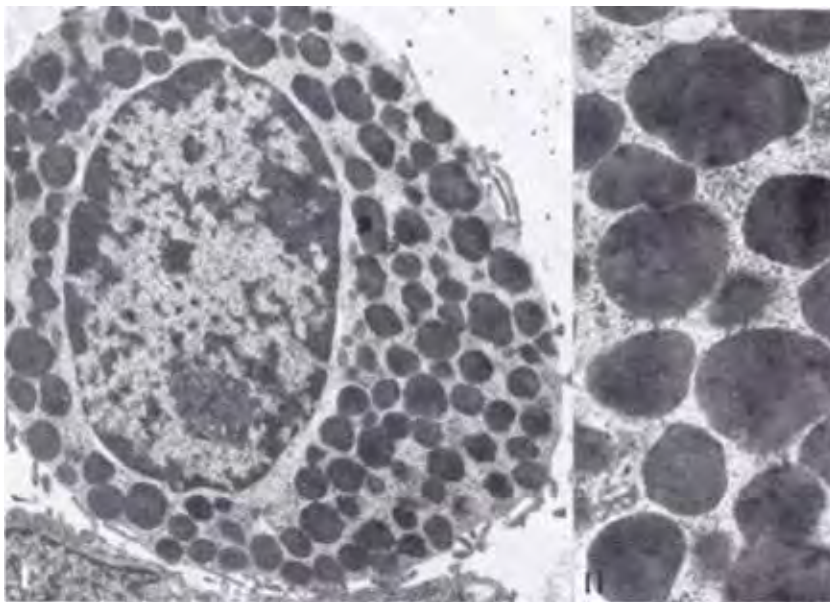


Fig. 13. The granules are large and filled with dense homogenous material. Lamellar structure is seen dubious. No distinct enclosing membrane is found. Left-hand figure $\times 5,000$. Right-hand figure. $\times 20,000$.

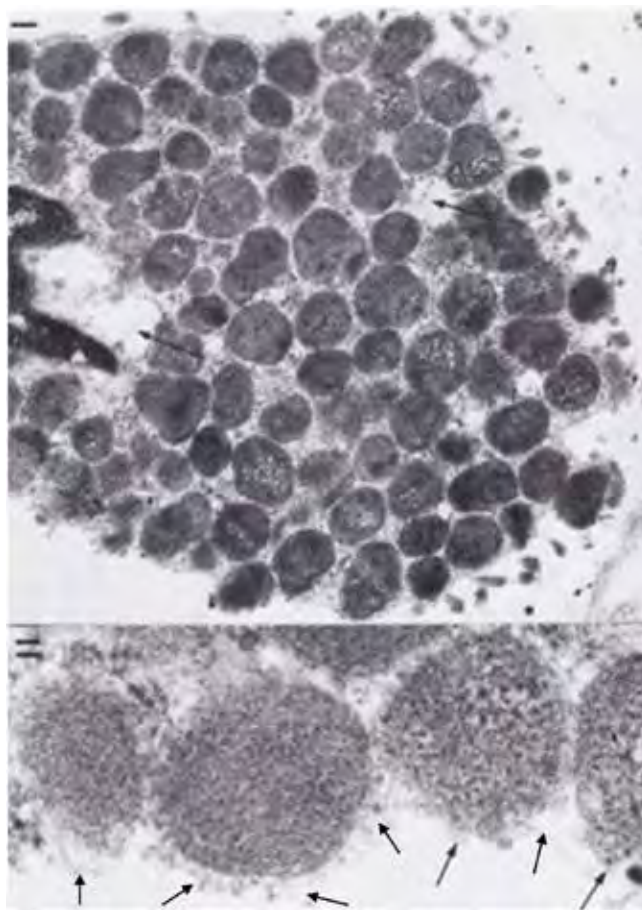


Fig. 14. Mast cell in myxoedema. The upper figure shows mast cell with disintegrating granules. The granules are filled of homogenous material but lamellar structure are indistinct. Arrows point out honeycomb structure. $\times 5,000$. The lower figure shows extracellular granules. Glycosaminoglycan figures on the granule surface and no enclosing membrane is seen. Arrows point details of the granules without enclosing membrane and glycosaminoglycan figures on the granule surfaces. $\times 20,000$.



Fig. 15. Mast cell in myxoedema. The upper figure shows a mast cell filled of large lucent homogeneous granules. $\times 5,000$. The lower figure shows the large homogenous granules in details. The granules are filled with lucent homogenous material but lamellar structure is scarcely seen. Arrows point at distinct enclosing membrane. The granules are in hydropic-like condition. Such change of mast cell granules are often seen in myxoedematous dermis. $\times 20,000$.

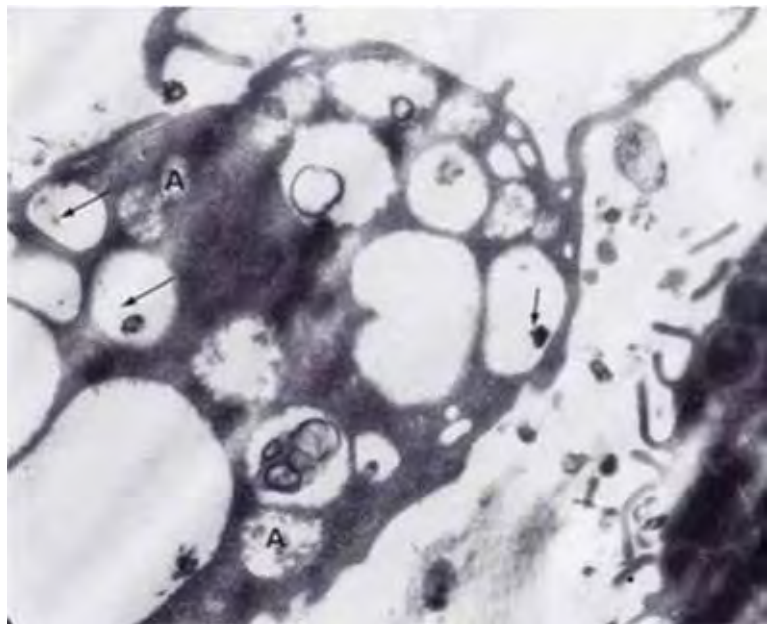


Fig. 16. Mast cell in myxoedema. Honeycomb structure in the cytoplasm. Arrows point at rests of glycosaminoglycan figure. A: amorphous material. $\times 5,000$.

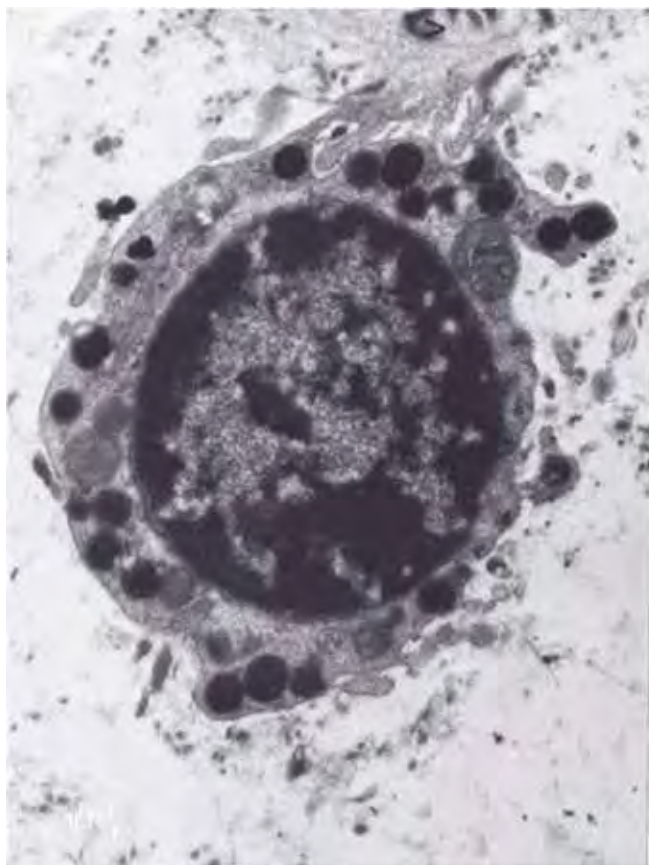
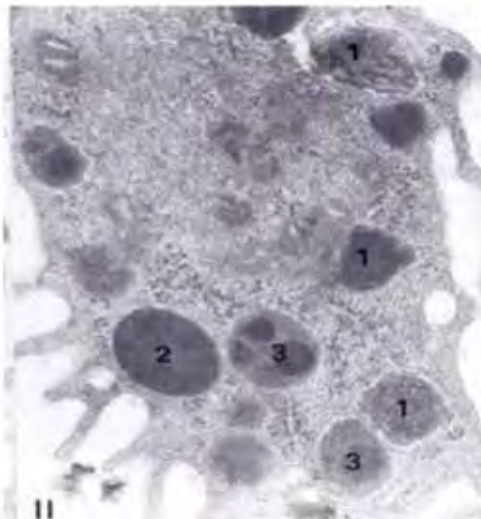


Fig. 17. Mast cell in myxoedema. Left-hand figure shows mast cell with small granules with dense homogenous content and scarce lamellar structures. $\times 5,000$. The right-hand figure shows mature and abnormal granules. 1. Mature granule. 2. Abnormal granules containing diffuse homogenous content (seen like lysosome). 3. Granules with dense central core. $\times 20,000$.



Scleromyxoedema [6]



Fig. 18. Scleromyxoedema [6]. A mast cell shows degranulation. The granules with dense coarse granular content and distinct enclosing membrane (g, h). A thick arrow shows example of distinct enclosing membrane. Thin arrows show scrolls. H: honeycomb structure. $\times 10,000$.

Morphoea

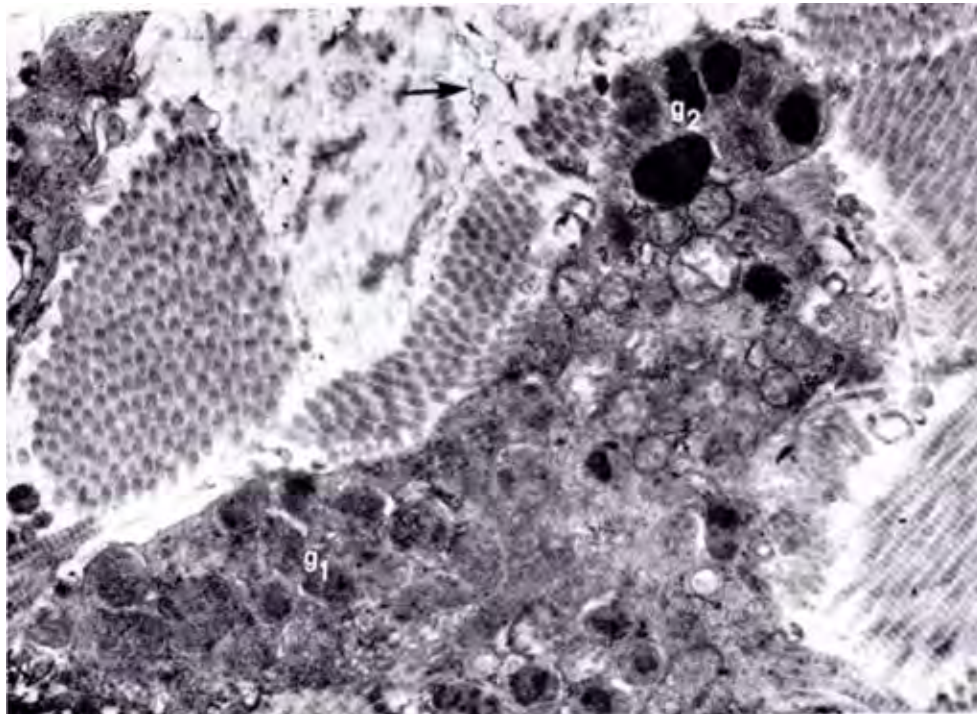


Fig. 19. Mast cell in the inflammatory zone of morphea [7]. The inflammatory zone is clinically called "lilac ring". The disease process is progressing into normal area. The dermis is myxoedematous, identical with localized myxoedema and generalized scleroderma. Mast cells in the area contain mature granules with disintegration. g_1 : disintegrating granules, g_2 : mature granules. Myxoedematous dermis presents glycosaminoglycan figure (arrow shows an example). $\times 70,000$.

Generalized scleroderma [8]

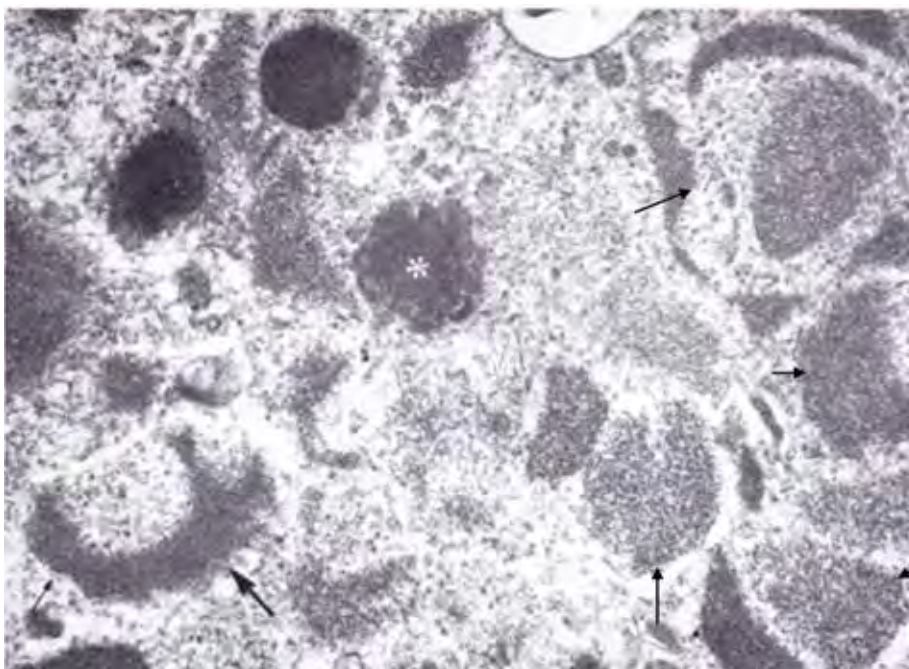


Fig. 20. Generalized scleroderma [8]. Most of mast cell granules are disintegrating in the cytoplasm. The granules show no enclosing membrane (thick and thin arrows) and contain coarse granular material of uneven distribution, some showing scrolls (asterisk) and dense compact mass. These abnormal figures imply intracytoplasmic dissolution of the granules. No degranulation or villi are found. Mature granules are few. $\times 15,000$.

Fibrodysplasia ossificans progressiva [9]

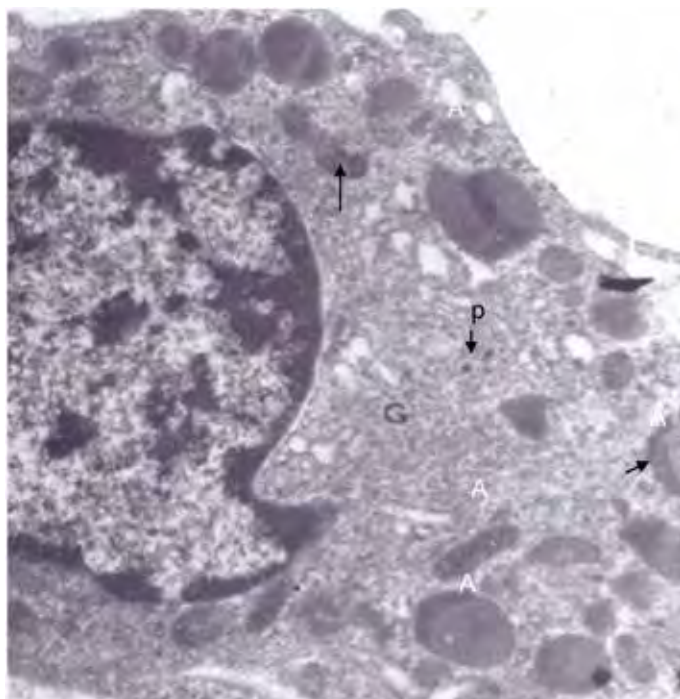


Fig. 21. The dermis presents myxoedematous area and fibrotic area. Myxoematous area contains numerous glycosaminoglycan filaments and some mast cells. Left: mast cell containing prominent Golgi area (G) (arrow with p; progranule) and abnormal granules of dense homogenous content and enclosing membrane. Arrow-pointed granules contain coarse granular material (asteriks). Enclosing membrane is preserved (arrows). $\times 10,000$. Right: granules in a high-power. Thin arrows point at filaments of glycosaminoglycan. $\times 20,000$. Mast cells seem to stimulate granulation but produced granules are abnormal missing lamellar structure. No degranulation occurs. Dermis is not myxoedematous.

Amyloidosis [10]

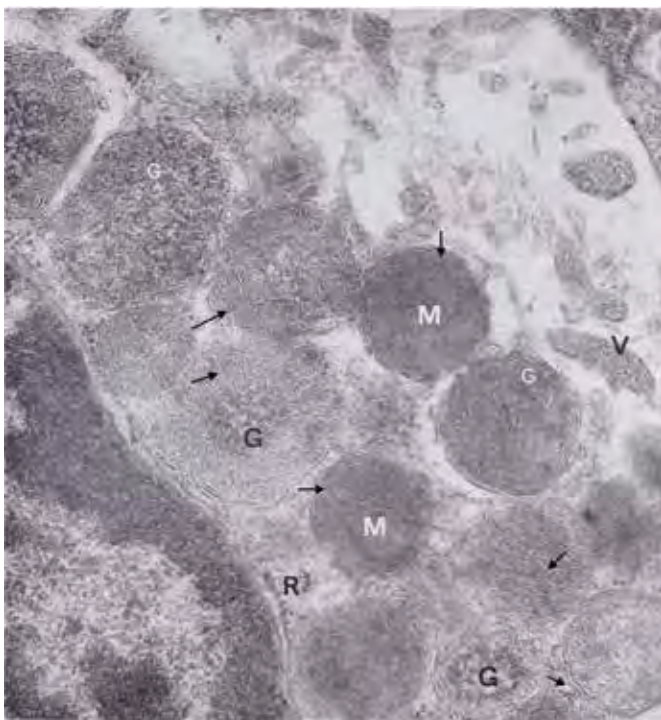


Fig. 22. Systemic amyloidosis. Abnormal granules (G) show coarse dense material and mature granules (M). Both types of granules show lamellar structures (arrows). Abnormal granules with coarse granular material (G). Villous protrude of cytoplasm is few (V). $\times 20,000$.

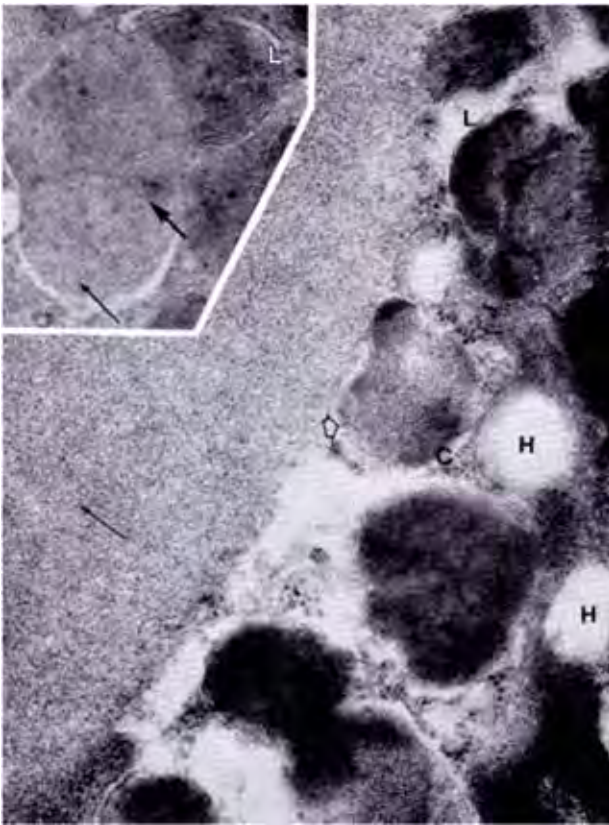


Fig. 23. Mast cell granules and amyloid mass [10]. Mast cells in the same biopsy as the previous figure. Mast cell granules shows dense granular material and lamellar structure (framed arrow). L: lamellar structure, H: honeycomb structure. Amyloid mass shows amyloid filaments (thin arrow). Inset show a mast cell granule. Lamellar structure (L) and amyloid mass (thick arrows). $\times 20,000$. The figure implies a close relation of mast cell granule to amyloid mass. This case show also elastic fibre matrix in masses of amyloid. $\times 20,000$. Details of amyloid filaments are demonstrated in section Elastic system.

Mast cells in basal cell carcinoma [11]

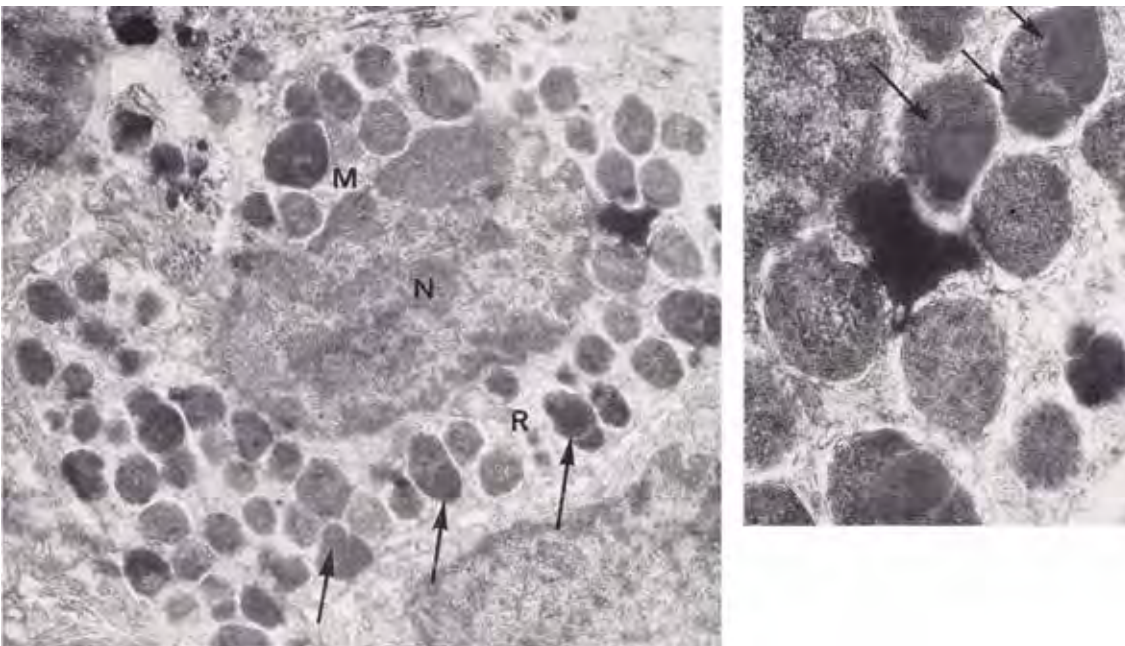


Fig. 24. Mast cells in the vicinity of cancer tissue. Mast cells reveal varied shapes of the granules corresponding to the areas of cancerous tissue. In the area outside the cancer tissue, mast cells are large (approx. $0.38 \mu^2$ in size) and dense. Left-hand figure shows an example of the mast cells. Arrows point at the granules material. Right-hand figure shows details of the granules containing fine granular material and lamellae (arrows). M: mitochondria, N: nucleus, R: granular endoplasmic reticulum. Left: $\times 5,000$. Right: $\times 20,000$.

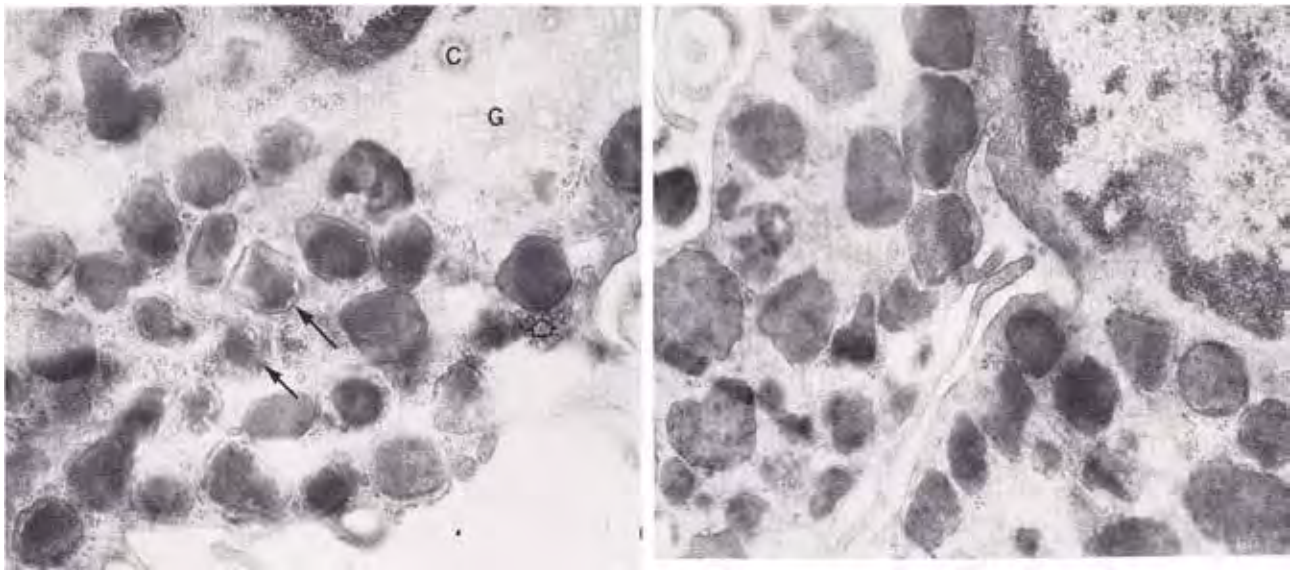


Fig. 25. Mast cells in the cancer infiltrate. The mast cell granules show varied figures. The granules are classified as types I to VI by the ultrastructure. Left: Mast cell granules. Type I is small, $0.05 \mu^2$ in size, containing unparallel arranged lamellae and fine dense granules. No distinct enclosing membrane. $\times 6,000$. Right: Mast cell granules. Type II are approx. $0.2 \mu^2$ in size, showing parallel lamellae and scrolls. Granular material is fine with crystalline structure. No enclosing membrane is found. $\times 6,000$.

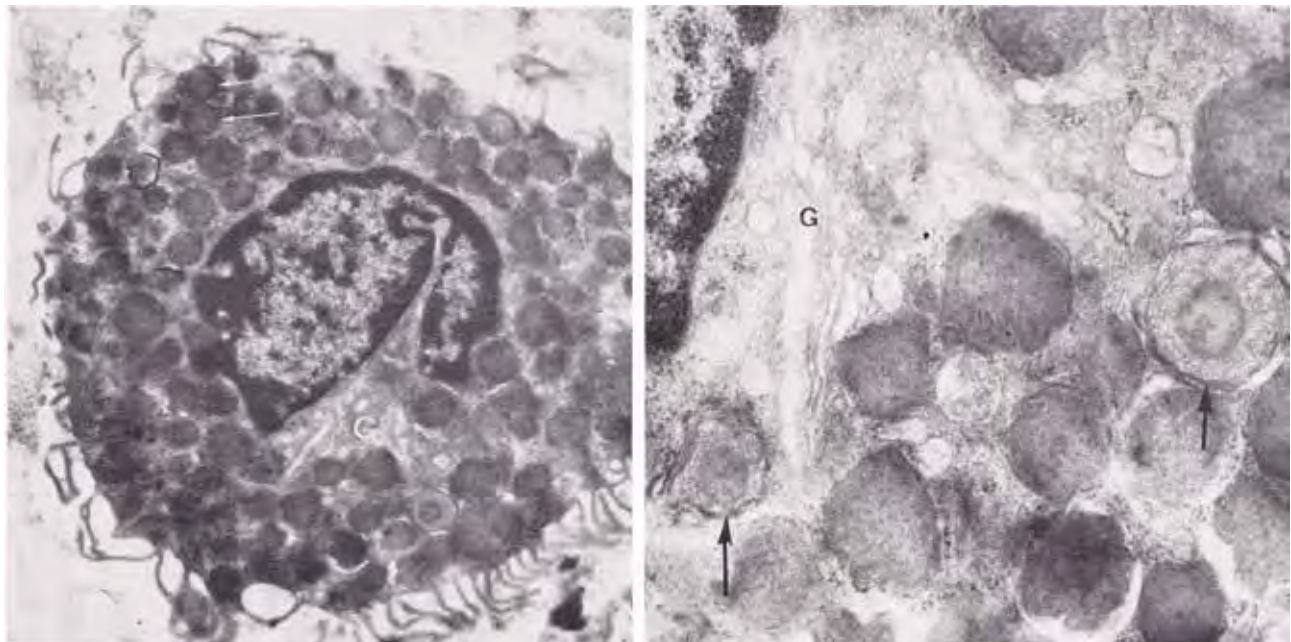


Fig. 26. Mast cells in the cancer infiltrate. Mast cell granule type III. Type III granules are $0.2 \mu^2$ in size, showing parallel lamellae and coarse granular material with a central core (arrows in the right-hand figure). No enclosing membrane is found. The mast cells show numerous finger-like protrusions of cytoplasm on the cell surface. Left: $\times 6,000$. Right: $\times 15,000$.

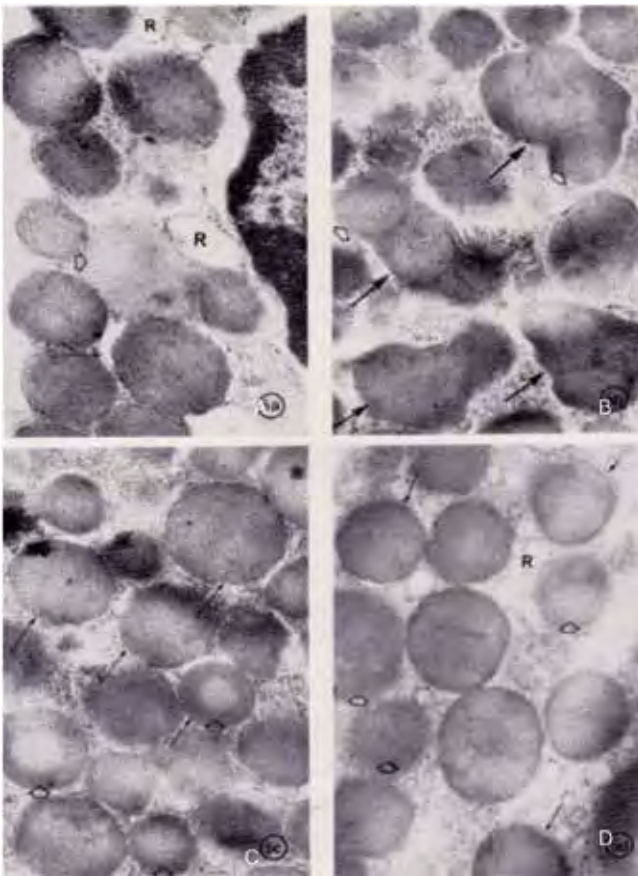


Fig. 27. Mast cell in the cell infiltrate. Type IV. Type IV granules are approx. $0.28 \mu^2$ or larger in size. The granules are filled of lucent homogeneous material (Figs. A, B, C, D in white letters.). Thin arrows point at lamellae in the periphery. Thick arrows indicate granules that looked like confluent. Enclosing membrane is indistinct. Similar granules are seen in myxoedematous dermis. R: dilated cisterna of the reticulum. $\times 20,000$.

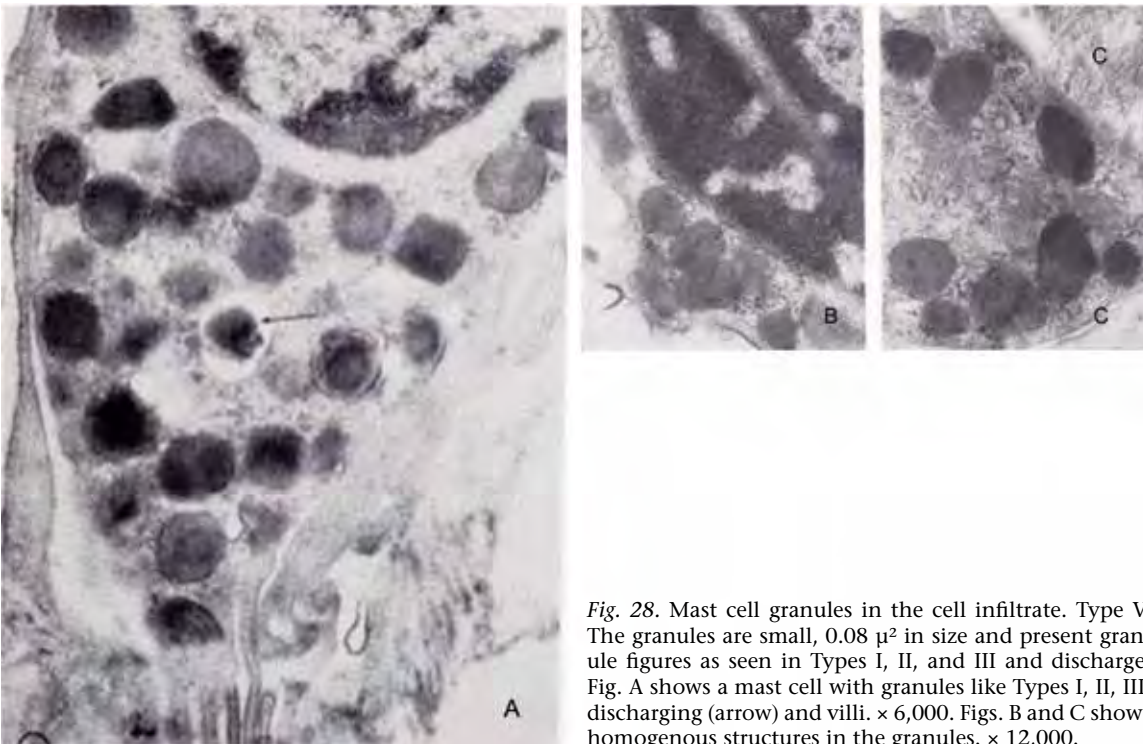


Fig. 28. Mast cell granules in the cell infiltrate. Type V. The granules are small, $0.08 \mu^2$ in size and present granule figures as seen in Types I, II, and III and discharge. Fig. A shows a mast cell with granules like Types I, II, III, discharging (arrow) and villi. $\times 6,000$. Figs. B and C shows homogenous structures in the granules. $\times 12,000$.

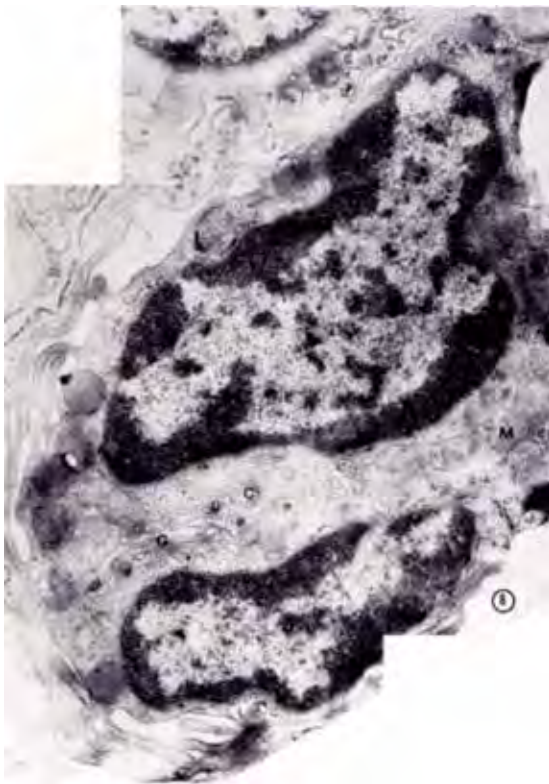


Fig. 29. Mast cell granule type VI. Small mast cell with a few small granules, $0.04 \mu^2$ in size. The granule content is seen homogeneous with indistinct internal structures. $\times 6,000$.

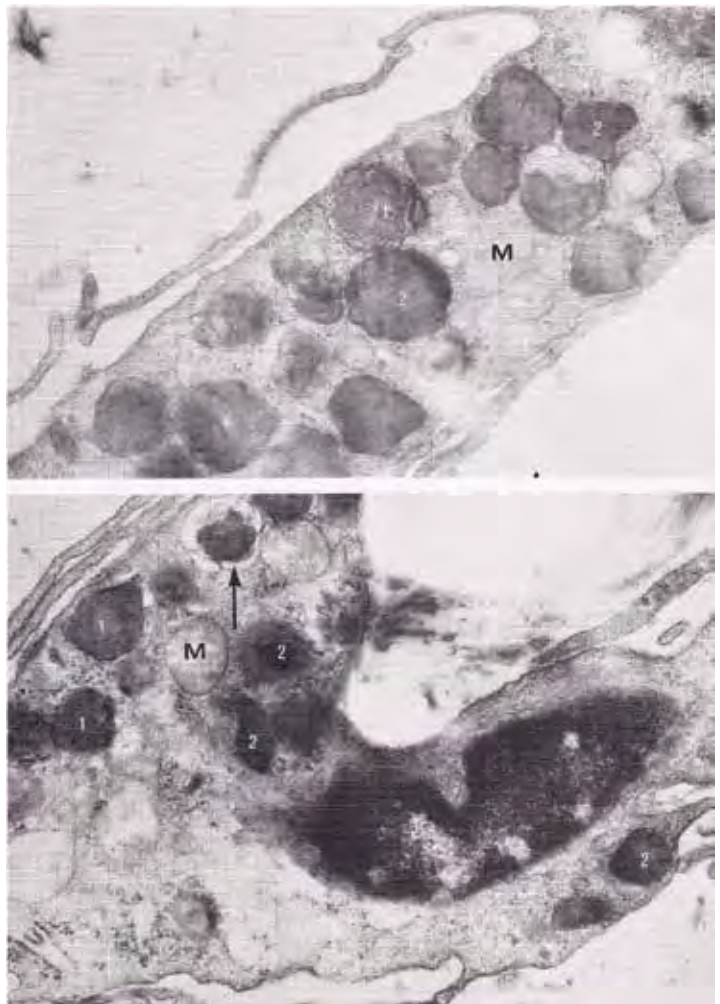


Fig. 30. Mast cells close to the basal cell carcinoma. The granules are $0.13 \mu^2$ and show the internal structure, responded to types I–VI. Both figures show long cytoplasmic protrudes. $\times 6,000$.

Table I. Mast cell granules and basal cell carcinoma. Various shapes of granules (Type I to VI), related to in situ location of basal cell carcinoma. Granule type I–VI shows similar structure but size becomes smaller if mast cells locate close to the cancer tissue of basal cell carcinoma. Seemingly cancer cells suppress granule formation of mast cell. The changes are summarized that poor lamella and homogenous material filled in the granule. Type IV granules are large, hydropic-like as seen myxoedematous dermis. This may be related to mucinous stroma of basal cell carcinoma.

Location of mast cells	Granule type	Frequency of appearance (%)	Maximum area of granules (μ^2)	Maximum diameter of granules (μ)	Coexistence with	Membrane-enclosed granules* (%)
Outside cell infiltrate			0.38	0.7	–	0
In cell infiltrate	I	4.7	0.05	0.25	II, III	0
	II	21.3	0.2	0.5	I, III, IV	2.7
	III	0.6	0.2	0.5	I, II, IV	9.0
	IV	60.4	0.28	0.6	II, III	10.6
	V	11.1	0.08	0.33	VI	10.1
	VI	1.9	0.04	0.23	V	11.1
Close to tumour			0.13	0.41		5.3
Mean						6.1

*Numbers of membrane-enclosed granules in relation to total number of each granule type.

Squamous cell carcinoma [12]

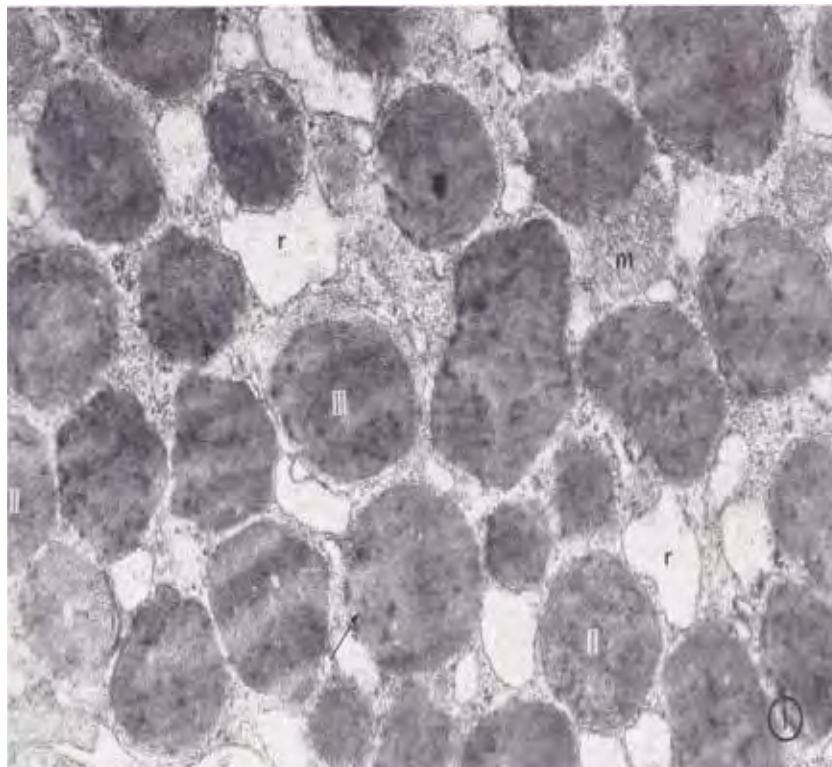


Fig. 31. Mast cell granules in cancer tissue are classified types I, II and III by ultrastructure. The variation of the granule ultrastructure seems to occur by cancer cell (see Fig. 37). Type I granule: Lamella and granular material like normal mature granule. Size $0.163\text{--}0.306\ \mu^2$, $0.4\text{--}0.5\ \mu$ across. The granules are shown in this figure. Details are seen in Fig. 33. Type II granule: Lamella and granular material in an irregular pattern. Size $0.16\ \mu^2$, $0.4\text{--}0.5\ \mu$ across (Figs. 34, 35, 36). Type III granule: Uncomponents. Size $0.98\ \mu^2$, $0.3\text{--}0.4\ \mu$ across (Figs. 33–36).

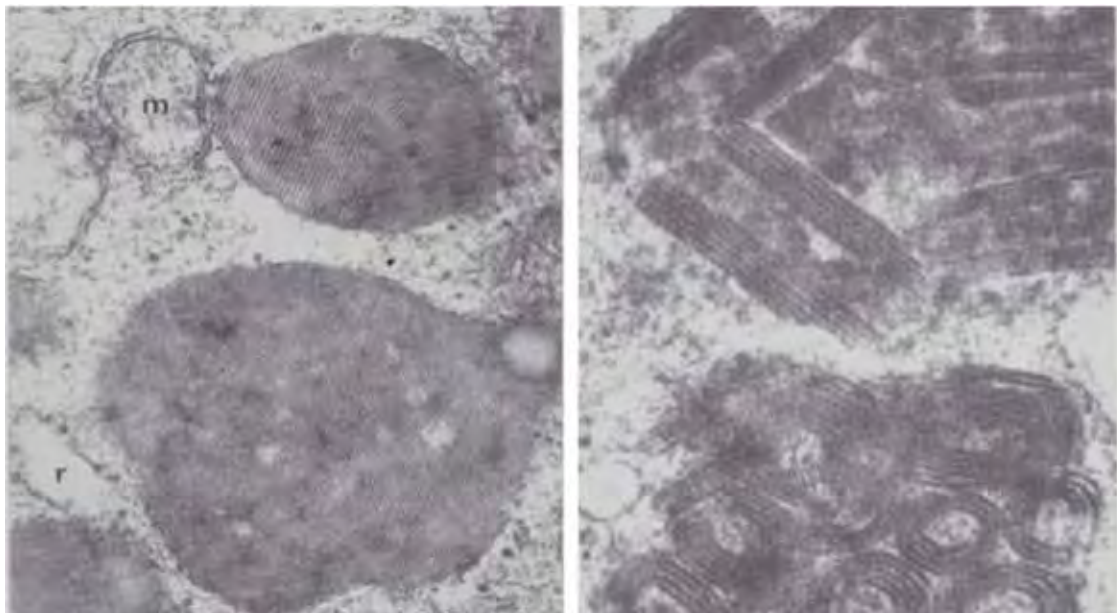


Fig. 32. Mast cell granules. Details of type I granules, in Fig. 31. Left: distinct crystalline figure and faint lamellae. The crystalline shows 60 Å and 120 Å and cross at angles 30° and 60°. × 40,000. Right: distinct lamellae and scrolls. × 80,000.

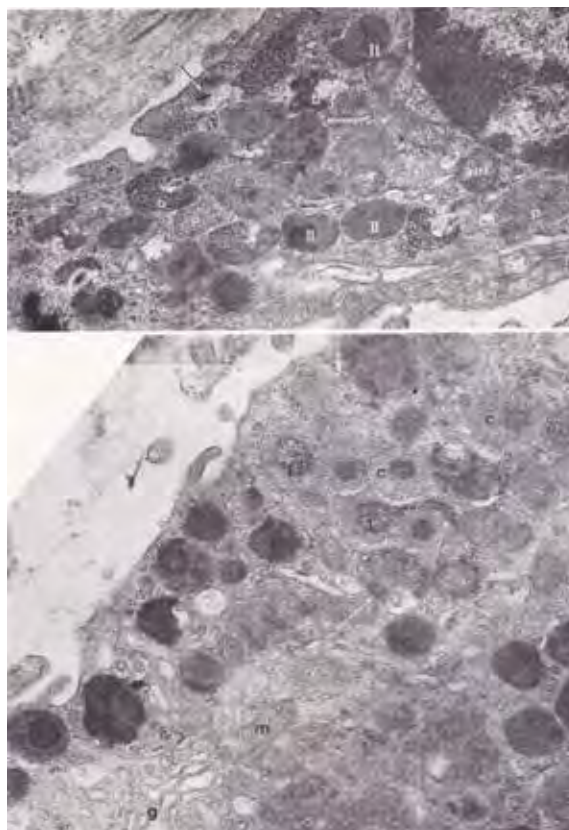


Fig. 33. Mast cell granules close to the infiltrate of squamous cell carcinoma. Mast cell granules of type II (marked by II) are 0.16 μ^2 in area, and rest of them (no marks) are type III. Type II granule shows lamellae in periphery of the granule and granular material is coarse with a central core. Type III granules are without mark, 0.098 μ^2 in size showing various sized central core. White arrows in the lower figure point at wavy lamellae. × 10,000.

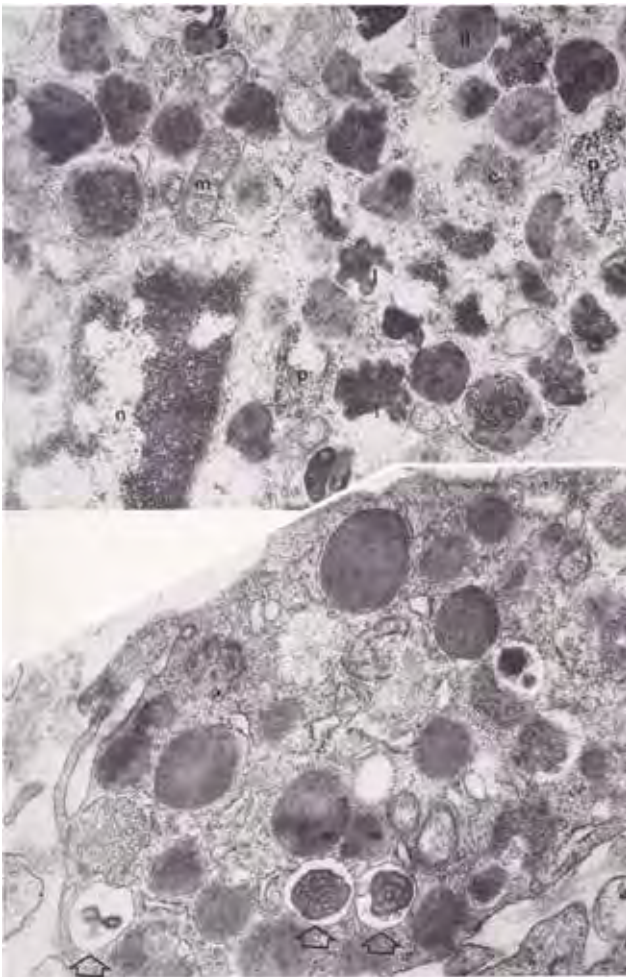


Fig. 34. Mast cell granules close to the cancer infiltrate. The mast cells show types I, II, III, but all the granules are small ($0.16 \mu^2$). Framed arrows in the lower figure indicate distinct enclosing membrane. $\times 20,000$. Mast cells stimulate granule formation in the vicinity of cancer tissue but suppressed the formation and form small and altered granules in the cancer tissue. No hydrope-like granules appear.

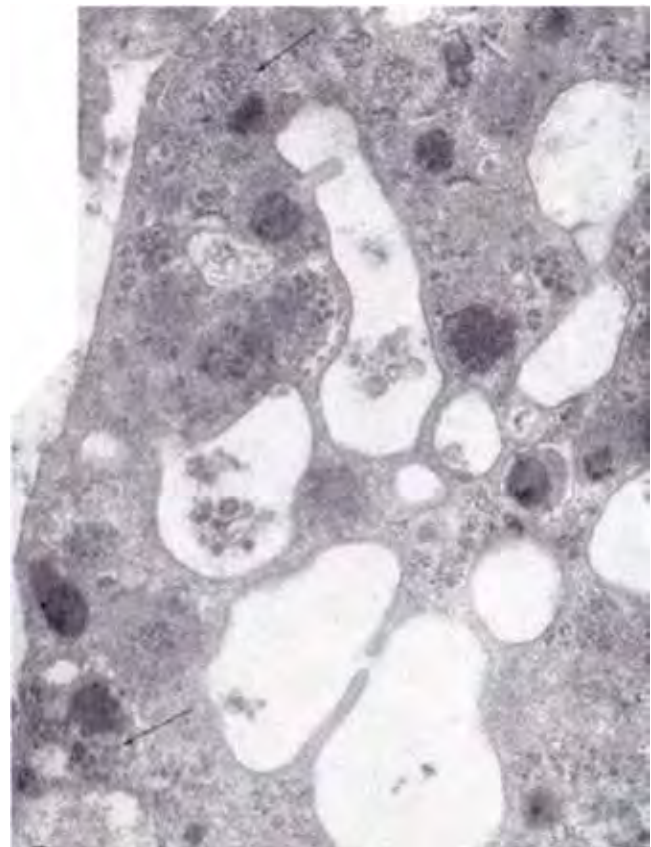


Fig. 35. A mast cell in epidermis. Mast cells immigrate epidermis around cancer tissue. The mast cells show honey comb structure and types II and III granules. $\times 20,000$.

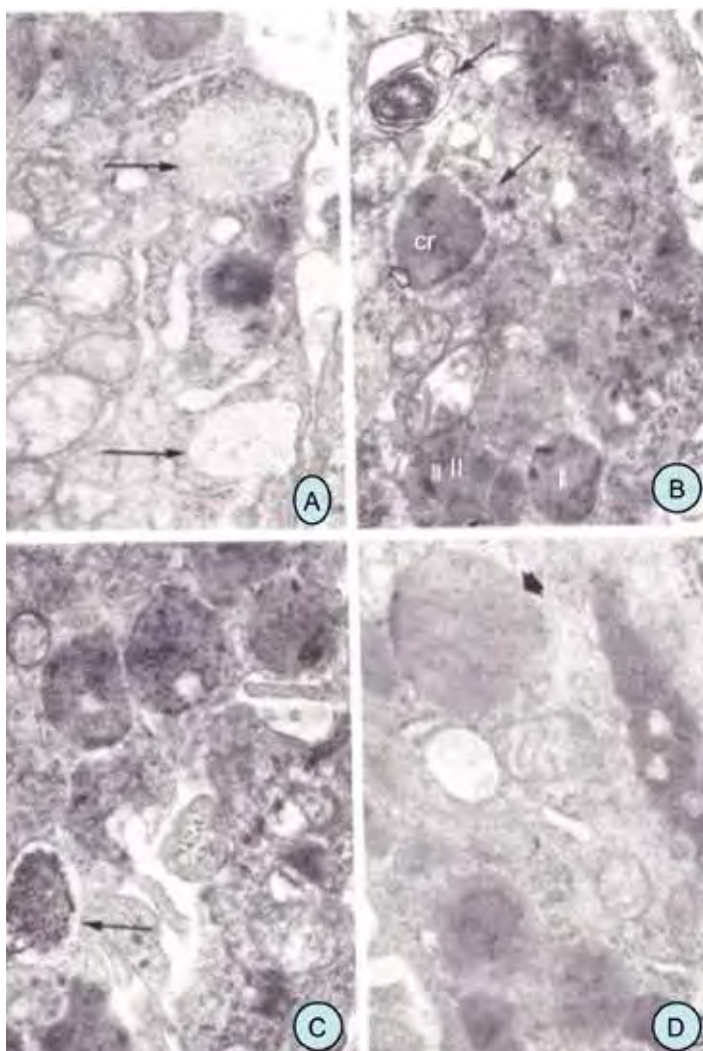


Fig. 36. Mast cell granules in epidermis. Granule types I, II, and III and enclosing membrane. × 20,000 Arrows in Figs. A, B, C show distinct enclosing membrane. Fig. B shows a large granule with crystalline structure (cr) and types I and II. Fig. C shows coarse granular material and lamellar structures. Fig. D shows crystalline figure and lamellae (thick arrow). Rest of the granules in Fig. D are type III.

Types ^{*)} and per cent of granules				Membrane enclosed granules	Location	
				I	II	III
I 85%				10%	5%	Far from the cell infiltrate
I 53%				11%	35%	31% Near the cell infiltrate
I 21%	II 8%	III 71%		6% In the cell infiltrate		
I 11%	II 12%	III 77%		14% In the epidermis		

*) Numbers I, II and III indicate each granule type.

Fig. 37. Mast cells in the infiltrate of squamous cell carcinoma. The results imply that cancer cells of squamous cell carcinoma interfere with granule formation. The formation is stimulated in the area around cancer tissue. The granules are large with distinct lamellar structure and thick granular material (type I). Type III granules are small and contain abnormal content. However small type I granules are also admixed. Type II granules are probably intermediate type between type I and III. It seems that mast cells do not produce normal granules in cancer tissue. The mast cells produce small abnormal granules and some small mature granules with distinct lamellae (type III). Mast cells are interfered with granule formation by cancer cells. The mast cells produce small mature and abnormal granules. Mast cells are also found in epidermis. The granules are type III and excreted granule content leaving honeycomb structure.

VI. Mesenchymal cell lineage

Overview	
• Survey of the lineage for interpreting the results	Figure 1
• Cell culture	Figures 2–6
• Transformation in vitro (in cultivated dermis)	Figures 7–9
• Cytochemistry	Figures 10–13
• Immunoglobulin to myofibroblast	Figures 14–15
• TCF-beta	Figures 16–17
• Suggestive transformation to adipose cell	Figure 18
• Transformation in vitro (in fibrotic dermatoses)	Figures 19–22
• Fibrotic dermatoses	
- Shagreen patch	Figures 23–24
- Ulcus cruris	Figures 25–26
- Spontaneous keloid	Figures 27–29
- Pretibial myxoedema	Figure 30
- Morphoea	Figures 31–33
- Acrosclerotic scleroderma	Figures 34–37
- Linear sclerosis	Figure 38

Survey of the mesenchymal cell lineage

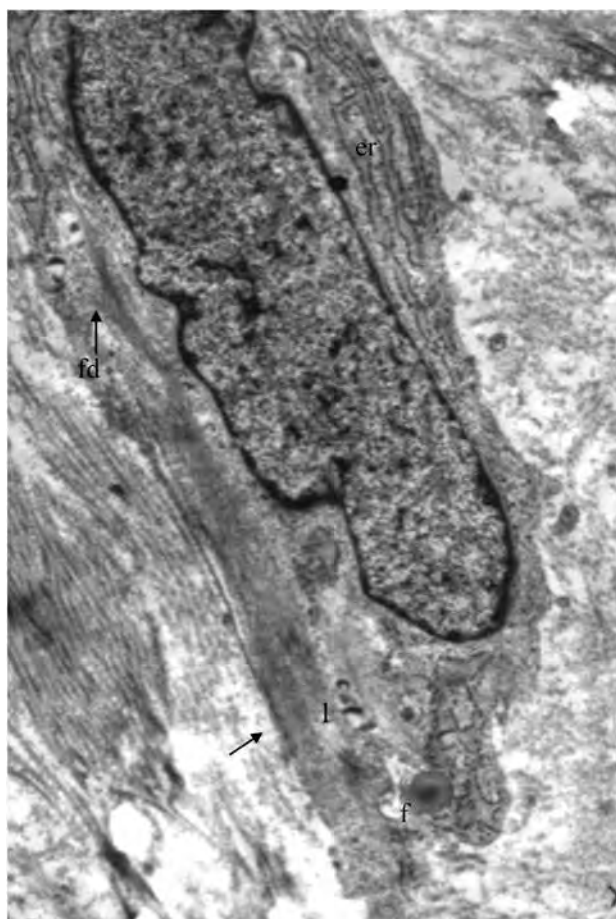


Fig. 1. Myofibroblast. Ultrastructure [1–9, 17]. Mesenchymal cell lineage includes pericyte, myofibroblast, fibroblast and fibrocyte. These four cells contain similar cytoplasmic organelles in different proportion and maintain dermal connective tissue in stable condition. The cytoplasmic organelles are grouped in secretory and contractile component. The secretory component consists of Golgi apparatus, ribosomes, endoplasmic reticulum and lysosomes. Secretory component produces material of connective tissue for renewal and repair. The contractile component includes intracytoplasmic filaments and hemidesmosomes, and acts tissue contraction. Fibroblast contains rich in secretory component. Myofibroblasts contains rich in contractile component with characteristic structures such as fibronexus and focal density [3]. Fibroblast and myofibroblast secrete collagen. Besides collagen secretion, myofibroblasts contract dermal connective tissue but the contraction is weak and lasts longer than smooth muscle cells, except myofibroblast in foetus that do not contract wounds [4]. Pericyte exhibits cytoplasmic organelles, similar with myofibroblast and covered by basal lamina. Pericyte transformation to myofibroblasts is the essential process of fibrosis. Pericyte is the cell reservoir for the mesenchymal cell lineage. Fibrocyte seems to be on the rest stage of the lineage. × 10,000. Er: granular endoplasmic reticula, Fd: focal density, F: fat droplet, L: lysosome. Arrow: fibronexus.

Cell culture

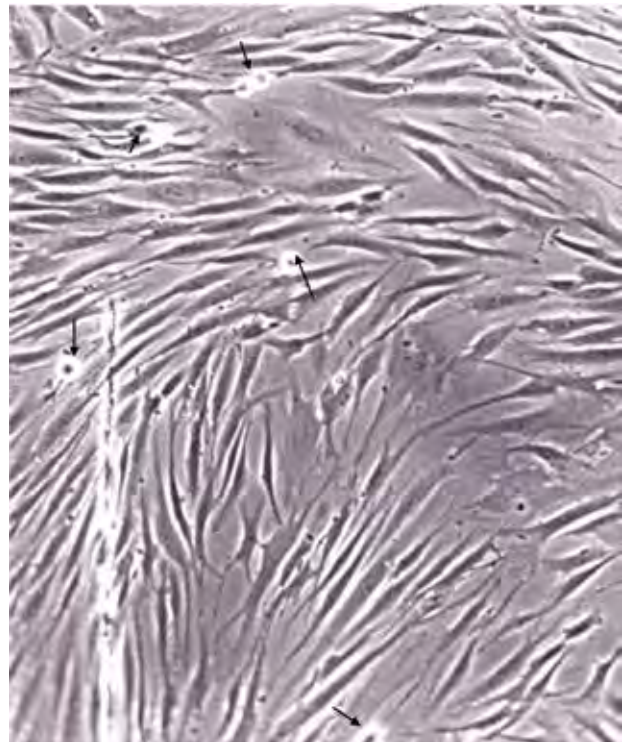


Fig. 2. Established cell culture of myofibroblast (fibroblast) from normal human dermis. When pieces of normal dermis is implanted for culture, spindle-shaped cell growth is first noticed after about 10 days of cultivation. These cells are just called fibroblasts. The cell growth can be trypsinized several times and obtained lots of spindle-shaped cells. The spindle-shaped cell growth shown in the figure is the culture maintained for 2 years. Cell structure is demonstrated in the next figure. When the cells grow, secretory component firstly becomes manifest and contractile component is followed as shown (Nos 4, 5, and 6). Nos 7, 8 and 9 demonstrate transformation of pericyte in vascular wall and perineurium. Arrows point at mitosis. $\times 40$. Ultrastructure is shown in the following figures. The myofibroblast of this culture used for preparation of immunoglobulins (see Appendix).

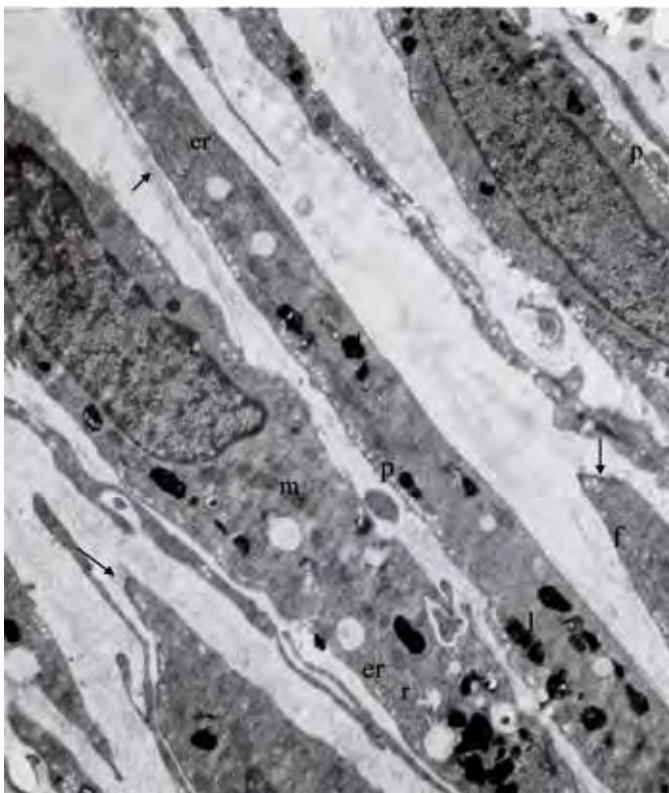


Fig. 3. Established cell culture of myofibroblasts from dermis of normal human adult (Fig. 2). The cells contain an oval nuclei, mitochondria (m), and secretory and contractile component. Secretory component are poor. Granular endoplasmic reticulum (er), ribosomes (r), Golgi apparatus, lysosomes (l), and pinocytotic vesicles (p). Contractile component is rich. Intracytoplasmic filaments with focal density (f). Desmosome-like thick cell membrane with basal lamina-like cell coat (fibronexus) [3] (arrows). These cells are myofibroblasts. $\times 5,000$. The cell culture is applied to prepare anti immunoglobulin to myofibroblast (see Appendix).



Fig. 4. Fibroblasts grown from normal dermis. A piece of dermis is implanted in Falcon culture flask. Spindle-shaped cells begin to grow after about 10 days and soon covers the surface of the flask bottom. Grown cells present as distinct figures of granular endoplasmic reticulum with dilated cisterna (c), ribosomes, granular endoplasmic reticula (r) (Secretory component), but contractile component is poor. An arrow points at desmosome-like thickened cell membrane with basal lamina. Two cells in the figure shows fat-droplet with surrounding glycogen particles (f). $\times 5,000$. Figs 4, 5 and 6 present development of cytoplasmic organelles.

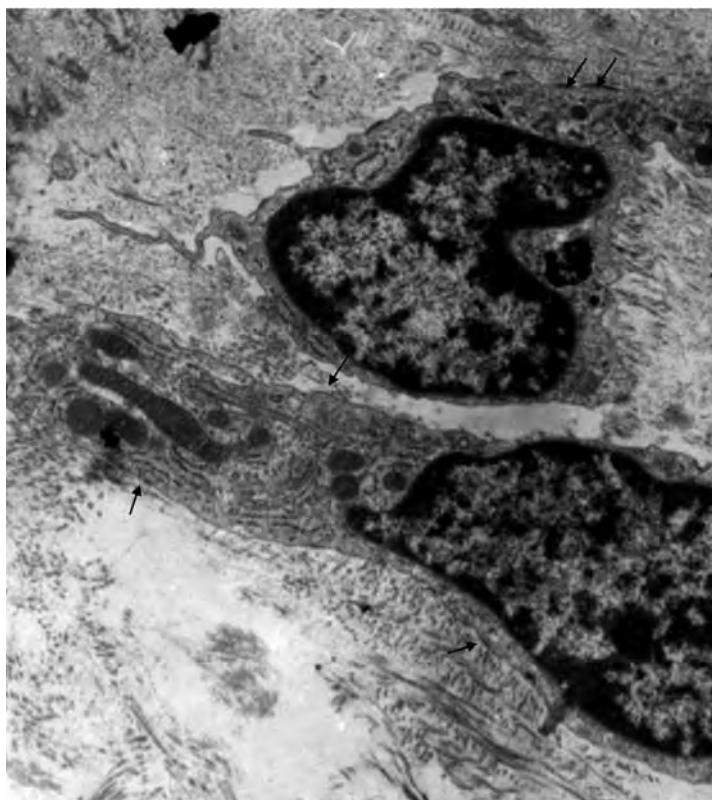


Fig. 5. Fibroblast culture from normal dermis, cultivated for 10 days. Spindle-shaped fibroblasts are rich in granular endoplasmic reticulum and poor in contractile component. Basal lamina is scarcely seen. Arrows point at localized thickening of cell membrane. Contractile component is poor. No basal lamina is seen. The cells may be called fibroblasts. $\times 5,000$.

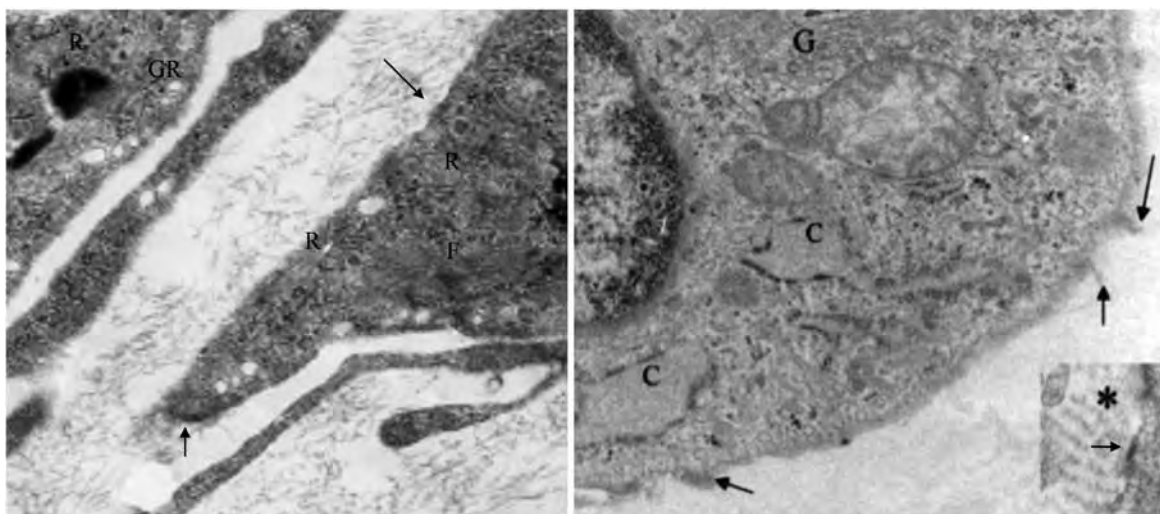


Fig. 6. Myofibroblast. Cytoplasm is rich in ribosomes (R), granular endoplasmic reticulum (GR) and intracytoplasmic filaments with focal density (F). Arrows point out desmosome-like thickening of cell membrane “Fibronectus” [3]. × 20,000. Cisterna of granular endoplasmic reticulum is dilated (C). The limiting membrane of the reticulum is associated with numerous ribosomes. Intracytoplasmic filaments are poor. Golgi zone (G). Arrows point at thickening of cell membrane. Inset shows collagen aggregate (asterisk) and cell membrane thickening (arrow). See Section II Collagen: Collagen aggregate. The cell is fibroblastic. × 20,000.

Transformation of pericytes to myofibroblast in vitro (cultivated dermis)

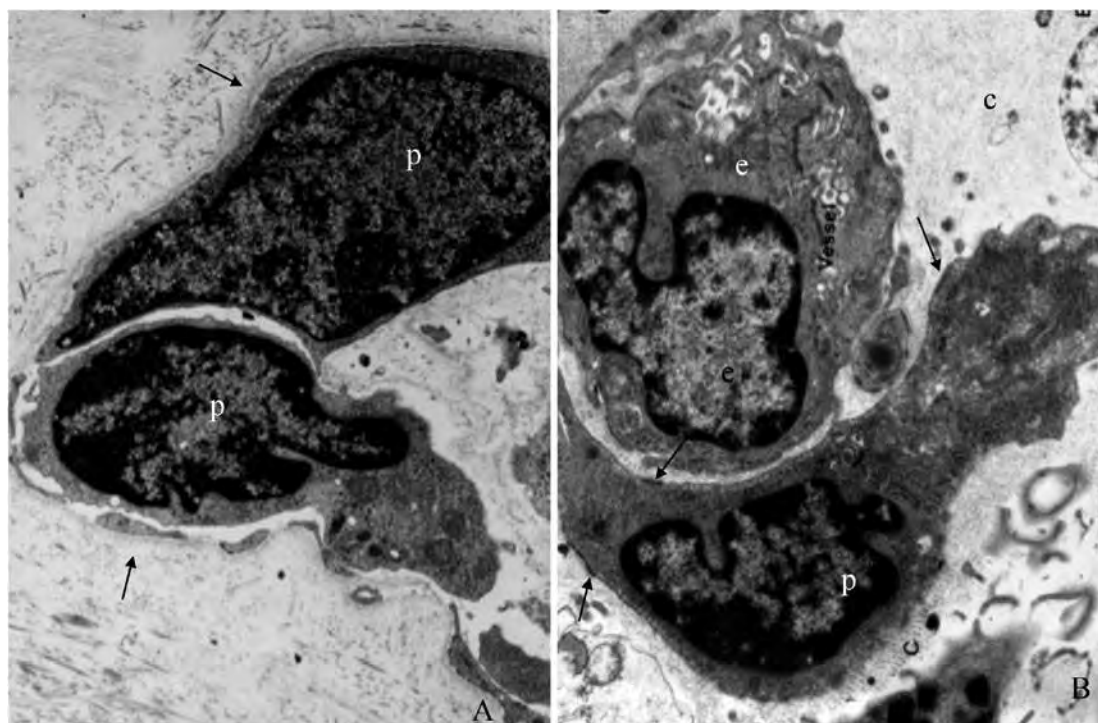


Fig. 7. Vascular wall of normal dermis, cultivated for 3 days. Pericytes show transformation to myofibroblasts. Picture A shows immature pericytes (p) and thin basal lamina (arrows). Picture B shows a transforming pericyte (p) with fragments of basal lamina (arrows). Endothelial cell of a small vessel (e). Collagen fibrils (c). × 5,000. Pericyte transformation to myofibroblast in dermatoses are shown in the following figures.

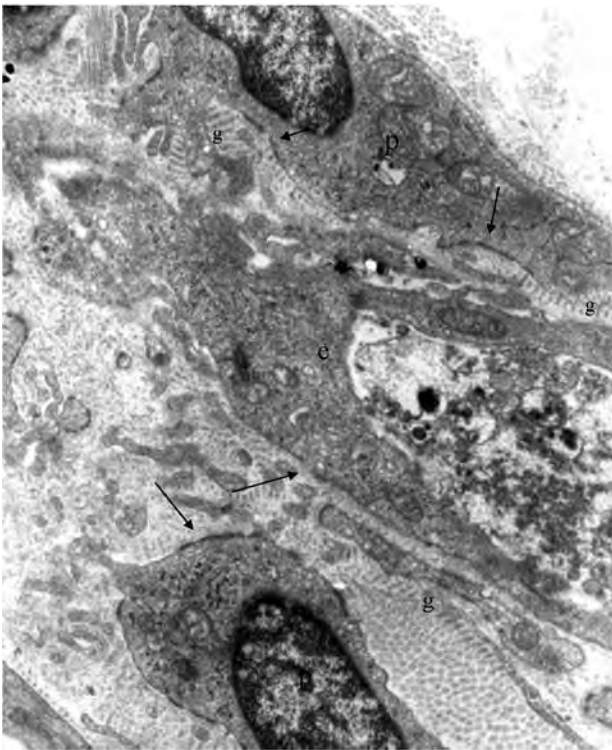


Fig. 8. Pericytes under transformation. Dermis in 7 days culture. Pericytes (p) and an endothelial cell of vessels (e) are activated, exhibiting dominant in granular endoplasmic reticulum and distinct hemidesmosomes (arrows). Basal lamina is interrupted. Collagen aggregates indicate degradation of collagen fibrils (g). $\times 5,000$. Increased amount of granular endoplasmic reticulum and fragmented basal lamina indicate that the pericytes are activated to transformation.

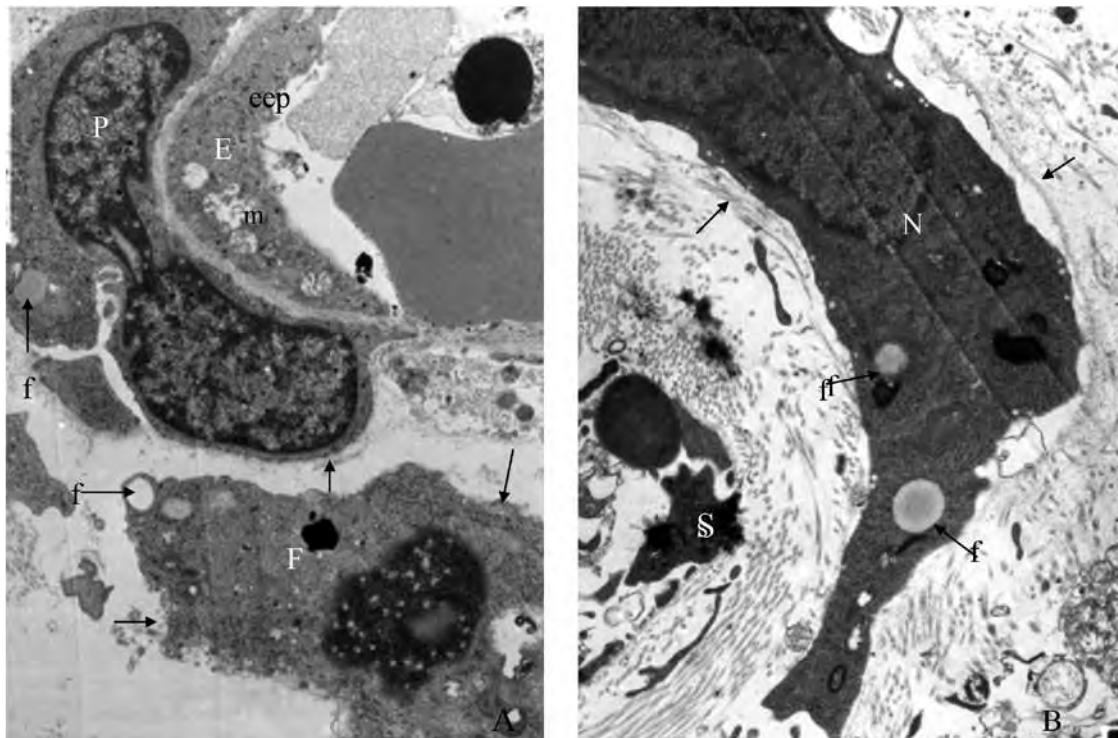


Fig. 9. Dermis cultivated for 2 weeks. Activated pericytes. Fig. A shows vascular wall and Fig. B peripheral nerve. Endothelial cell (E), pericyte (P), myofibroblast (F), perineural cell (N) Schwann cell (S). These cells contain well-developed granular endoplasmic reticulum, lysosome and mitochondria (m). Fat droplet (arrow with f). Basal lamina (arrows) is fragmented in picture A and discontinued in picture B. $\times 5,000$.

Cytochemistry

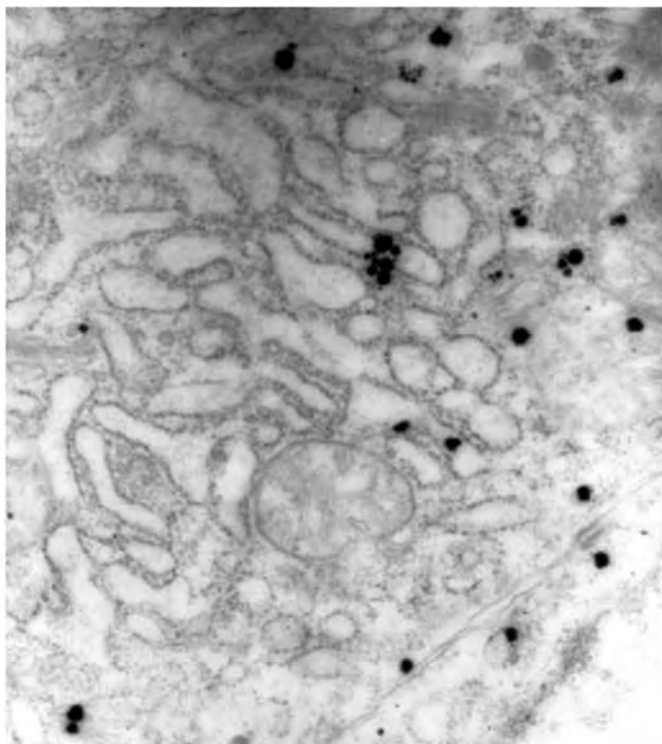


Fig. 10. A myofibroblast of chick embryo. Radioautograph of Prolin-C 14. Silver grains in varied sizes locate on the ribosomes and in cisterna of granular endoplasmic reticulum. $\times 20,000$. Radioautograohic technique is complicate and time-required. Technique is not for daily study-work. Used technique does not appear in Appendix (Contact the Author for the technique, if interested). [Unpublished]

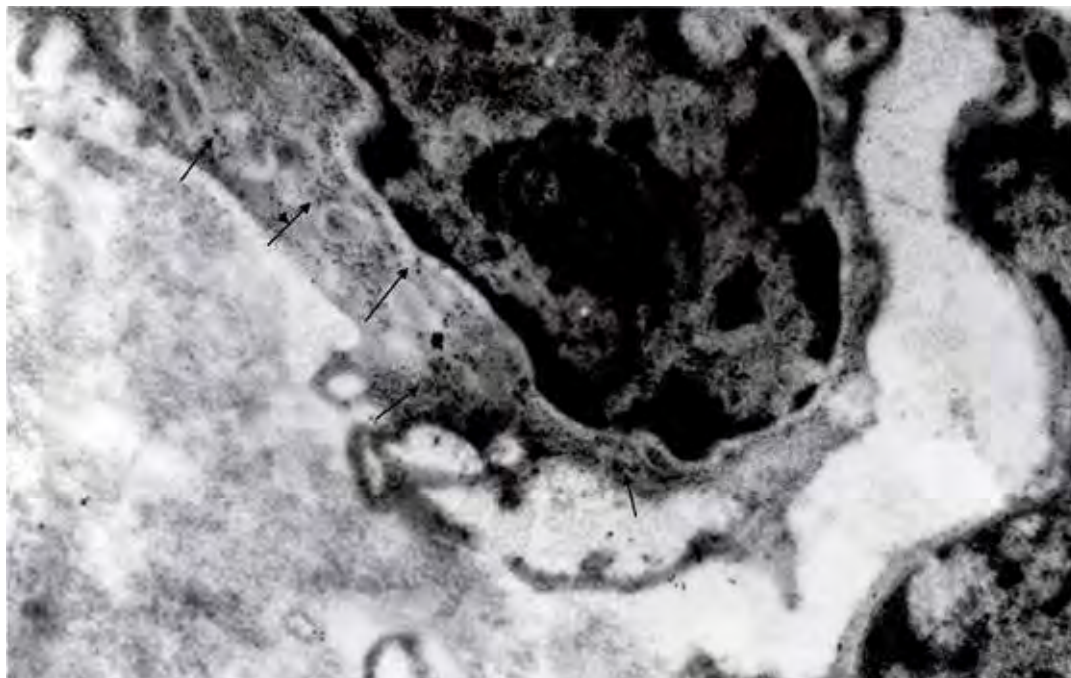


Fig. 11. Myofibroblast, stained with antiserum to vimentin [20]. Gold particles are found in the cytoplasm of myofibroblast (arrows). Positive vimentin reaction indicates that the cell is mesenchymal. $\times 10,000$.

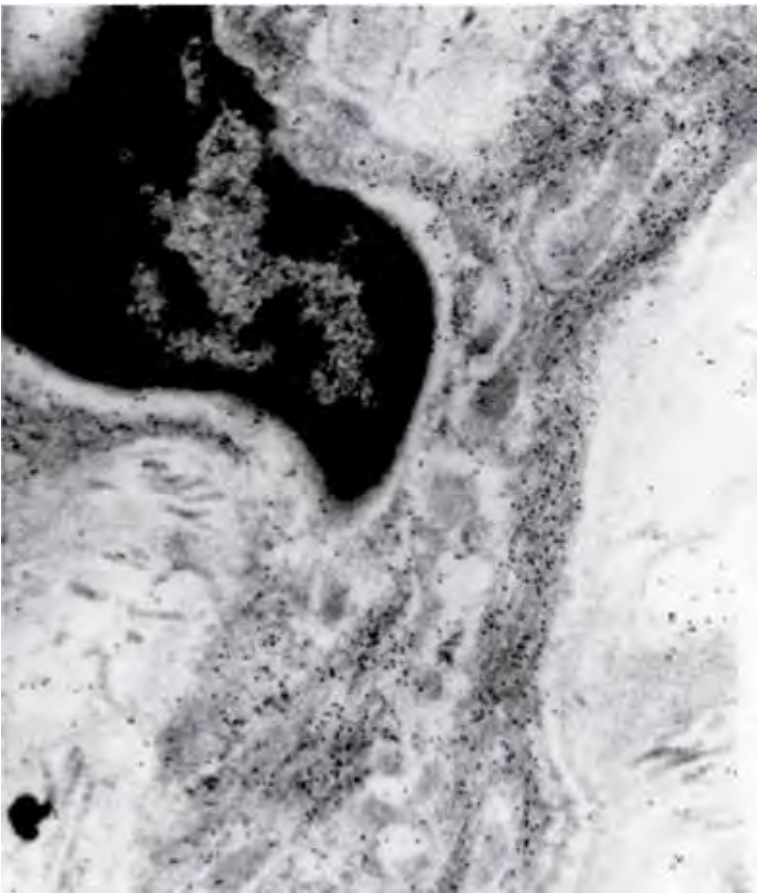


Fig. 12. A myofibroblast in cultivated dermis, stained by antibody to smooth cell actin and detected 10 nm gold particles. Gold particles lying on the intracytoplasmic filaments. $\times 10,000$.

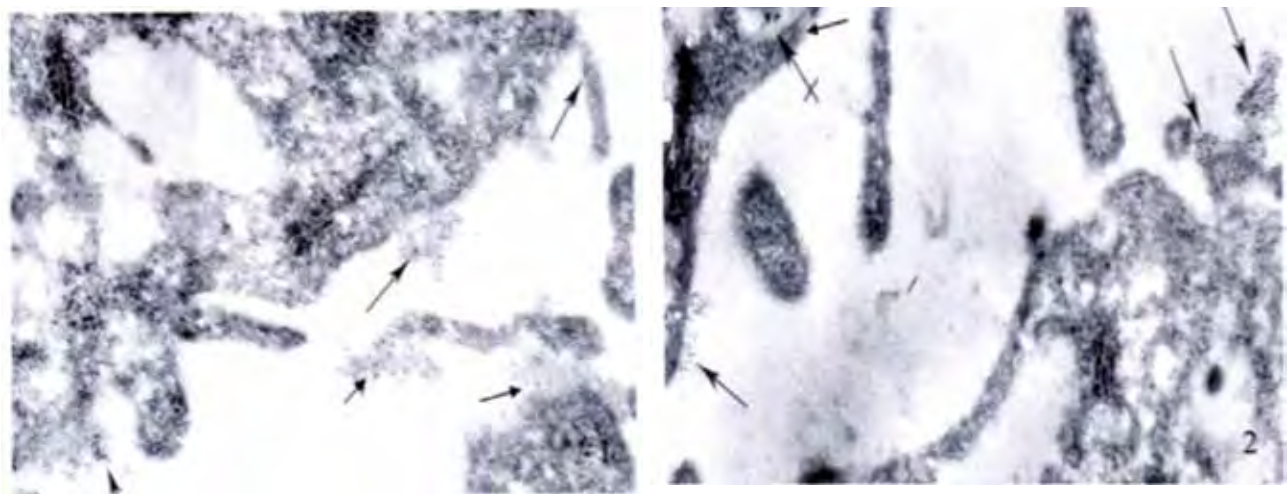


Fig. 13. Myofibroblasts in cell culture, stained by antiserum to type IV collagen (Left) and to fibronectin (Right). Arrows show gold particles on the cell surface. $\times 20,000$. The positive results of the immunochemical staining represent the cultivated cells are mesenchymal and have characters of smooth muscle, i.e. myofibroblast.

Staining with immunoglobulin to myofibroblast

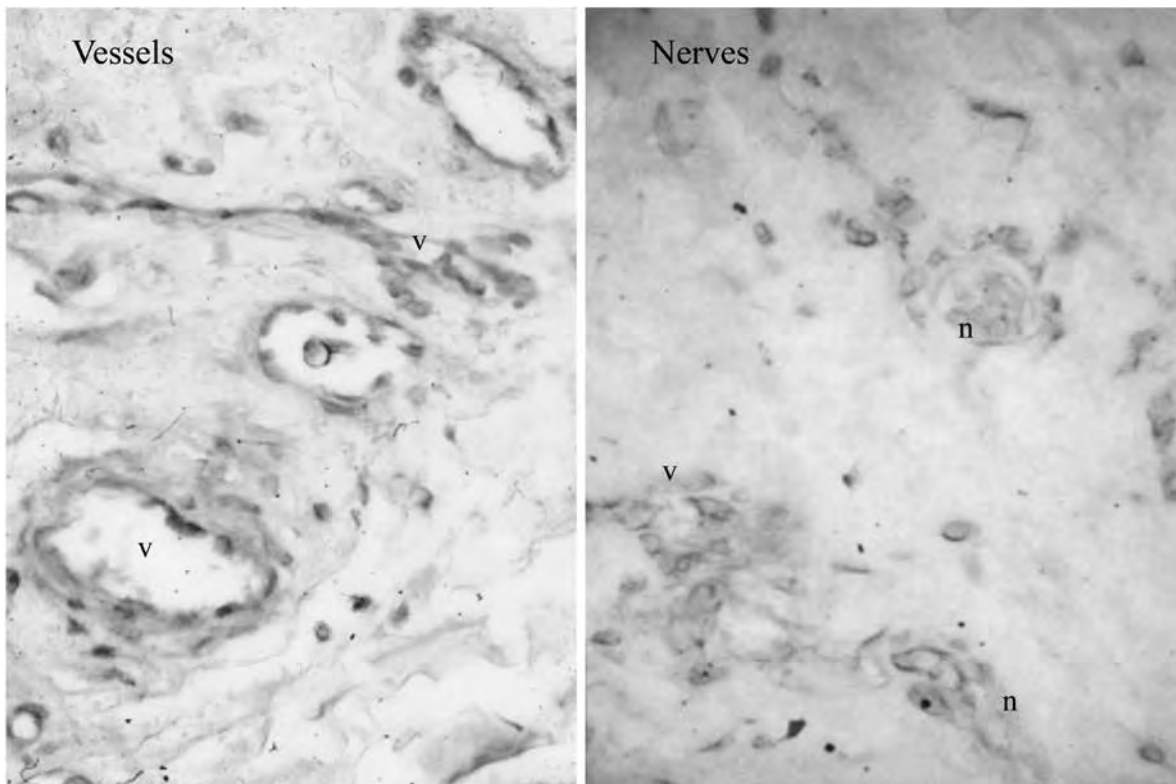


Fig. 14. Dermis. Vascular wall and nerve. Organ culture skin for 10 days is stained with immunoglobulin to myofibroblast (see Appendix). Positively stained cells are endothelial cells and myofibroblasts in vascular wall, peripheral nerve and spread in dermis. Vascular wall (v), nerve (n). Dermis: × 400 Nerve: × 600 (nerve).



Fig. 15. Endothelial cell (E) and pericyte (P) in vascular wall, stained by immunoglobulins to myofibroblast *in vitro* [Appendix]. Gold particles were seen in the cytoplasm of pericyte and endothelial cell. × 20,000.

TGF- β and myofibroblast in vitro

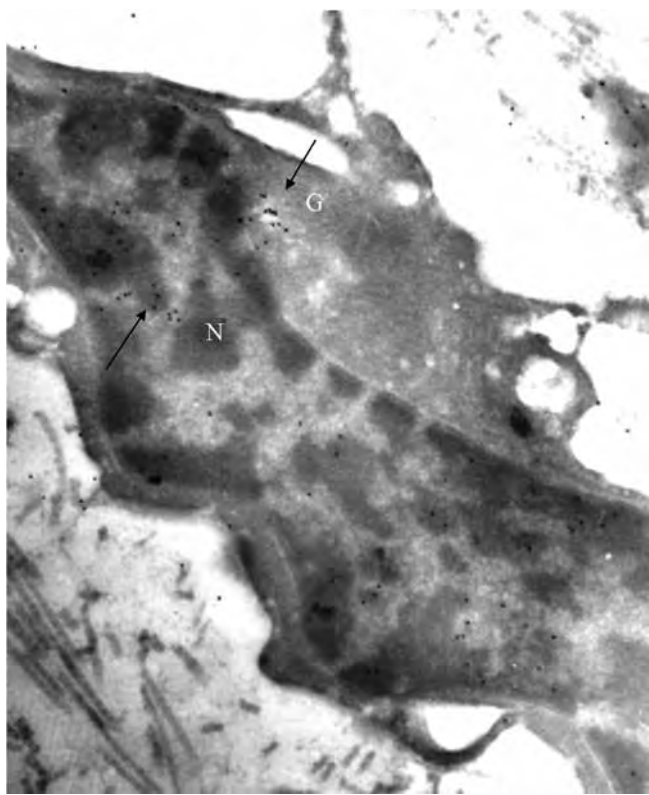


Fig. 16. The figure shows myofibroblast in vitro are stained by antiserum of TGF- β visualized by biotin-avidin-gold method. Gold articles 10 nm are found in Golgi area (G) and spread in the nucleus (N) (arrows) [6, 21]. Myofibroblast secretes TGF- β . $\times 10,000$. Myofibroblast is paracrine cells and secretes TGF- β [7, 8].

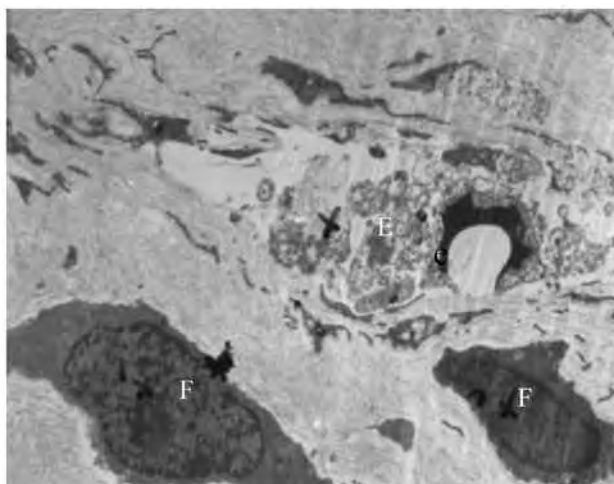
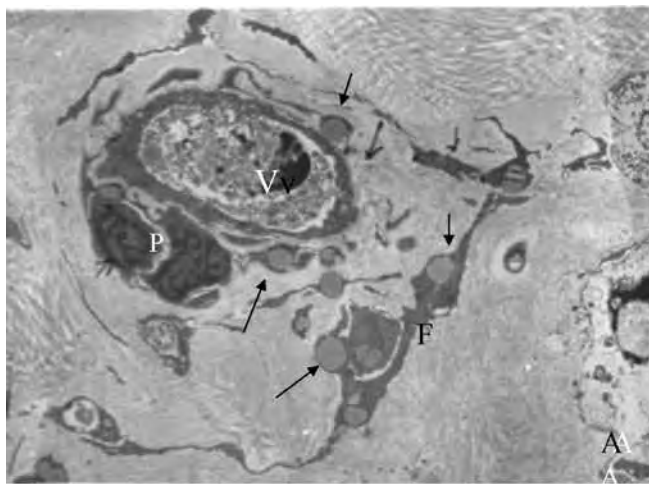


Fig. 17. Influences of external TGF- β for the transformation [18–21]. Fig. A: Organ culture of dermis (media with TGF- β , 2 $\mu\text{g/ml}$ for 15 days cultivation) shows myofibroblasts with fat-droplets (arrows). The transformation seems not to be suppressed. Vascular lumina (V). Two pericytes (P) are well developed but growth of myofibroblasts (F) around the vessel are suppressed. The myofibroblasts are thin and contain fat-droplets (arrows). $\times 5,000$. Fig. B: Organ culture of dermis (media with TGF- β , 4 $\mu\text{g/ml}$ for 10 days) shows disintegrated endothelial cells and pericytes of vascular wall (E). The endothelial cells and pericytes are disintegrated and the transformation is interrupted, while myofibroblasts are stimulated growth (F). $\times 5,000$. Previous report described TGF-1 mediate terminal differentiation to myofibroblast [7]. Myofibroblast is considered a paracrine cell [8]. Present results indicate that TGF- β 2 mg in the media show not influence on the transformation. The myofibroblasts do not grow well. TGF- β 4 mg/ml in the media interfere with the transformation, while the growth of myofibroblasts are stimulated. Besides, factor XIIIa shows no visible effect over the myofibroblasts [20].

Suggestive transformation to adipose cell

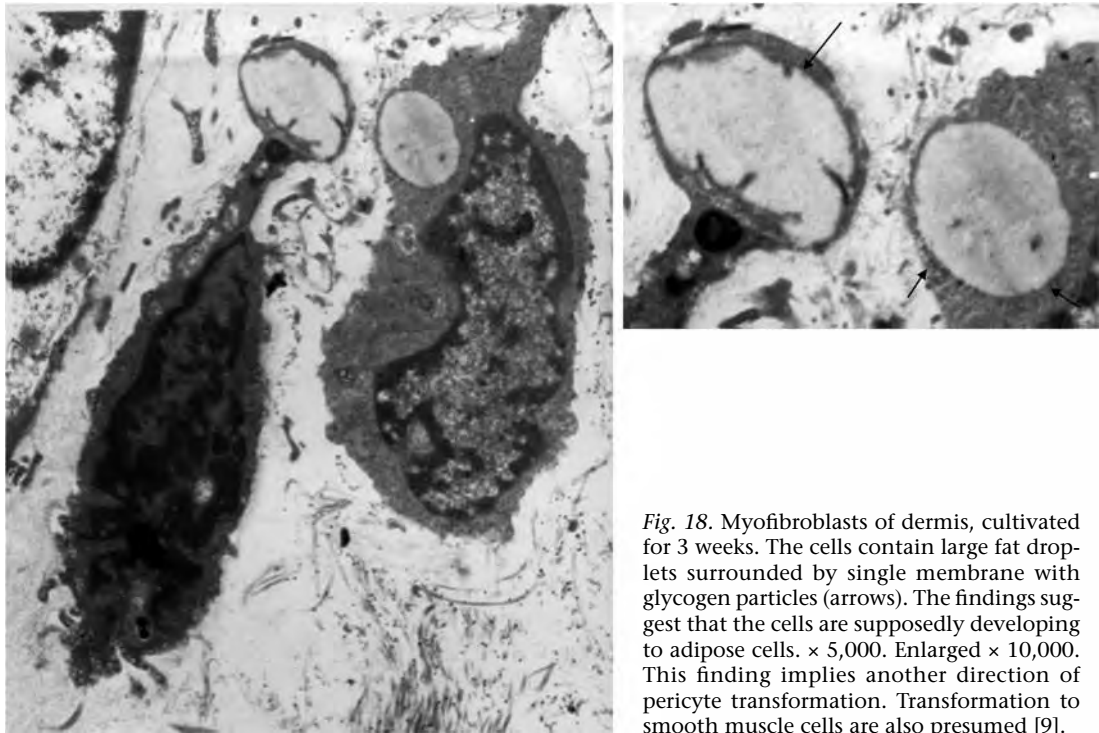


Fig. 18. Myofibroblasts of dermis, cultivated for 3 weeks. The cells contain large fat droplets surrounded by single membrane with glycogen particles (arrows). The findings suggest that the cells are supposedly developing to adipose cells. × 5,000. Enlarged × 10,000. This finding implies another direction of pericyte transformation. Transformation to smooth muscle cells are also presumed [9].

Transformation of pericyte to myofibroblast *in situ* in fibrotic dermatoses

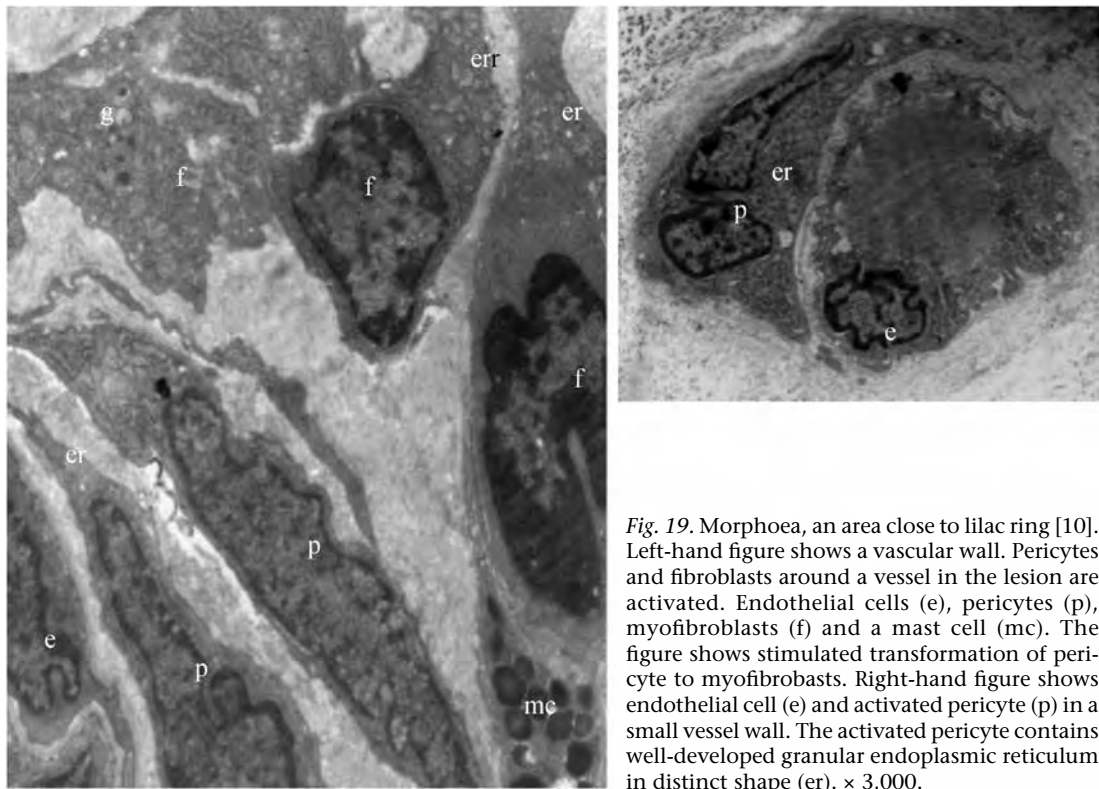


Fig. 19. Morphea, an area close to lilac ring [10]. Left-hand figure shows a vascular wall. Pericytes and fibroblasts around a vessel in the lesion are activated. Endothelial cells (e), pericytes (p), myofibroblasts (f) and a mast cell (mc). The figure shows stimulated transformation of pericyte to myofibroblasts. Right-hand figure shows endothelial cell (e) and activated pericyte (p) in a small vessel wall. The activated pericyte contains well-developed granular endoplasmic reticulum in distinct shape (er). × 3,000.



Fig. 20. Peripheral nerve in morphea [11]. Perineurial cells, pericyte of nerve (p) are activated. The cells contain ribosomes and granular endoplasmic reticulum (er). No distinct basal lamina on the cell surface. Thick basal lamina-like material locates close to the dermal surface of the cell (arrows). A: axon. $\times 10,000$. Ultrastructural signs for the pericyte transformation can be recognized by enlarged Golgi apparatus, enriched ribosomes and granular endoplasmic reticulum and fragmentation of basal lamina on the dermal surface of the pericyte. When cytoplasmic protudes of pericyte are seen in dermis, the transformation is ongoing.

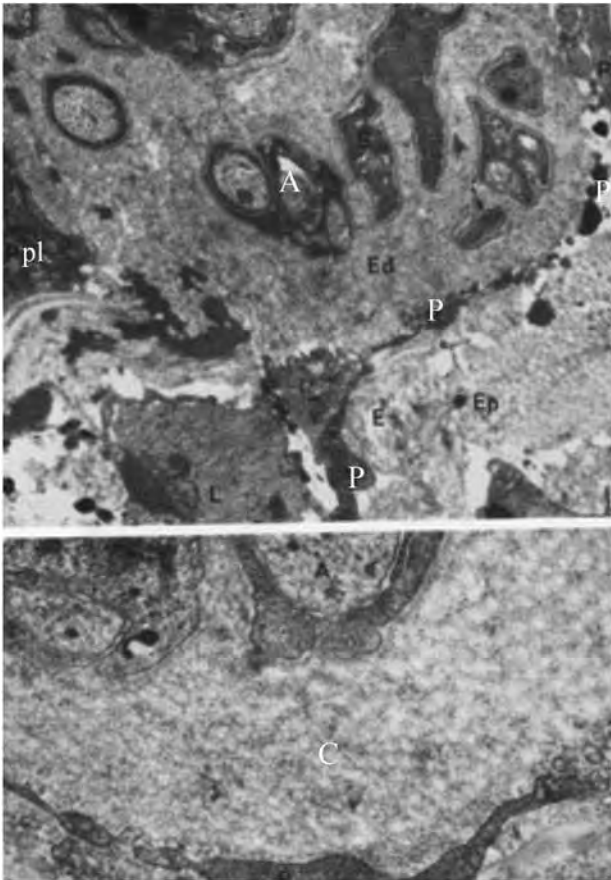


Fig. 21. Morphea [11]. Upper figure: Peripheral nerve. Pericytes (perineurial cell) are retracted and show no basal lamina (P). Schwann cell with axon (A) is exposed to the dermis. $\times 13,000$. Lower picture: The collagen fibrils in perineurium show various thickness. $\times 26,000$. P: perineurium, PC: perineurial cell, A: axon, E: elastic fibre, C: collagen fibrils in endoneurium, L: lymphocyte.

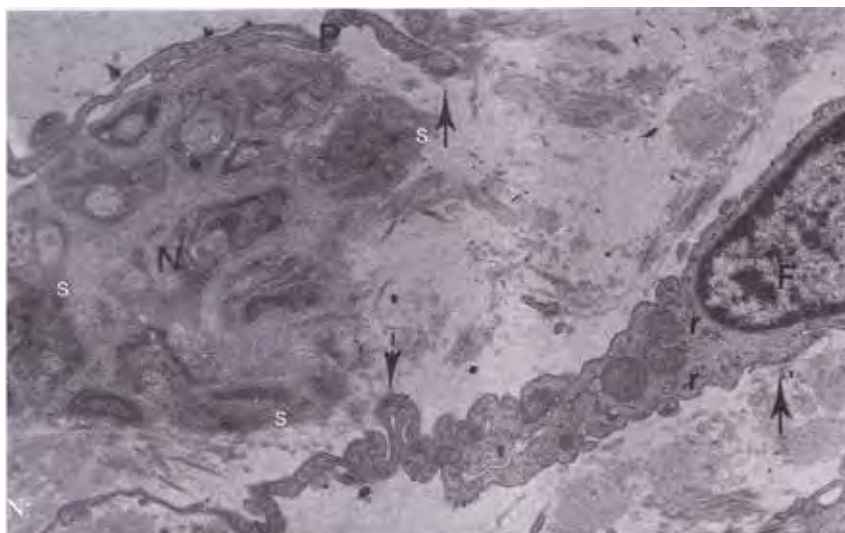


Fig. 22. Transformation of pericyte of perineurium to myofibroblast, Ehlers-Danlos syndrome type III [12]. Peripheral nerve (N) lost perineurial cells and is exposed to dermis. Arrows point at released perineurial cell (F). × 5,000.

Fibrotic dermatoses

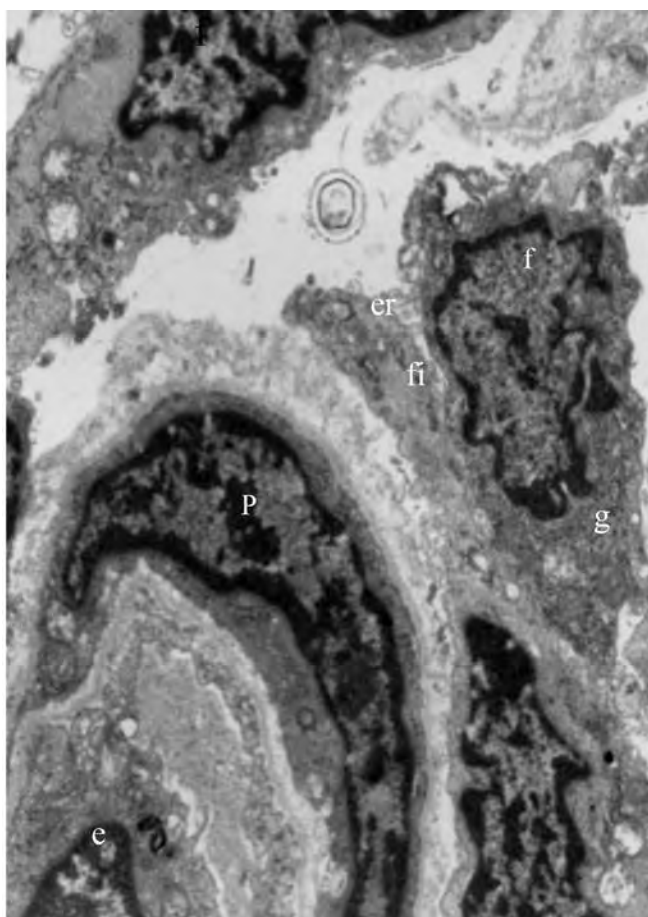


Fig. 23. Shagreen patch [13]. Vascular endothelial cells (e), pericytes (p) and myofibroblasts (f) around a vessel. Pericyte is hypertrophic. Myofibroblasts show well-developed endoplasmic reticula (er) and Golgi apparatus (g). Intracytoplasmic filaments (fi) are in a limited area. Cytoplasmic structure suggests that the myofibroblasts in this disorder is fibroblastic. × 2,000.



Fig. 24. Shagreen patch. A hypertrophic fibroblast in dermis. The cell presents widened Golgi apparatus (g), granular endoplasmic reticulum (er) and ribosomes in free and rosette form. Intracytoplasmic filaments (f) are scanty. $\times 5,000$. The findings represent that the transformation is not suppressed and fibroblast develops, however myofibroblasts are not developed.

Ulcus cruris

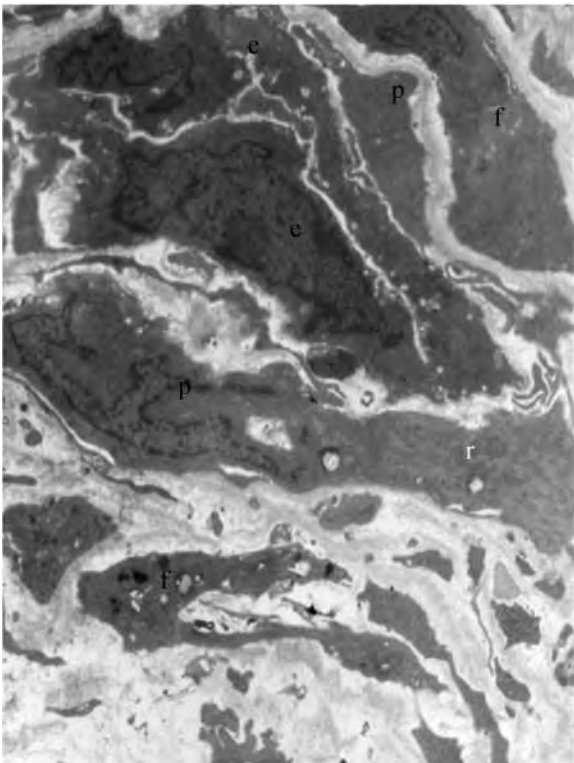


Fig. 25. Ulcus cruris [13]. Peripheral area of ulcer. Vascular wall shows large hypertrophic endothelial cell (e), pericytes (p) and fibroblast (f). Ribosomes and granular endoplasmic reticula (r). The figure indicates that pericytes are activated for the transformation. $\times 2,000$.

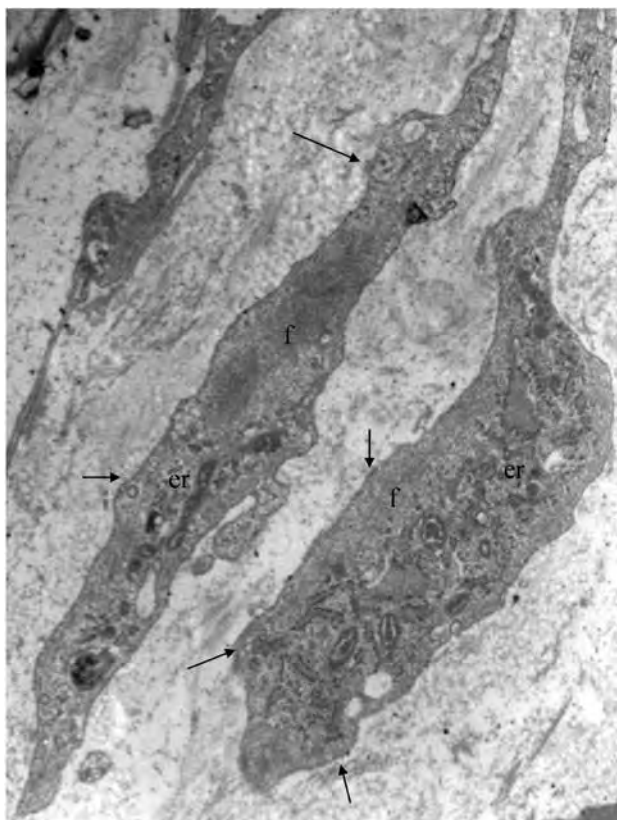


Fig. 26. Ulcus cruris. Myofibroblasts in fibrous area of dermis shows granular endoplasmic reticula (er), bundles of intracytoplasmic filaments with focal density (f) and fibronexus (arrows). × 5,000. Pericyte transformation is stimulated and myofibroblasts develop in the lesion.

Spontaneous keloid

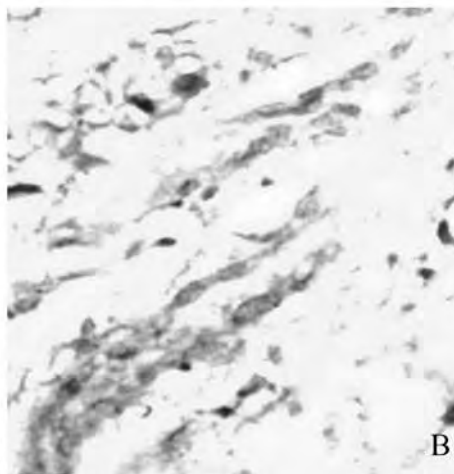
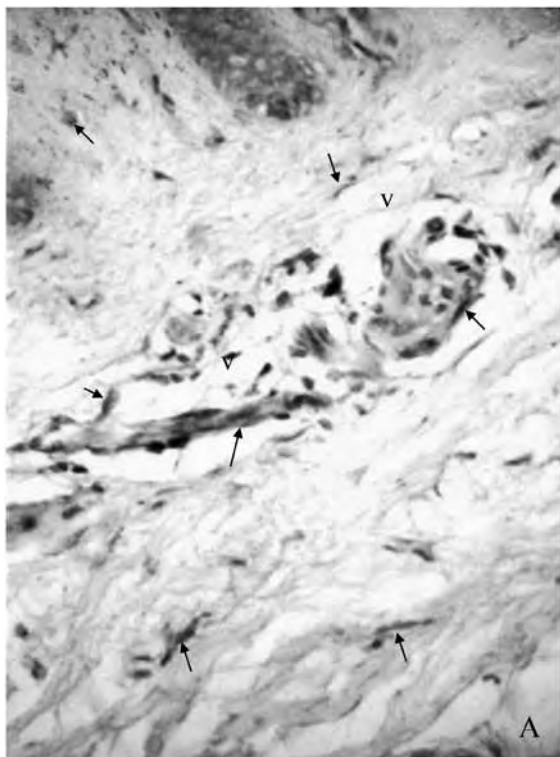


Fig. 27. Keloid tissue is stained with immunoglobulins to myofibroblast and visualized by biotin-avidin-peroxidase method [13] [Appendix]. Cells in vascular wall and around vessels (v) and between dermal fibres are stained positively. These cells are myofibroblasts. × 40. Arrows in Fig. A point at some of the positive cells for the staining. Fig. B is in high resolution. × 80.



Fig. 28. Spontaneous keloid. A vessel in keloid lesion. Endothelial cells are thin. Pericytes are hypertrophic (p), showing granular endoplasmic reticulum (er) and Golgi apparatus (g). Endothelial cell (e). Myofibroblast (f). The figure represents that pericyte transformation is stimulated in the vascular wall. $\times 3,000$.

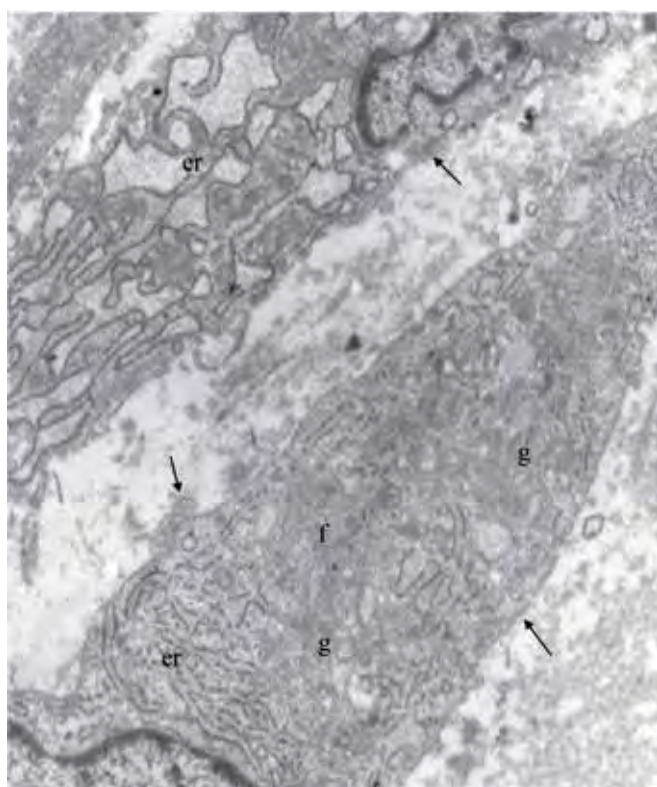


Fig. 29. Spontaneous keloid. Fibrous lesion. Fibroblasts in the lesion presents different cytoplasmic structure. The cell in the lower part presents cytoplasm filled of granular endoplasmic reticulum with dilated cisterna and closely associated ribosomes (er). Golgi apparatus is enlarged (g). Contractile component are scanty and indistinct (f) (arrows). The cell is fibroblasts under active formation of collagen fibrils. The other fibroblast in the upper has supposedly reduced activity for collagen formation. Threads are filled in the dilated cisterna. Ribosomes on the granular reticula are seen denser than those of the lower cell. $\times 5,000$.

Pretibial myxoedema

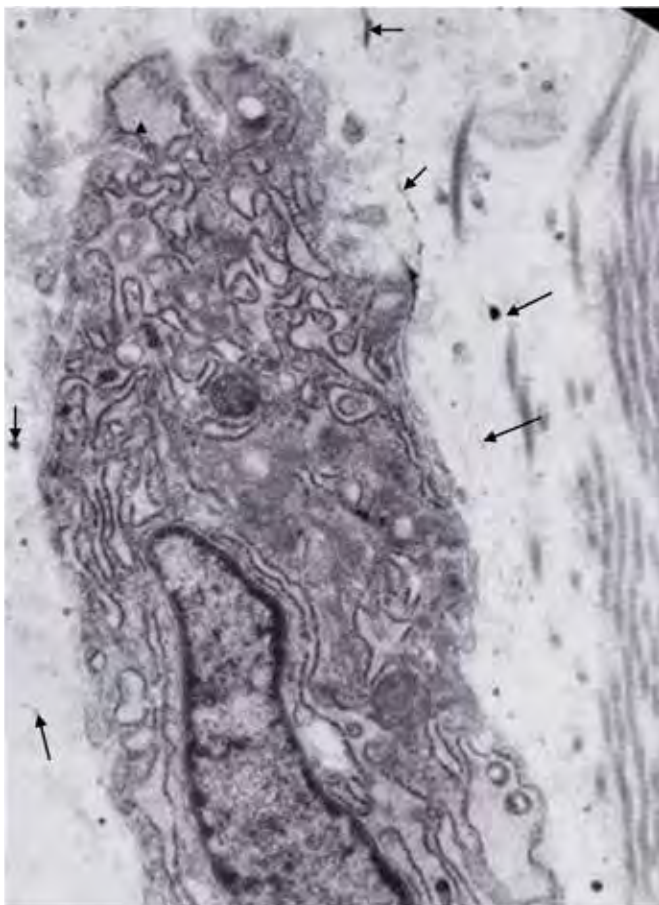


Fig. 30. Pretibial myxoedema. Myofibroblast shows distinct shape of granular endoplasmic reticulum with dilated cisterna and distinct dense ribosomes. Contractile components are scarcely seen. The cell may be called fibroblast. Cisterna of the granular endoplasmic reticulum is dilated and contain faint filamentous figures, supposedly glycosaminoglycan, are seen in the dilated cisterna (arrow-head, in the dilated cisterna, top of the cell). The ribosomes have lost their ordinary function and produced neither collagen nor proteoglycan. Glycosaminoglycan figures are in the extra-cellular space (arrows). × 10,000. Based on the description in this section and sections for Collagen, Ground substance, and Mast cell, it may be hypothesised that the ribosomes of the granular endoplasmic reticula alter the function. Neither collagen nor proteoglycan is produced but glycosaminoglycans appear in the cisterna. This seems to be the main source of the interstitial ground substance. [Unpublished]

Morphoea

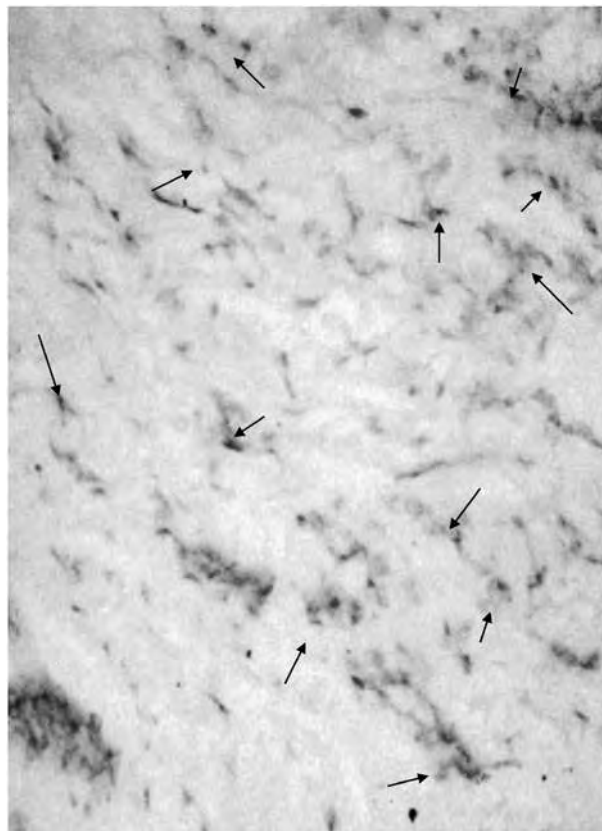


Fig. 31. Tissue sections from fibrotic area of morphoea are stained by immunoglobulin to myofibroblast and visualized by peroxidase anti peroxidase method (Appendix). The fibrotic dermis shows numerous myofibroblasts. Arrows show some examples. × 400. [Unpublished]

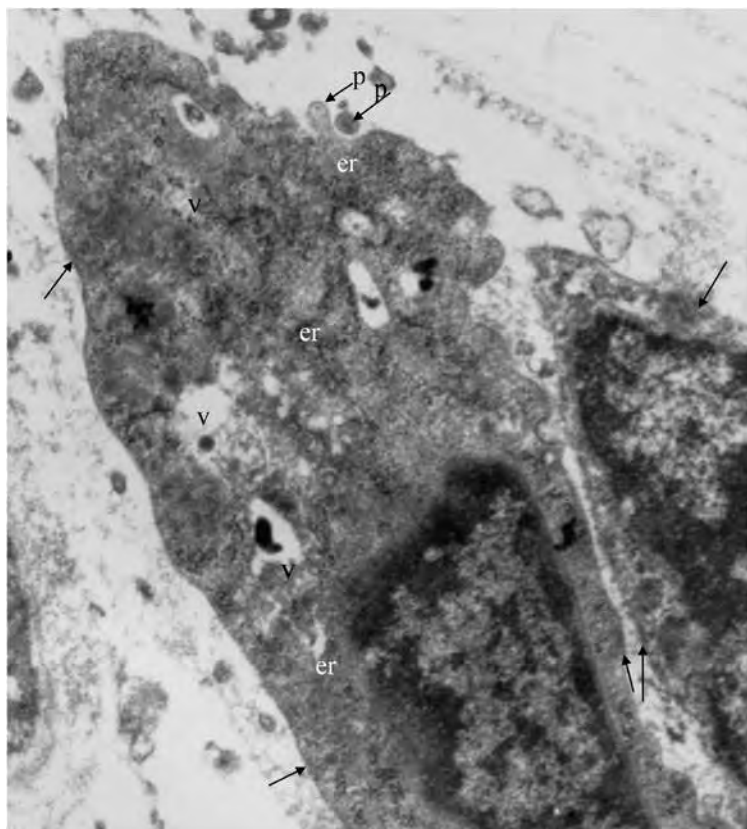


Fig. 32. Morphoea. Myofibroblasts in the lesion are probably apoptotic [14]. Fibroblasts show vacuoles with dark dots of glycosaminoglycans in the cytoplasm (v). Abnormal endoplasmic reticula (er) reveal conglomerates of ribosomes and indistinct limiting membrane (er). Scarce intracytoplasmic filaments are in the cytoplasm. Round cytoplasmic protrudes on the cell surface are supposedly apoptotic body (arrows with p). Ill-defined hemidesmosome-like thickening (arrows). × 5,000. Fibroblasts are abnormal. Myofibroblasts are scarcely found. [Unpublished]



Fig. 33. Nuclear changes of myofibroblasts in morphoea. The nuclei contain thick peripheral condensates and columns of chromatin (n). Nuclear envelop is hardly seen. Cytoplasm shows indistinct cell organelles. The nuclear change represent that those myofibroblasts are disintegrated probably by aponecrosis. × 5,000.

Cell death, aponecrosis: Apoptosis can be recognized in ultra-structural level [14]. Suggestive signs are:

1. Chromatin condensation in nucleus as seen in column formation and peripheral condensation.
2. Degradation of limiting membrane in cytoplasm. This change reveals defect of endoplasmic reticulum, loss of inner cell membrane and nuclear envelop.
3. Conglomerated intracytoplasmic filaments, probably resulted from apoptotic body formation and loss of cellular connection. These changes are often confused with necrosis. Then it is better to call it aponecrosis. [Unpublished]

Acrosclerotic scleroderma

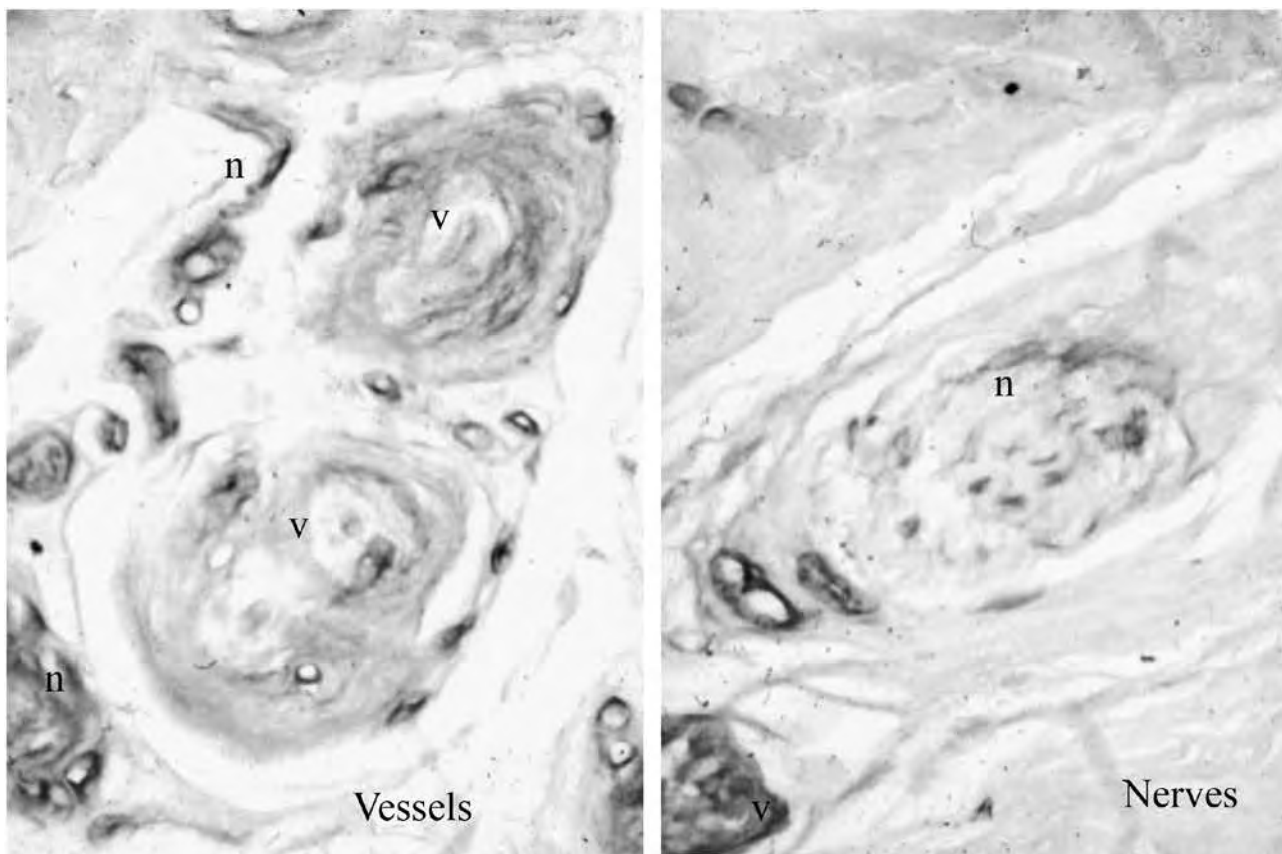


Fig. 34. Acrosclerotic scleroderma [18]. Stained by antiserum to myofibroblast and visualized by streptavidin-peroxidase-diaminobenzidin. Myofibroblasts and pericytes of vessel and nerves are stained positively. × 400. Myofibroblasts are noticed in sclerotic dermis [15]. Present findings indicate that myofibroblasts are found in vascular wall and nerve of scleroderma lesion.

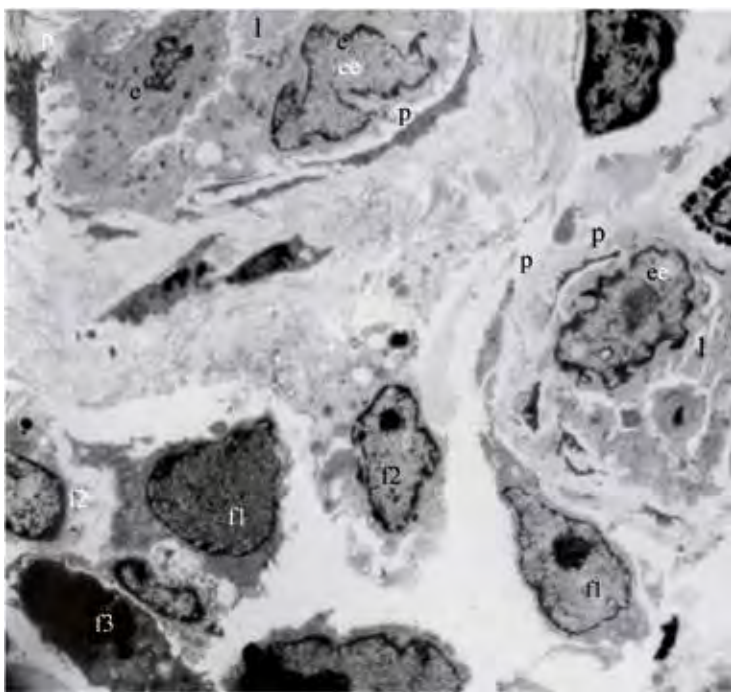


Fig. 35. Acrosclerotic scleroderma [18]. Vessels and infiltrated cells in the periphery of scleroderma lesion. The vessels show hypertrophic endothelial cells (e), thin condensed cytoplasm in pericytes (p) and narrow lumen of vessel (l). Fibroblasts around vessels appear in various cytoplasmic structures. Fibroblasts (f1) are seen as rather active endoplasmic reticulum and fibroblast (f2) are vacuolated, while fibroblast (f3) contains condensed nuclear chromatin (apoptotic). × 2,000. Myofibroblast and its apoptosis is important in the pathogenesis of systemic scleroderma [16].

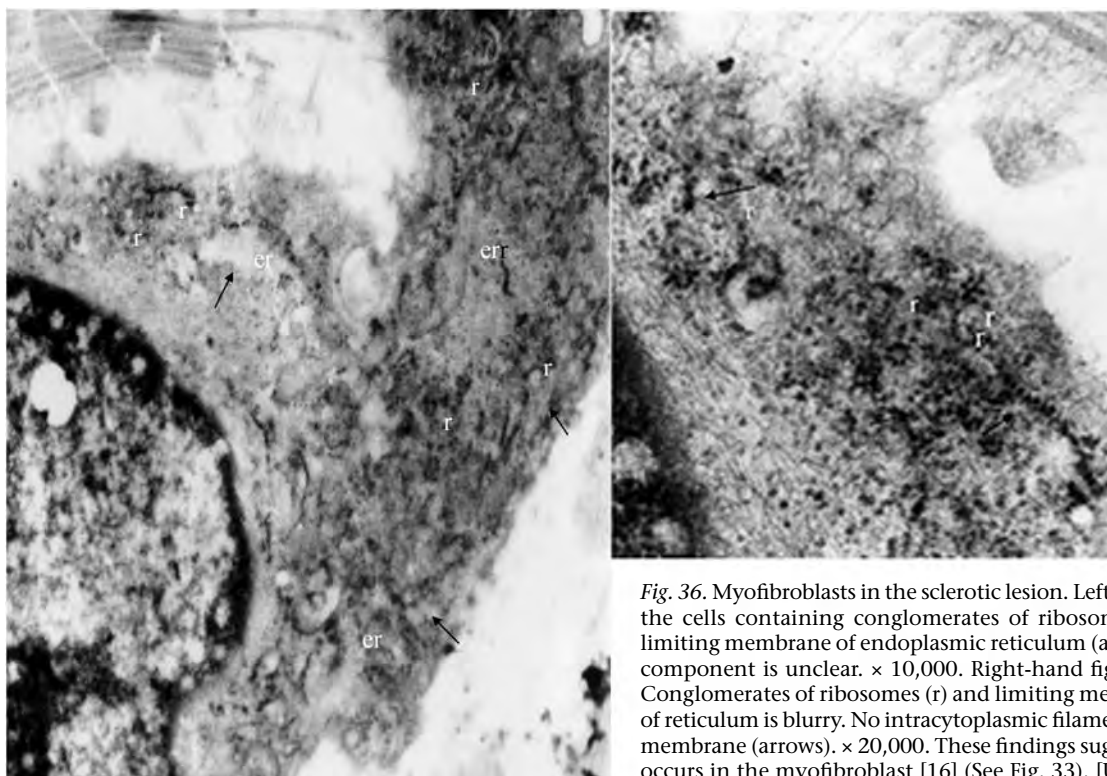


Fig. 36. Myofibroblasts in the sclerotic lesion. Left-hand figure shows the cells containing conglomerates of ribosome (r) and blurred limiting membrane of endoplasmic reticulum (arrows). Contractile component is unclear. $\times 10,000$. Right-hand figure shows details. Conglomerates of ribosomes (r) and limiting membrane of cisterna of reticulum is blurry. No intracytoplasmic filaments attached to cell membrane (arrows). $\times 20,000$. These findings suggest that apoptosis occurs in the myofibroblast [16] (See Fig. 33). [Unpublished]

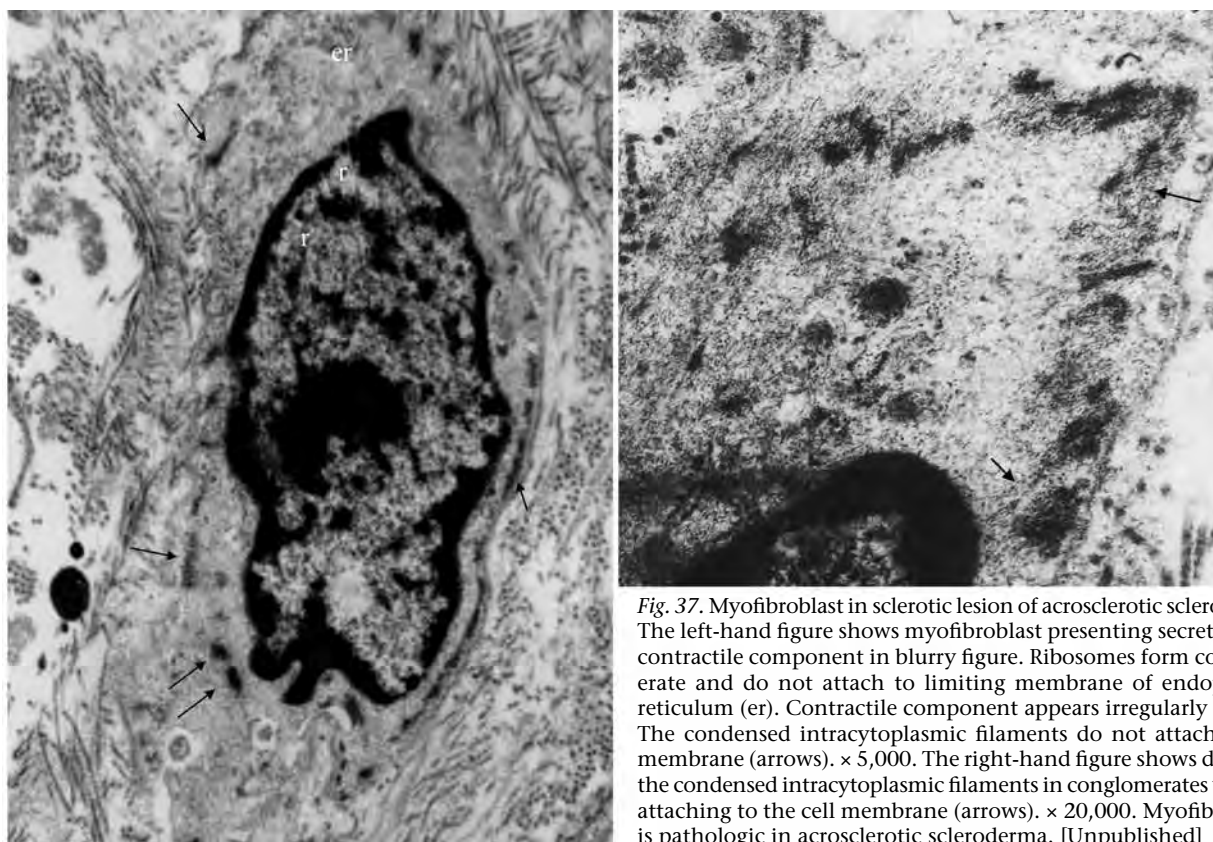


Fig. 37. Myofibroblast in sclerotic lesion of acrosclerotic scleroderma. The left-hand figure shows myofibroblast presenting secretory and contractile component in blurry figure. Ribosomes form conglomerate and do not attach to limiting membrane of endoplasmic reticulum (er). Contractile component appears irregularly shaped. The condensed intracytoplasmic filaments do not attach to cell membrane (arrows). $\times 5,000$. The right-hand figure shows details of the condensed intracytoplasmic filaments in conglomerates without attaching to the cell membrane (arrows). $\times 20,000$. Myofibroblasts is pathologic in acrosclerotic scleroderma. [Unpublished]

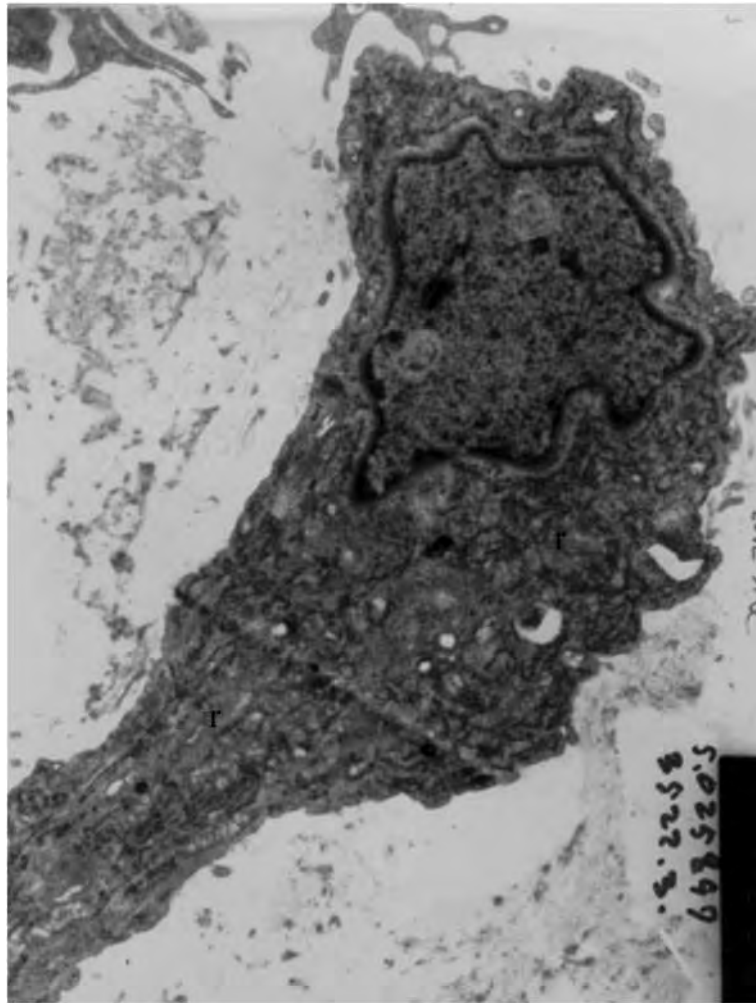


Fig. 38. Linear scleroderma. Myofibroblasts in sclerotic lesion show distinct structure of granular endoplasmic reticulum (r) with dilated cisterna. Degeneration of myofibroblasts are not serious lesion. $\times 10,000$. [Unpublished]

Description for ultrastructural histopathology of dermal connective tissue

The dermis is constructed of connective tissue that holds the epidermis and mesenchymal cell tissues in a stable condition. The connective tissue of the dermis is composed of elastic system fibres, collagen fibrils and ground substance. Epidermis and mesenchymal cell tissues form a junction structure and anchor to elastic system fibre. Mast cells and myofibroblasts migrate freely into the dermis, maintaining it in a stable condition.

I. Elastic system fibre

Elastic system fibres consist of elastic microfibrils and elastic matrix and present in various shapes. Elastic microfibril is a hollow fibril 10 nm across that occurs in straight and wavy shapes. Matrix is lucent homogenous with dense grainy stripes. Matrix appears in the bundle of elastic microfibrils and gradually covers the whole bundle in adult dermis. Elastic matrix is not a binding material for bundles of elastic microfibrils, but elastic matrix is a component of elastic fibre. Elastic system fibres present various shapes.

Elastic system fibre of typical construction is called "elastic fibre proper", and presents homogenous lucent matrix with dense stripes inside and microfibrils on the surface. Broad elastic fibre is a common variant seen in normal dermis. Broad elastic fibre is fully covered by elastic matrix with indistinct thin internal stripes; microfibrils are scarcely seen on the matrix surface of broad elastic fibre. Elastic fibre and bundles of microfibrils form a plexus under the epidermis (subpapillary elastic plexus) and bundles of elastic microfibrils ascend from the plexus and fuse to the basal lamina of the epidermis (ascending rami). Elastic microfibrils in the dermis join the basal lamina of mesenchymal cell tissues. Keratinocytes and mesenchymal cells secrete basal lamina and anchor themselves to the elastic microfibrils and elastic system fibre. Such a network of elastic system fibre holds the dermis in stable form against external forces.

Elastic matrix contains elastomucin, which is susceptible to pancreatic elastase. Elastic microfibrils are not susceptible to the influence of elastase. Elastic microfibrils contain fibrillin and disulfide bonds. Elastic microfibrils are disintegrated by dithioerythritol. In reticular dermis, bundles of straight microfibrils, probably elastic in nature, are occasionally found. This microfibril bundle is called oxytalan fibre, by Cotta-Pevetria et al. [7]; its function is unknown.

It is unclear which cells secrete elastic microfibrils. Pericytes are thought to be the first candidate for production of elastic

microfibrils. The turnover-rate of elastic fibre is unknown. It has been suggested that the turn-over rate is very long or that no turn-over occurs.

Elastic fibre degenerates with age, disorders and external influences for instance sun-exposure. Degenerate elastic fibre exhibits a loss of elastic microfibrils, a dense grainy coat over the matrix surface, widened dense internal stripes, and calcium spots. Degenerate matrix is separated into bands. Calcium spots are dense round spots, in which calcium apatite crystals are demonstrated. Calcium spot is a sign for aging. Globus elasticus is a large round matrix with occasional calcium spots inside and a few elastic microfibrils on the surface. Globus elasticus is found in the papillary dermis of aged persons [6].

Age-dependent alteration is divided into 4 age-patterns: infantile, adolescent, adult and senile. Age-dependent changes in the ultrastructure of elastic fibre become manifest in adult age, usually around 35 years of age in the reticular dermis in normal females. Sun-exposure provokes the initiation and stimulates the intensity of the age-dependent change. Phospholipid dots also appear in heavily exposed areas. Exposure-dependent degeneration of elastic fibre begins in the papillary dermis during the twenties in intensively exposed areas of the body and expands into the surrounding areas and deeply into the reticular dermis.

Abnormal calcification is seen in bizarre annular form inside the lucent matrix with no dense matrix stripes. Abnormal calcification is found in pseudoxanthoma elasticum. If the calcification is due to external influence, such as corrosion due to Norwegian salpêtre or some diseases, calcium precipitation is found on the surface of normal elastic fibre.

Amyloid fibrils seem to develop in the elastic fibre matrix and masses of amyloid fibrils deposit in the elastic matrix. Amyloid fibrils also precipitate on basal lamina of the epidermis and perineurium. In necrobiosis and myxoedema, glycosaminoglycans are found on the surface of elastic matrix. Elastic matrix is disintegrated in morphea and acrosclerotic scleroderma. Lupus erythematosus reveals needle-shaped elastic microfibrils.

Among the inherited hypermobile disorders, Ehlers-Danlos syndrome shows no definite special changes in elastic fibre, but exposure-dependent degeneration seems to start at an earlier age than normal, being apparent at around 5 years of age. Characteristic ultrastructural variation in elastic fibre is noticed in Marfan syndrome, osteogenesis imperfecta and homocystinuria, while exposure-dependent alterations are not clearly demonstrated in these disorders. Inheritance-dependent changes in Marfan syndrome reveal diminished microfibrils on the matrix surface. Glycosaminoglycan figures and dense surface coat on the matrix surface appear at infantile and adolescent ages. In adult age, the matrix surface is covered by dense material with no microfibrils. Osteogenesis imperfecta

type I reveals numerous wavy elastic microfibrils on the surface of the lucent matrix in infantile age. After ageing, matrix becomes lucent homogenous with indistinct internal stripes and reduced numbers of microfibrils. At adult age, matrix becomes lucent round with no internal stripes and scarce microfibrils on the matrix surface. Elastic fibres in the eruptions of juvenile elastoma and connective tissue nevi reveal changes resembling osteogenesis imperfecta. Homocysteinuria shows numerous straight and wavy elastic microfibrils on the matrix surface.

II. Collagen fibrils

Collagen fibrils are straight fibrils with round and oval cut-surfaces. Collagen fibrils tend to bundle and fill in the space of the networks of elastic system fibres. Collagen fibrils are identified by their characteristic axial periodicity of 60 nm.

The thickness of collagen fibril in normal dermis ranges from 30 to 150 nm. Papillary dermis has a thickness ranging from 30 to 60 nm, with a sharp peak at 50 nm, and reticular dermis has a distribution of 50 to 130 nm, with a slow peak ranging from 83 to 120 nm. Thin collagen fibrils are found in the perivascular area of normal dermis and in the lesion of keloid and atrophoderma. Scleroderma presents a distribution of 17–160 nm in bimodal distribution in active proceeding lesions. Sclerotic lesion shows thick fibrils of 150–160 nm or more.

Collagen fibrils of the dermis are constructed of types I and III collagen. Thinner collagen fibrils have a lower ratio of I/III and thicker collagen fibrils have a higher ratio of I/III. In addition, type V collagen binds collagen types I and III to form fibrils and pack collagen fibrils in bundles. Furthermore, type V collagen binds the other fibrillar components, i.e. elastic fibres, basal lamina and ground substance (see sections, I, III, IV).

Twisted collagen fibrils are the specific sign for inherited malformation of the collagen fibrils. A person with twisted collagen fibrils has inherited abnormality of collagen fibril formation. The normal skin of the patients with inherited hypermobile disorders, and even normal persons in the pedigree, shows twisted collagen fibrils. Twisted collagen fibrils have a flower-like (or firework-like) cut surface appearance and wire-like shape in longitudinal section. Twisting occurs clockwise by 15 degrees. Twisted collagen fibrils are usually thicker than 100 nm. Increased winding of the collagen fibrils is seen in the curled form of thinner collagen fibrils. The curled form of collagen fibrils are found in tuberous sclerosis. Experimentally twisted collagen fibrils can be produced in normal collagen fibrils by treatment with citrate buffer pH 3.1.

Collagen aggregate is notable in pathological dermis, as demonstrated by characteristic figure, that is, filament bundle with cross-bands in diseased dermis. Collagen aggregate represents an intermediate product of *in situ* degradation of collagen fibrils. Collagen aggregate has been demonstrated in the dermis of the inflammatory dermatoses and mesenchymal cell

tumour; however, no collagen aggregate has been found in basal and spinous cell carcinoma (ectodermal origin).

Experimentally, collagen aggregate can be produced by clostridial collagenase and collagenolytic factor, separated from the culture media of human myofibroblast of dermis and organ culture of normal dermis.

Calcification of collagen fibrils shows calcium apatite crystals on the fibril surface along the collagen molecules.

III. Ground substance

Ground substance reveals a specific figure, “filaments and dots”, in the interfibrillar space of the dermis. This figure is distinct after routine glutaraldehyde fixative supplemented by 7.5% sucrose. The figure is composed of filamentous collagen type VI associated with glycosaminoglycan. Dots present a high content of acid glycosaminoglycan. Positive staining with ruthenium-red indicates a high content of acid glycosaminoglycan (hyaluronic acid). The filamentous figure of collagen VI joins each other by type V collagen and forms networks in the interfibrillar space. Type V collagen further binds ground substance to collagen fibres, elastic fibres, basal lamina and cell surface.

Increased numbers of the specific figure suggest myxoedematous condition in the dermis. Myxoedematous dermis is demonstrated in the lesion of localized myxoedema, popular mucinosis, lupus erythematosus, morphea, basal cell carcinoma and fibrodysplasia ossificans progressiva. Mast cell granules in the lesion of those disorders show glycosaminoglycan figure. The granules seem to be closely related to form myxoedematous dermis, but the exact roles of mast cells in the myxoedematous process is obscure (for further information, see Section VI. Mesenchymal cell lineage).

In addition, proteoglycan appears as dense fine granular material. Proteoglycan is demonstrated by periodic acid-silver proteinate method on the cell surface and in the cisterna of granular endoplasmic reticulum of myofibroblasts, cross-bands of collagen fibrils and anchoring fibrils.

IV. Junction

Junction covers the connective tissue surface of the dermis and anchors ectodermal and mesenchymal cell tissues to underlying connective tissue, especially with elastic microfibrils. The junction under the epidermis is well developed and reveals distinct structure in detail, while the junction structure under mesenchymal cell tissue is poorly developed and only shows basal lamina and hemidesmosomes, such as vessel, nerve, smooth muscle cells and adipose cells. The junction under the epidermis (dermoepidermal junction) is found as follows. Basal lamina binds to hemidesmosomes of basal keratinocytes by anchoring filaments. Anchoring fibrils extrude from basal

lamina into the dermis and end free between the fibrils in the papillary dermis. Basal lamina is formed of a three-dimensional mesh structure of type IV collagen and glycoprotein. Anchoring filaments are composed of collagen IV and laminin, a variant of laminin of Rousselle (1991). Anchoring fibrils are composed of type VII collagen. Anchoring fibrils present cross-bands of proteoglycans.

Clostridial collagenase and pancreatic elastase completely remove junction structure, while collagenolytic factor from myofibroblasts does not influence basal lamina except the joint-area of anchoring fibrils to basal lamina. Dithioerythritol also influences the basal lamina. Seemingly, disulphide bonds are included in the construction of basal lamina.

Organ culture of skin grafts disclosed the process of formation of new dermoepidermal junction and multiple layers of basal lamina. The junction is formed by basal keratinocytes. Hemidesmosomes first develop on the dermal aspect of keratinocyte and then anchoring filaments and basal lamina. Basal lamina left on the dermal surface becomes dense and numerous anchoring fibrils develop on the dermal surface of the basal lamina (double layers of basal lamina). Keratinocytes join directly to elastic matrix and microfibrils without junction. Collagen fibrils under the basal cells are disintegrated. Cell culture of keratinocyte, free from contamination by mesenchymal cells, has confirmed the secretion of type IV collagen by keratinocytes.

Destruction of the dermoepidermal junction produces blisters in the skin. Blisters are classified by the damaged level in the junction, i.e. epidermal, subepidermal, sublaminal and dermolytic. Epidermal separation is produced by altered desmosomes and hemidesmosomes in different form, i.e. spongiotic, acantholytic and necrotic. Epidermal blisters are found in various hereditary, inflammatory and degenerative dermatoses. Subepidermal separation includes real and false variants.

Both variants develop in the subepidermal space. Real subepidermal blister presents well-preserved cell membrane on the blister roof and intact basal lamina on the blister floor. Real subepidermal blister is found in epidermolysis bullosa junctionalis, bullous pemphigoid, linear IgA dermatosis and suction blister of normal skin. False subepidermal separation occurs by destruction of both or either blister roof or floor. This type of blister is found in dermatitis herpetiformis, diabetic blister and epidermolysis dystrophica recessiva. Dermolytic blister presents with separation in the papillary dermis. The blister roof is dermoepidermal junction in normal shape and the floor is dermal fibres. False subepidermal blister is found in epidermolysis bullosa dystrophica of dominant variant and early phase of recessive variant and epidermolysis bullosa acquisita. Dermolytic blister in the deep reticular dermis is found in generalized scleroderma. The character of the changes in

blister roof and floor, and the damaged level of the junction provide clues for clinical diagnosis.

Productive change in the dermoepidermal junction presents multiple layers of basal lamina, diffuse and localized thickening of basal lamina, globes of anchoring fibrils and precipitation of immune reactant, hyaline, amyloid and proteoglycan. Amyloid precipitation on basal lamina of the epidermis and perineurium is notable.

The cytoplasmic protrusion of both basal and squamous carcinoma cells penetrates through normal junction and forms its own junction in the dermis. Basal cell carcinoma diminishes the junction structure and, finally, the junction appears like pieces of dense cell coat on the cancer cell surface. Squamous cell carcinoma produces an irregular form of the junction, thickened basal lamina with or without anchoring fibrils. Hemidesmosomes and anchoring filaments are sometimes found. Dislocated basal lamina with distinct anchoring fibrils is formed between invaded cancer cells of squamous cell carcinoma.

V. Mast cell

Mast cells are easily identified by specific granules with a lamellar structure (often seen in scroll form), dense granular material with a crystalline structure and an indistinct enclosing single membrane. Ruthenium red stain granular materia.

Mast cells function according to the granule content. When mast cells begin to degranulate, the single enclosing membrane of the granule becomes dense and thick. Degranulation proceeds in two ways. Firstly, the granule content in the cytoplasm is disintegrated and the content flows out of the cell, leaving round empty spaces in the cytoplasm (honeycomb structure). Secondly, whole granules are extruded into the extracellular space, leaving long villi on the cell surface. The extruded granules are dissolved in the extracellular space. The latter probably occurs during the acute response. Glycosaminoglycan figures are seen on the surface of the degranulated granules. Regranulation begins in the Golgi apparatus soon after degranulation is over. Progranule and immature granules are seen in the Golgi apparatus. In the case of urticaria pigmentosa, simply stroking with a blunt instrument provokes degranulation within 5 minutes and the degranulated mast cells are fully regranulated by approximately 30 minutes after stroking.

Mast cells play a significant role in introducing myxoedematous change in the dermis. Lots of the figure "filaments and dots" appear on the surface of disintegrated granules. In amyloidosis, mast cell granules are filled with amyloid fibrils. Mast cells also play significant roles in the allergic process, collagenolytic process, and in remodelling connective tissue. Myxoedema, morphoea, scleroderma and fibrodysplasia are notable examples.

Mast cells are influenced significantly by basal and squamous cell cancer. Mast cells have stimulated granule formation in the area surrounding basal and squamous cell carcinoma and suppressed granule formation in the cancer tissue. In basal cell carcinoma, mast cells in surrounding areas reveal large granules containing lucent homogenous material similar to myxoedema. The granules become smaller close to basal cell carcinoma tissue. In squamous cell carcinoma, mast cells in surrounding areas exhibit large granules with distinct large lamellae with scarce homogenous material. The granules are smaller close to the cancer tissue. However, the lamellae are distinct and homogenous material is scanty. Mast cells are also found in epidermis around squamous carcinoma. The granules are small and degranulated, leaving a honeycomb structure.

VI. Mesenchymal cells

Mesenchymal cell lineage includes pericyte, myofibroblast (fibroblast) and fibrocyte. The cells contain identical cytoplasmic organelles, i.e. secretory and contractile cytoplasmic components. Besides, pericyte is covered on cell surface with basal lamina. These cells function to remodel the structure of connective tissue of dermis. Pericytes of vessel wall and perineurium transform to myofibroblasts and immigrate into dermal connective tissue. The transformation begins with enlargement of Golgi apparatus, distinct ribosomes and granular endoplasmic reticula. Basal lamina is fragmented and the cells are released and immigrate into the dermal connective tissue. The cells are myofibroblasts. Fibrocyte is the cell in the resting stage. Vascular endothelial cells are probably the origin of myofibroblast. Myofibroblasts are paracrine cells and secrete transforming growth factor β . Transforming growth factor β is probably to suppress the transformation. Tuberous sclerosis, spontaneous keloid, ulcer cruris, and the other common fibrotic process present the transformation. Concerning myxoedematous change, dysfunction of ribosomes on the granular endoplasmic reticula seems to be the main process for myxoedema formation.

Abnormal findings in the myofibroblasts in morphea and acrosclerotic scleroderma, indicate that both sclerodermic disorders probably have abnormal conditions on the inner cell membrane system of myofibroblast. The suggestive signs are *in morphea*, loss of nuclear membrane with chromatin column formation and apoptotic body on cell surface, and *in acrosclerotic scleroderma*, loss of granular endoplasmic reticulum, i.e. conglomerate of ribosomes (loss of smooth-surfaced endoplasmic reticulum and disattachment of intracytoplasmic filament to inner leaflet of cell membrane). Myofibroblasts occasionally contain fat-droplets surrounded by glycogen particles. This sign implies possible conversion of myofibroblast to adipose cell. Malignant myofibroblast is unknown in this respect.

In conclusion, pericytes of vascular wall and perineurium are the cell reservoir for mesenchymal cell lineage in dermis. Transformation of pericyte to myofibroblast is the essential

cell process in fibrosis. Granular endoplasmic reticula of myofibroblasts seems to play significant role for connective tissue disorders.

References

I. Elastic system fibre

- 1a. Kobayasi T. Electron microscopy of the elastic fibres and the dermal membrane in normal skin. *Acta Derm Venereol* 1968; 48: 303–312.
- 1b. Kobayasi T. Elastic fibre. In: Hirone T, Suzuki K, editors. *Electron Microscopy in Clinical Dermatology*. Kodansha: Tokyo, p. 26–27, 1989.
2. Kobayasi T. Anchoring of basal lamina to elastic fibres by elastic fibrils. *J Invest Dermatol* 1977; 68: 389–390.
3. Kobayasi T, Karlsmark T, Asboe-Hansen G. Degradation of dermal fibrillar structure. Effect of collagenase, elastase, dithioerythritol and citrate. *Acta Derm Venereol* 1977; 57: 379–387.
4. Kobayasi T, Karlsmark T. Type V and VI collagen for cohesion of dermal fibrillar structures. *J Submicrosc Cytol Pathol* 2006; 38: 103–108.
5. Kobayasi T. Dermal elastic fibres in the inherited hypermobile disorders. *J Dermatol Sci* 41 2006: 175–185.
6. Ebner H, Gebhart W. Elastic globes. *Arch Dermatol* 1974; 249: 329–339.
7. Cotta-Peveria G, Rodorigo FG, Bittencourt-Sampaio S. Oxytalan, elanuin and elastic fibres in the human skin. *J Invest Dermatol* 1976; 66: 143–148.
8. Danielsen L, Kobayasi T. Regeneration of dermal elastic fibres in relation to age and light-exposure. *Acta Derm Venereol* 1972; 52: 1–10.
9. Danielsen L, Kobayasi T, Larsen H-W, Midtdaard K, Christensen HE. Pseudoxanthoma elasticum. *Acta Derm Venereol* 1970; 50: 353–373.
10. Danielsen L, Kobayasi T. Internal elastic lamina of gastric arteries in pseudoxanthoma elasticum. *Acta Pathol Microbiol Scand A* 1972; 80: 697–704.
11. Danielsen L, Kobayasi T. An ultrastructural study of cutaneous amyloidosis. *Acta Derm Venereol* 1973; 53: 13–21.
12. Otkjær Nielsen A, Christensen OB, Hentzer B, Johnson E, Kobayasi T. Salpeter induced dermal changes electron microscopically distinguishable from pseudoxanthoma elasticum. *Acta Derm Venereol* 1978; 58: 323–327.
13. Otkjær-Nielsen A, Johnson E, Hentzer B, Kobayasi T. Dermatomyoitis with universal calcinosis. *J Cutan Pathol* 1979; 6: 486–491.
14. Kobayasi T, Asboe-Hansen G. Ultrastructure of skin in primary systemic amyloidosis. *Acta Derm Venereol* 1979; 59: 407–413.
15. Kobayasi T, Danielsen L, Asboe-Hansen G. Ultrastructure of localized myxedema. *Acta Derm Venereol* 1976; 56: 173–185.
16. Kobayasi T, Danielsen L, Asboe-Hansen G. Ultrastructure of necrobiosis lipoidica diabetorum. *Acta Derm Venereol* 1974; 54: 427–431.
17. Kobayasi T, Asboe-Hansen G. Ultrastructural changes in the inflammatory zone of localized scleroderma. *Acta Derm Venereol* 1974; 54: 105–112.
18. Kobayasi T, Asboe-Hansen G. Ultrastructure of generalized scleroderma. *Acta Derm Venereol* 1972; 52: 81–93.
19. Kobayasi T, Asboe-hansen G. Ultrastructure of lupus erythematosus. Dermal connective tissue. *Acta Derm Venereol* 1974; 54: 23–28.
20. Danielsen L, Kobayasi T, Jacobsen G. Ultrastructural changes in disseminated connective tissue nevi. *Acta Derm Venereol* 1977; 57: 93–101.
21. Kobayasi T, Bartosik J, Ullman S. Elastic fibre in dermis of juvenile elastoma. *J Dermatol* 1998; 25: 5–9.

II. Collagen fibrils

1. Kobayasi T, Karlsmark T. Type V and VI collagen for cohesion of dermal fibrillar architectures. *J Submicroscop Cytol Pathol* 2006; 38: 104–108.

2. Luse SA. Electron microscopic studies of brain tumor. *Neurology (NY)* 1960; 10: 881-905.
 3. Kobayasi T, Asboe-hansen G, Tsurufuji S. Filamentous aggregates of collagen. Ultrastructural evidence for collagen-fibril degradation in situ. *Arch Dermatol Res* 1985; 277: 214-219.
 4. Kobayasi T, Hentzer B, Asboe-Hansen G. Degradation of dermal fibrillar structures: Effects of collagenase, elastase, dithioerythritol and citrate. *Acta Derm Venereol* 1977; 57: 379-387.
 5. Hentzer B, Kobayasi T, Hentzer B, Kobayasi T. Ultrastructural change of human skin in organ culture. *IRCS. J Med Sci* 1975; 3: 221.
 6. Kobayasi T, Asboe-Hansen G. Ultrastructure of generalized scleroderma. *Acta Derm Venereol* 1972; 52: 81-93.
 7. Kobayasi T, Karlsmark T, Ullman S. Ultrastructural aspects in scleroderma. In: Nishioka K, Krieg Th, editors. Pathogenesis and management of scleroderma and connective tissue disorders. Osaka 1993, p. 29-39.
 8. Kobayasi T, Danielsen L, Asboe-hansen G. Ultrastructure of necrobioid lipoidica diabetorum. *Acta Derm Venereol* 1974; 54: 427-431.
 9. Kobayasi T, Asboe-Hansen G. Ultrastructural changes in the inflammatory zone of localized scleroderma. *Acta Derm Venereol* 1974; 54: 105-112.
 10. Serup J, Weismann K, Kobayasi T, Ammitzbøll T, Møller R. Local panatropy with linear distribution: A clinical, ultrastructural and biochemical study. *Acta Derm Venereol* 1982; 62: 101-105.
 11. Kobayasi T, Oguchi M, Asboe-hansen G. Dermal changes in Ehlers-Danlos syndrome. *Clinical Genetics* 1984; 25: 477-484.
 12. Kobayasi T. Abnormality of dermal collagen fibrils in Ehlers-Danlos syndrome. Anticipation of the abnormality for the inherited hypermobile disorders. *Eur J Dermatol* 2004; 14: 221-229.
 13. Danielsen L, Kobayasi T, Larsen H-W, Midtgaard K, Christensen HE. Pseudoxanthoma elasticum. A clinico-pathological study. *Acta Derm Venereol* 1970; 50: 355-373.
 14. Danielsen L, Kobayasi T. Pseudoxanthoma elasticum. An ultrastructural study of scar tissue. *Acta Derm Venereol* 1974; 54: 121-128.
 15. Danielsen L, Kobayasi T. Pseudoxanthoma elasticum. An ultrastructural study of oral lesion. *Acta Derm Venereol* 1974; 54: 173-196.
 16. Kobayasi T, Wolf-Jurgensen P, Danielsen L. Ultrastructure of shagreen patch. *Acta Derm Venereol* 1973; 53: 275-278.
 17. Danielsen L, Kobayasi T, Jacobsen GK. Ultrastructural changes in disseminated connective tissue nevi. *Acta Derm Venereol* 1977; 57: 93-101.
 18. Kobayasi T, Asboe-Hansen G. Ultrastructure of skin in primary systemic amyloidosis. *Acta Derm Venereol* 1979; 59: 407-413.
 19. Kobayasi T, Ullman S. Twisted collagen fibrils in dermis. Significance for differentiation of hypermobile patient. Presentation in the 29th Nordic Congress of Dermatology and Venereology. Gothenburg, Sweden, 2001.
- ### III. Ground substance
1. Kobayasi T, Danielsen L, Asboe-Hansen G. Hyaluronate (?) microfibrils in human dermis. *Acta Derm Venereol* 1971; 51: 27-34.
 2. Kobayasi T, Asboe-Hansen G. Ruthenium red staining of ultrathin sections of human mast cell granules. *J Microscopy* 1971; 93: 55-60.
 3. Thierry JP. Mise en evidence des polysaccharides sur coupes fines en microscopie electronique. *J Microscopie* 1967; 6: 987.
 4. Kobayasi T. Argentaffin reaction of the dermoepidermal zone. *Acta Derm (Kyoto)* 1960; 56: 247.
 5. Kobayasi T, Danielsen L, Asboe-Hansen G. Ultrastructure of localized myxedema. *Acta Derm Venereol* 1976; 56: 173-185.
 6. Danielsen L, Kobayasi T. Ultrastructural changes in scleromyxedema. *Acta Derm Venereol* 1975; 55: 451-460.
 7. Kobayasi T, Asboe-Hansen G. Ultrastructure of systemic lupus erythematosus. Dermal connective tissue. *Acta Derm Venereol* 1974; 54: 23-28.
 8. Kobayasi T, Asboe-Hansen G. Ultrastructural changes in the inflammatory zone of localized scleroderma. *Acta Derm Venereol* 1974; 54: 105-112.
 9. Hentzer B, Kobayasi T, Asboe-Hansen G. Ultrastructure of dermal connective tissue in fibrodysplasia ossificans progressiva. *Acta Derm Venereol* 1977; 57: 477-485.
 10. Kobayasi T, Asboe-Hansen G. Ultrastructure of mast cell granules in basal cell carcinoma. *Acta Derm Venereol* 1969; 49: 111-124.
- ### IV. Junction
1. Kobayasi T. An electron microscope study on the dermo-epidermal junction. *Acta Derm Venereol* 1961; 41: 481-491.
 2. Kobayasi T. Electron microscopy of the elastic fibres and the dermal membrane in normal human skin. *Acta Derm Venereol* 1968 48: 303-412.
 3. Kobayasi T. Dermo-epidermal junction of normal skin. *Jap J Dermatol* 1978; 5: 157-165.
 4. Kobayasi T, Asboe-Hansen G. Die dermoepidermale Verbundzone bei Hautkrankheiten. *Hautarzt* 1979; 30: 353-359.
 5. Kobayasi T. Anchoring of basal lamina to elastic fibres by elastic fibrils. *J Invest Dermatol* 1977; 68: 389-390.
 6. Kobayasi T. Argentaffin reaction of the dermo-epidermal zone. *Acta Dermatol (Kyoto)* 1960; 56: 247-249.
 7. Kobayasi T, Hentzer B, Asboe-Hansen G. Degradation of dermal fibrillar structures. Effect of collagenase, elastase, dithioerythritol and citrate. *Acta Derm Venereol* 1977; 57: 379-387.
 8. Kobayasi T. Development of fibrillar structures in human fetal skin. *Acta Morph Neerl Scand* 1966; 6: 257-269.
 9. Hentzer B, Kobayasi T. Dissociation of human adult epidermal cells by disulfide reducing agents and subsequent trypsinization. *Acta Derm Venereol* 1976; 56: 19-25.
 10. Hentzer B, Kobayasi T. Enzymatic liberation on viable cells of human skin. *Acta Derm Venereol* 1978; 58: 197-202.
 11. Oguchi M, Kobayasi T, Asboe-Hansen G. Secretion of type IV collagen by keratinocytes of human adult. *J Invest Dermatol* 1985; 85: 79-81.
 12. Kobayasi T, Karlsmark T. Type V and VI collagen for cohesion of dermal fibrillar structures. *J Submicrosc Cytol Pathol* 2006; 38: 103-108.
 13. Weismann K, Kvist N, Kobayasi T. Bullous acrodermatitis due to zinc deficiency during total parenteral nutrition: An ultrastructural study of the epidermal changes. *Acta Derm Venereol* 1983; 63: 143-146.
 14. Kobayasi T. The dermo-epidermal junction in bullous pemphigoid. *Dermatologica* 1967; 134: 157-156.
 15. Kiistala U, Mustakallio KK. Dermoepidermal separation with suction. *J Invest Dermatol* 1967; 48: 466.
 16. Hentzer B, Kobayasi T. Suction blister transplantation for leg ulcers. *Acta Derm Venereol* 1975; 55: 207-209.
 17. Kobayasi T. Dermoepidermal junction in the recessive type of epidermolysis bullosa. An electron microscopic study. *Acta Derm Venereol* 1967; 47: 57-59.
 18. Kobayasi T, Willeberg A, Serup J, Ullman S. Generalized morphea with blister. *Acta Derm Venereol* 1990; 70: 454-456.
 19. Kobayasi T, Asboe-Hansen G. Ultrastructure of generalized scleroderma. *Acta Derm Venereol* 1972; 52: 81-93.
 20. Kobayasi T, Asboe-Hansen G. Ultrastructure of systemic lupus erythematosus skin. Dermo-epidermal junction. *Acta Derm Venereol* 1973; 53: 417-424.
 21. Kobayasi T, Asboe-Hansen G. Ultrastructure of systemic lupus erythematosus. Dermal connective tissue. *Acta Derm Venereol* 1974; 54: 23-28.
 22. Kobayasi T. Dermo-epidermal junction in basal cell carcinoma. *Acta Derm Venereol* 1970; 50: 401-411.
 23. Kobayasi T. Dermo-epidermal junction in invasive squamous cell carcinoma. *Acta Derm Venereol* 1969; 49: 445-457.
 24. Kobayasi T, Danielsen L, Asboe-Hansen G. Ultrastructure of localized myxedema. *Acta Derm Venereol* 1976; 56: 173-185.
 25. Kobayasi T, Asboe-hansen G. Ultrastructure of skin in primary systemic amyloidosis. *Acta Derm Venereol* 1979; 59: 407-413.
 26. Sboukis D, Kobayasi T, Stravianeas N, Karameris A. Hyalinosis cutis et mucosae: Excessively secreted basal lamina by pericytes and

myofibroblasts and its conversion to hyaline. *J Eur Acad Dermatol Venereol* 2003; 17: 97–98.

27. Kobayasi T, Asboe-Hansen G. Ultrastructural changes in the inflammatory zone of localized scleroderma. *Acta Derm Venereol* 1974; 54: 105–112.
28. Kobayasi T, Hentzer B. Ultrastructure of human keratinocyte growth in vitro. Presentation in the 15th Annual meeting for the Society of Cutaneous Ultrastructure Research, 1988.
29. Hentzer B, Kobayasi T. Ultrastructural changes of human skin in organ culture. *IRCS J Med Sci* 1975; 3: 221.
30. Kobayasi T, Karlsmark T, Ågren M. Formation of dermoepidermal junction in organ culture. Presentation in the 26th Annual Meeting of Society for Cutaneous Ultrastructural Research in Florence, Italy, 1999.

V. Mast cells

1. Kobayasi T, Midtgaard K, Asboe-Hansen G. Ultrastructure of human mast cell granules. *J Ultrastruct Res* 1968; 23: 153–165.
2. Kobayasi T, Asboe-Hansen G. Ruthenium red staining of ultrathin-sections of human mast cell granules. *J Microscopy* 1971; 93: 55–60.
3. Kobayasi T, Asboe-Hansen G. Degranulation and regranulation of human mast cells. *Acta Derm Venereol* 1969; 49: 369–381.
4. Kobayasi T, Asboe-Hansen G. Human mast cells influenced by adrenocortical steroids. *Uppsala J Med Sci* 1977; 82: 138.
5. Kobayasi T, Danielsen L, Asboe-Hansen G. Ultrastructure of localized myxedema. *Acta Derm Venereol* 1976; 56: 173–185.
6. Danielsen L, Kobayasi T. Ultrastructural changes in scleromyxedema. *Acta Derm Venereol* 1975; 55: 451–460.
7. Kobayasi T, Asboe-Hansen G. Ultrastructural changes in the inflammatory zone of localized scleroderma. *Acta Derm Venereol* 1974; 54: 105–112.
8. Kobayasi T, Asboe-Hansen G. Ultrastructure of generalized scleroderma. *Acta Derm Venereol* 1972; 52: 81–93.
9. Hentzer B, Kobayasi T, Asboe-Hansen G. Ultrastructure of dermal connective tissue in fibrodysplasia ossificans progressiva. *Acta Derm Venereol* 1977; 57: 477–485.
10. Danielsen L, Kobayasi T. An ultrastructure study of cutaneous amyloidosis. *Acta Derm Venereol* 1973; 53: 13–21.
11. Kobayasi T, Asboe-Hansen G. Ultrastructure of mast cell granules in basal cell carcinoma. *Acta Derm Venereol* 1969; 49: 111–124.
12. Kobayasi T, Asboe-Hansen G. Ultrastructure of mast cell granules in squamous cell carcinoma. *Acta Derm Venereol* 1969; 49: 233–240.

VI. Mesenchymal cells

1. Kobayasi T. Pericyte transformation to myofibroblast. *Jap J Dermatol* 1991; 101: 1465–1466.
2. Schurch W, Seemeyer T, Gabiani G. The myofibroblast: A quarter century after its discovery. *Am J Surg Pathol* 1998; 22: 141–147.
3. Eyden B. The myofibroblast: A study of normal, reactive and neoplastic issues with an emphasis on ultrastructure. Part 1. Normal and reactive cells. *J Submicrosc Cytol Pathol* 2005; 37: 109–204.
4. Krummel TM, Ehrlich P, Nelson JM, Michna BA, Thomas BL, Hayens JH, et al. Fetal wounds do not contract in utero. *Surg Forum* 1989; 40: 613–615.
5. Kobayasi T. Vascular pericytes transform to myofibroblasts. Presentation in the 20th World Congress of Dermatology, Paris, 2002. IC 1396.
6. Karlsmark T, Kobayasi T. Transforming growth factor beta-3. Effects on the cells of vascular wall. *J Invest Dermatol* 1996; 107: 657.
7. Evans RA, Tian YC, Philips AO. TGF-beta 1-mediated fibroblast-myofibroblast terminal differentiation-the role of smad proteins. *Exp Cell Res* 2003; 282: 90–100.
8. Powell DW, Miffin JD, Crowe VSE, Saada JI, West AB. Myofibroblast.

I. Paracrine cells important in health and disease. *Am J Physiol Cell Physiol* 1999; 277: C1–C19.

9. Requena L, Kutzner H, Hugel H, Rutten A, Furio V. Cutaneous adult myofibroma: A vascular neoplasm. *J Cutan Pathol* 1996; 23: 445–457.
10. Kobayasi T, Serup J. Vascular changes in morphea. *Acta Derm Venereol* 1985; 65: 116–120.
11. Kobayasi T, Serup J. Nerve changes in morphea. *Acta Derm Venereol* 1983; 63: 321–327.
12. Kobayasi T, Oguchi M, Asboe-Hansen G. Dermal changes in Ehlers-Danlos syndrome. *Clin Genetics* 1984; 25: 477–484.
13. Kobayasi T, Ullman S, Karlsmark T. Mesenchymal cell lineage in fibrosis and scleroderma. 2007. (Unpublished data).
14. Hacker G. The morphology of apoptosis. *Cell Tissue Res* 2000; 301: 5–17.
15. Kobayasi T, Asboe-Hansen G, Serup J. [Ultrastructural histopathology at sclerodermia]. *Ugeskrift for Laege* 1984; 146: 1617–1619 (in Danish).
16. Kissin E, Korn JH. Apoptosis and myofibroblast in the pathogenesis of systemic sclerosis. *Curr Rheumatol Rep* 2002; 4: 129–135.
17. Kobayasi T. Transformation of pericyte to myofibroblasts. An experimental study. Presentation in the 2nd International Symposium on Cutaneous Development, Aging and Repair. Padua, Italy, 1991.
18. Kobayasi T, Karlsmark T, Ullman S. Fibrotic process of scleroderma. Presented in the 21st Annual Meeting for the Cutaneous Ultrastructure Research. Leiden, Holland, 1991.
19. Kobayasi T, Karlsmark T. Transforming growth factor beta. Effects on cells of vascular wall. Presented in the 19th Annual Meeting for Cutaneous Ultrastructure Research. Lyon, France, 1992.
20. Kobayasi T, Karlsmark T. Dermal myofibroblasts react with antibodies to factor XIIIa. Human myofibroblast in vitro and vimentin. Presented in the 22nd Annual Meeting for Cutaneous Ultrastructure Research. Heidelberg, Germany, 1995.
21. Karlsmark T, Kobayasi T. Effects of transforming growth factor beta 3 on cells of vascular wall. Presented in the 23rd Annual Meeting for Cutaneous Ultrastructure Research. Brescia, Italy, 1996.

Acknowledgements

The author expresses sincere respect and gratitude to Professor Gustav Asboe-Hansen MD, Leader in the Department of Dermato-venereology with the Connective Tissue Research Laboratories, University of Copenhagen Rigshospital. Professor Asboe-Hansen was fascinated by ultrastructural study of connective tissue of dermatoses and constantly supported and encouraged me with valuable comments on the studies from 1959 until the day of his death in 1988. I extend sincere and profound thanks to Tonny Karlsmark, Dr med., who was my co-worker in myofibroblast research. I also extend profound thanks to my colleagues in the laboratory who studied dermal connective tissue, whose publications were cited in this article. I also extend my gratitude to my assistants who worked in the laboratory and helped me with their skilful techniques. Finally, I thank Kiyoshi Nishioka, MD, Emeritus Professor in Dermatology, Tokyo Medical and Dental University, Tokyo Japan, and Keiji Iwatuki, MD, Professor of Dermatology, University of Okayama, Japan for their comments.

APPENDIX. Description of techniques

The techniques described here are specially developed in the laboratory. Routine methods only describe the modified matters in the laboratory.

It is important to find the most significant area of the change in the specimen in the orientation section and prepare ultrathin sections in the areas for electron microscopy. Qualified experiences in clinic and laboratory work are required.

For routine study, the fixative is supplemented sucrose at 7.5%. No other modification is performed in routine preparation and staining of uranyl acetate and lead citrate. Embedding in epoxy-resin and staining in uranyl acetate and lead citrate is as usual. Used uranyl acetate is recycled. (Unpublished method). The used uranyl solution is deposited in aqueous solution of 1N NaOH after staining. Precipitated uranyl acetate is gathered by centrifugation and prepared saturated solution in 70% ethanol for staining. Distilled water for the staining is necessary to boil and remove carbon dioxide.

For immune electron microscopy the ultrathin sections are prepared as follows:

Preparation of ultrathin section for immune chemical stain. The tissue specimens are fixed in 4% paraformaldehyde solution of phosphate-buffered saline (PBS) pH 7.4 with 7.5% sucrose and embedded in Technovit 7100 (Kulzer), a water-soluble resin, without dehydration in ethanol and transitional solvent. Tissue specimens are cut in the size of 4–5 mm blocks and placed on the surface of the column of the infiltration solution of Technovit without harder. The specimens sink down to the bottom. This procedure is repeated 2–3 times for making sure of complete exchange of water by infiltration solution of Technovit. When water in the specimens are exchanged completely to the infiltration solution, the specimens lay down on the bottom of the infiltration solution. The specimens are moved on the surface of the infiltration solution with harder (embedding solution) in capsules. When the specimens sink down on the bottom of the capsules, the capsules are then placed in a glass desiccators with silica gel for polymerization. Polymerization is carried out at room temperature (20°C). Polymerization is completed for about 2 days. For ultramicrotomy, water-free glycerol is used in troughs. Silver-coloured ultrathin sections are floating on the surface of the water-free glycerol. Ribbons of the ultrathin sections are picked up on formvar-coated nickel-grid. Ultrathin sections on the grids are covered by glycerol and can be stored in the grid box for couples of weeks. Immune staining is carried out after the ultrathin sections on grids. The grids with ultrathin sections are washed in PBS with 0.02 M glycine for 20 min and de-masked by neutral protease (Sigma P-5380) 5 m/10 ml PBS at 35°C for 7 min. After these steps, immune staining is proceeded by usual techniques as described. Counter stain is carried out only by uranyl acetate, saturated in 70% ethanol for a couple of minutes.

Technique for preparation of keratinocyte culture from normal human skin (unpublished data, 1988)

Preparation for growth-active keratinocyte suspension from human adult skin:

1. Skin graft in split-thickness is removed corium by a pair of scissors as thin as possible and cut 4 cm² in size.
2. The skin grafts are incubated in a clostridial collagenase solution for 2.5 h at 37°C, with vigorous shaking. The clostridial collagenase solution is prepared in Worthington collagenase CLS 4, 10 mg dissolved in the culture medium, pH 7.3 with 0.005% calcium chloride and 20% fetal calf serum solution. Incubation is carried out at 36°C for about 1.5 h. When edges of the graft are released from epidermis, sheets of epidermis is peeled from dermis by forceps and washed quickly in Hanks BBS.
3. The sheets of epidermis are incubated in the solution of dithioerythritol (3 mg/ml Hanks BBS. pH 7.6 is adjusted by 7.5% Na bicarbonate). 80 ml DTE solution for approximately 7–8 epidermal sheets is suitable. The sheets are incubated at 37°C for 8 min and then 60 ml of 0.2% trypsin in PBS is poured. The solution with the epidermal sheets is shaken vigorously for 3 min. The trypsin solution becomes muddy by the released cells. The keratinocytes in basal and lower Malpighian layers are dissociated and released from the sheets but most of the cells in the upper layers of the sheets are not dispersed from the sheet. The epidermal sheets are discarded.
4. The solution is diluted 4 times by the culture medium and spun at 800 G for 5 min. The cells of the sediment are re-suspended in small volume of the culture medium.
5. Growth-active keratinocytes are isolated from the suspension by centrifuge on a continuous gradient of Percoll (Pharmacia, Sweden).

Preparation of continuous Percoll gradient: The original Percoll (10 times concentrated) is diluted by 1/10 volume of BBS solution and the diluted Percoll solution is further diluted at a concentration of 40% by Hanks balanced salt solution and spun at 60,000 G for 30 min.

6. The epidermal cell suspension is layered on the top of the continuous Percoll gradient and spun at 800 G for 20 min. The cells are separated into two layers, the upper conglomerate and the lower disc (Fig. 1, left-hand drawing). The lower disc contains growth-active cells released from basal and lower Malpighian layers (about 15% of the cell suspension) and about 85% of the cells come in the upper conglomerate (keratinized cells and dendritic cells in Malpighian cell layers). The cells of both parts are re-suspended in the culture-media. Two and three drops of the suspension are placed on the flask bottom and left on the table for about 20 min. Ordinary cell culture media is gently poured in flasks and cultivated at 37°C. The unsettled cells are removed by the medium change.

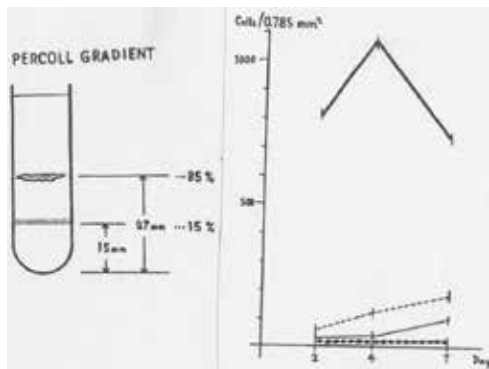


Fig. 1. Preparation of continuous Percoll gradient.

Keratinocyte growth after 4 days cultivation is shown in Figs 29 and 30 in Section IV Junction. In right-hand drawing of Fig. 1, the thick continuous line, shows keratinocyte growth from the lower disc and thick broken line shows dendritic cell growth from the upper conglomerate. (Thin lines show unsettled non-grown cells.) The grown cells in 9 days cultivation are shown in Figs 2 and 3. Keratinocytes from the lower disc start to grown. Mitotic figures are found

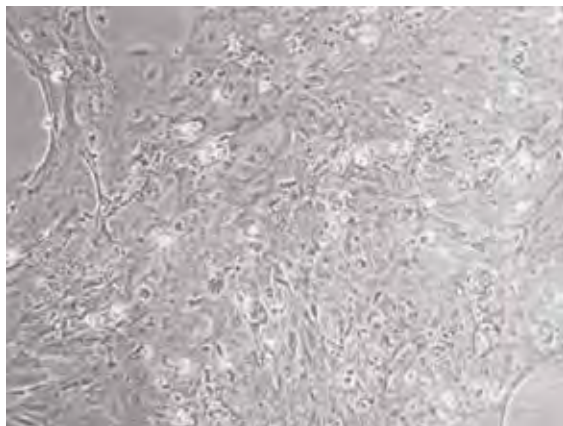


Fig. 2. Keratinocyte culture from the disc after 9 days cultivation.

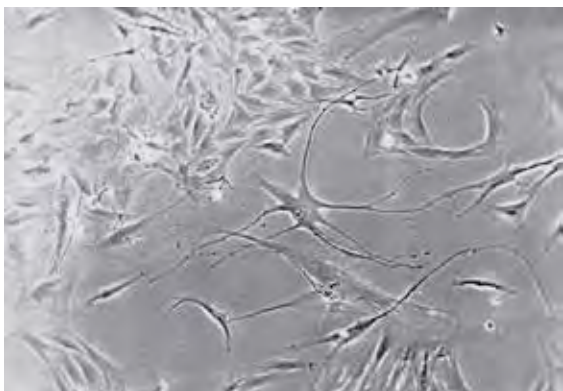


Fig. 3. Dendritic cell growths from the upper conglomerate after 9 days cultivation.

in the 4th day culture. (Page 85, IV. Junction, Fig. 29.) The grown cells expand cytoplasm and form round membranous growth. Keratinization is seen distinctly in the 9 days culture (Fig. 2). Thereafter, the membranous growth of the keratinized keratinocytes is released from the flask bottom, keeping round membranous growth. Dendritic cells grown from the upper conglomerate appear dendritic and spindle-shaped. The cells increase slowly in number to the 9th day of culture (Fig. 3) and grow further.

Rabbit immunoglobulins to human myofibroblast (5)

Antigen (Human myofibroblast) preparation and immunization:

Cell suspension of human myofibroblasts and Cytodex 2 microcarriers (Pharmacia) is mixed. The cell suspension (1,000 cells/ml culture media) is mixed in 10 ml of the microcarriers and are suspended in 50 ml culture media in a Falcon flask and myofibroblasts *in vitro*. The air in the flask is exchanged with sterilized air with 5% carbon dioxide. The culture is carried out at 37°C under gentle shaking for 3–4 weeks with the media change twice a week. When the cells grow well on the microcarriers, the culture is washed in MEM without foetal calf serum and injected subcutaneously in rabbit, twice in one week.

Immunoglobulins to myofibroblast, preparation and qualification:

Immunoglobulins are isolated from the rabbit serum by salt diffusion and further rinsed by CNBr sepharose 4B-collagen column (Pharmacia). The eluted solution of the immunoglobulins is concentrated by salt precipitation and qualified reactivity to human fibroblast *in vitro* by enzyme-linked immune absorbent assay. For immune staining, a dilution of 8,000 times is applied for staining.

Reactivities of the immune globulins to *in vitro* myofibroblasts and some other connective tissue components are demonstrated in Fig. 4.

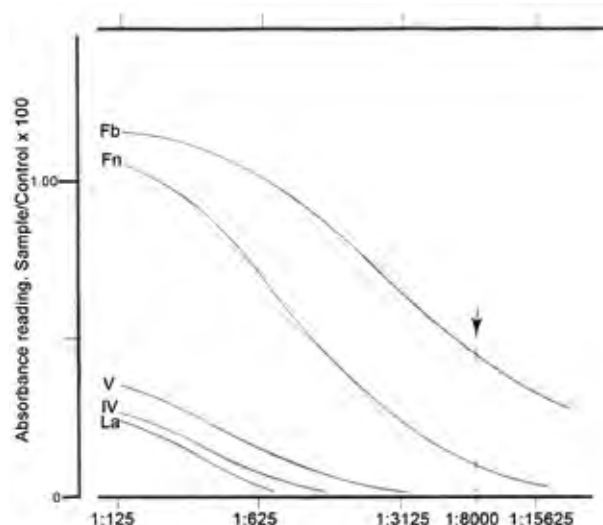


Fig. 4. Fb: Myofibroblast *in vitro*. Fn: Fibronectin. V: Collagen type V. IV: Collagen type IV. La: Laminin. Arrow indicates a suitable dilution of the antibody for immune staining, 1:8,000.

Sender:
Forum for Nordic Dermato-Venereology
S:t Johannesgatan 22A
SE-753 12 Uppsala
Sweden

B

SVERIGE
PORTO BETALT
PORT PAYÉ